



UNIVERSITÀ DEGLI STUDI DI MILANO

Ph.D. School in MOLECULAR AND CELLULAR BIOLOGY
Cycle XXXIII

Department of Excellence of Bioscience



Molecular design of a novel Dual-purpose Barley Variety

LISA ROTASPERTI
Matricola: R11969

Supervisor: Prof. Paolo Pesaresi
Tutor: Dr. Luca Tadini
Ph.D. School Coordinator: Prof. Martin Kater

Academic year 2019-2020

Index

Abstract	4
Riassunto	6
1 – Introduction	8
1.1 - The current state of the agricultural land availability	8
1.2 - Fossil fuels: a problem that must be solved	8
1.3 - Dual-purpose crops as a sustainable strategy for future agriculture	10
1.4 - Barley, an ideal model organism for the realization of a dual-purpose crop	12
1.4.1 - Barley diversity: natural and induced genetic variability	14
1.5 - Photosynthesis and photosynthesis regulation	16
1.6 - Engineering the photosynthetic process to improve the biomass production	20
1.6.1. Optimization of the antenna size	21
1.6.1.1 The importance of pale phenotype	23
1.6.2 - Improving the adaptation to fluctuating light: dissipation of excess energy through Non-Photochemical Quenching (NPQ)	25
1.6.2.1 - The xanthophyll cycle	28
2 - Aims of the project	31
3 - Materials and methods	33
3.1- <i>In silico</i> analysis	33
3.2 - Plant lines and growth conditions of <i>Hordeum vulgare</i>	33
3.3 - <i>Arabidopsis thaliana</i> lines and growth conditions	34
3.4 - Crossing of selected barley plants	35
3.6 - Genotyping procedures	36
3.7- Exome capture and sequencing	38
3.8 - RNA extraction from leaf material	41
3.9 - DNase treatment and cDNA synthesis	41

3.10 - High fidelity PCR	42
3.11 - Complementation experiments introducing <i>Hordeum vulgare</i> genes in <i>Arabidopsis thaliana</i>	42
3.12 - Quantitative real-time PCR (qRT-PCR)	44
3.13 - Protein preparation and immuno-blot analysis	45
3.14 - Coomassie Brilliant Blue staining	46
3.15 - Thylakoid membrane extraction	46
3.16 - Pigment extraction and quantification	47
3.17 - Measurement of photosynthetic efficiency	48
3.18 - Yeast two hybrid assay	49
3.19 – TEM (Transmission Electron Microscope)	51
4 - Results and discussions	52
4.1 - Characterization of the barley pale mutant <i>hus1</i>	52
4.2 - Exome capture analysis allowed for the identification of <i>hus1</i> mutation	54
4.3 - Functional characterization of <i>HUS1</i> gene	60
4.4 - <i>Arabidopsis chaos</i> mutant complementation with barley <i>HUS1</i> gene	66
4.5 Identification of putative <i>hus1</i> allelic variants in the Whealbi collection	68
4.6 - Phenotypical description of a TILLMore mutant line altered in photosynthesis	75
4.7 HUS1 physical interacts with barley cpSRP54 protein	78
4.8 – Characterization of barley <i>VDE</i> allelic variants	82
4.9 - Complementation assay with <i>VDE</i> allelic variants of <i>Arabidopsis thaliana npq1</i> mutant	87
4.10 - Preliminary characterization of barley <i>ZEP</i> allelic variant	89
5 - Conclusions and future perspective	91
6 - Bibliography	95
7 – Acknowledgments	112
8 – Appendices (Manuscripts)	113

Abstract

By mid-century the bio-based economy is expected to have grown significantly in Europe and all around the world. A pillar of this, both now and in the future, is the sustainable processing of biomass into a spectrum of marketable products and energy. That will depend largely on the availability of a reliable supply of appropriate quantities of biomass in a sustainable manner and at fair prices. Among the primary sources of agriculture-derived biomass, crop residues have a great potential to supply large, reliable, and sustainable quantities of biomass.

This Ph.D. thesis work was aimed to address this issue using barley as model crop, since its straw is characterized by the largest content of carbohydrates among cereals, thus a valuable product for its potential conversion into biofuels and other eco-friendly products. Especially, we tried to explore the possibility to increase barley biomass production, without penalty on grain yield, by improving the light phase of photosynthesis through:

- i) decreasing the light harvesting antenna size of photosystems, thus reducing the excess of light absorption on top of the canopy, together with the consequent decrease in photo-damage, and favoring a more uniform light absorption and photosynthesis throughout the canopy;
- ii) the fine-tuning of the photoprotective mechanism, known as Non-Photochemical Quenching mechanism (NPQ), with aim to have a more rapid induction/relaxation of this mechanism, hence a better photosynthetic performance.

Within this frame, we have characterised into details the *hus1* (*happy under the sun*) barley mutant, isolated by a forward genetics approach within the HorTILLUS chemical mutagenize population. *hus1* plants are characterised by pale-green leaves, a reduced antenna size of photosystems and an improved photosynthetic performance with respect to cv. Sebastian, used as control. Segregation analysis performed on the

F₂ population obtained by crossing *hus1* with Morex indicates that the *hus1* phenotype is caused by a monogenic recessive allele. Using exome capture sequencing of DNA pools from 50 WT and 50 *hus1*-like plants, the putative SNP mutation has been identified in the *Arabidopsis thaliana* homologous *CHAOS* gene, encoding the Chloroplast Signal Recognition Particle 43 (cpSRP43), a stromal chaperone that upload the antenna proteins into the thylakoid membranes. As a matter of fact, immune-blot analyses confirmed that barley *hus1* and the *Arabidopsis chaos* mutants have a similar reduction in the levels of antenna protein accumulation. Furthermore, using an allele mining strategy, the natural genetic variability of *HUS1 locus* has been studied in the exome sequences of the Whealbi collection. 26 accessions with different polymorphisms have been identified in *HUS1 locus*. A preliminary screening led to the identification of few pale lines that seem to have a higher photosynthetic activity compared to the corresponding WT. These natural accessions have been collected from different regions of the planet and represent an invaluable genetic material to understand how photosynthesis adapt to the different growth conditions.

With respect to fine-tuning of NPQ, a reverse genetic approach has been used to identify allelic variants of Violaxanthin De-Epoxidase (VDE) and Zeaxanthin Epoxidase (ZEP) enzymes both involved in the xanthophyll cycle, an integral part of NPQ photoprotective mechanism. Five allelic variants of the *VDE* gene and one of *ZEP* gene have been found. Most of the mutant plants show a Sebastian-like phenotype under green-house growth conditions, but they show very different NPQ kinetics, thus representing the ideal genetic material to investigate the impact of NPQ alteration on photosynthetic performance and biomass accumulation.

Riassunto

Entro la metà del secolo l'economia green dovrebbe crescere in modo significativo in Europa e in tutto il mondo. Un pilastro di questo, sia ora che in futuro, è la trasformazione sostenibile della biomassa in una gamma di prodotti ed energia commerciabili. Ciò dipenderà in gran parte dalla disponibilità di una quantità adeguata di biomassa prodotta in modo sostenibile e a prezzi equi. Tra le primarie fonti di biomassa derivate dall'agricoltura, i residui delle colture hanno un grande potenziale per fornire grandi quantità affidabili e sostenibili di biomassa.

Lo scopo di questo lavoro di tesi di dottorato è stato quello di affrontare questo problema utilizzando l'orzo come pianta modello, poiché la sua paglia è caratterizzata dal maggior contenuto di carboidrati tra i cereali, risultando quindi un prodotto prezioso per la sua potenziale conversione in biocarburanti e altri prodotti eco-compatibili. In particolare, abbiamo cercato di esplorare la possibilità di aumentare la produzione di biomassa di orzo, senza penalizzare la sua resa in granella, migliorando la fase luminosa della fotosintesi attraverso:

- i) la riduzione delle dimensioni dell'antenne di raccolta della luce legate ai fotosistemi, riducendo così l'eccesso di assorbimento della luce sulla sommità della chioma, insieme alla conseguente diminuzione del danneggiamento dovuto alla luce, e favorendo un assorbimento della luce e fotosintesi più uniforme attraverso tutta la chioma;
- ii) la modulazione del meccanismo foto-protettivo, noto come Non-Photochemical Quenching (NPQ), con l'obiettivo di avere una più rapida induzione/rilassamento di questo meccanismo, quindi una migliore prestazione fotosintetica.

All'interno di questo quadro, abbiamo caratterizzato nel dettaglio il mutante di orzo *hus1* (felice sotto il sole), isolato mediante un approccio di genetica diretta all'interno

della popolazione mutagenizzata chimicamente HorTILLUS. Le piante *hus1* sono caratterizzate da foglie verde chiaro, una ridotta dimensione dell'antenne dei fotosistemi e una migliore prestazione fotosintetica rispetto alla cultivar Sebastian, usato come controllo. L'analisi di segregazione eseguita sulla popolazione F₂ ottenuta incrociando *hus1* con Morex mostra che il fenotipo *hus1* è causato da un allele monogenico recessivo. Sequenziando l'esoma tra il pool di DNA di 50 piante WT e 50 piante pallide come *hus1*, la putativa mutazione SNP è stata identificata nel gene omologo di *Arabidopsis thaliana* *CHAOS*, che codifica per la molecola di riconoscimento del segnale del cloroplasto 43 (cpSRP43), un chaperone stromale che trasporta le proteine antenna nelle membrane tilacoidi. In effetti, le analisi di immunoblot hanno confermato che i mutanti di orzo *hus1* e *Arabidopsis chaos* hanno una riduzione simile nei livelli di accumulo delle proteine antenna. Inoltre, utilizzando una strategia di allele mining, è stata studiata la variabilità genetica naturale del locus *HUS1* nelle sequenze degli esomi della collezione Whealbi. Da questa analisi sono state identificate 26 accessioni con differenti polimorfismi nel locus *HUS1*. Uno screening preliminare ha portato all'identificazione di alcune linee pallide che sembrano avere una maggiore performance fotosintetica rispetto al controllo WT. Queste varianti alleliche naturali sono state raccolte da diverse regioni del pianeta e rappresentano un materiale genetico inestimabile per capire come la fotosintesi si sia adattata alle diverse condizioni di crescita.

Per quanto riguarda la modulazione dell'NPQ, è stato utilizzato un approccio di genetica inversa per identificare varianti alleliche degli enzimi Violaxantina De-Epossidasi (VDE) e Zeaxantina Epossidasi (ZEP) entrambi coinvolti nel ciclo delle xantofille, che risulta parte integrante del meccanismo foto-protettivo NPQ. Cinque varianti alleliche del gene *VDE* e una del gene *ZEP* sono state identificate. La maggior parte delle piante mutanti mostra un fenotipo simile a Sebastian in condizioni di crescita in serra, ma mostrano una cinetica dell'NPQ molto diversa, rappresentando così il materiale genetico ideale per lo studio dell'impatto dell'alterazione dell'NPQ sulla performance fotosintetica e sull'accumulo di biomassa nella pianta.

1 – Introduction

1.1 - The current state of the agricultural land availability

More and more frequently, cataclysms, storms, floods, droughts, sudden changes in temperature put a strain on global agricultural production. In addition to climate change, the increasing world's population, which is expected to reach 9.1 billion people by 2050, also pushes for ever-greater competition for land occupation. The on-going struggle between crops for food and those for bioenergy production has now brought to the end the problem of deforestation of the world's green lungs. In the last 300 years, land occupation for agricultural practices has led to the disappearance of about 7-11 million km² of forests, contributing enormously to deforestation [1]. Around 80% of deforestation worldwide between 2000 and 2010 was caused by agriculture [2]. The growing urbanization of developing countries implies a greater demand for food, leading to the need of increasing agricultural production. About 40% of the land surface is occupied by croplands and pastures which make them the most expanded terrestrial biomes [1] and the most extensive form of land use [3]. It is estimated that around 10 million km² of land will be needed to meet future agricultural demand by 2050, which is about 8% of the ice-free land [3]. However, it must be considered that the available soil is limited by various factors such as environmental, climatic, topographical and geological factors [4]. The scarcity and preciousness of new soil to cultivate, together with the need to preserve natural habitats with their high biodiversity, led to the design of a new concept of management of the already-anthropogenic soil.

1.2 - Fossil fuels: a problem that must be solved

Among the various causes of climate change, perhaps the most problematic is the use of fossil fuels for energy production. This is one of the main causes of the CO₂

increasing concentration in the atmosphere and together with other greenhouse gases is responsible for the temperatures rise. The high pollution produced by fossil fuels together with their exhaustible quantity of extraction led to the search for new alternative sources for energy production [5]. A solution to this problem could come from renewable sources such as biofuels made from plant tissue and organic products [6]. There are several sources from which it is possible to produce biofuels, for example, oil and starch grains, cellulosic material and organic waste [7]. In recent years there has been a growth in demand for biofuels including ethanol, produced from feed-stocks rich in sugars (such as sugarcane and sugar beet), starch (such as maize, wheat and barley) or cellulose, and biodiesel, produced by combining vegetable oil or animal fat with alcohol. While nowadays only 10% of the energy used comes from bioenergy (FAO, 2011), the production of biofuel is estimated to grow significantly in the next few years by competing both soil and water resources with crops for food. The first implication of this feud is also on an economic-social level: the greater demand for grain to produce biofuels raises the prices of the latter, having an impact on the food chain [8]. An alternative to first generation biofuels, produced directly from edible biomass, are those produced from biomass waste, particularly from non-edible lignocellulosic biomass, called second generation biofuel [6]. In addition to the increase in biomass production, another important aspect remains to improve the quality of the lignocellulosic material in terms of sugar content to optimize the biofuel production chain [9] [10]. This material is mainly obtained from the parts of plants left on the fields after harvesting [11], representing a very cheap and abundant resource. Partly used for animal feed, straw is largely unused or burned in the open field [12]. In this scenario, where the use of new arable land is impossible, increasing the biomass production of cultivated crops is necessary to avoid the excessive exploitation of natural resources [13].

1.3 - Dual-purpose crops as a sustainable strategy for future agriculture

During the “Green Revolution” of the XX century, a selection of very high grain yielding dwarf varieties was carried out, leading to the maximum potential limit of grain production in a plant. The next challenge for a sustainable agriculture is to increase the biomass production without penalizing grain yield, thus creating a dual-purpose crop, in order to minimize the competition between food and energy demand. The dual-purpose crop will be able to supply the grain for the production of animals feed and for human nutrition and, at the same time, a large amount of straw, useful for the production of biofuels.

To optimize the development of a dual-purpose crop, different traits can be modified (**Figure 1**):

- **Canopy architecture.** Increasing the number of tillers and the leaf size or modifying the leaf angle [14] could have a positive impact on the biomass production [15]. Moreover, having vertical leaves in the upper part of the canopy and horizontal leaves in the lower part would allow a better distribution of light through the so-called "smart" canopy and more efficient photosynthesis [16].
- **Nitrogen uptake and allocation.** The manipulation of nitrate and ammonium ion absorption from the soil, distribution and efficient utilization could have positive impact on the photosynthetic process and plant development [17] improving the accumulation of the biomass. Furthermore, the generation of cultivars that are more efficient in the usage of nitrogen would allow sparing the application of fertilizers to the soil, leading to less pollution of groundwater and economic savings for farmers.
- **Photosynthetic performance.** As described below, photosynthesis can be implemented from two different points of view: reducing the size of the antenna complexes that absorb light and modifying the kinetics of the photo-protection mechanism. In the first case, the exposure of the upper part of the canopy to high light

radiation can cause damage to the photosynthetic apparatus. The possibility of having reduced antenna complexes in the upper part of the canopy would facilitate the distribution of light through the whole canopy, especially in the lower part that is usually reached by dim light, leading to a general improvement in light absorption throughout the canopy [18][19]. In the second case, accelerating the dissipation process in the form of heat of the excess absorbed energy, known as NPQ (Non-Photochemical Quenching of chlorophyll fluorescence), would lead to an increase in photosynthetic efficiency up to 60% [20].



Figure 1 - Traits to be manipulated in order to improve biomass production in a dual-purpose crop.

The development of a dual-purpose crop is the aim of the European BarPLUS project that involves the University of Milan, CREA (Fiorenzuola d'Arda), University of Silesia, University of Potsdam and University of Lleida. This thesis work was realised within the frame of BarPLUS. The project's goals are the identification of genes, plant lines and alleles that might be helpful in increasing the biomass production without any penalty to the grain yield in barley (barplus.wordpress.com). Given its peculiar characteristic of having the highest sugar content in straw, barley (*Hordeum vulgare*) is an excellent candidate for the production of biofuels from its field waste [21].

1.4 – Barley, an ideal model organism for the realization of a dual-purpose crop

Barley is a self-pollinating monocotyledonous plant that belongs to the *Poaceae* family, a grass family that includes several important crops for agriculture. Barley is the fourth major crop after maize, wheat and rice in terms of annual grain tonnage, about 141 million tons (2018/2019) (FAOSTAT, 2020). The 75% of its global production is for animal feed, 20% for alcoholic and non-alcoholic beverages in brewing industry and 5% for human nutrition. Barley has a high content of beta-glucan, a beneficial fibre that can reduce cholesterol levels in the blood.

Since ancient times, man has selected plants for greater grain production, greater resistance to biotic and abiotic stresses, sensitivity to changes to photoperiod and nutritional value [22]. The domestication of the wild species *Hordeum vulgare* ssp. *spontaneum* dates circa 10000 BC in the Fertile Crescent [23], especially in Israel-Jordan region [24]. During the early domestication the main features selected were i) the non-shattering of the seeds, to facilitate grain collection [25], ii) reduced secondary ramification and vegetative plant biomass, to avoid lodging, iii) increased grain and fruit production quality, iv) loss of seed dormancy, to synchronize the germination [26]. *Hordeum vulgare* shows several differences with respect to *Hordeum spontaneum* as shorter stem and awns, tough ear rachis, broader leaves, a shorter and thicker spike and larger grains [27]. *H. spontaneum*, as *H. vulgare* is a very rustic and versatile plant that can grow in heterogeneous habitats and climates from the Arctic Circle to the tropics [28]. This composite resilience due to a high natural variability makes barley an excellent model for investigating crop adaptation to biotic stresses such as cold, drought, alkalinity and salinity.

During the last century, barley was one of the first crops to be exploited in cereal improvement programs using various induced mutagenesis strategies. Pioneering experiments using different types of radiation, such as X-rays and UV light, led to the discovery and study of different chlorophyll-deficient and virescent phenotypes

mutants such as *albina*, *xantha*, *alboviridis*, *viridis*, *tigrina*, *striatae maculata*. It was used as model plant to dissect the molecular and physiological mechanisms of chloroplast biogenesis and the fundamental processes of photosynthesis as reviewed in [29].

As significant model of the second half of the last century for the study of chloroplast, barley slowly lost its centrality in favor of the more famous model plant *Arabidopsis thaliana*, considered the “golden” model plant of the last 20 years. However, for the study of some traits of photosynthesis *Arabidopsis* is still a limited model.

Arabidopsis does not produce a true canopy therefore it is not a good model organism for studying the plant architecture and optimization of photosynthesis under field conditions [30][31]. Moreover, the biogenesis of the chloroplast is very different between monocotyledons and dicotyledons [32]. Along the leaf of the monocotyledon it is possible to observe a gradient of the chloroplast development process (**Figure 2**), since leaves have a basal meristem with youngest cells, carrying proplastid, while at the tip of the leaf, older cells with mature chloroplasts are present [33][34][35].

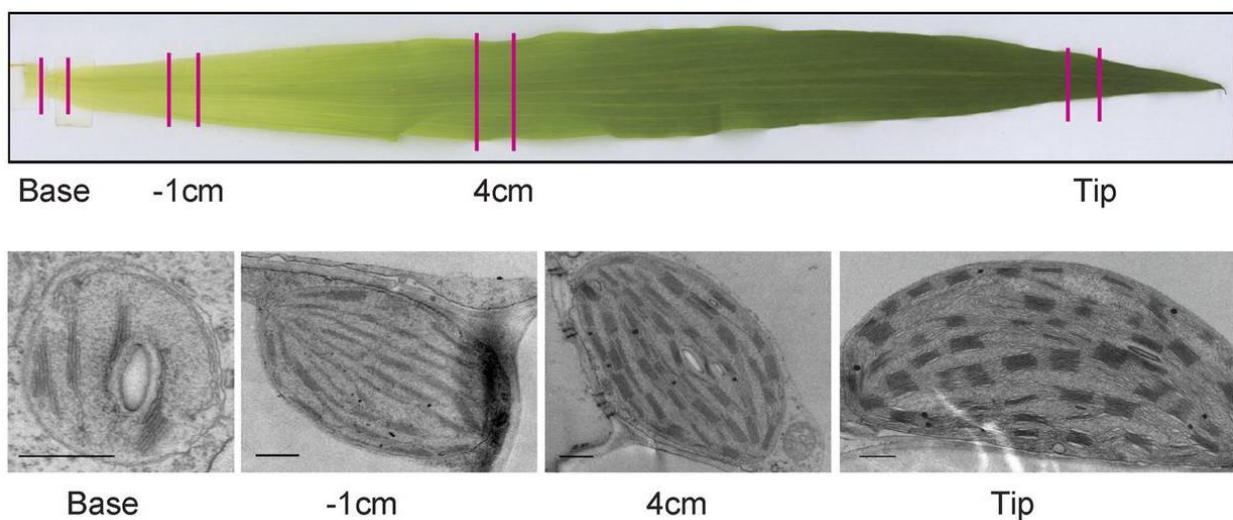


Figure 2 - The chloroplast developmental gradient of a maize leaf (Monocot plant, as barley). Adapted from [36].

1.4.1 - Barley diversity: natural and induced genetic variability

Investigating and understanding the enormous genetic variability of barley is an essential prerequisite for developing a dual-purpose crop. During domestication much of the genetic diversity was lost due to the selection of only some traits to the detriment of others through the phenomenon known as "domestication bottleneck" [37].

Landraces and wild barley varieties are therefore very precious genetic resources of natural variability useful to be introduced in modern breeding programs. Fortunately, over the years, several institutes around the world have preserved this variability making it available to breeders. Among the most important collections scattered all over the world we find ICARDA Collection with 222,704 accessions of barley, while at European level the IPK genebank contains most probably 300,000 accessions and the Whealbi collection (WHEAt and barley Legacy for Breeding Improvement collection), which includes 511 accessions, are the most representative. The Whealbi collection includes cultivars, landraces, wild barley varieties from Europe, Africa, the Middle East and Asia. Among these accessions a subset of 371 domesticated lines were analysed through exome sequencing [38] (**Figure 3**).

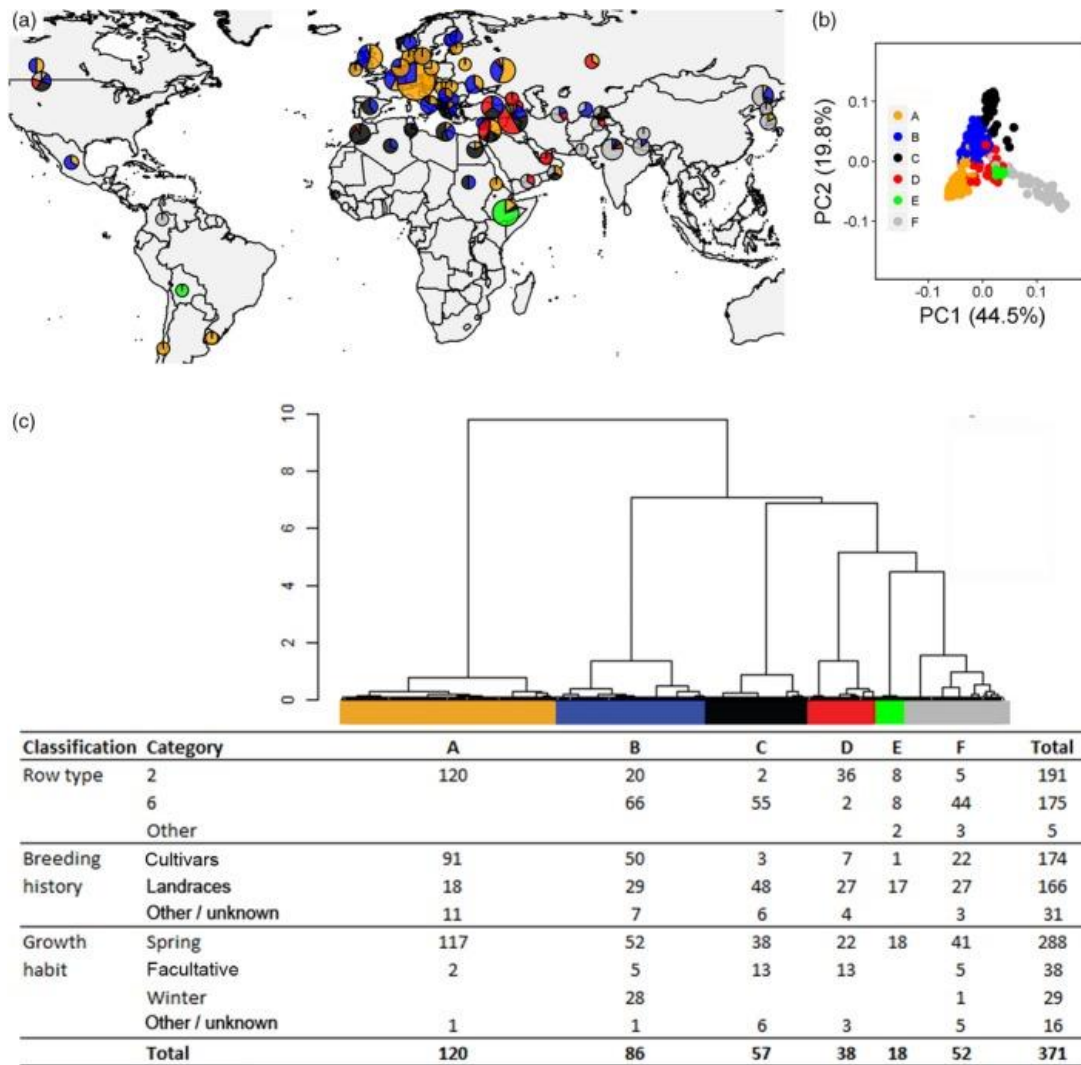


Figure 3 - Geographical distribution of six sub-populations for 371 barley genotypes that are part of the Whealbi collection [38].

In addition to natural allelic variability, a great role in understanding the correlation between gene functions and a particular phenotype is the availability of induced mutants. Always used as a model for chemical and physical mutagenesis studies, we have different populations of mutagenized cultivars for barley as listed in [29]. Among them in this work two chemical mutagenized population were taken in consideration. The first one is HorTILLUS (Hordeum-TILLING-University of Silesia) derived from the spring barley cultivar Sebastian treated with NaN_3 and MNU [39] and the second one is TILLMore, a sodium azide-mutagenized population of cv. Morex with 4906 M_3 families [40]. Another important population to mention was created by mutagenizing

the cultivar Golden Promise which turns out to be the reference variety for genetic transformation [41].

In recent years, numerous genes involved in the development and morphology of the plant have been identified using a forward genetic approach, starting from the analysis of mutagenized population [42][43][44][45][46]. Among the reverse genetic approach, TILLING, Targeting Induced Local Lesions In Genomes [47], has taken hold as a powerful method in gene validation studies. TILLING produced allelic series are useful in cases where the knock-out is lethal or where new protein functions are to be characterized. The gene of interest is amplified in a DNA pool which forms heteroduplex containing allelic mismatches that undergo enzymatic cleavage. The cleaved strands are detected on polyacrylamide gels and sequenced to confirm the allelic difference [48]. Thanks to the advance of NGS (Next Generation sequencing) and the availability of updated versions of genomes, the use of this strategy in combination with exome capture is increasingly used to study multiple genes simultaneously [41][49]. An important aspect to take into consideration is that mutagenized plants are not considered Genetically Modified (GM) and therefore can be used in the field trials of countries where GM organisms are forbidden.

1.5 - Photosynthesis and photosynthesis regulation

Plants, together with other photosynthetic organisms, carry out the most essential and important biochemical process on Earth: photosynthesis, fixing atmospheric carbon into sugars (dark reactions, also called Calvin-Benson-Bassham cycle) by means of the energy supplied by light radiation (light reactions, generating reducing power in form of NADPH and ATP). This process takes place in a subcellular compartment called chloroplast (**Figure 4**).

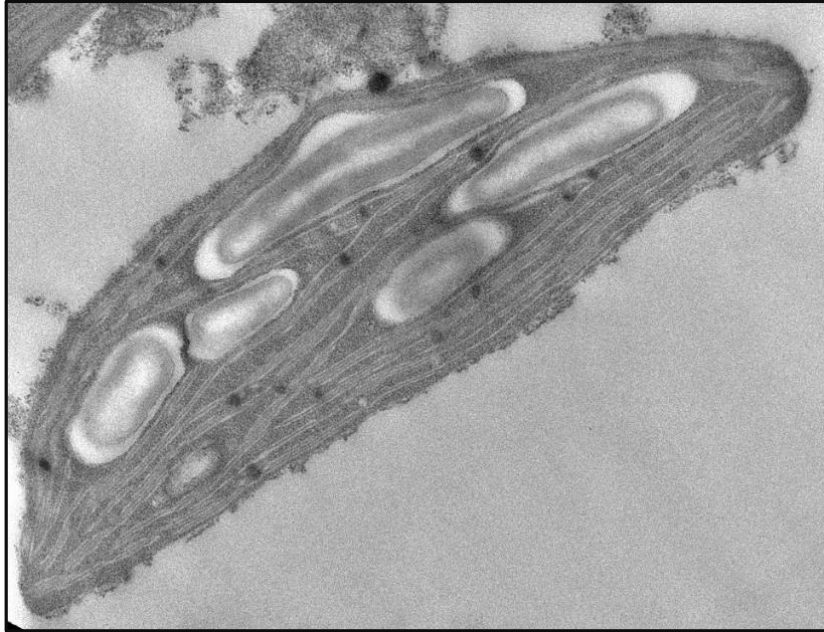


Figure 4 – Chloroplast structure (TEM image).

With the help of chlorophylls and other pigments the photosynthetic apparatus converts photons into chemical energy. Inside the chloroplast the thylakoid membranes are immersed in the stroma containing soluble enzymes responsible for the metabolism of carbon whose products are exported out of the chloroplast and distributed in all the cells of the plant [50].

The conversion of light energy into chemical free energy in the form of ATP and NADPH are due to the main components of the ETC (Electron Transport Chain) (**Figure 5**) as photosystem II (PSII), photosystem I (PSI), cytochrome b_6f (cyt b_6f), several electron carriers as plastoquinone and plastocyanin and the ATPase complex.

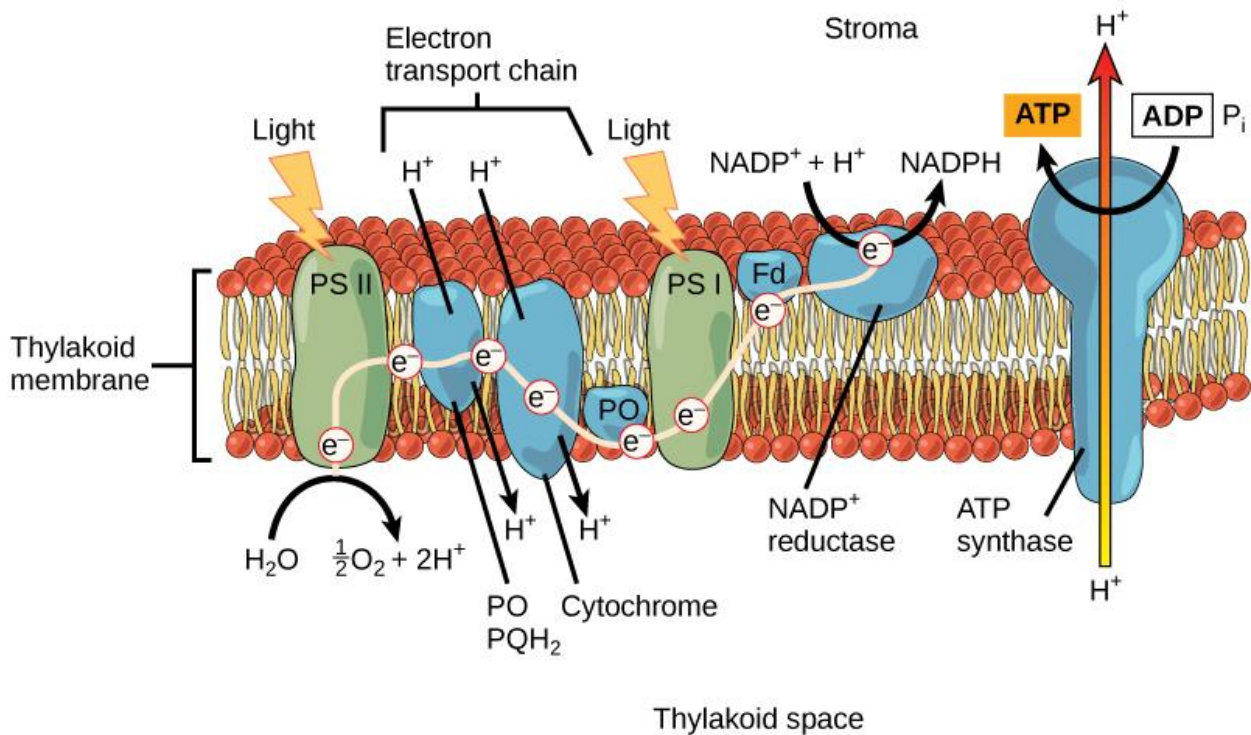


Figure 5 – Schematic overview of the major components involved in the light reaction (From <https://courses.lumenlearning.com>)

The antenna complexes, also called Light Harvesting Complexes (LhcAs associated to PSII and LhcBs related to PSI), are multimeric protein complexes containing chlorophyll pigments, especially the type b and other accessory pigments, as the carotenoids. The LHCs, responsible for increasing the harvesting of light, surround the reaction centres. The absorption peak of the PSI reaction centre is 700 nm, while for the PSII is 680 nm. The combination of the reaction centres and the antenna complexes form the multi-subunit protein complexes called photosystems I (PSI) and II (PSII). When the plant is hit by light, the PSII absorbs light through the LhcBs by exciting the reaction centre formed by a pigment dimer that is oxidised, triggering the flow of electrons throughout the ETC. As soon as the PSII is oxidised, its positive charge attracts electrons from OEC (Oxygen Evolving Complex), which splits the H₂O molecules into molecular oxygen (O₂), 4 protons (H⁺) and 4 electrons (e⁻). In the next steps intermediates carriers transfer electrons to the plastoquinones pool, the cytochrome b₆f, plastocyanin and finally they arrive at the PSI Fe-S proteins and

ferredoxin. When a NADP^+ molecule is present in the stroma, ferredoxin transfer electrons to NADP^+ , forming NADPH.

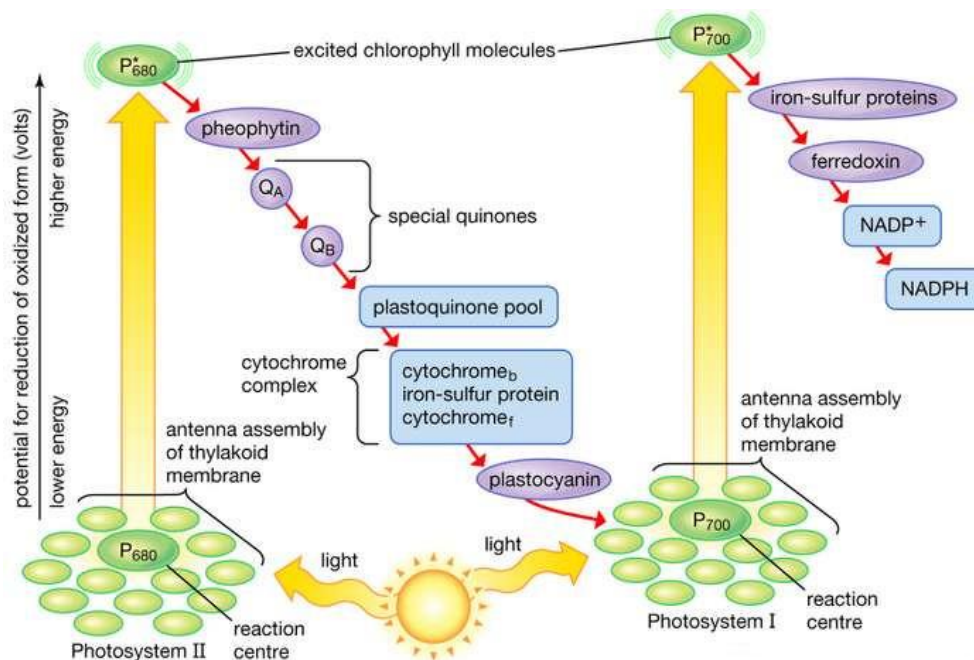


Figure 6 - Flow of electrons during the light reaction stage of photosynthesis, known as Z-scheme. Arrows pointing upward represent light reactions that increase the chemical potential, and arrows slanting downward represent the flow of electrons via carriers in the membrane (from Encyclopædia Britannica)

The flow of electrons through the two PSs and the intermediate carriers from the water to the ferredoxin is named linear electron flow (**Figure 6**), while the one that returns from the ferredoxin to the intermediate carries cyclic electron flow. The water splitting, together with the plastoquinone cycle, cause an increase proton (H^+) concentration in the lumen, producing a trans-thylakoid electrochemical gradient, known as the proton motive force (pmf) that allow ATP synthase to convert ADP and inorganic phosphate (P_i) to ATP and water. In the second phase of photosynthesis, called dark phase or Calvin-Benson-Bassham cycle (**Figure 7**), three CO_2 molecules are transformed into a glyceraldehyde-3-phosphate molecule, consisting of three carbon atoms. For each molecule of carbon dioxide fixed, two molecules of NADPH and three molecules of

ATP are needed. A molecule of five-carbon ribulose 1,5-bisphosphate (RuBP) reacts with a molecule of CO₂ thanks to the activity of nature's most abundant enzyme, Rubisco. The product of this reaction is split in two molecules of 3-phosphoglycerate (3-PGA). 1,3-bisphosphoglycerate (DPGA) and ADP are obtained from the phosphorylation of 3-PGA with ATP by the activity of phosphoglycerate kinase. Glyceraldehyde-3-phosphate dehydrogenase reduces DPGA with NADPH to give a three-carbon compound, the glyceraldehyde 3-phosphate (Gal3P) that can be transported out of the chloroplast or converted into starch. An alternative fate of Gal3P is to regenerate RuBP molecules, with a series of enzymatic reactions, that close the cycle.

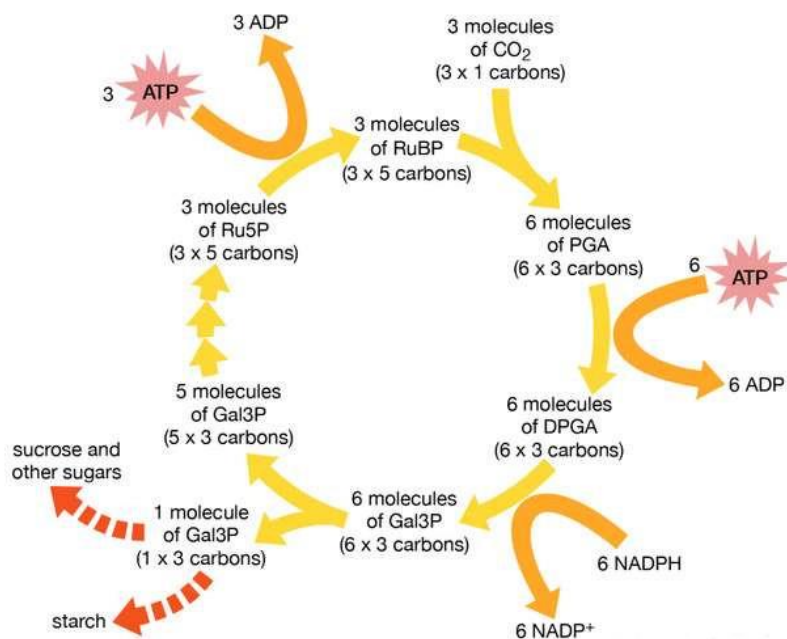


Figure 7 – Schematic representation of the dark phase of the photosynthesis (Calvin-Benson-Bassham) (from Encyclopædia Britannica)

1.6 - Engineering the photosynthetic process to improve the biomass production

For the next years, improving photosynthesis will prove to be strategic for creating plants that are more productive and more resistant to climatic adversities [51]. It must

be remembered that during the enormous agricultural improvements brought by the "Green Revolution", little or nothing was done about manipulating the photosynthetic mechanism. Photosynthesis therefore remains an unexplored field with respect to the genetic improvement of cereals. The theoretical maximum efficiency of the conversion of solar energy into biomass in a C3 plant, as barley, is estimated to be around 4,6%, decreasing to 2,4% under field conditions leaving a large margin of loss to be recovered. Among the different targets within the photosynthetic process that can be manipulated there are: the optimization of the antennas size in crop canopies (see below **chapter 1.6.1**), with an efficiency gain of 20-50% [31][52][30] and the fine tuning of the NPQ (Non-Photochemical Quenching) (see below **chapter 1.6.2**) [53] with an efficiency gain of 30%. One of the major problems responsible of the low yield of the conversion of light energy is due to the light saturation of the photosynthetic machinery, as the best yield efficiency is obtained at low light intensities. In C3 plants, indeed, the 25% of the maximum sunlight is able to saturate the photosynthetic machinery [54].

1.6.1. Optimization of the antenna size

Antenna polypeptides in green algae and plants are all members of a nuclear-encoded multigenic family of proteins called LHCs (Light Harvesting Complexes) [55], that surround the core of pigment–protein complexes, photosystems I and II (PSI and PSII). The antenna system of PSI (LHCI) comprises four major proteins, Lhca1-4, arranged in a half-moon structure adjacent to the PsaF/PsaJ subunits of the PSI core [56]. The LHCs associated with PSII are the monomeric antennae Lhcb4, Lhcb5 and Lhcb6 and the trimeric light-harvesting complex II (LHCII), composed of Lhcb1, Lhcb2 and Lhcb3 [55].

In nature, shading caused by neighbouring plants has led to the selection of large antennae at the top of the canopy for the competition of light [57][18], thus in a cultivated monoculture field this would result in a disadvantage, with saturated antenna

complexes in the upper part of the canopy and not enough light in the bottom leaves. On the contrary, the selection of small antennas in the upper part of the canopy would lead to major advantages, including the saving of metabolic resources for the production of antennas and activation of photo-protection mechanisms and at the same time would allow a better, uniform penetration of irradiance in the canopy, decreasing the loss of absorbed energy into heat and fluorescence [50][18][20] (**Figure 8**).

The reduction of the antenna complexes in the upper part of the canopy would lead to a better functioning of the light absorption and a greater portion of absorbed photons could be converted into biomass [19].

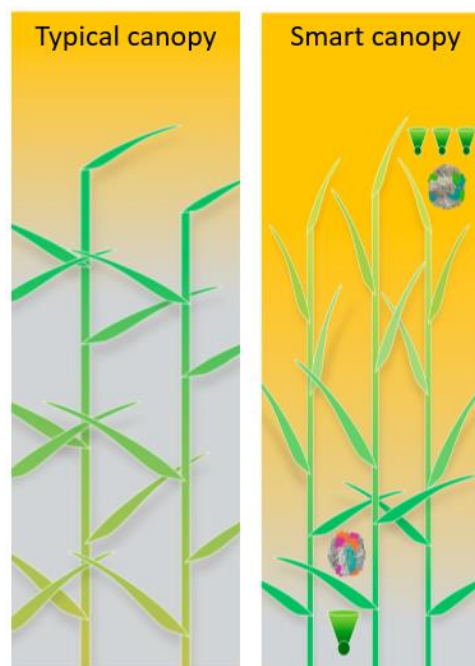


Figure 8 - In a typical canopy (left), most light is absorbed by the upper leaves, which are dark green and often tend toward being horizontal. A smart canopy (right) would have paler leaves at the top of the canopy, with a reduced leaf angle, and dark green horizontal leaves at the base (adapted from [19]).

Several studies have shown how reducing the size of the antennae can improve photosynthetic performance. A 50% increase in photosynthetic yield was observed in

an engineered strain of *Chlamydomonas reinhardtii* with a reduced size of antenna complexes [58]. A common photosynthetic organism with a reduction of 33% of antenna could shift the light-response curve for photosynthesis, so that photosystems would be saturated at higher intensities avoiding photo-damage [50].

1.6.1.1 The importance of pale phenotype

In this scenario, the pale phenotype, with reduced antenna complexes and chlorophyll content, could be a good solution to diminish the loss of absorbed energy and improve solar radiation conversion. Several works demonstrated that mutants lacking chlorophylls have similar or higher leaf photosynthetic efficiency compared with “green” varieties of the same species [59][60][31][61][62][63].

In high light and high temperature environments a pale-green phenotype could be evolutionarily advantageous [64][60], attenuating the damaging effects of high radiation and high leaf temperature as it can be observed in wild grasses and cereal landraces adapted to semi-arid environments [60][65][66]. In *Nicotiana tabacum*, pale green mutants with decreased antenna size, show an increase of about 25% in plant biomass accumulation under high-density cultivation [31]. The same trend was observed in rice plant with pale leaves under high light conditions [60].

A new frontier of bio-geo-engineering (**Figure 9**) would be to introduce the pale phenotype into crops around the world. This would have the effect of increasing the reflectance of solar radiation and therefore increasing the albedo of the cultivated area [59][67], finally mitigating the global increase in temperature.

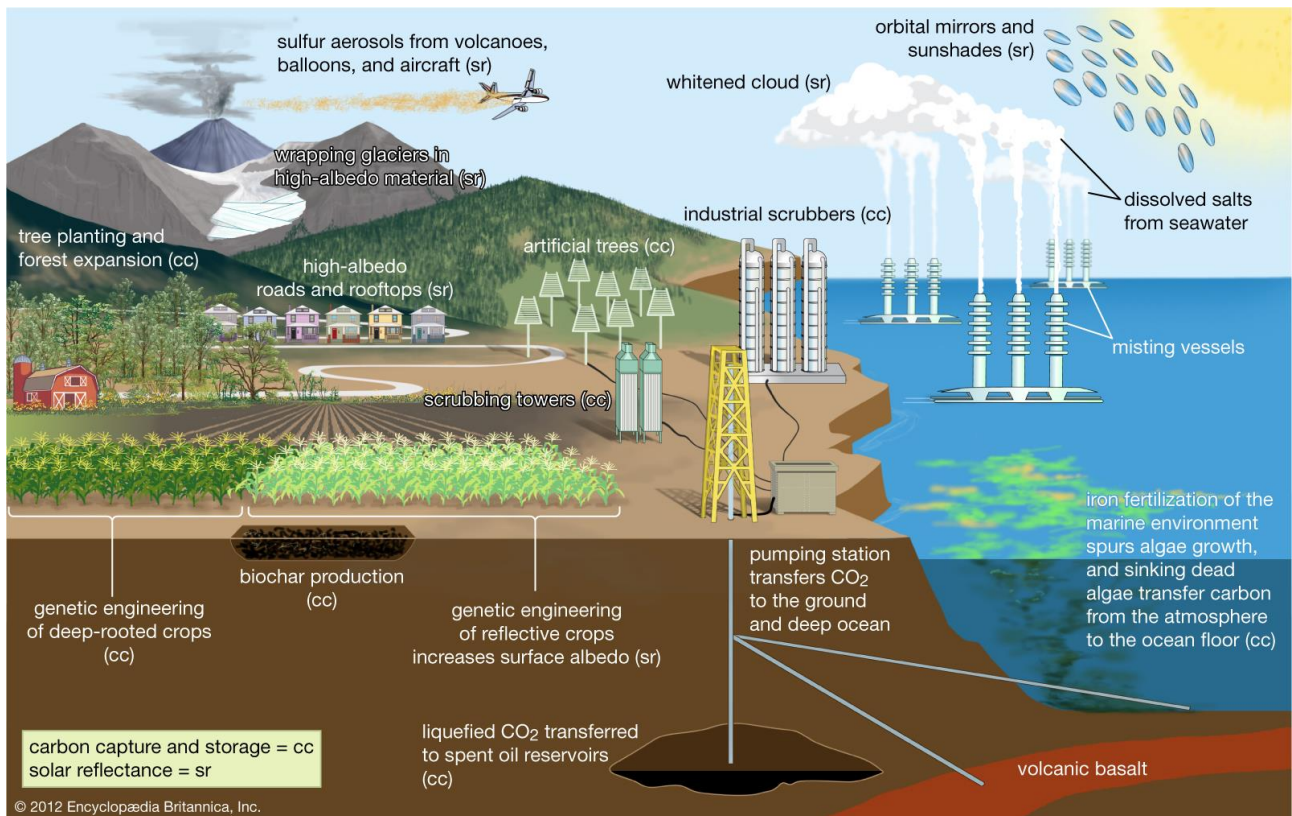


Figure 9 – Bio-geo-engineering possible strategies to counteract the global warming (from Encyclopædia Britannica)

Albedo is the measure of solar radiation that is reflected by a surface and returns to space. It is a value between 0 (which corresponds to a black body, therefore a surface not able to reflect), and 1 (a hypothetical white body able to reflect all the solar radiation). The light not reflected is absorbed by the atmosphere and by the surface and provides the energy input for driving the motions of atmosphere and oceans, maintaining the climate, and making the earth habitable [68]. The albedo can be defined as the ratio between the reflected solar radiation over the incoming solar radiation [69]. Usually, fresh snow has an albedo of about 0.9, while fresh asphalt can reach 0.04. The albedo is an essential component of the climate, its variation can lead to local meteorological changes up to climate changes on a global scale. The more solar radiation is absorbed, the higher the ground level temperature, when less energy is reflected, then there will be a warming effect. In this context, pale croplands could be a solution to counteract climate change by reflecting a greater amount of solar radiation

and therefore decreasing the temperature near the canopy and on a large scale also affect the global climate [70][67][71]. Experiments conducted on a pale soybean mutant have shown that the canopy of the latter reflects a significantly higher fraction (about 14% more) than the green control in the second half of July 2016, with a marginal decrease in surface canopy temperature [59].

1.6.2 - Improving the adaptation to fluctuating light: dissipation of excess energy through Non-Photochemical Quenching (NPQ)

A plethora of short-term photo-protective mechanisms are in place to regulate the flow of electrons in the ETC in response to fluctuating light as reviewed by [72]:

- “State Transitions,” i.e. optimization of light absorption between PSI and PSII achieved upon phosphorylation of the ‘mobile pool’ of LHCII that can move between PSI and PSII [73][74]. During State Transitions (**Figure 10**), the binding of PQH₂ to the Q_o site of the cytochrome works as a signal to activate the STN7 kinase to phosphorylate the LHCII, promoting its migration to PSI, thus increasing the light harvesting capacity of PSI (State I-to-State II transition). LHCII is dephosphorylated by the TAP38/PPH1 phosphatase, upon increased oxidation of PQH₂, promoting the migration of LHCII back to PSII, thus balancing the redox state of the PQ pool [73][75][76][77][78][79].

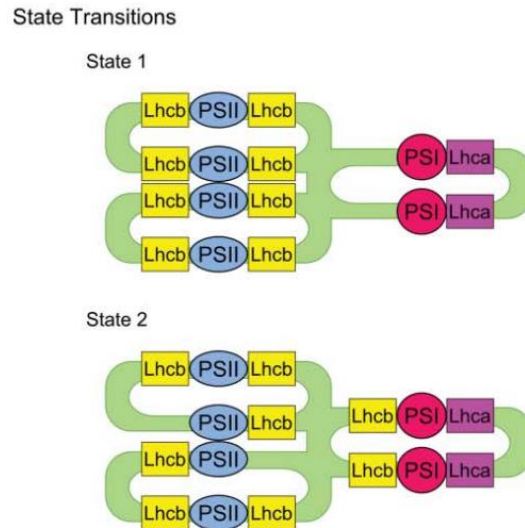


Figure 10 – Redistribution of Lhcbs between PSII and PSI, during state transitions. State 1, LHCII remain attached to PSII; State 2, the mobile pool of LHCII migrates to PSI (from [72]).

- “Alternative Electron Transport Routes,” i.e., redistribution of electron fluxes through different alternative pathways, including Cyclic Electron Transport (CET) mediated by either the NADH dehydrogenase-like (NDH) complex or the PRG5-PGRL1 protein complex [80][81][82]. PGR5 (Proton Gradient Regulation 5) together with PGRL1 (PGR5-like photosynthetic phenotype 1) form the protein complex that mediates cyclic electron transport around PSI, accepting electrons from ferredoxin (Fd) and reducing the PQ pool, thus acting as an Fd-PQ reductase (FQR).

- “Photosynthesis Control,” i.e., regulation of electron transport by the Cyt b_6f complex, modifying the pH of thylakoid lumen and stroma [83][84][85][86]. Thylakoid lumen acidification is essential for preserving energy balance during photosynthesis. Cyclic electron flow around PSI is activated to diminished lumen pH, when the leaf is under a stress situation [87]. In particular, lumen acidification reduces Cyt b_6f activity, thus decreasing the rate of electron transfer [88].

- “Non Photochemical Quenching (NPQ),” i.e. pH-dependent dissipation of excess energy in form of heat, in the LHCII to protect the photosynthetic apparatus against photo-oxidation [89][90][91].

Non-Photochemical Quenching (NPQ) is the most important photoprotective system in higher plants and involves several mechanisms based on the time scale of relaxation kinetics after pre-illumination via chlorophyll fluorescence quenching [92][93]. The qI (slow phase), which occurs on a timescale of hours, is a photo-inhibitory process in which PSII core components act as quenchers. The qT component (state transition), in which part of LHCII moves to the PSI complex, is detectable within 30 min. The qZ, which is detectable in 10–15 min, contributes to the thermal dissipation of violaxanthin to antheraxanthin and zeaxanthin via de-epoxidation (xanthophyll cycle). The qE, that occurs within seconds, relies on thylakoid lumen acidification-dependent energy dissipation within LHCII.

Therefore, the second trait that can be manipulated to increase photosynthetic efficiency and therefore biomass production is through the tuning of the NPQ (Non-Photochemical Quenching) mechanism. Engineering this trait would allow the plants to better adapt to fluctuating light intensity, as it happens under field conditions. This photo-protection mechanism allows the dissipation of the excess energy absorbed in the form of heat, avoiding oxidative damage. When the light is too intense, the excess of e^- absorbed could react with the available O_2 , creating ROS (Reactive Oxygen Species) as *O_2 (singlet oxygen), H_2O_2 (hydrogen peroxide) and OH^- (hydroxide ions). The high reactivity of ROS can cause damage to different components of the photosynthetic apparatus, such as reaction centres and membrane proteins and lipids [94], leading the chloroplast to bleaching.

The activation and relaxation of this mechanism takes from seconds to minutes, making it much slower than the changes in light intensity that occurs in the canopy. This results in a loss of photosynthetic efficiency since the dissipation of energy in the form of heat continues even when light does not exceed the photosynthetic capacity [95]. Over-expression of genes involved in NPQ in tobacco shows about 20% increase in biomass accumulation under both greenhouse and field conditions [53], while in rice leads to improve canopy radiation use efficiency and grain yield under fluctuating light [96].

Other studies have been able to support the notion that the manipulation of the photoprotective mechanism is useful to enhance crop productivity [96][97][98][53].

1.6.2.1 - The xanthophyll cycle

The dissipation of the excess energy in the form of heat by the carotenoids, through the xanthophyll cycle (**Figure 11**) is one of the most relevant photo-protection mechanisms [99] that is found in higher plants, green algae, mosses and diatoms and a similar mechanism exists also in the red algae and Cyanobacteria [100]. In high light condition, the lumen pH begins to acidify (pH around 5.2) due to the increasing quantity of protons that accumulate in the lumen upon ETC activation. In this situation, VDE (Violaxanthin De-Epoxidase), that is in the inactivated form in the lumen, is activated by interacting with the thylakoid membranes and catalyzes the conversion of violaxanthin pigment into the intermediate antheraxanthin and into the zeaxanthin, by removing two epoxy groups. The binding of this enzyme to the thylakoid membrane occurs most likely through the charged C-terminal domain of the enzyme, principally due to the presence of histidine residues [101]. Different protonation of specific residues contributes to regulate the binding of VDE to the thylakoid membrane and influences the stability of the active homodimer [101]. When the light intensity decreases the opposite reaction is catalyzed by another enzyme, ZEP (Zeaxanthin EPoxidase), which is located in the stroma at optimum pH of 7.5 and reacts about 5 to 10 times slower compared to VDE. In the lipid membrane the zeaxanthin acts as an antioxidant and a membrane dynamics regulator, making the membrane more rigid, while the violaxanthin make it more fluid [102].

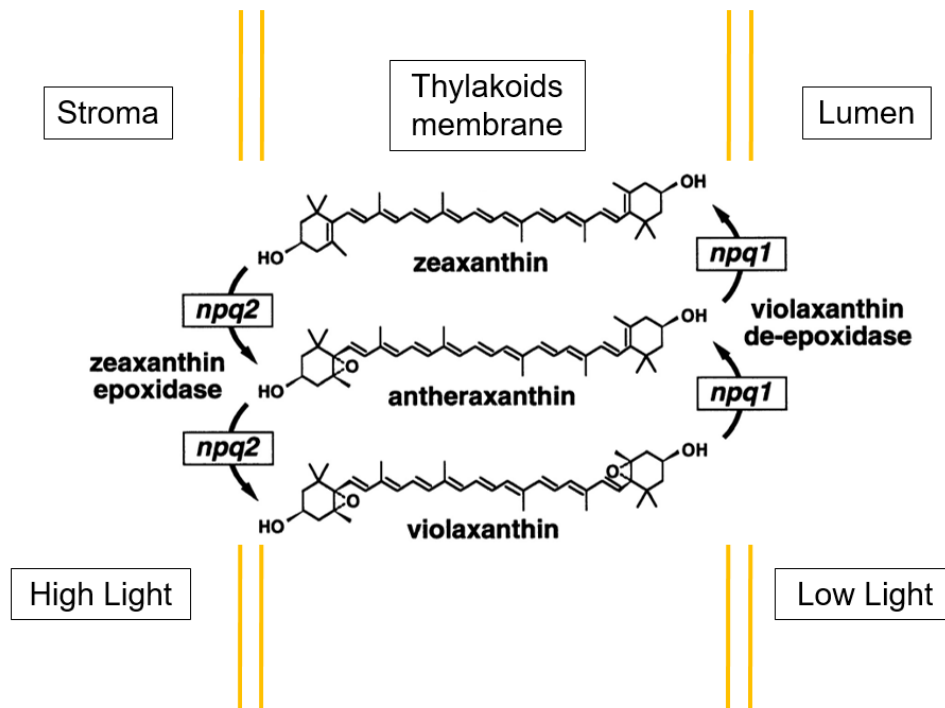


Figure 11 – In the xanthophyll cycle, two enzyme VDE and ZEP convert the violaxanthin into zeaxanthin and viceversa (Adapted from [103]).

Another fundamental protein, named PsbS (PSII subunit 22kDa protein) participates in the regulation of this process. PsbS sits between the PSII core and most peripherals LHCII. As soon as the pH of the lumen falls (**Figure 12**), PsbS binds to zeaxanthin allowing the pigment to de-excite the chlorophylls through energy transfer, allowing NPQ, i.e. dissipation as heat of the excess of absorbed energy [104].

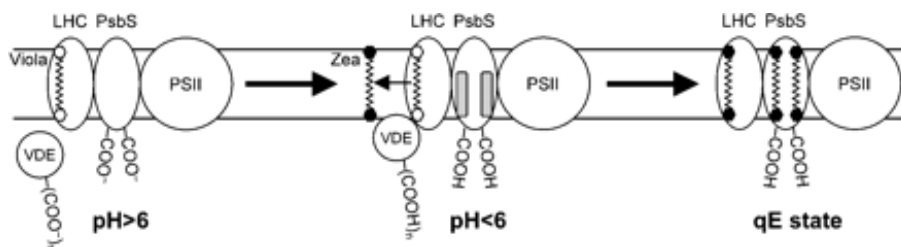


Figure 12 – The conversion of violaxanthin into zeaxanthin mediated by PsbS protein, releases the excess of energy absorbed as heat (From [104]).

Therefore, manipulating the kinetics of NPQ to minimize the waste of energy, which on the contrary could be used for carbon fixation, appears to be an important trait to increase plant yield and production [53] . In the evergreen oak (*Quercus coccifera*) photo-inhibition was observed to lead to a daily loss of 7.5-8.5% of the potential carbon gain in the upper part of the canopy and a loss of 3% in the lower part [105].

As show in the (**Figure 13**) in a common situation when a plant is subjected to high light some delay in NPQ activation may be observed, causing a loss of energy.

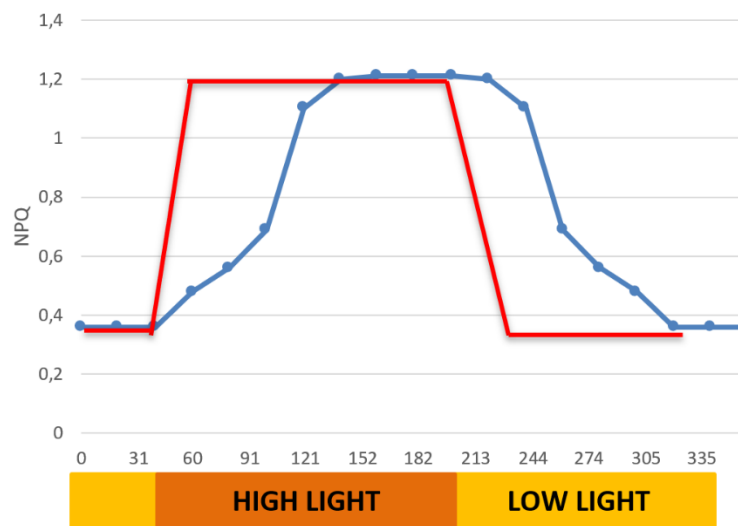


Figure 13 – Schematic representation of the NPQ kinetics in high light e low light condition between an ideal plant (in red) and a normal plant (in blue). The faster NPQ kinetic of an ideal plant (in red) compared to a normal plant (in blue) could improve the photosynthetic efficiency of a plant.

On the other hand, the kinetics of an ideal plant are shown in red where NPQ is activated and switched off very rapidly, allowing this mechanism to protect from photo-damage the chloroplasts during the entire period of exposure to high light and to be completely inactive in low light.

2 - Aims of the project

The generation of a dual-purpose barley variety (*Hordeum vulgare*), with an improved biomass production, without penalty on grain yield, was the aim of the European BarPlus project, of which my Ph.D. work was part. The goal of my thesis was to isolate new genes, alleles and barley plant lines with improved photosynthetic performance and modified photosynthesis regulation.

To this aim we focused the attention on barley mutants with i) reduced light capture antenna system and ii) heterogeneous kinetics of the photo-protection process NPQ (Non-Photochemical Quenching).

The mutant *hus1* was isolated within the chemically mutagenized barley population HorTILLUS, as pale-green mutant with improved photosynthetic yield, and reduced photosystem antenna size.

The goals of this first part of the project are:

- The identification of the causative mutation responsible for *hus1* phenotype;
- The characterization of *hus1* at the phenotypic, physiological and biochemical level;
- The validation of the causal relationship between the candidate mutated gene and the *hus1* phenotype by:
 1. similarity with other plant species, as *Arabidopsis thaliana*, and by introduction of *HUS1* wild-type and mutated alleles in *Arabidopsis* mutants for complementation tests;
 2. the isolation of a second allele of *hus1* within the natural genetic available in the Whealbi collection, examining the natural diversity in this locus;
 3. the isolation of a second allele of *hus1* in the chemically mutagenized population TILLMore;

As the second part of the project, we aim to characterize allelic variants of the *VDE* (Violaxanthin De-Epoxidase) and *ZEP* (Zeaxanthin Epoxidase) genes both of them encoding enzymes involved in the xanthophyll cycle, previously isolated from the HorTILLUS population, in order to explore whether variations in NPQ kinetics have impact on the plant physiology.

The goals of this second part are:

- The characterization, at physiological and biochemical level, of plant lines carrying polymorphisms in the *VDE* genes, by studying the NPQ process and the xanthophyll cycle;
- The introgression and characterization of the 5 allelic variants of barley *VDE* with the knock-out mutant of *Arabidopsis thaliana npq1-2* [103] with abolished NPQ;
- The preliminary characterization of the only *ZEP* allelic variant.

The investigation of these lines and traits, such as the altered size and composition of the photosystem antenna complexes, suitable for light absorption optimization, and the heterogeneous kinetics of the NPQ, suitable for photo-protection optimization, might be valuable traits for breeding programs, not only for barley but also for other cultivated species. The selection of these traits could lead to cultivars that are more resistant and resilient to environmental changes, and more suitable for agriculture practices.

3 - Materials and methods

3.1- *In silico* analysis

Nucleic acid and amino acid sequences were obtained from Ensembl Plants database (www.plants.ensembl.org/Hordeum_vulgare/Info/Index), Phytozome (www.phytozome.jgi.doe.gov/pz/portal.html), Barlex (<https://apex.ipk-gatersleben.de/apex/f?p=284:10>), NCBI (National Center for Biotechnology Information, www.ncbi.nlm.nih.gov), TAIR (The Arabidopsis Information Research, www.arabidopsis.org), and UniProt (www.uniprot.org/). Homologous gene sequences were searched with BLAST (Basic Local Alignment Search Tool, <https://blast.ncbi.nlm.nih.gov/Blast.cgi>), IPK Barley Blast Server (https://webblast.ipk-gatersleben.de/barley_ibsc/) and Clustal Omega (www.ebi.ac.uk/Tools/msa/clustalo/). Sequence analysis and editing were performed on SnapGene Viewer (www.snapgene.com) and GeneRunner (www.generunner.net). Sub-cellular localization and chloroplast transit peptide prediction were performed by consulting the TargetP database (www.cbs.dtu.dk/services/TargetP). Plasmid sequences were obtained from AddGene database (<https://www.addgene.org/>). Phylogenetic analyses were conducted using MEGA version X (www.megasoftware.net/). Exome capture data analysis was performed according [106].

3.2 - Plant lines and growth conditions of *Hordeum vulgare*

Barley plants (*Hordeum vulgare*) were cultivated on acid soil (Vigor plant growing medium, Irish and Baltic peats based, pH 6.0) in greenhouse-controlled conditions at long-day photoperiod, 16 hours of light ($250 \mu\text{mol photons m}^{-2} \text{s}^{-1}$) and 8 hours of dark. Temperatures were set at 20°C during the day and 16°C at night, with Relative Humidity set at 30%. Spring cultivars required to be incubated at 37°C for 7 days

before sowing to break dormancy and induce germination. Before sowing, the seeds were treated with Redigo fungicide (Bayer) and Osmocote fertilizer was added to the soil. The barley lines of interest were selected among the HorTILLUS population [39], the WHEALBI collection (WHEAT and Barley Legacy for Breeding Improvement, <http://www.whealbi.eu/>) and the TILLMore population [40]. ‘Morex’ and ‘Sebastian’ cultivars were used as controls. Other *HvCHAOS* alleles were searched in the TILLMore population, using a forward genetic approach while the WHEALBI collection was screened using a reverse genetic strategy. A subset of 24 lines from TILLMore and a subset of 26 WHEALBI accessions were taken into consideration for *HvCHAOS* analysis.

3.3 - *Arabidopsis thaliana* lines and growth conditions

Arabidopsis thaliana Columbia (Col-0) ecotype wild-type and mutants (**Table 1**) plants were grown on soil in growth chambers under long day conditions, photoperiod set as 16 hours light (150 μ E), 8 hours dark, with growing temperature set at 22°C. Dry seeds were stored at 4°C before sowing. Seeds were soaked at 4°C on wet paper for two days for stratification, in order to induce synchronized germination.

Gene	Allele	AGI Code	Reference	Mutation type
<i>CAO</i>	<i>chaos</i>	At2g47450	[107]	<i>En</i> transposon
<i>NPQ1</i>	<i>npq1-2</i>	At1g08550	[103]	Unknown - Possible deletion or gene rearrangement (Fast neutron bombardment)

Table 1 – List of *Arabidopsis* mutants and related genes analysed in this thesis.

3.4 - Crossing of selected barley plants

For successful crossing, timing is a crucial factor and sowings need to be tightly scheduled. The emasculation of the female parent was performed when the awns were begun to emerge from the flag leaf auricles, at this stage the pistil should be at 2-4 days before the anthesis, this would prevent self-pollination. The spike was unwrapped from the flag leaf sheath and the awns were trimmed off using a little and sharp scissors. The tip of spikelets was cut, the palea and lemma were slightly opened with a tweezer and the three green not mature anthers were removed. If the spikelets were ready for the emasculation, the anther tips should be circa half way up the lemma. After 2-4 days from emasculation, the stigma was ready for pollination. The pollen was taken from other ready spikelet opening the flowers and using a tweezer the pollen was spread gently on the stigma of the emasculated spikelet. After emasculation and pollination the spikes were always covered with a paper bag. If the spikelets were successfully pollinated, the developing caryopses were begun visible around 5 days after pollination.

3.5 - Genomic DNA extraction

For genotyping purposes genomic DNA was extracted in 360 µl of DNA Extraction Buffer (250 mM Tris-HCl pH 7.5; 25 mM EDTA; 250 mM NaCl) by mechanical homogenization using Tissue lyser (Qiagen) (1 minute with a pulse frequency of 30 s⁻¹) and three steel beads. After homogenization, 40 µl of SDS 10% (w/v) were added to the sample and samples were centrifuged for 30 minutes at 13000 g. The supernatant was transferred into a new tube containing 320 µl of isopropanol (about 0.8 volumes of EB). After a centrifugation step of 15 minutes at 13000 g the supernatant was discarded. The pellet was washed with 300 µl of 70% EtOH, resuspended in 50 µl RNase A solution (10 µg/ml in bi-distilled water) and incubated at 37°C for 30 minutes, to remove RNA.

For exome capture analyses, barley leaf material was collected from 50 plants displaying a wild-type-like phenotype and 50 plants displaying a clear chlorotic phenotype. The 50 samples per each phenotype were pooled and grinded with liquid nitrogen and 700 µl Extraction Buffer (0.1 M Tris-HCl pH 7.5, 0.05 M EDTA pH 8.0, 1.25% SDS, 1 µl of RNase A (10 mg/ml; w/v)) (preheated to 65°C) was added and incubated 40 minutes at 65°C. Samples were incubated for 15 minutes at 4°C before adding 350 µl 6M ammonium acetate and incubated for 15 more minutes at 4°C. The samples were centrifuged for 20 minutes at 18000 g at 4°C. 800 µl of supernatant was collected per each sample, 600 µl of isopropanol was added and was left at room temperature for 10 minutes. The sample were centrifuged for 20 minutes at 18000 g at 4°C. The pellet was washed twice with 500 µl of EtOH 70% and resuspended in 60 µl of 10 Mm Tris-HCl, pH 8.0 at 4°C overnight.

3.6 - Genotyping procedures

For barley genotyping, 1 µl of DNA was used as a template for a standard PCR analysis, in a total volume of 20 µl containing 4 µl of 5x GoTaq-Green Buffer (Promega), 0.5 µl of 2.5 mM dNTPs, 0.5 µl of 10 mM primers and 0.05 µl of GoTaq polymerase (Promega) per sample. The PCR products were diluted to 100 µl with bi-deionized water and precipitated adding 300 µl of 100% EtOH and 10 µl of 3M sodium acetate pH 5.2. After 20 minutes at -20° C, the sample was centrifuged for 20 minutes at 4° C at 13000 g. The pellet was washed with 70% EtOH and was resuspended in 15 µl of bi-deionized water. Samples were then sent for Sanger sequencing. The primers used for barley genotyping were listed in **Table 2**.

Primer ID	Sequence (5' → 3')	Description	Gene
HV_001	CAGATTTTACCGGCAAG TGG	Fw primer of <i>HvVDE</i>	<i>HORVU.MOREX.r2.2H</i> <i>G0133130.1</i> (<i>HORVU2Hr1G068610</i> .2)
HV_002	CCAAGTTCAGCTGATCC AAG	Rev primer of <i>HvVDE</i>	<i>HORVU.MOREX.r2.2H</i> <i>G0133130.1</i> (<i>HORVU2Hr1G068610</i> .2)
HV_007	GACGAGACTGAATGCCA GAT	Fw primer of <i>HvVDE</i>	<i>HORVU.MOREX.r2.2H</i> <i>G0133130.1</i> (<i>HORVU2Hr1G068610</i> .2)
HV_012	GGGGACAAGTTTGTAC AAAAAAGCAGGCTATG GAGGCCGTCCTGCGAC	Fw primer with <i>attB1</i> site and complementary to the 5' of <i>HvCHAOS</i>	<i>HORVU.MOREX.r2.4H</i> <i>G0341350.1</i>
HV_013	GGGGACCACTTTGTAC AAGAAAGCTGGGTTC CCCTGCAAATGTCTCCG CC	Rev primer with <i>attB2</i> site and complementary to the 3' of <i>HvCHAOS</i>	<i>HORVU.MOREX.r2.4H</i> <i>G0341350.1</i>
HV_014	AGGTGGAGAAGGTGGTG GAC	Fw primer of <i>HvCHAOS</i>	<i>HORVU.MOREX.r2.4H</i> <i>G0341350.1</i>
HV_047	GGTGGTACCGATCCTGA GAA	Fw primer of <i>HvZEP</i>	<i>HORVU.MOREX.r2.2H</i> <i>G0142080</i>
HV_054	TACCGACAAAGGTCCCA GAC	Rev primer of <i>HvZEP</i>	<i>HORVU.MOREX.r2.2H</i> <i>G0142080</i>

Table 2 – List of primers used in *Hordeum vulgare* for genotyping.

For genotyping *Arabidopsis thaliana* mutants, the standard PCR was prepared using primers listed in **Table 3** and coupled in **Table 4**.

Primer ID	Sequence (5' → 3')	Description
Atp_7124	ATGCAAAAGGTCTTCTTGGC	Fw primer for <i>AtCHAOS</i>
Atp_7125	CCTCTCTCGTCTTCCACTTC	Rev primer for <i>AtCHAOS</i>
AtP_3341	GAGCGTCGGTCCCCACACTTCTAT AC	En-specific primer EnR
Atp_6898	CTGCAATAACCGTCCAGATG	Fw primer for <i>AtNPQ1-2</i>
Atp_6899	CATATCCATCCCAAGCATCG	Rev primer for <i>AtNPQ1-2</i>

Table 3 – List of primers designed to determine plant genotypes in *Arabidopsis thaliana*.

Allele	Type of mutant	WT-version	Mutated-version
<i>chaos</i>	En transposon	Atp_7124 - Atp_7125	Atp_3341 - Atp_7125
<i>npq1-2</i>	Fast neutron bombardment	Atp_6898 - Atp_6899	X

Table 4 – The primer combinations used for genotyping in *Arabidopsis thaliana*

3.7- Exome capture and sequencing

The paired-end exome capture libraries for Illumina sequencing were prepared using KAPA High Throughput Library Preparation Kit, SeqCap Adapter Kit A with TrueSeq Index Adapters (Roche) and dedicated SeqCap EZ reagent Kits (Roche). The exome capture probes were synthesized according to the SeqCap EZ Developer probe pool design 120426_Barley_BEC_D04.EZ, as described by [108].

The purified DNA from each of F₂ pools was digested enzymatically by mixing 5 µl of KAPA Fragmentation Buffer (10x), 10 µl of KAPA Fragmentation Enzyme Mix and 700 ng of genomic DNA in a total volume of 50 µl. The mix was placed in precooled thermocycler and enzymatic digestion was performed at 37°C for 25 min. Such proportion of DNA and enzyme mix together with the 25 min of digestion reaction allowed to obtain the highest number of fragments with the average size between 250 and 350 bp. The digestion was followed by end repair reaction and was performed by adding to the digestion mixture 7 µl of KAPA End-repair/A-tailing Buffer and 3 µl of

KAPA End repair/A-tailing Enzyme Mix. Such mix was then placed again in precooled thermocycler and the end-repair reaction was performed at 65°C for 30 min. The index adapters were then ligated to the restriction fragments by adding 30 µl of Ligation Buffer, 10 µl of DNA ligase, 5 µl of PCR-grade water and 5 µl of an appropriate index adapter. Such mixture was incubated for 15 min at 20°C and then purified using AMPure beads (Beckman Coulter). The purified fragments were then suspended in 50 µl of 10 mM Tris-HCl (Sigma).

Next, the dual size selection of fragments was performed using AMPure Beads. In the first step 0.7 volume of AMPure beads was added to the libraries and after mixing and incubation at room temperature (RT) for 10 min, 80 µl of supernatant was transferred into a new tube. This allowed to recover fragments smaller than approximately 450 bp. In the second step 10 µl of AMPure beads were added to the supernatant, followed by careful mixing, incubation at RT for 10 min. and subsequent washes with 80% ethanol. After drying of beads they were re-suspended in 23 µl of 10 mM Tris-HCl and later 20 µl of supernatant was transferred into a new tube. This step allowed to recover fragments larger than approximately 250 bp.

In order to enrich the libraries, the pre-capture LM-PCR (ligation –mediated PCR) reaction was performed in a total volume of 50 µl. The reaction mix contained 20 µl of purified library after adapter ligation, 25 µl of 2x KAPA HiFi HotStart Ready Mix and 5 µl of 10 x Library Amplification Primer Mix. The PCR program was as follows: 98°C for 45 min, 4 cycles of 98°C for 15 s, 60°C for 30 s, 72°C for 30 s, then one cycle of 72°C for 1 min. In each step of the reaction the ramp of 2.5°C/s was used. The enriched libraries were then purified using AMPure beads and the DNA fragments were re-suspended in 50 µl of PCR-grade water. The size range of pre-capture LM-PCR library were examined using Agilent 2100 Bioanalyzer DNA 1000 Chip.

The preparatory step before the hybridization with exome capture probes was performed. The 1 µg of pre-capture LM-PCR library was mixed with 10 µl of SeqCap Developer Reagent (Roche), 1 µl of SeqCap HE Universal Oligo to block the universal

segment of library adapters during the hybridization and 10 µl of SeqCap HE Index Oligo to block the index segment of library adapter. Next, 2 volumes of AMPure beads were added to the above mixture and after 10 min of incubation at RT the supernatant was removed and the beads were washed with 80% of ethanol and aired dried. Later, the 7.5 µl of 2x Hybridization Buffer was mixed with 3 µl of Hybridization component A (SeqCap EZ Hybridization & Wash Kit, Roche) and 10.5 µl of this mixture was used to re-suspend the pre-capture LM-PCR library fragments immobilized in AMPure beads. Then, 10.5 µl of the library was combined with 4.5 µl of SeqCap EZ Probe Pool containing barley exome capture probes. After 5 min denaturation at 95°C, the hybridization with capture probes was performed at 47°C for about 18 hours.

The hybridization was followed by series of washes. In this step the 1x Stringent Wash Buffer, 1x Wash Buffer I, 1x Wash Buffer II and 1x Wash Buffer III, together with 1x Bead Wash Buffer (SeqCap EZ Hybridization & Wash Kit, Roche) were prepared. The Capture Beads (SeqCap EZ Pure Capture Bead Kit, Roche) were purified and re-suspended in 50 µl 1x Bead Wash Buffer. The Exome Capture libraries were then bind to Capture Beads and after 15 min of incubation at 47°C were subjected to post-hybridization washes in the following order: 1x Wash Buffer I (100 µl), double wash with 1 x Stringent Wash Buffer (200 µl), 1x Wash Buffer I (100 µl), 1x Wash Buffer II (100 µl) and 1x Wash Buffer III (100 µl). Washes with the Stringent Wash Buffer lasted for 5 min. and were performed at 47°C and the remaining ones lasted for 1 min at RT. After the last wash, the libraries were suspended in 15 µl of PCR-grade water.

The last step of the procedure included Post-Capture LM-PCR reaction. It was performed by mixing 25 µl of 2x KAPA HiFi HotStart Ready Mix, 5 µl of 5 µM Post-LM-PCR Oligos 1&2 (SeqCap EZ Accessory Kit v2, Roche) and 20 µl of Exome Capture libraries. The following program was used for the reaction: 98°C for 45 min, 14 cycles of 98°C for 15 s, 60°C for 30 s, 72°C for 30 s, one cycle of 72°C for 1 min. In each step of the reaction the ramp of 2.5°C/s was used. After Post-Capture LM-PCR the libraries were purified using AMPure beads and suspended in 50 µl of 10 mM Tris-HCl. The size range of exome capture fragments were analyzed using Agilent 2100

Bioanalyzer DNA 1000 Chip, the A260/A280 ratio (1.7–2.0) was analyzed on a NanoDrop1000 spectrophotometer and the quantity of the library was examined using qPCR with KAPA Library Quantification Kit (Roche) according to the manufacturer protocol.

The Post-Capture LM-PCR libraries were then subjected to paired-end sequencing on HiSeq4000 Illumina Instrument using HiSeq 3000/4000 PE Cluster Kit and HiSeq 3000/4000 SBS Kit (Illumina) according to the manufacturer protocol.

3.8 - RNA extraction from leaf material

For the RNA extraction, the leaf material was ground in liquid nitrogen using a pestle and mortar and 800 µl of RNA extraction buffer (100 mM Tris-HCl pH 7.5; 100 mM LiCl; 10 mM EDTA; 1% SDS) was added. 800 µl of acid phenol (pH 4) were added to the homogenized sample and mixed. The sample was incubated at 55°C for 5 minutes and then centrifuged at 13000 g for 10 minutes at 4°C in order to separate the two phases. The supernatant was collected and 800 µl chloroform:isoamyl alcohol (24:1) was added. The sample was then centrifuged at 13000 g for 10 minutes at 4°C. The supernatant was mixed with 800 µl of LiCl (8M) and incubated at 4°C overnight. The sample was centrifuged at 13000 g for 30 minutes at 4°C, the pellet was washed with EtOH 75% and resuspended in 50 µl of nuclease-free water. RNA concentration and purity were measured by NanoDrop (Thermo Fisher) and agarose gel run.

3.9 - DNase treatment and cDNA synthesis

For cDNA synthesis, the iScript™ gDNA Clear cDNA Synthesis Kit (Bio-Rad) was employed. 1 µg of total RNA was diluted to 14 µl of water. 2 µL of Master Mix DNase solution 5X (0.5 µL of iScript DNase and 1.5 µL of DNase Buffer) were added and

samples were incubated for 5 minutes at 25°C, to allow DNA digestion, followed by 5 minutes at 75°C for DNase inactivation. 4 µL of iScript Reverse Transcription Supermix were added to the DNase-treated RNA sample. The single strand cDNA was synthesized in the thermocycler, according to the following program: 5 minutes at 25°C (Priming), 20 minutes at 46°C (Reverse transcription), 1 minute at 95°C (RT inactivation). To test the presence of genomic DNA and assure the quality of cDNA sample, PCR analyses, using *ACT7* primers (**Table 6**), were performed.

3.10 - High fidelity PCR

For cloning purposes, coding sequences of the genes of interest were amplified from cv ‘Sebastian’ cDNA, *hus1*, *vde-a*, *vde-b*, *vde-g*, *vde-l*, *vde-h*, WB-146, WB-401, WB-418 with the Q5 High-Fidelity DNA Polymerase (New England BioLabs). Reactions were performed in a total volume of 30 µl each. The reaction contained 6 µl of 5X Q5 Reaction Buffer, 6 µl of 5X Q5 High GC Enhancer, 1 µl of 10 mM dNTPs, 1 µl of 10 µM of each primer and 0.8 µl of Q5 DNA Polymerase. The PCR-products were loaded on a 1% agarose gel and then cut from the gel and purified via the Macherey Nagel gel extraction kit following the producer’s instructions.

3.11 - Complementation experiments introducing *Hordeum vulgare* genes in *Arabidopsis thaliana*

The cloning of *HvCHAOS*, *Hvchaos*, *HvVDE*, *Hvvde-a*, *Hvvde-b*, *Hvvde-g*, *Hvvde-l*, *Hvvde-h* was performed in binary vectors using the GATEWAY™ reaction strategy (Invitrogen). The coding sequences (CDS) of these genes were amplified using High fidelity PCR, the cDNA as template and the following primers (**Table 5**):

Primer ID	Sequence (5' → 3')	Description	Gene
HV_005	GGGGACAAGTTTGTAC	Fw primer with <i>attB1</i>	<i>HORVU2Hr1G068610.2</i>
	AAAAAAGCAGGCTCAA ATGTTGTCGCGGCAGTG	site and complementary to the 5' of <i>HvVDE</i>	
HV_006	GGGGACCACTTTGTAC	Rev primer with <i>attB2</i>	<i>HORVU2Hr1G068610.2</i>
	AAGAAAGCTGGGTCTAT CTTAGCTTCCTTATCGG	site and complementary to the 3' of <i>HvVDE</i>	
HV_007	GACGAGACTGAATGCCA GAT	Fw primer of <i>HvVDE</i>	<i>HORVU2Hr1G068610.2</i>
HV_012	GGGGACAAGTTTGTAC	Fw primer with <i>attB1</i>	<i>HORVU.MOREX.r2.4H</i> <i>G0341350.1</i>
	AAAAAAGCAGGCTATGG AGGCCGTCCTGCGAC	site and complementary to the 5' of <i>HvCHAOS</i>	
HV_013	GGGGACCACTTTGTAC	Rev primer with <i>attB2</i>	<i>HORVU.MOREX.r2.4H</i> <i>G0341350.1</i>
	AAGAAAGCTGGGTTCAC CCTGCAAATGTCTCCGCC	site and complementary to the 3' of <i>HvCHAOS</i>	
HV_014	AGGTGGAGAAGGTGGTG GAC	Fw primer of <i>HvCHAOS</i>	<i>HORVU.MOREX.r2.4H</i> <i>G0341350.1</i>

Table 5 – List of primers designed to clone genes of interest.

The BP reaction (Invitrogen GATEWAY™) was performed according to the instruction. The Donor vectors used in this work were the pDONR201 and pDONR207. DH10B *E. coli* strain was transformed through electroporation and heat shock with the obtained Entry vectors, containing the CDS of interest. After purification of the Donor vector from *E. coli* (NucleoSpin Plasmid, Mini kit for plasmid DNA Macherey-Nagel, following producer's instructions), the second Gateway reaction was catalysed by LR clonase, which had recombined the Entry vector with the 35S Destination vector (pB2GW7). Once the recombination occurred DH10B *E. coli* strain was transformed through electroporation and heat shock with the obtained Expression vectors as described before. The Expression vectors were transferred in *Agrobacterium*

tumefaciens electrocompetent cells. To transform *Arabidopsis thaliana* plants the inflorescences were dipped in transformed *Agrobacterium tumefaciens* suspension, through floral dipping procedure [109]. The T₁ generation of transformant plant was selected using the BASTA herbicide.

3.12 - Quantitative real-time PCR (qRT-PCR)

The quantitative polymerase chain reaction (qRT-PCR) was performed in a final volume of 12 µl adding to the 2 µl of cDNA, 6 µl of SYBR master mix 2X and 0.4 µl of each primer (10 mM). qRT-PCR analysis was carried out on a CFX96 Real-Time system (Bio-Rad), the primers used are listed in **Table 6**. *ACT7* was used as internal standard. Data from three biological and three technical replicates were analysed with Bio-Rad CFX Maestro software.

Primer ID	Sequence (5' → 3')	Description	Gene
HV_003	GGGCAGAAGGATGCTTA TGT	Fw primer of <i>HvACT7</i> in barley	<i>HORVU.MOREX.r2.1H</i> <i>G0001540.1</i>
HV_004	CCATCACCAGAGTCGAG AAC	Rev primer of <i>HvACT7</i> in barley	<i>HORVU.MOREX.r2.1H</i> <i>G0001540.1</i>
HV_026	CTGCGACATCCATCCCTT TC	Fw primer of <i>HvCHAOS</i> in barley per RT	<i>HORVU.MOREX.r2.4H</i> <i>G0341350.1</i>
HV_027	CTCCTCGTCTTCTTCATC GC	Rev primer of <i>HvCHAOS</i> in barley per RT	<i>HORVU.MOREX.r2.4H</i> <i>G0341350.1</i>
HV_064	GCTGACGAAGGAAACCA TTG	Fw primer of <i>HvcpSRP54-1</i> in barley per RT	<i>HORVU.MOREX.r2.4H</i> <i>G0293270</i>

HV_065	GTCGGATTCCTCGGATAA CA	Rev primer of <i>HvcpSRP54-1</i> barley per RT	<i>HORVU.MOREX.r2.4H</i> G0293270
HV_066	AAGGTCCCGCTGCCTTCC	Fw primer of <i>HvcpSRP54-2</i> barley per RT	<i>HORVU.MOREX.r2.4H</i> G0293280
HV_067	CTCCTTTGTCAGTCGATC GA	Rev primer of <i>HvcpSRP54-2</i> barley per RT	<i>HORVU.MOREX.r2.4H</i> G0293280

Table 6 – Barley’s primers used for Real-time PCR

3.13 - Protein preparation and immuno-blot analysis

The total protein was carried out homogenizing plant material in 2X Laemmli buffer (200 mM Tris-HCl pH 6.8, 4% SDS, 20% glycerol, 5% β -mercaptoethanol), by adding 10 μ l of Laemmli buffer per 1 mg of leaf fresh weight, and solubilized for 15 minutes at 65°C. After a centrifugation step (13000 g, 10 min) the supernatant was incubated at 95°C for 5 minutes to allow protein denaturation. Protein samples were loaded onto a Tris-glycine 12% PAA (w/v) SDS-PAGE [110]. Proteins were then transferred on PVDF membranes, activated with methanol, using a semi-dry electro-blotter (Biorad) and the Bjerrum Schafer-Nielsen Buffer (48 mM Tris, 39 mM glycine, 20% methanol, 1.3 mM SDS (pH 9.2)). To avoid non-specific binding the membrane was incubated at least one hour in a solution of 5% milk powder (w/v) and TBST buffer (200 mM Tris-HCl pH 8; 300 mM NaCl; 0.1% Tween-20 v/v). The membranes were immuno-decorated with primary antibody diluted in 5% milk TBST solution for 4 hours at room temperature or overnight at 4°C. After 3 washing steps of 10 minutes each with TBST buffer, the secondary antibody diluted in 5% milk TBST solution was added and incubated for 1 hour. After 3 washing steps of 10 minutes each with TBST buffer, the membrane was incubated with chemo-luminescence substrate (ECL Star Enhanced

Chemiluminescent Substrate Euroclone), which allowed the imaging of protein detection.

3.14 - Coomassie Brilliant Blue staining

After the Tris-glycine 12% SDS-PAGE separation, total proteins could be visualized within the gel by permanently Coomassie Brilliant Blue (C.B.B.) staining. The gel was incubated in staining solution (40 % methanol (v/v); 10 % acetic acid (v/v); 0.1 % Coomassie Brilliant Blue R-250 (w/v)) for at least 1 hour. To remove the background, the gel was washed in de-staining solution (40 % methanol (v/v); 10 % acetic acid (v/v)), which removes the unbound dye from the gel by diffusion.

3.15 - Thylakoid membrane extraction

500 mg of leaf fresh weight was frozen in liquid nitrogen and ground using mortar and pestle. The powder was resuspended in 4 ml of Homogenization Buffer (HB 0.45 M sorbitol, 20mM Tricine-KOH pH 8.4, 10 mM EDTA, 10 mM NaHCO₃ and 0.1% BSA w/v). The suspension was filtered through the Miracloth (Millipore) filter paper, in order to eliminate debris, and then was centrifuged at 4°C at 2000 g for 10 minutes, in order to enrich the chloroplast fraction, preserving their integrity. The supernatant was discarded and the pellet was resuspended in 250 µl of Extraction Buffer (EX 100 mM HEPES-KOH pH 8.0, 15 mM MgOAc and 60 mM KOAc) supplemented with protease inhibitors cocktail (SERVA protease-inhibitor Mix M). In order to obtain chloroplasts burst, samples were subjected to mechanical rupture, forcing the suspension to pass into a syringe. Samples were then centrifuged at 4°C at 13000 g for 10 minutes. Supernatant contained stromal soluble proteins was collected and stored at -80°C, the remaining pellet contained insoluble thylakoid membrane proteins was resuspended in

500 μ l of EX buffer and the centrifugation step was repeated. The pellet was resuspended in 10 μ l of Laemmli buffer for 1 mg of leaf fresh weight in order to extract the thylakoids proteins as described in paragraph **3.13**.

3.16 - Pigment extraction and quantification

Fresh material was collected and weighted before being frozen in liquid nitrogen. Samples were then ground in liquid nitrogen, resuspended in 95% acetone (v/v) solution and centrifuged at 13000 g for 10 minutes at 4°C. The supernatants containing the pigments were sent for a detailed analysis using HPLC or measured using a spectrophotometer into quartz cuvette. The total amount of chlorophyll (Chla + Chlb) and the ratio (Chla/Chlb) was calculated using the spectrophotometer. Since the Chla absorption peak is at 663 nm while the Chlb peak is at 646 nm, the chlorophyll content, expressed as μ g/mg, was calculated following these equations:

$$Chla = \frac{(12,25 * A663) - (2,55 * A646)}{m * V} * DF$$

$$Chlb = \frac{(20,31 * A646) - (4,91 * A663)}{m * V} * DF$$

$$Chla + Chlb = \frac{(17,76 * A646) + (7,43 * A663)}{m * V} * DF$$

A is the absorbance, *m* is the weight of fresh material (mg), *V* is the volume of acetone (mL) and *DF* is the dilution factor.

3.17 - Measurement of photosynthetic efficiency

The Handy-PEA chlorophyll fluorometer (Hansatech Instruments, www.hansatech-instruments.com) was used to measure F_v/F_m upon light exposure and after 30 minutes of dark adaptation. The photosynthetic efficiency of barley was measured *in vivo* with the non-invasive Dual-PAM-100 (Walz, www.walz.com/). After 30 minutes of dark adaptation the minimal fluorescence (F_0) was measured. With a pulse (0.8 sec) of saturating white light ($5000 \mu\text{mol photon m}^{-1} \text{s}^{-1}$) the maximum fluorescence (F_m) was determined. The ratio $(F_m - F_0)/F_m$ was calculated as F_v/F_m , the maximum quantum yield of PSII. After the exposure to the actinic red light ($80 \mu\text{mol photon m}^{-1} \text{s}^{-1}$), the steady state fluorescence (F_s) was measured and with a second saturation pulse the F_m' was determined. The PSII effective quantum yield (Φ_{II}) was calculated as the ratio $(F_v - F_s)/F_m'$. In particular, Light Curves and Induction-Relaxation were performed following the pre-sets (see DUAL-PAM-100 P700 & Chlorophyll Fluorescence Measuring System manual). Moreover, the Imaging-PAM (Walz, www.walz.com/) was exploited to acquire images of photosynthetic activity in a spatio-temporal way. The Imaging-PAM allows for the acquisition of images of the entire leaf providing an overall view of photosynthetic parameters. Each saturation pulse provides an image with a chromatic scale indicating the intensity of the emitted signal. The fluorescence parameter F_t is continuously monitored. F_0 and F_m are assessed after dark adaptation, serving as reference for fluorescence quenching analysis by the saturation pulse method. Besides F_v/F_m (where $F_v = F_0 - F_m$, F_0 = minimal fluorescence yield, F_m = maximal fluorescence yield), the PSII quantum yield after dark acclimation, also the PSII quantum yield during illumination, $Y(II)$, and the quantum yields of regulated and non-regulated energy dissipation ($Y(NPQ)$ and $Y(NO)$ respectively) as well as the electron transport rate (ETR and PS) can be imaged.

3.18 - Yeast two hybrid assay

For yeast two hybrid analyses, the restriction enzymes cloning strategy was chosen. The PCR products (primers listed in **Table 7**) were digested with one or two enzymes for 60 min at 37°C, for the cutting procedure EcoRI-HF, XhoI and SacI-HF were used in a single or double digest in CutSmart buffer.

Genes	Sense primer (5' → 3')	Antisense primer (5' → 3')
<i>HvCHAOS</i> (AD-Vector)	GTGAATTCGCAGCAAG CAAGGGGGGC	GTCTCGAGTCACCCTGCA AATGTCTCC
<i>Hvchaos</i> (AD-Vector)	GTGAATTCGCAGCAAG CAAGGGGGGC	GTCTCGAGTCACCCTGCA AATGTCTCC
<i>HvcpSRP54</i> (AD-Vector)	GTGAATTCACGTTCCGG GCAGCTCACCAC	GTGAGCTCTCAAGGCCT ACTGGCGCCAC
<i>HvCHAOS</i> (BD-Vector)	GTGAATTCGCAGCAAG CAAGGGGGGC	GTGAATTCTCACCCTGCA AATGTCTCC
<i>Hvchaos</i> (BD-Vector)	GTGAATTCGCAGCAAG CAAGGGGGGC	GTGAATTCTCACCCTGCA AATGTCTCC
<i>HvcpSRP54</i> (BD-Vector)	GTGAATTCACGTTCCGG GCAGCTCACCAC	GTGAATTCTCAAGGCCTA CTGGCGCCAC

Table 7 – Primers sequences employed in the Y2H assay.

HvCHAOS wild type and mutated sequences (*Hvchaos*), were cloned using EcoRI-HF and Xcho for the pGADT7 (AD-Vector-Clontech) plasmid, while for the pGBKTP7 (BD-Vector-Clontech) a single EcoRI-HF digest. *HvcpSRP54* was cloned using EcoRI-HF and SacI-HF for the pGADT7 plasmid, while for the pGBKTP7 a single EcoRI-HF digest. The AD-Vector and BD-Vector were cut with a restriction reaction incubating them for 2 hours at 37°C and for 20 minutes at 65°C to inactivate the enzyme. To avoid self-ligation of the plasmids, Calf Intestine Phosphatase (NEB) was added to the reaction and incubated at 37°C for 30 min. The plasmids were then

purified with the Qiagen PCR Purification Kit. The ligation step was performed at 4°C for 24 hours using a T4 DNA ligase (NEB).

The *Saccharomyces cerevisiae* strain AH109 (Clontech Laboratories, Palo Alto, CA, USA) was inoculated in 25 ml of liquid medium (20 g/l yeast extract, 40 g/l tryptone), containing also 2% (v/v) of glucose, over-night at 28°C. The inocule was diluted in a total volume of 150 ml of liquid medium containing glucose and was grown for 2 hours. The cells were spun down in the centrifuge for 10 minutes at 3000 g. After centrifugation, the supernatant was removed and the cells were washed with 1 ml sterile ddH₂O. The cells were centrifuged again for 10 minutes at 3000 g, the supernatant removed and the pellet washed in 1ml µl LiTe buffer (10 mM Tris-HCl pH 7.5, 1 mM EDTA pH 8, 100 mM LiAc). The centrifugation-step was repeated and the pellet was resuspended in 100 µl LiTe buffer. For co-transformation 25 µl of the washed yeast cells, 1 µg of each construct, 20 µl Carrier-DNA (DNA from fish sperm 2 mg/ml), 20 µl dimethylsulfoxid (DMSO) and 300 µl LiTePEG (10 mM Tris-HCl pH 7.5, 1 mM EDTA pH 8, 100 mM LiAc, 40% PEG v/v) were combined. These preparations were incubated for 30 minutes at 30°C and for 15 minutes at 42°C. Afterwards the cells were centrifuged down for 10 minutes at 3000 g, resuspended in 100 µl of sterile ddH₂O and plated on SC-Drop-out (-W-L) plates. The plates were incubated at 30 °C. Of each positive plate a few colonies were streaked out on SC-Drop-out (-W-L-H) plates. For semi-quantitative analyses, colonies of the SC-Drop-out (-W-L) plates were inoculated in 10 ml liquid SC-Drop-out (-W-L) medium overnight. The OD₆₀₀ was measured and brought to the same value. The cells were then centrifuged down at 3000 g for 10 minutes and resuspended in 40 µl sterile H₂O. 20 µl of the cell suspension was then brought as a drop onto SC-Drop-out (-W-L-H) and SC-Drop-out (-W-L-H + 3mM 3AT)-plates. The SC-Drop-out was prepared with 6.67 g/l yeast nitrogen base (w/o amino acids), 20 g/l glucose, 0.83 g/l Synthetic Complete Drop Out Mix (-W-L/ -W-L-H/-W-L-H+3mM 3-Amino-1,2,4-triazole; pH 5.6).

3.19 – TEM (Transmission Electron Microscope)

Barley (Sebastian, *hus1*) and *Arabidopsis thaliana* (Col0, *chaos*) second leaves fragments (2 mm x 3 mm) were manually dissected and immediately were fixed in 2.5% glutaraldehyde in 0.1 M sodium cacodylate buffer, placed in a vacuum desiccator for 4 h at room temperature and, subsequently, overnight at 4°C. Then samples were rinsed 2 times for 10 minutes with sodium cacodylate buffer 0.1 M, post-fixed in 1% osmium tetroxide in 0.1 M cacodylate buffer for 2 hours at 4°C. After 2 rinses with bi-distilled water, samples were counter-stained with a 0.5% uranyl acetate in bi-distilled water overnight at 4°C in the dark. After rinsing with bi-distilled water, the tissues were dehydrated with a series of solutions containing increasing concentrations of ethanol (70%, 80%, 90%) for 10 minutes each. Subsequently, the samples were dehydrated with 100% ethanol for 15 min, 2 times. The tissues were then permeated twice with 100% propylene oxide for 15 min. Meanwhile, Epon-Araldite resin was prepared mixing properly Embed-812, Araldite 502, dodecenylsuccinic anhydride (DDSA) and Epon Accelerator DMP-30 according to manufacturer specifications. Samples were gradually infiltrated first with a mixture of Epon-Araldite and propylene-oxide 1:2 for 2 hours, then with Epon-Araldite and propylene-oxide 1:1 for 1 hour and left in a mixture of Epon-Araldite and propylene-oxide 2:1 overnight at room temperature. The samples were finally put in pure resin before polymerization at 60°C for 48 hours. Resin embedded samples were cut with the ultramicrotome (PowerTome XL, RMC) in semi-thin sections of 0.5 µm thickness with a glass knife, stained with 0.1% toluidine blue in 0.1 M sodium phosphate buffer and observed at the optical microscope to identify the region of the sample to investigate at the ultrastructural level. Ultra-thin sections of 70 nm were cut with a diamond knife (Ultra 45°, DIATOME) and collected on copper grids (G300-Cu, Electron Microscopy Sciences). Samples were observed at the transmission electron microscope (TEM) (Talos L120C, Thermo Fisher Scientific) at 120 kV and images were acquired with a digital camera (Ceta CMOS Camera, Thermo Fisher Scientific).

4 - Results and discussions

4.1 - Characterization of the barley pale mutant *hus1*

The M₄ plants, from nine-hundred M₃ generation mutated lines from the chemically mutagenized barley population HorTILLUS [39] cv. Sebastian, were screened for increased photosynthetic performance under field condition, at the breeding station in Bochuchwalowice village, University of Silesia, Poland. From this preliminary screening, seven lines were selected for pale phenotype and altered photosynthetic performance. Among those, the line 283/001/7/1 was selected as the most interesting candidate to be studied since it showed a wild-type-like growth rate, size and grain production, a clear leaf pale-green phenotype (**Figure 1A**) and an increased photosynthetic efficiency compared to the wild-type reference Sebastian upon low- and high-light illumination. Because of this last feature the mutant line was named *happy under the sun1* (*hus1*). A preliminary phenotypical analysis allowed defining that the pale-green pigmentation of leaves is due to lower chlorophylls content (Chl a+b) in the leaves, with a pronounced reduction of chlorophyll b, the pigment mainly associated to the antenna complexes (**Figure 1B**). Thylakoid proteins of *hus1* and the Sebastian were extracted from an equal amount of fresh weight leaf material (second leaf) and fractionated onto SDS-PAGE gel, stained with Coomassie Brilliant Blue (C.B.B.). The protein fractionation showed a reduction of the antenna proteins Lhca and Lhcb in the mutant, while the rest of the proteins remained mainly unchanged (**Figure 1C**). To assess the photosynthetic performance of *hus1* mutant, and corroborate the analyses performed in field conditions, dark-adapted leaves were subjected to increasing actinic light intensities (0 to 1287 $\mu\text{mol}\cdot\text{photons m}^{-2}\cdot\text{s}^{-1}$) and the effective PSII quantum yield ($Y_{(II)}$), was measured by Dual-PAM 100 fluorometer. By increasing actinic light, decreased $Y_{(II)}$ values could be observed in *hus1* and Sebastian, due to the fact that photo-protective mechanisms were activated. However, at each light intensity, *hus1* showed higher $Y_{(II)}$ values compared to Sebastian and lower NPQ, non-photochemical

quencing, indicating that *hus1* has a more efficient photosynthetic performance as a consequence of reduced photo-protection (**Figure 1D-E**).

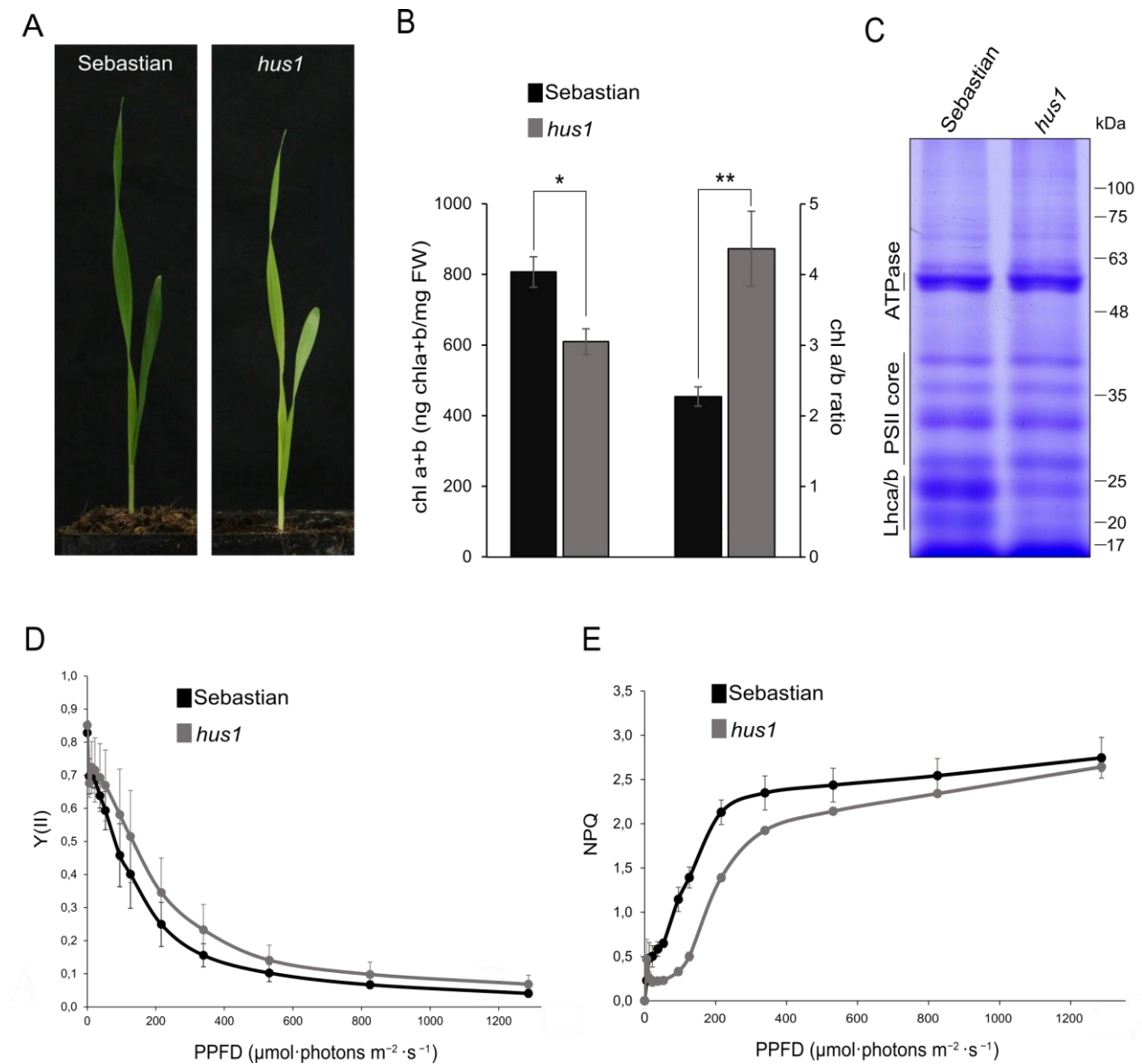


Figure 1 – Phenotypical analysis of *hus1* mutant. (A) The mutant line *hus1* shows a pale-green leaf phenotype compared to the wild-type cv. Sebastian. (B) Total chlorophyll (Chl a+b) content, normalized on FW (Fresh Weight) is decreased in *hus1* compared to Sebastian, especially in the Chl b content as shown by the increased Chl a/b ratio (t-Test, p-value < 0,05 *, p-value < 0,01**). Error bars in the histogram indicate standard deviation (SD). (C) SDS-PAGE of thylakoid proteins from Sebastian and *hus1* was stained with Coomassie Brilliant Blue (C.B.B.). Note that in the region between 25 and 20 KDa, the accumulation of Lhca and Lhcb subunits was reduced in *hus1* mutant. (D-E) Light curve analysis was performed using the Dual-PAM 100 fluorometer. The Y_(II), the

effective quantum yield of PSII, and the NPQ, non-photochemical quenching, were calculated at increasing light intensity (from dark to 1287 $\mu\text{mol}\cdot\text{photons m}^{-2}\cdot\text{s}^{-1}$) (x-axis, PPFD = Photosynthetic Photon Flux Density). The charts represent the average of three biological replicates and error bars indicate standard deviation.

4.2 - Exome capture analysis allowed for the identification of *hus1* mutation

In order to identify the putative mutation leading to *hus1* phenotype, two different back-crossing populations were generated, one by crossing *hus1* mutant (background cv. Sebastian) and cv. Sebastian, for cleaning the genome from secondary mutations caused by the chemical mutagenesis, and the second one by crossing *hus1* mutant and cv. Morex, whose genome has been fully sequenced and annotated [111]. The F₂ generation, from two different F₁ plants of the *hus1* x Morex backcross, was analysed into details. The *hus1*-like plants (pale) segregated in a ratio of 1/4 vs 3/4 wild-type like plants, a segregation typical for a monogenic recessive mutation (**Figure 2A**). The χ^2 (chi-square test, one degree of freedom) value of 0.386, calculated on the entire F₂ generation (311 plants) indicated a P (Probability) > 0.05, validating the hypothesis of a monogenic recessive mutation.

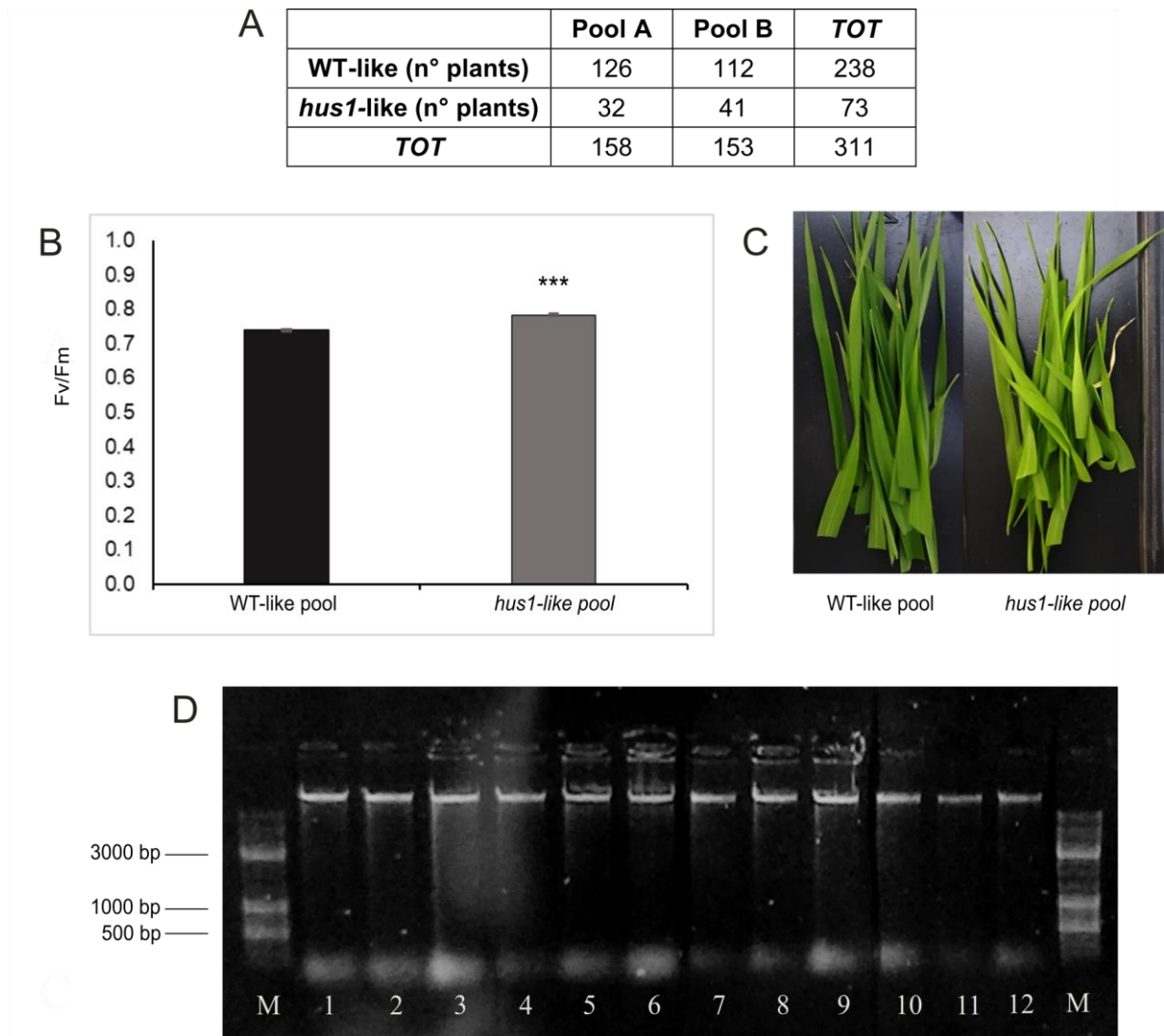


Figure 2 – Analysis of F₂ generation of the backcross *hus1* x Morex. (A) Number of plants analysed in the F₂ generation showing Sebastian (WT-like) and *hus1*-like phenotype and (B) Fv/Fm, maximum quantum yield of PSII, measurements performed in the greenhouse using Handy-PEA fluorimeter between the pale green pool and the dark green pool. Error bars indicate standard deviation. Statistically (t-Test, p-value < 0,001***). (C) The two different pools used for genomic DNA extraction and exome capture analysis. (D) Agarose gel containing the genomic DNA of 6 sample (from 1 to 6) belonging to WT-like pool, together with 6 sample (from 7-12) belonging to the *hus1* pool, for sequencing purposes.

The 73 pale plants (*hus1*-like pool) showed an increased maximum quantum yield of PSII (Fv/Fm), performed using the Handy-PEA fluorimeter, compared to WT-like pool (dark green leaves) (**Figure 2B**). The genomic DNA of 50 individuals from WT-like

pool and 50 individuals from the *hus1*-pool (**Figure 2C**) was extracted and the genomic DNA was bulked in an equal proportion to generate the wild-type bulked DNA pool and the mutant bulked DNA pool. Different replicates of genomic DNA were loaded onto agarose gel (**Figure 2D**) to control the integrity of DNA samples. The DNA material was sent to the collaborator partners at the University of Silesia for library preparation and for exome capture sequencing. The purified DNA from each pool was digested enzymatically to obtain the highest number of fragments with the average size between 250 and 350 bp. After the end-repair reaction that add adapters to the fragments, the dual size selection of fragments was done using AMPure Beads. The enrichment of the libraries through pre-capture LM-PCR (ligation-mediated PCR) was done; the libraries were purified and hybridized with exome capture probes design according to the [108]. Then the libraries were subjected to paired-end exome capture HiSeq4000 Illumina sequencing. Thanks to the collaboration of the bio-informatic group at the Department of Biosciences, the output of exome capture sequencing was analysed. Reads were mapped onto the improved annotated reference genome sequence assembly of cv. Morex [111] and single nucleotide polymorphisms (SNPs) were detected. Allele frequency shows a single sharp peak on the long arm of chromosome 4H, where the frequency of the mutant allele increased to over 97% and dropped to about 20% in the wild-type pool. The candidate region of 4.5 Mbp (**Figure 3A**) contained circa a hundred of annotated genes, of which 41 genes (**Table 1**) contain missense variant between the two bulks, but only the *HORVU.MOREX.r2.4HG0341350* gene was found to be highly expressed in the green leaves (IPK Barley Server), was localized in the chloroplast, and its coding sequence contained a Single Nucleotide Polymorphism (SNP) in homozygosity causing the presence of a stop codon.

Gene ID	Localization
HORVU.MOREX.r2.4HG0340750.1	/
HORVU.MOREX.r2.4HG0340770.1	/

HORVU.MOREX.r2.4HG0340780.1	Secretory pathway
HORVU.MOREX.r2.4HG0340790.1	/
HORVU.MOREX.r2.4HG0340800.1	/
HORVU.MOREX.r2.4HG0340810.1	/
HORVU.MOREX.r2.4HG0340820.1	Mitochondrion
HORVU.MOREX.r2.4HG0340830.1	Mitochondrion
HORVU.MOREX.r2.4HG0340850.1	/
HORVU.MOREX.r2.4HG0340890.1	Chloroplast
HORVU.MOREX.r2.4HG0340940.1	Mitochondrion
HORVU.MOREX.r2.4HG0340960.1	/
HORVU.MOREX.r2.4HG0340970.1	Mitochondrion
HORVU.MOREX.r2.4HG0340980.1	/
HORVU.MOREX.r2.4HG0341000.1	Secretory pathway
HORVU.MOREX.r2.4HG0341010.1	Chloroplast
HORVU.MOREX.r2.4HG0341020.1	/
HORVU.MOREX.r2.4HG0341030.1	/
HORVU.MOREX.r2.4HG0341040.1	/
HORVU.MOREX.r2.4HG0341050.1	/
HORVU.MOREX.r2.4HG0341060.1	/
HORVU.MOREX.r2.4HG0341070.1	Chloroplast
HORVU.MOREX.r2.4HG0341080.1	/
HORVU.MOREX.r2.4HG0341110.1	/
HORVU.MOREX.r2.4HG0341130.1	Secretory pathway
HORVU.MOREX.r2.4HG0341140.1	Mitochondrion
HORVU.MOREX.r2.4HG0341400.1	Secretory pathway
HORVU.MOREX.r2.4HG0341430.1	Chloroplast
HORVU.MOREX.r2.4HG0341440.1	/
HORVU.MOREX.r2.4HG0341500.1	/
HORVU.MOREX.r2.4HG0341530.1	/
HORVU.MOREX.r2.4HG0341580.1	/
HORVU.MOREX.r2.4HG0341650.1	/
HORVU.MOREX.r2.4HG0341670.1	Chloroplast
HORVU.MOREX.r2.4HG0341700.1	Mitochondrion

HORVU.MOREX.r2.4HG0341710.1	Mitochondrion
HORVU.MOREX.r2.4HG0341790.1	Secretory pathway
HORVU.MOREX.r2.4HG0341830.1	/
HORVU.MOREX.r2.4HG0341840.1	Secretory pathway
HORVU.MOREX.r2.4HG0341890.1	/
HORVU.MOREX.r2.4HG0341910.1	/

Table 1 – List of the genes identified in the candidate region of 4.5 Mbp. These genes have a different allele frequency in the WT-like pool and *hus1*-pool due to the presence of missense variants.

As expected from a mutagenized population obtained through the treatment with sodium azide (NaN_3) and N-methyl-N-nitrosourea (MNU), the SNP in *HORVU.MOREX.r2.4HG0341350* gene caused the change from G (Guanine) in position 885 of the coding sequence (CDS) into A (Adenine), causing a non-sense mutation that turns the Tryptophan (W) in position 295 into a STOP codon (**Figure 3B**). The identified mutation was verified in an F_2 population generated by crossing *hus1* with Sebastian. All the dark green plants had the Guanine in position 885 (88 plants), while the heterozygous ones (174 plants) showed a WT-like phenotype and displayed both G and A at +855 bp from the ATG translation starting codon. As expected, all the pale-green, *hus1*-like plants (84 plants) had the mutated nucleotide A in position +885 bp (**Figure 3C**). Moreover, the analysis of the transcript level of *HORVU.MOREX.R2.4HG0341350* in Sebastian and *hus1* plants revealed a marked reduction of the transcript accumulation in *hus1* genetic background (**Figure 3D**). This is in agreement with previous findings, where mRNAs with premature stop codons have been shown to be recognized by a surveillance complex and to be selectively degraded [60][112].

Given the strong association of G885A SNP with the *hus1* phenotype and the specific expression of *HORVU.MOREX.R2.4HG0341350* gene in leaves and the almost

complete suppression of its expression in *hus1* mutant background, this gene was considered to carry the causal mutation responsible of the *hus1* phenotype.

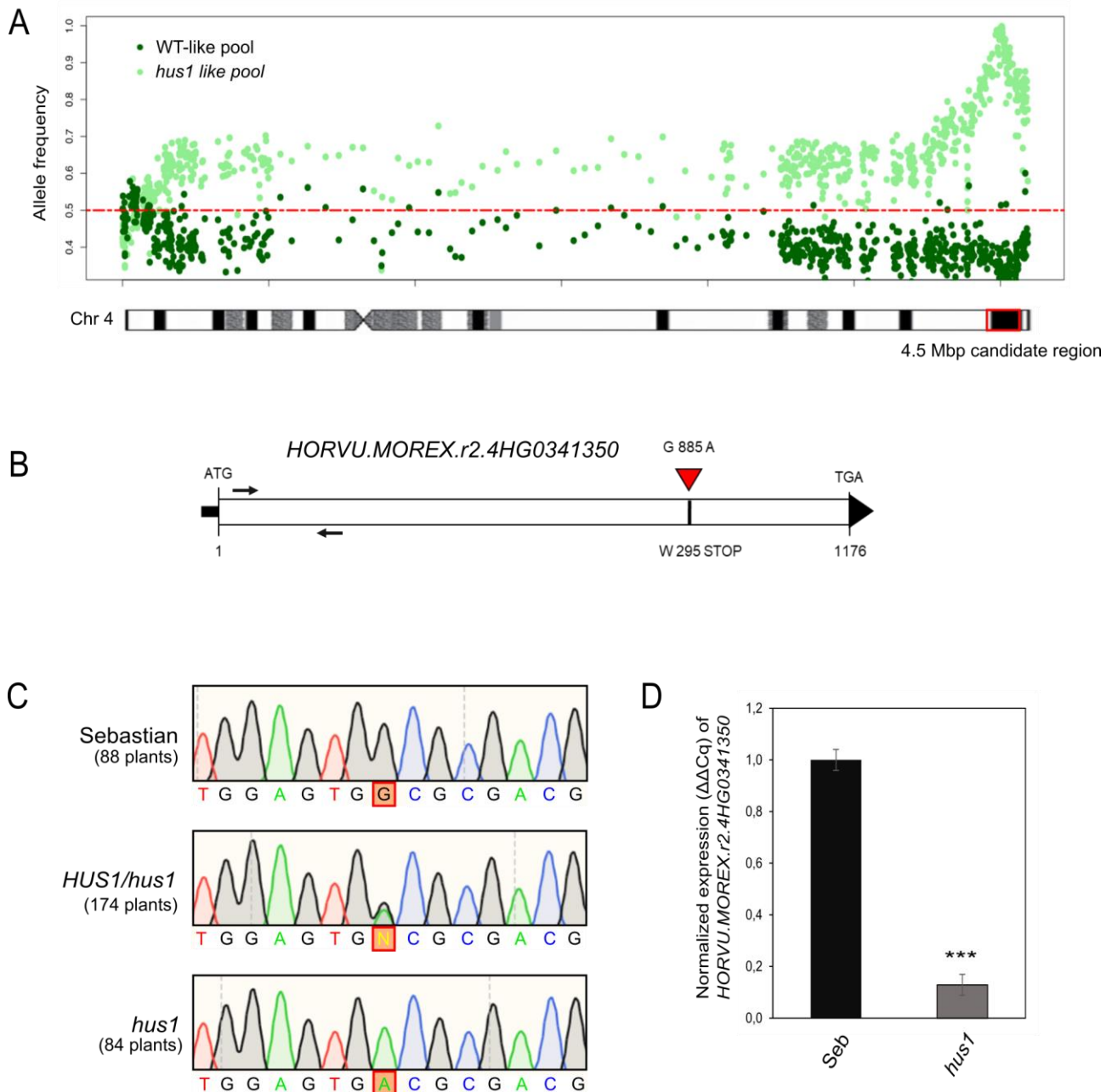


Figure 3 – Identification of the SNP mutation in *HORVU.MOREX.r2.4HG0341350* gene. (A) Allele frequency of the chromosome 4 highlighted a peak in the *hus1* pool around the 600 millions bp position. In this region of 4.5 Mbp, distinct polymorphisms were found between the two pools. (B) The schematic structure of *HORVU.MOREX.r2.4HG0341350* gene, annotated as a single exon gene. The red triangle indicates the position of the SNP, at nucleotide 885 from the START codon of the CDS. The two arrows indicated the positions of the primers used for the real-time PCR analysis,

reported in **(D)**. **(C)** The segregation analysis of the mutation is shown as chromatograms: the dark-green Sebastian-like leaves (88 plants), the dark-green leaves of the heterozygous plant (174 plants) and pale-green leaves of the *hus1* mutant (84 plants). **(D)** qRT-PCR performed on *HORVU.MOREX.r2.4HG0341350* transcript. Histograms represent the average of three technical replicates and error bars indicate standard deviation. Analysis was performed on three biological replicates and one representative experiment is shown. The *HORVU.MOREX.r2.4HG0341350* transcript level in the *hus1* mutant is dramatically reduced, resembling the one of a knock-down mutant (t-Test ,*** p-value < 0.001).

4.3 - Functional characterization of *HUS1* gene

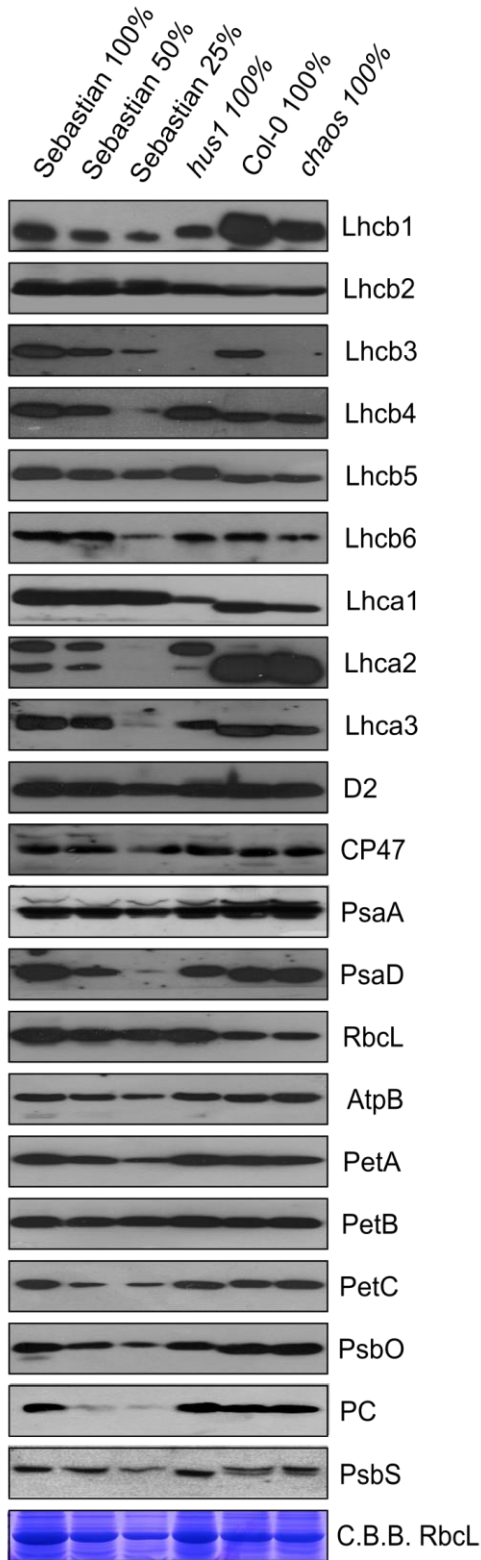
The *HORVU.MOREX.r2.4HG0341350* gene encodes a protein characterised by 48% amino acid sequence identity and 62% similarity with the chloroplast Signal Recognition Particle 43 kDa protein (cpSRP43; [113] [114]) of *Arabidopsis thaliana*. Furthermore, this protein is highly conserved in land plants (**Figure 4**). cpSRP43 is a chaperone of the chloroplast Signal Recognition Particle (SRP) pathway and it is required for post-translational targeting of LHCPs into the thylakoid membrane, thus contributing to the biogenesis and maintenance of the thylakoid membranes and the associated electron transport chain. In *Arabidopsis*, the corresponding mutant, known as *chaos* (for chlorophyll a/b binding protein harvesting-organelle specific), shows a leaf pale-green phenotype [113] very similar to the one that characterises *hus1* mutant plants.

Figure 4 – Homology of cpSRP43 protein in photosynthetic organisms. (A) The evolutionary history of *cpSRP43* gene was inferred by using the Maximum Likelihood method and JTT matrix-based model [115]. The tree with the highest log likelihood (-24185.86) is shown. Initial tree(s) for the heuristic search were obtained automatically by applying Neighbor-Join and BioNJ algorithms to a matrix of pairwise distances estimated using the JTT model, and then selecting the topology with superior log likelihood value. This analysis involved 29 land plants amino acid sequences. There was a total of 430 positions in the final dataset. Evolutionary analyses were conducted by MEGA X [116]. (B) Alignment of HUS1 and AtpSRP43 protein sequence, using Clustal Omega. In green the cTPs (Chloroplast Transit Peptide) of the two proteins are indicated; in light blue the three CHROMO domains and in yellow the four ANK (Ankarin) domains of the *Arabidopsis thaliana* protein are shown. BLAST alignment shows a 186/384 (48%) of identity and 241/384 (62%) similarity between the two sequence.

In order to investigate whether barley *HUS1* gene is the functional orthologue of *Arabidopsis cpSRP43*, a detailed biochemical and physiological analysis, comparing *hus1* and the *Arabidopsis chaos* mutant, was performed. Immuno-blot analyses displayed a general and very similar reduction in the accumulation of antenna complexes of both photosystems, in the two mutants with respect to the corresponding wild-type controls (Sebastian and Col-0, respectively) (**Figure 5A**). In particular, while the accumulation of Lhcb4, Lhcb5 and Lhca2 remained unchanged, Lhcb1, Lhcb6 and Lhca1 showed a reduced accumulation, and Lhcb3 was completely absent in both *hus1* and *chaos* thylakoids. The accumulation of several other proteins of the thylakoid electron transport chain, i.e. subunits of photosystem cores, cytochrome b_6f and ATPase, was not altered by the mutation, corroborating the hypothesis that *hus1* and *chaos* mutations affect, specifically, the uploading of few antenna proteins into the thylakoid membranes in a similar way.

Furthermore, the photosynthetic performance was measured in barley and *Arabidopsis* leaves. The Imaging-PAM fluorometer was used to measure $Y_{(II)}$ and confirmed the increased photosynthetic performance of leaves of both mutants, compared to the corresponding controls (**Figure 5B**).

A



B

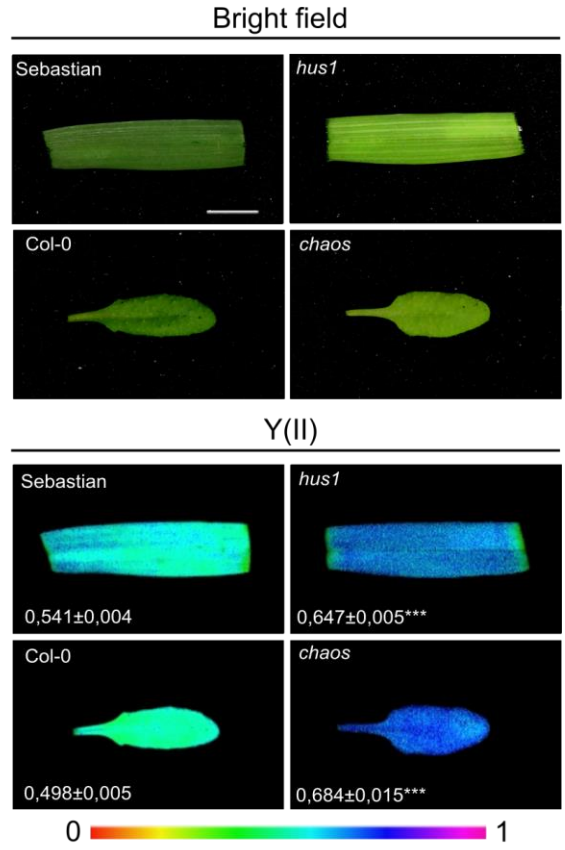


Figure 5 – Biochemical and physiological analysis in *hus1* and *chaos* leaves. (A) Immuno-blot of the total protein content of Sebastian, *hus1*, Col-0 and *chaos* genetic backgrounds using antibodies specific for the main subunits of thylakoid protein complexes, normalized on fresh weight. Coomassie Brilliant Blue (C.B.B.) of SDS-PAGE RbcL-migrating region is shown for equal loading. (B) Imaging-PAM values of $Y_{(II)}$ upon exposure of leaves for 5 minutes to actinic light intensities ($36 \mu\text{mol}\cdot\text{photons m}^{-2}\cdot\text{s}^{-1}$) are displayed in false colours. The colour scale is shown below, violet colour corresponds to 1 and red to 0. The picture is a representative point of 5 independent induction curves obtained for each genotype (not shown). Difference between WT and mutants are statistically significant (t-Test, *** p-value < 0.001)

The leaf pigment content was also analysed by using HPLC (High Performance Liquid Chromatography), in collaboration with the laboratory of Prof. Peter Jahns at the University of Düsseldorf (Germany). Total pigments were extracted from equal amounts of fresh leaf weight and separated and quantified by using HPLC. As show in **Table 2** the two mutants displayed a very similar reduction of total (Chl a+b) content and an increased Chl a/b ratio. Furthermore, the level of carotenoids such as Neoxanthin (Nx), Lutein (Lut) and Violaxanthin (Vx) content was reduced in the two mutants as well, whereas carotenoids that are not present in the antenna of photosystems, such as β -carotene, exhibited even an increase in the mutant leaves, supporting further the primary alteration of Lhc-associated pigments.

	Nx	Vx	Ax	Lut	Zx	Chl b	Chl a	Car	VAZ	Chl a/b	Chl a+b
Sebastian	90±12	123±20	6±1	249 ± 27	3 ± 1	774 ± 54	2579 ± 271	97 ± 32	132 ± 22	3.33 ± 0.129	3353 ± 325
<i>hus-1</i>	32±4	74±20	7±2	92 ± 21	3 ± 1	311 ± 23	1253 ± 105	121 ± 67	83 ± 23	4.03 ± 0.108	1564 ± 128
	***	**	ns	***	ns	***	***	ns	**	***	***
WT Col-0	45±4	50±4	2	146 ± 25	0	359 ± 36	1141 ± 106	84 ± 30	52 ± 4	3.18 ± 0.036	1500 ± 142
<i>chaos</i>	22±1	40±4	2	90 ± 11	1 ± 1	200 ± 10	826 ± 50	92 ± 27	43 ± 5	4.13 ± 0.047	1026 ± 60
	***	**	ns	**	*	***	***	ns	**	***	***

Table 2 - HPLC analysis of pigment content in Sebastian, *hus1*, Col-0 and *chaos*. The pigment content is normalized on leaf FW (Fresh Weight) and is reported as pmol per mg FW. Nx = Neoxanthin; Vx = Violaxanthin; Ax = Antheraxanthin; Lut = Lutein; Zx = Zeaxanthin; Chl = Chlorophyll; VAZ= Vx+Ax+Zx; Car = β -carotene; DEPS = De-epoxidation. t-Test, *p-value < 0.05, ** p-value < 0.01, *** p-value < 0.001, ns = not significant.

Furthermore, analyses conducted with Transmission Electron Microscopy (TEM) revealed a similar size of chloroplasts in all the genetic background analysed, although the *hus1* chloroplasts contained less starch grains (**Figure 6 b,c**), similar to *chaos* (**Figure 6 e,f**). TEM analysis also revealed a different organization of the thylakoid membranes with thinner grana stacks in *hus1* and *chaos*, when compared to the corresponding wild-type controls (**Figure 6 a,b**).

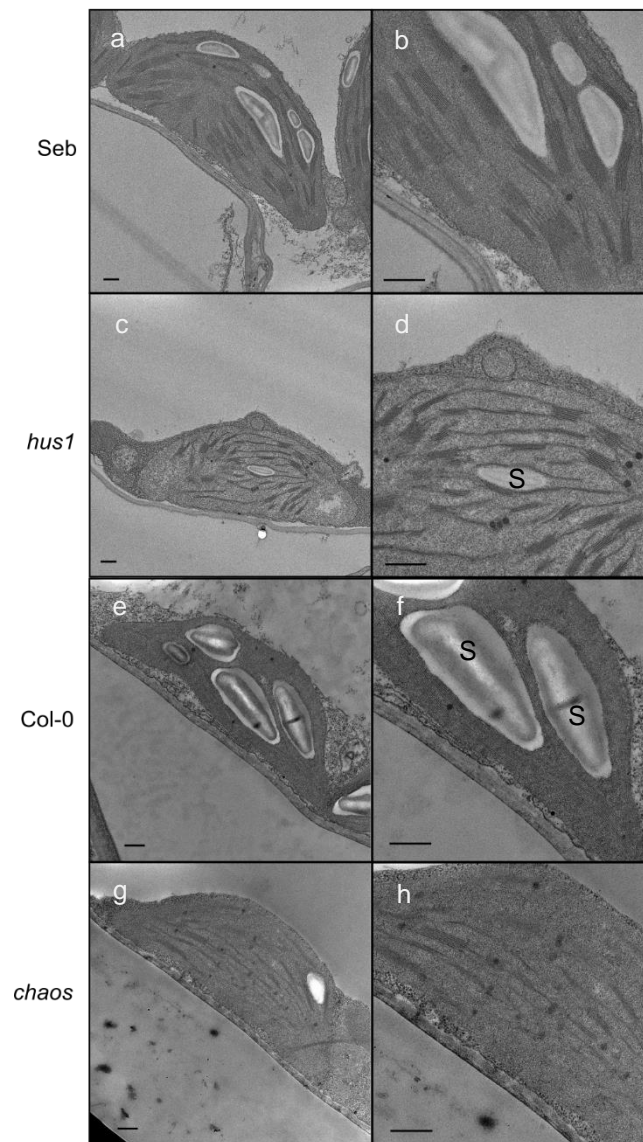


Figure 6 - Transmission electron microscopy (TEM) analysis of chloroplast ultrastructure. (a, b), wild-type barley plant Sebastian, (c, d), *hus1* barley mutant, (e, f) wild type Arabidopsis plant Col-0 and (g, h) Arabidopsis *chaos* mutant. Scale-bar equals to 500 nm. S, starch granule.

4.4 - Arabidopsis *chaos* mutant complementation with barley *HUS1* gene

In order to verify if the *HUS1* gene is the functional orthologue of *cpSRP43* of Arabidopsis and that the identified SNP is the actual causal mutation of *hus1* phenotype, complementation experiments were carried out. The *HUS1* wild-type and *hus1* mutated Coding Sequences (CDS) were expressed under the control of CaMV35S Promoter in the *Arabidopsis thaliana chaos* mutant, resulting in *chaos+35S::HUS1* and *chaos+35S::hus1* transgenic lines. The wild-type version of barley *HUS1* gene was able to revert the pale-green phenotype of *chaos* mutant, restoring a Col-0-like pigmentation, while *chaos+35S::hus1* showed no complementation effect in terms of leaf pigmentation and $Y_{(II)}$ parameters (**Figure 7A**). The pigments content measurement allowed to corroborate this observation. Indeed, *chaos* and *chaos+35S::hus1* Arabidopsis lines had very similar values of total chlorophyll content (Chl a+b) and Chl a/b ratios, that differ from the almost identical values observed in Col-0 and *chaos+35S::HUS1* lines (**Figure 7B**). qRT-PCR performed to monitor *HUS1* transcript accumulation in the two transformant lines showed comparable expression of *HUS1* gene in *chaos+35S::hus1* and *chaos+35S::HUS1* lines (**Figure 7C**). Ruling out any possible defect in *hus1* gene expression at the basis of the failed complementation of *chaos+35S::hus1*, immuno-blot analysis of antenna proteins (**Figure 7D**) among Col-0, *chaos*, *chaos+35S::HUS1* and *chaos+35S::hus1* displayed the characteristic absence of Lhcb3, in all the lines lacking a functional cpRP43 protein, i.e. *chaos* and *chaos+35S::hus1* (see also **Figure 5A**). The other antenna proteins analysed, such as Lhcb1, Lhcb2, Lhca3, were also decreased in these two lines, while Lhca3 remain unchanged. Taken together these observations allow to state that barley *HUS1* gene is the functional orthologue of the Arabidopsis *cpSRP43/CHAOS*. In addition, the failure to complement the *chaos* mutation with *hus1* mutated gene indicated that the stop codon introduced in *hus1* sequence is able to impair the HUS1 protein function in chloroplasts.

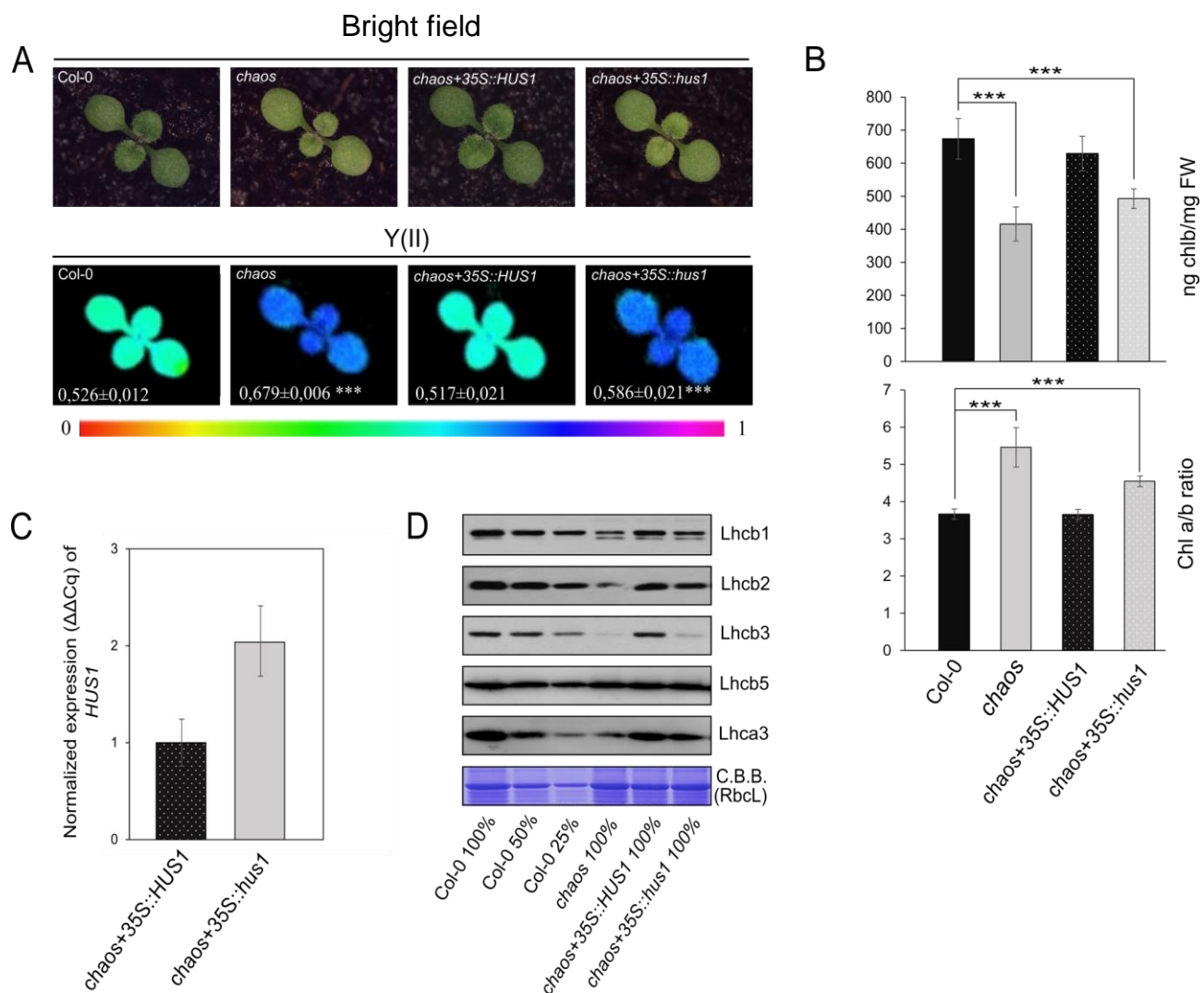
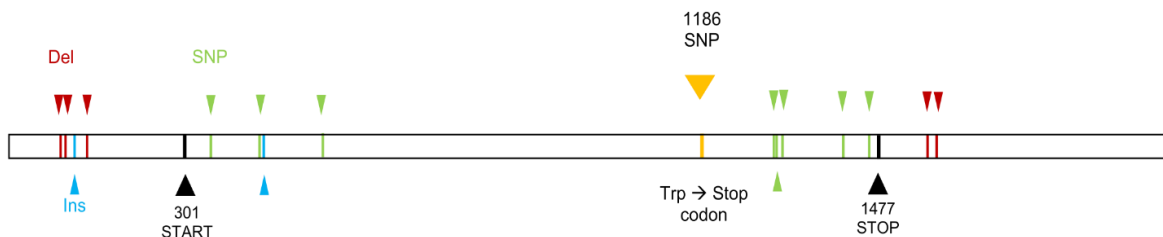


Figure 7 – *HUS1* complement Arabidopsis *chaos* mutant. (A) Visible phenotype and photosynthetic performance of Col-0, *chaos*, *chaos+35S::HUS1* and *chaos+35S::hus1* Arabidopsis lines at 8 days after sowing. Imaging-PAM values of $Y_{(II)}$ after actinic light exposure (5 minutes actinic light intensity $36 \mu\text{mol}\cdot\text{photons m}^{-2}\cdot\text{s}^{-1}$) are displayed in false colours. The increased $Y_{(II)}$ in the *chaos* and *chaos+35S::hus1* lines are statistically significant compared to Col-0 (t-Test, *** p-value < 0.001). (B) Chlorophyll a+b and the ratio a/b is shown (t-Test, p-value < 0,001 ***). (C) qRT-PCR performed on *HUS1* transcript in the two transformant lines. Histograms represent the average of three technical replicates and error bars indicate standard deviation. Two independent replicates were performed and a representative experiment is shown. (** p-value < 0.01). (D) Immuno-blot of the total protein content of Col-0, *chaos*, *chaos+35S::HUS1* and *chaos+35S::hus1* using antibodies against the antenna proteins of PSII and PSI, normalized on leaf fresh weight. Coomassie Brilliant Blue (C.B.B.) of SDS-PAGE showing the RbcL-migrating region is used as loading control.

4.5 - Identification of putative *hus1* allelic variants in the Whealbi collection

The natural genetic variability of the Whealbi collection was investigated using an allele mining approach, i.e. a reverse genetics approach, to search for a second *hus1* allele. The Whealbi collection is made of barley accessions from all over the world and includes landraces, *Hordeum spontaneum* and cultivars representing a large natural allelic variability. The exome of around 300 accessions of this collection was searched for variants in the *HUS1* gene, thanks to the collaboration with CREA of Fiorenzuola d'Arda. In these analyses, SNPs and In-Del (Insertion-Deletion) polymorphisms in the 5' UTR, CDS and 3' UTR of genes were searched (**Figure 8**). Among the 300 lines, 26 accessions were selected as possible candidates for novel *hus1* alleles (**Table 3**).

A



B

POS	REF	ALT		
620482952	CGACACACTAAATTTTAGT	C	Deletion	
620482944	CGGTA	C	Deletion	
620482938	A	AGC	Insertion	
620482931	TTCAACAAGCGCGCGGTAGCGCGACACAC	T	Deletion	
620482694	G	A	SNP	Pro16Ser
620482612	G	C	SNP	Ala43Gly
620482605	C	CGCG	Insertion	Ala45dup
620482512	G	C	SNP	Ile76Met
620481763	G	A	SNP	Ala326Val
620481734	C	G	SNP	Ala336Pro
620481733	G	C	SNP	Ala336Gly
620481721	C	A	SNP	Gly340Val
620481616	T	A	SNP	Gln375Leu
620481568	C	A	SNP	Gly391Val
620481485	GCTA	G	Deletion	
620481466	CACAACAATCTCTCGGA	C	Deletion	

Figure 8 – (A) Schematic representation of the *HUS1* locus with the positions of allelic variants of Whealbi accessions (SNPs are indicated in green, Deletion in red and Insertion in blue) and the *hus1* mutation (indicated in yellow), selected for this work. (B) The colour code indicates the type of mutation listed in table. POS = position on the chromosome. REF = sequence of the reference accession. ALT = alternative allele.

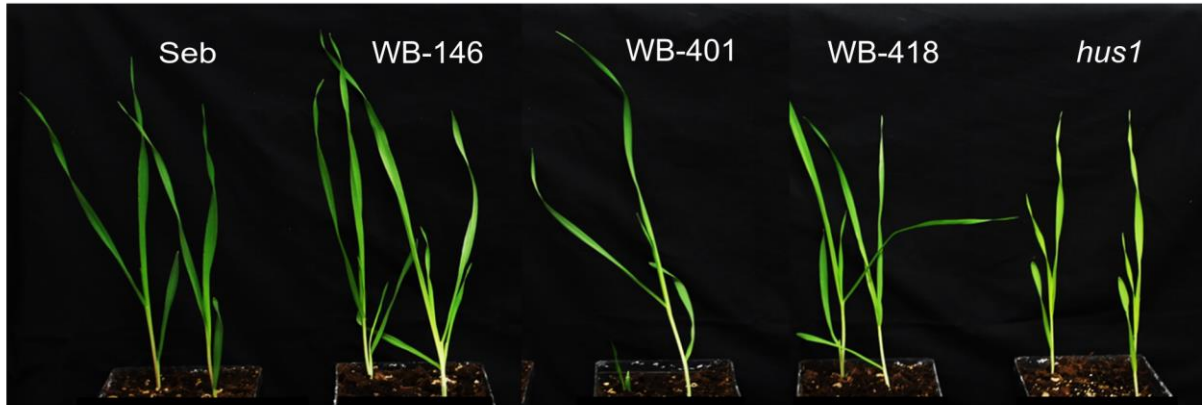
Line ID	Variety-Country of origin	Barley group category
WB-003	KW Cassia (UK)	Formally-bred cultivar
WB-033	Iran	<i>Hordeum spontaneum</i>
WB-106	Ursa-gebeizt (Germany)	Formally-bred cultivar
WB-119	IG 31424 (Syria)	Landrace
WB-122	K-14943 (Tajikistan)	Landrace
WB-146	Nigatsuko (Japan)	Formally-bred cultivar
WB-147	Buhobori (Republic of Korea)	Formally-bred cultivar
WB-149	Hyanmaeg (Republic of Korea)	Formally-bred cultivar
WB-151	Sariweon Yugmobori 1 (Republic of Korea)	Formally-bred cultivar
WB-160	Aliso (Mexico)	Formally-bred cultivar
WB-165	Compana (USA)	Formally-bred cultivar
WB-166	Diamond (Canada)	Formally-bred cultivar
WB-167	FNC 1 (Uruguay)	Breeding/research material
WB-175	Munsing (USA)	Formally-bred cultivar
WB-263	Unumli-Arpa (Uzbekistan)	Formally-bred cultivar
WB-274	Pallidum 45 (Russia)	Formally-bred cultivar

WB-284	Pallidum 4 (Ukraine)	Formally-bred cultivar
WB-291	HOR 750 (Albania)	Landrace
WB-294	FAO 3413 (Iran)	Landrace
WB-309	HOR 12830 (Syria)	Landrace
WB-361	HOR 6957 (Yemen)	Landrace
WB-401	HOR 5939 (Ethiopia)	Landrace
WB-418	HOR 10619 (Iraq)	Landrace
WB-484	FT872 (Uzbekistan)	<i>Hordeum spontaneum</i>
WB-496	HID114 (Lebanon)	<i>Hordeum spontaneum</i>
WB-500	HID219 (Afghanistan)	<i>Hordeum spontaneum</i>

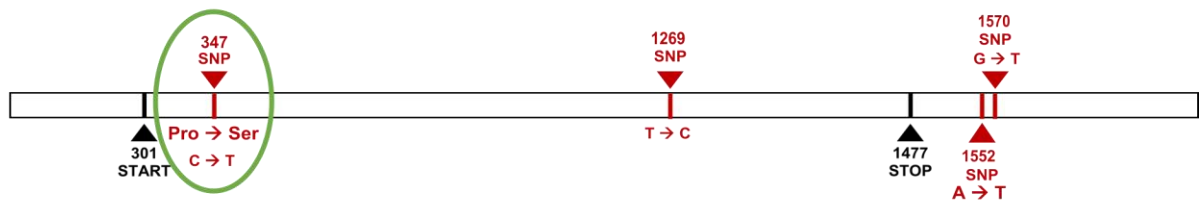
Table 3 - List of barley lines from Whealbi collection used for identifying *HUS1* allelic variants. For each line, the Line ID, the Country of origin and barley group category are indicated.

Among the 26 accessions taken into consideration, only three showed a pale-green leaf phenotype, namely WB-146, WB-401 and WB-418 (**Figure 9A**). The *HUS1* locus for these three lines was cloned and sequenced, confirming the presence of polymorphisms. The WB-146 line contained four SNPs, but only one caused a non-synonymous substitution (Proline into Serine) (**Figure 9B**), in the WB-401, a Glycine was substituted by a Valine (**Figure 9C**), while in WB-418 two SNPs led to change an Alanine into a Valine and a Glutamine into a Leucine (**Figure 9D**).

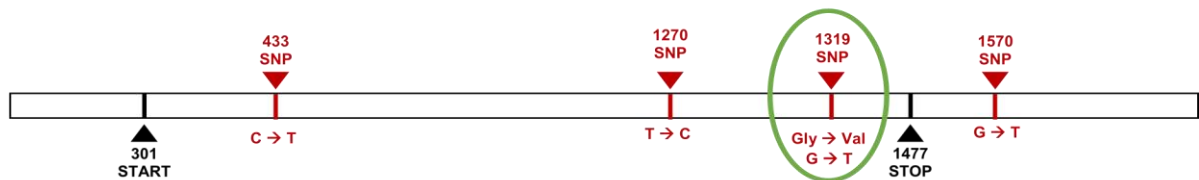
A



B



C



D

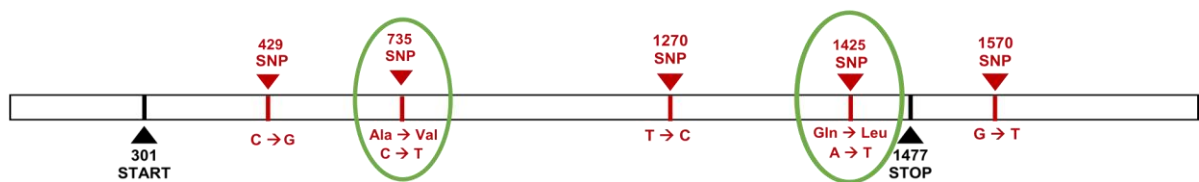


Figure 9 – WB-146, WB-401 and WB-418 phenotypes and allelic variants in *HUS1* locus. (A) Pale phenotype accessions from Whealbi collection containing allelic variants in *HUS1* locus, next to the dark green Sebastian and the pale mutant *hus1*. **(B)** Schematic representation of *HUS1* gene

with corresponding allelic variants in WB-146, (C) WB-401 and (D) WB-418. Polymorphisms resulting into amino acid changes are circled.

In order to study the photosynthetic performance, physiological analyses were conducted on these three accessions. After 30 minutes of dark-adaptation plant leaves were subjected to increasing actinic light intensities for 40 minutes (0 to 1287 $\mu\text{mol}\cdot\text{photons m}^{-2}\cdot\text{s}^{-1}$) and the $Y_{(II)}$ and the NPQ parameters were measured by using the Dual-PAM 100 fluorometer. Under increasing light intensity WB-401 showed a markedly higher photosynthetic efficiency and a reduction of NPQ as showed in **Figure 10A, B**, while WB-146 showed values similar to *hus1*. On the other hand, WB-148 had a trend similar to Sebastian control. Pigment content analysis (**Figure 10C**) showed the reduction of chlorophyll b compared to the chlorophyll a in all the three accessions, displaying an intermediate level between the pale mutant *hus1* and the dark green Sebastian, as displayed by chlorophyll a+b and chl a/b values. Immuno-blot analysis on leaf total proteins showed that the levels of accumulation of antenna proteins in the three lines remained unchanged compared to Sebastian, while Lhcb2, Lhcb3 and Lhca1 were dramatically reduced in *hus1* (**Figure 10D**).

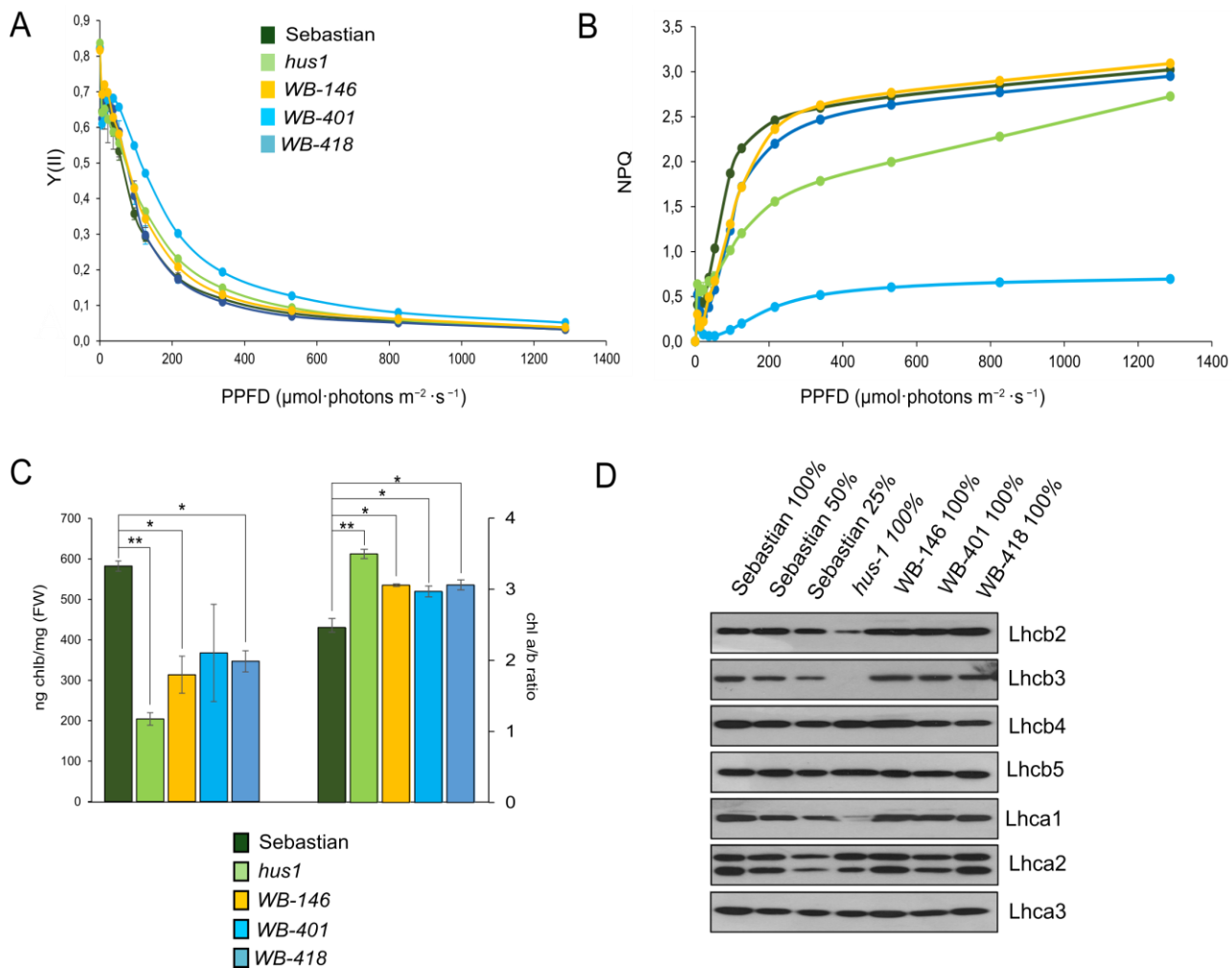


Figure 10 – (A) and (B). Light curves were performed using the Dual-PAM fluorometer. The $Y(II)$ and the NPQ values were measured under increasing light intensity from 0 to 1287 $\mu\text{mol}\cdot\text{photons m}^{-2}\cdot\text{s}^{-1}$ (x-axis, PPF = Photosynthetic Photon Flux Density). Curves represent the average of three technical replicates and error bars indicate standard deviation. Two independent replicates were performed and a representative experiment is shown. (C) Chl b content, normalized on FW (Fresh Weight) is statistically (t-Test, p-value < 0,05 *, p-value < 0,01**) decreased in *hus1*, WB-146, WB-418 compared to Sebastian and Chl a/b ratio was increased. Error bars in the histogram indicate standard deviation. (D) Immuno-blot analysis of antenna proteins underlines the fact that there are no defects in the antenna proteins accumulation in the Whealbi lines, unlike *hus1*.

In order to test whether the allelic variants of *HUS1* are actually responsible for the pale-green pigmentation, the increased photosynthetic yield and the reduced content of chlorophyll b in the Whealbi lines, a complementation test of Arabidopsis mutant

chaos was carried out. The CDS of these three allelic variants was cloned and expressed under the control of the constitutive promoter CaMV35S into *chaos* genetic background. In the T₁ generation, all three constructs were able to restore the dark green phenotype and the photosynthetic parameters of the wild-type control (Col-0), proving that none of the identified allelic variants was a strong allele as *hus1* (**Figure 11**). Overall, the allelic variants identified in WB-401 and WB-418 resulted to have different characteristics with respect to the *hus1* allele, thus they were not instrumental for the identification of a second *hus1* allele. Nevertheless, crosses between *hus1* and WB-401 and WB-418 lines have been performed and the resulting F₁ generations, not available at the time this thesis is written, will allow to clarify whether these lines carry weak allelic versions of the strong *hus1* allele.

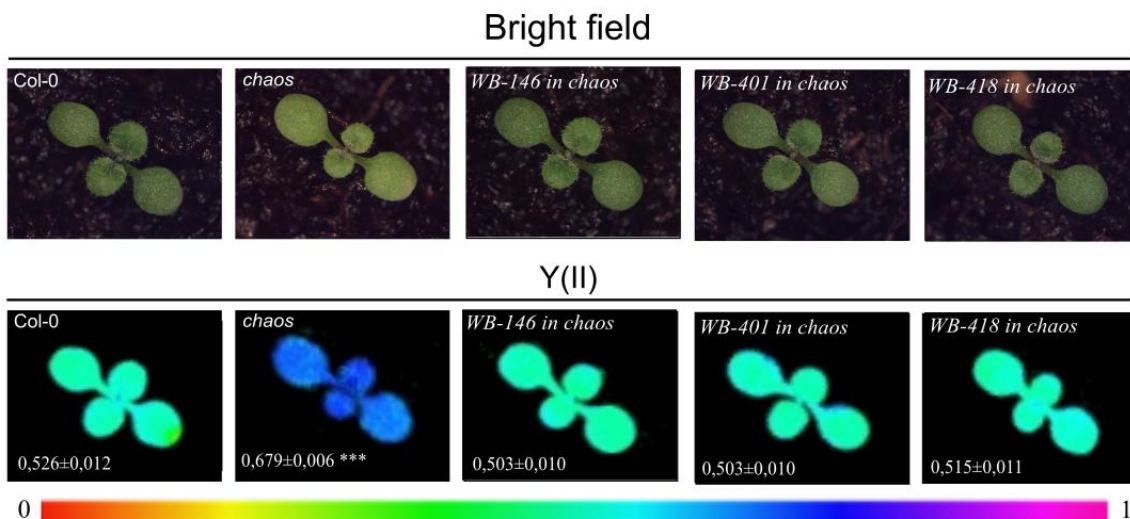


Figure 11 – Complementation test with Whealbi allelic variants. Imaging-PAM values of Y_(II) of Col-0, *chaos*, *chaos*+35S::*HUS1*(WB-146), *chaos*+35S::*HUS1*(WB-401) and *chaos*+35S::*HUS1*(WB-418) Arabidopsis lines at 8 days after sowing, displayed in false colours, after actinic light exposure (5 minutes to actinic light intensities 36 $\mu\text{mol}\cdot\text{photons m}^{-2}\cdot\text{s}^{-1}$). The difference in Y_(II) values between *chaos* and all the other genotypes is statistically significant (t-Test, *** p-value < 0.001).

4.6 - Phenotypical description of a TILLMore mutant line altered in photosynthesis

In attempt to identify a second mutated allele for *HUS1* gene, mutants with pale phenotype and altered in photosynthetic performance were searched in a chemically mutagenized population, the TILLMore [40]. Created by mutagenizing the Morex cultivar with sodium azide, the TILLMore population was screened in the field conditions, in collaboration with the Prof. Silvio Salvi at the University of Bologna. Among those a subset of 24 mutated lines were taken into consideration for increased photosynthetic efficiency and pale phenotype observed in the field. In greenhouse conditions, only the line *TM-2490* retained the pale phenotype and higher photosynthetic parameters, compared to Morex control, observed in the field (**Figure 12A**). Considering this, the line *TM-2490* seemed to be a good candidate for a second allele of *hus1* and the sequence of *HUS1* locus was analysed to verify the presence of possible mutations in *TM-2490*. Unfortunately no difference was found in *TM-2490* respect to the Morex control sequence and the *TM-2490* was excluded as a possible second allele for *hus1*.

However, *TM-2490* showed interesting features and was characterized more into details. *TM-2490* showed a wild-type-like growth rate, size and grain production (**Figure 12A**), a reduced accumulation of total chlorophylls (Chl a+b), and increased Chl a/b ratio, due to lower chlorophyll b content (**Figure 12B**). *TM-2490* showed an improved photosynthetic efficiency in low- and high-light conditions and a lower NPQ compared to Morex (**Figure 12C-D**).

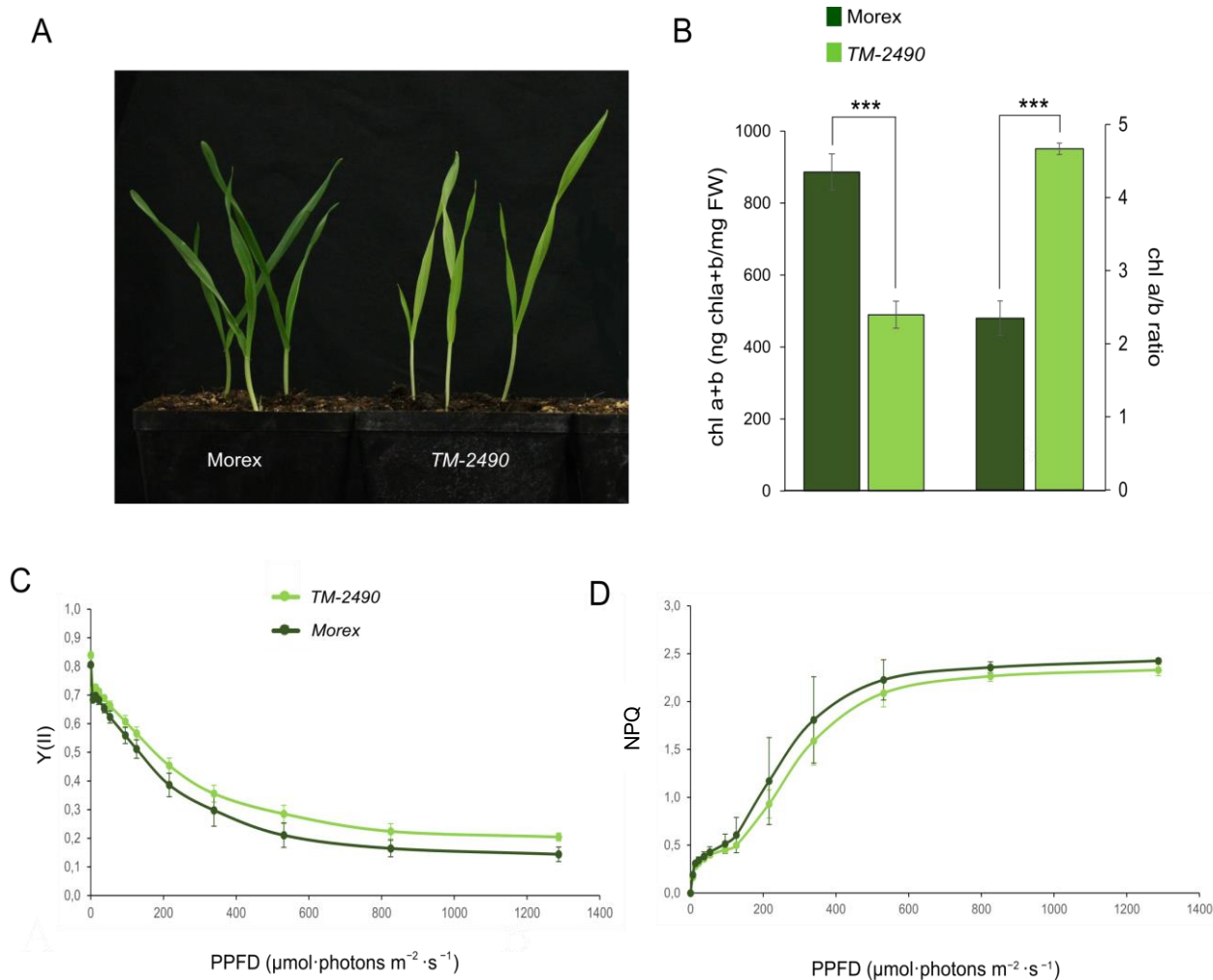


Figure 12 – Preliminary analysis of *TM-2490*. (A) and (B) display light curves of 40 minutes were performed using the Dual-PAM fluorometer. The Y(II) and the NPQ were taken under increasing light intensity from 0 to 1287 $\mu\text{mol}\cdot\text{photons m}^{-2}\cdot\text{s}^{-1}$ (x-axis, PPFD = Photosynthetic Photon Flux Density). Curves represent the average of three technical replicates and error bars indicate standard deviation. Two independent replicates were performed and a representative experiment is shown. *TM-2490* has an increased photosynthetic performance compared to the control Morex. (C) Chl a+b content, normalized on FW (Fresh Weight) is statistically (t-Test, p-value < 0,01***) decreased in *TM-2490*, compared to Morex, especially the Chl b content as show by the increasing ratio between Chl a and Chl b. Error bars in the histogram indicate standard deviation.

Immuno-blots on SDS-PAGE fractionated total proteins revealed no major differences with Morex regarding the accumulation of antenna proteins, except for Lhca1, Lhcb6 accumulation that seemed decreased (**Figure 13A**). Intriguingly, thylakoid isolated proteins fractionated by SDS-PAGE and stained with Coomassie Brilliant Blue show

that the antenna proteins Lhca and Lhcb are markedly reduced in *TM-2490*, compared to Morex (**Figure 13B**). This observation differs from the C.B.B. staining of total protein extraction and the immuno-blot analyses, suggesting that although the LHCs proteins might accumulate in the cell and in chloroplasts, they seem not to be correctly integrated in the thylakoid membrane and therefore to be not functional.

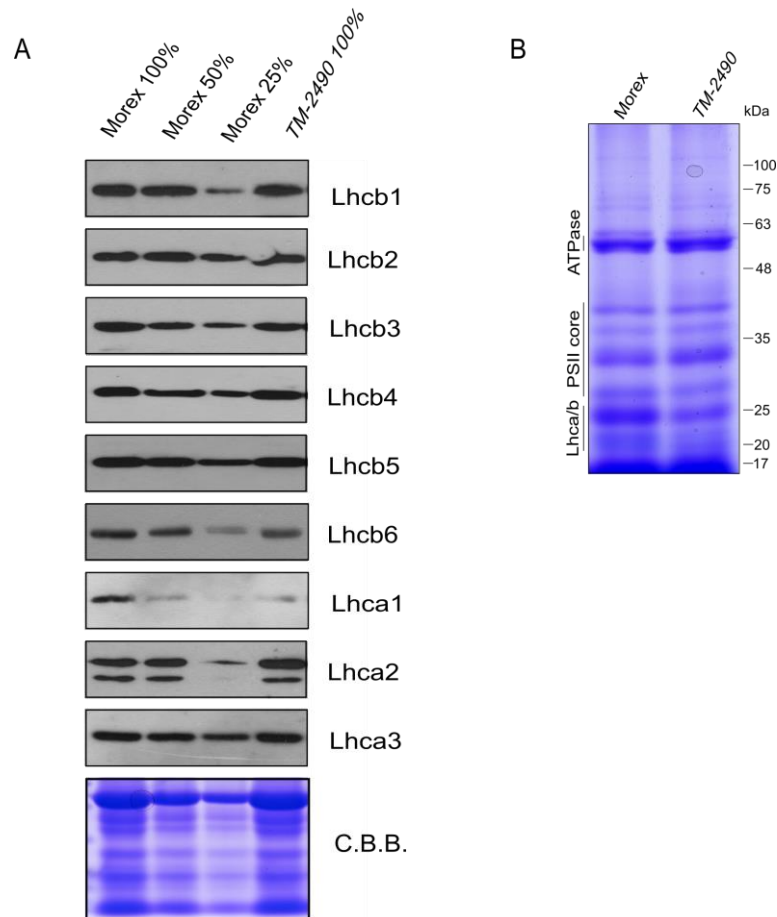


Figure 13 - (A) Immuno-blot analysis of several antenna proteins displays no defects in the antenna proteins accumulation in *TM-2490*. Coomassie Brilliant Blue (C.B.B.) of RbcL-migrating region was used as loading control. **(B)** SDS-PAGE gel was stained with Coomassie Brilliant Blue, containing the thylakoid proteins of Morex and *TM-2490*. The amount of Lhca and Lhcb proteins, see migration region between 25 and 20 KDa, are reduced in *TM-2490* mutant.

4.7 - HUS1 physical interacts with barley cpSRP54 protein

The light-harvesting chlorophyll a/b binding proteins (LHCP) are hydrophobic nuclear-encoded proteins that need the so-called “transit complex” to form a soluble complex in the stroma with the final aim to be integrated into the thylakoid membrane [117]. This “transit complex” is a heterodimer formed by the cpSRP43/cpSRP54 complex, well characterized in higher plants [118][119][114]. To investigate whether this complex is conserved also in barley, the amino acid sequence of the Arabidopsis cpSRP54 protein (At5g03940) was used to query the barley genome. The BLAST analysis on the IPK server identified two sequences of putative HvcpSRP54, *HORVU.MOREX.r2.4HG0293270* (from now on *HvcpSRP54-1*) and *HORVU.MOREX.r2.4HG0293280* (from now on *HvcpSRP54-2*). As show in **Figure 14A**, the alignment of these two sequences with the Arabidopsis cpSRP54, points out a higher homology between them. *HvcpSRP54-1* and *AtcpSRP54* have identities score of 361/498 with a percentage of 72%, while *HvcpSRP54-2* and *AtcpSRP54* an identity of 354/468 with a percentage of 76%. qRT-PCR performed on both transcripts in the background Sebastian showed the higher expression of *cpSRP54-1* with respect to *cpSRP54-2* (**Figure 14B**), revealing that one of the two gene prevails on the other one. Interestingly, in the *hus1* genetic background the *cpSRP54-1* transcript was found ten times down-regulated with respect the control Sebastian, suggesting that the altered expression of *cpSRP43* gene is able to influence the expression of *cpSRP54*, most probably with the aim to maintain the correct stoichiometry between the two chloroplast located proteins (**Figure 14C**).

Conserved amino acid are shown in red, strongly similar residues in yellow and light blue amino acids with weakly similar properties according to Clustal Omega software. (B) qRT-PCR performed on *HORVU.MOREX.r2.4HG0293270* (*HvcpSRP54-1*) and *HORVU.MOREX.r2.4HG0293280* (*HvcpSRP54-2*) transcripts in Sebastian background. (C) qRT-PCR performed on barley *cpSRP54-1*, *cpSRP54-2* and *HUS1* in Sebastian and *hus1* background represents the average of three technical replicates and error bars indicate the standard deviation. Two independent replicates were performed and a representative experiment is shown. (t.Test, ** p-value < 0.01 *** p-value < 0.001).

Once identified the *cpSRP54-1* as the best candidate for interaction tests with *HUS1/HvcpSRP43*, based on expression and similarity, the yeast two-hybrid assay was performed (**Figure 15**). The CDS, devoid of the cTP of *HUS1/HvcpSRP43* (wild-type and *hus1* mutated versions) and *HvcpSRP54-1* were cloned downstream the GAL4 DNA Binding Domain (BD) and the GAL4 DNA Activation Domain (AD), respectively. All the strains were able to grow on the permissive medium devoid of Tryptophan and Leucine (-W -L). On selective media lacking histidine (-W -L -H) and supplemented with 10 mM of 3-amino-1,2,4-triazole (3-AT), a competitive inhibitor for the HIS3 reporter gene, the interaction between cpSRP54 (AD) and cpSRP43 (BD), cpSRP43 (AD) and cpSRP54 (BD), and the homodimer of cpSRP43 were shown. This suggests that HUS1/cpSRP43 can form protein complexes with cpSRP54 and form cpSRP43-cpSRP43 homodimers, similarly to what observed in Arabidopsis [120], suggesting a functional conservation of the cpSRP complex also in barley. Intriguingly, no interaction between cpSRP54 and the mutated cpSRP43 encoded by *hus1* was observed, suggesting that the truncated version of HUS1 protein is unable to form heterodimers, thus causing the pale-green leaf phenotype observed in the *hus1* barley mutants.

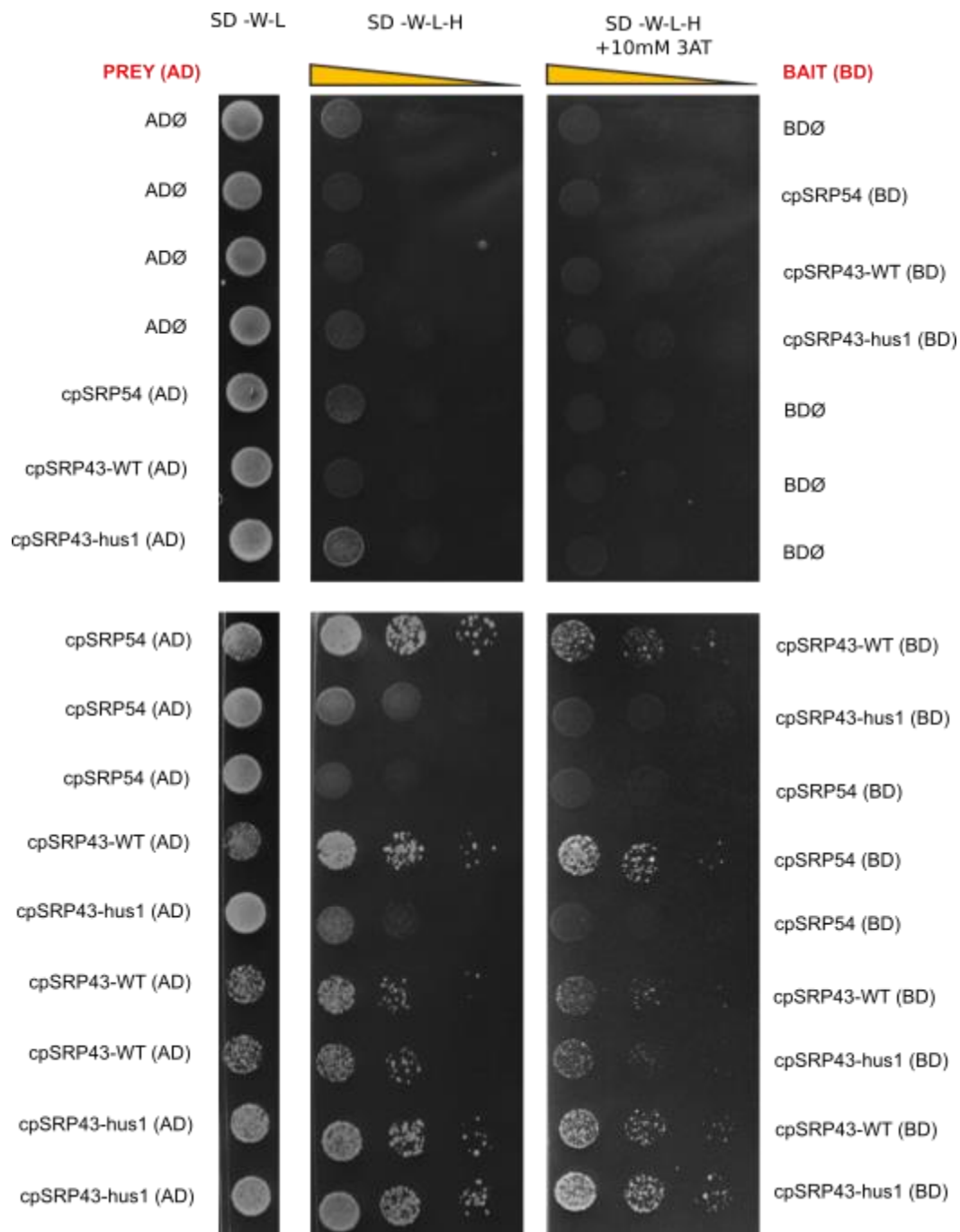


Figure 15 - Yeast two-hybrid interaction assay. cpSRP43 of Sebastian (HvcpSRP43-WT), cpSRP43 of *hus1* (HvcpSRP43-hus1) and cpSRP54 were tested for their physical interaction in both combinations with GAL4 DNA Binding Domain (BD) and the GAL4 DNA Activation Domain (AD). AD ∅ and BD ∅ empty vectors. -W -L, permissive medium devoid of Tryptophan and Leucine; -W -L -H, selective medium devoid of Tryptophan, Leucine, Histidine and supplemented with 10 mM 3-AT (3-Amino-1,2,4-triazole, a histidine biosynthesis inhibitor).

4.8 – Characterization of barley *VDE* allelic variants

As previously described (see introduction and aim of the work), in addition to the search for barley mutants and barley allelic variants with reduced antenna size, of great interest are also those barley lines carrying modifications in the regulation of photoprotection mechanisms, including NPQ (Non-Photochemical Quenching). This is particularly true, if the decrease in the antenna size causes a reduction in NPQ, as observed in *hus1* leaves. Therefore, a search was conducted with the aim to identify allelic variants for the genes involved in the xanthophyll cycle, a main constituent of NPQ. As first, the gene that codes for the enzyme involved in the conversion of violaxanthin into zeaxanthin, the *VDE* (Violaxanthin DEpoxidase) was taken into consideration. Using a TILLING approach, an allelic series for the *VDE* gene (*HORVU.MOREX.r2.2HG0133130.1*) was identified in collaboration with the University of Silesia in the chemical mutagenized population, HorTILLUS. Among them the *vde-a*, *vde-b*, *vde-g*, *vde-l*, *vde-h* (**Table 4**) were taken into consideration (**Figure 16**).

Allele	Mutation type	Nucleotide change	Amino acid change
<i>vde-a</i>	missense	C1178T	P248L
<i>vde-b</i>	missense	G1202A	G256E
<i>vde-g</i>	missense	C1496T	P327L
<i>vde-l</i>	missense	G1701T	E395D
<i>vde-h</i>	missense	G1630A	G372R

Table 4 – The five *VDE* allelic variants, their type of mutation together with nucleotide and the consequent aa exchange.

These five alleles contain mutations in two different protein domains: the lipocalin domain, where the catalytic site is present, and glu-rich domain, considered as the site for binding to the thylakoid membrane (**Figure 16B**).

Although plant lines carrying *vde-a*, *vde-b*, *vde-g*, *vde-l* and *vde-h* mutations showed no visible phenotype, similarly to what observed in other plant species as Arabidopsis [103], these mutants displayed an altered kinetics of NPQ (Non-Photochemical Quenching). In particular, after 30 minutes of adaptation to the dark, plants were subjected to an induction-relaxation curve, i.e. for 4 minutes under light ($36 \mu\text{mol}\cdot\text{photons m}^{-2}\cdot\text{s}^{-1}$) and then two minutes in the dark, using the Dual-PAM fluorometer. As it can be seen from **Figure 16C**, the *vde-b*, *vde-g*, *vde-l* and *vde-h* mutants showed heterogeneous induction and relaxation kinetics of NPQ, while *vde-a* mutant showed a Sebastian-like trend.

More into details, *vde-b*, *vde-g* and *vde-h* alleles displayed a total reduction of NPQ compared to the Sebastian control, particularly *vde-b* had a faster relaxation of this mechanism (**Figure 16C**). This suggests that the polymorphisms identified in *vde-b*, *vde-g*, *vde-l* and *vde-h* alter the enzymatic properties of VDE, resulting in altered NPQ induction and relaxation kinetics.

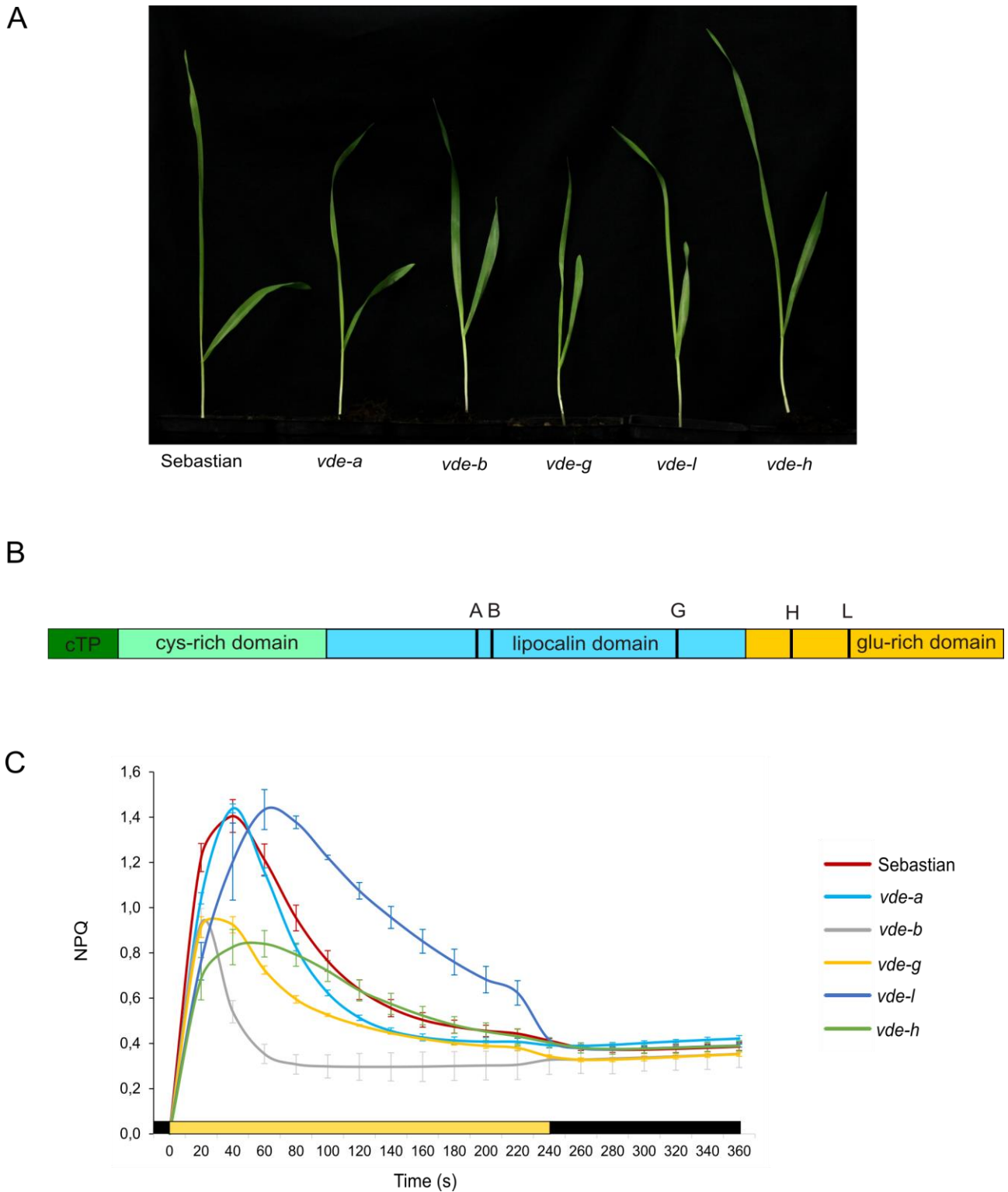


Figure 16 – Phenotype and genotype of 5 allelic variants of VDE gene from HortILLUS population. (A) The 5 VDE lines analysed in this work display a Sebastian like phenotype. (B) Schematic representation of VDE protein. *vde-a*, *vde-b*, *vde-g*, *vde-l* and *vde-h* (indicated as A, B, G, L and H) have SNPs located in different position, causing amino acid changes in the lipocalin domain and glu-rich domain. cTP (chloroplast Transit Peptide) is shown in dark green. (C) Induction-

relaxation curves of *VDE* alleles, NPQ measurements were performed using the Dual-PAM 100 fluorometer. After 30 minutes of dark adaptation the plants were subjected to light ($36 \mu\text{mol}\cdot\text{photons m}^{-2}\cdot\text{s}^{-1}$) for 4 minutes and then incubated for 2 minutes into the dark. Curves represent the average of three technical replicates and error bars indicate standard deviation. Three independent biological replicates were analysed and a representative experiment is shown.

In collaboration with Prof. Peter Jahns at the University of Duesseldorf, a detailed analysis of the xanthophyll cycle, obtained by measuring the xanthophyll accumulation in Sebastian, *vde-b*, *vde-g*, *vde-l* and *vde-h* plants, was performed. In **Figure 17A** the de-epoxidation state of the xanthophyll cycle pigments (DEPS), the percentage of Vx (Violaxanthin) and the percentage of Zx (Zeaxanthin) in the different alleles in dark conditions and after illumination are shown. DEPS indicates the rate of zeaxanthin conversion among the total concentration of the pigments involved in the xanthophyll cycle: lower value means lower concentration of zeaxanthin and less NPQ activation. *vde-b*, *vde-g* and *vde-l* showed a lower de-epoxidation rate at 130 μE , especially after 10 minutes illumination (L10), while *vde-a*, *vde-b* and *vde-g* seem to have a higher de-epoxidation rate at 1200 μE illumination **Figure 17A**. After 10 minutes of illumination, the percentage of Vx in low light (130 μE) was higher for *vde-b*, *vde-g* and *vde-l*, compared to Sebastian control, implying that those alleles have lower NPQ activation rate under this condition. *vde-a*, *vde-b* and *vde-g* show lower concentration of Vx, especially after 15 minutes of high light illumination (1200 μE), compared to the wild type. These results are confirmed by the increased Zx percentage, meaning that these mutant lines show a higher concentration of the pigment involved in NPQ, after 15 minutes of exposure to high light (1200 μE) (**Figure 17A**).

Immuno-blot analysis (**Figure 17B**) was also performed in order to study the proteins accumulation of the components involved in the xanthophyll cycle and in the ETC. The VDE enzyme, in all the barley mutants, accumulated as in the Sebastian control, indicating that the altered NPQ kinetics are not due to different amount of the enzyme, but rather to changes in the enzymatic properties. Similarly, the ZEP (Zeaxanthin

Epoxidase, the enzyme that carries the opposite reaction to the VDE) and PsbS, (Photosystem II 22 kDa protein, a thylakoid membrane protein involved in the VDE activation) amounts were unchanged, as the other components of the photosynthetic apparatus.

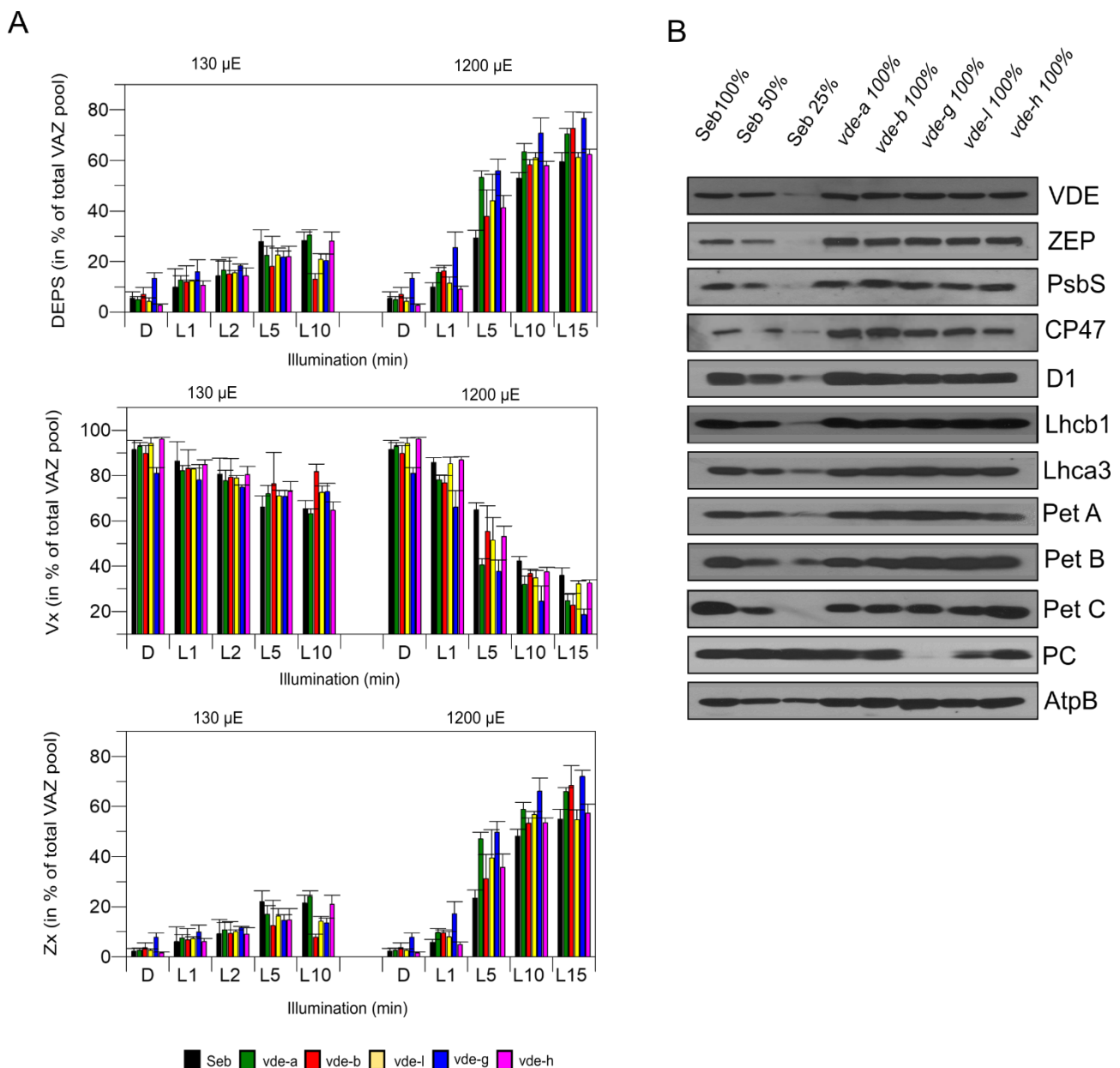


Figure 17– Characterization of the five VDE alleles. (A) Pigment measurements performed using HPLC. The leaf samples were collected from plants adapted to the dark (D) and after illumination: L1: one minute, L2: two minutes, L5: five minutes, L10: ten minutes, L15: fifteen minutes. Light intensity is 130 μ E or 1200 μ E. On the y-axis the DEPS = $[(Zx + Ax) / (Vx + Ax + Zx)] * 100$. Zx =

zeaxanthin, Ax = antheraxanthin, Vx = violaxanthin. **(B)** Immuno-blot analysis of total proteins of the xanthophyll cycle and proteins of the photosynthetic apparatus in Sebastian and in the 5 *VDE* allelic variants.

4.9 - Complementation assay with *VDE* allelic variants of *Arabidopsis thaliana npq1* mutant

To test whether the SNPs present in the *VDE* gene are responsible for the observed alteration of the NPQ kinetics and exclude the effect of other mutations in the barley genome, a complementation experiment where the barley allelic variants were introduced into the *npq1-2* (*non-photochemical quenching 1*; [103]) mutant of *Arabidopsis*, lacking the VDE enzyme, was carried out. *npq1-2* plants were transformed with a construct carrying the CDS of the five *HvVDE* allelic variants and *HvVDE* from Sebastian under the control of CaMV35S promoter. The presence of the constructs was verified by PCR in the T₁ generation and the accumulation of VDE protein was tested by immuno-blot analysis (**Figure 18A**). On the T₂ generations induction-relaxation curves analyses were performed using the Dual-PAM, i.e. for 4 minutes under light (36 $\mu\text{mol}\cdot\text{photons m}^{-2}\cdot\text{s}^{-1}$) and then two minutes in the dark. The barley VDE protein variants appeared to complement the phenotype of *npq1-2* and different kinetics were observed among the allelic variant with a similar trend as the measurements performed on barley plants for *vde-b* and *vde-g* complemented lines (**Figure 18B**). However, a detailed analysis of these lines is still missing. This preliminary analysis conducted on T₂ generation with Dual-PAM will be repeated in detail in the T₃ generation, where homozygous transgenic lines will be identified.

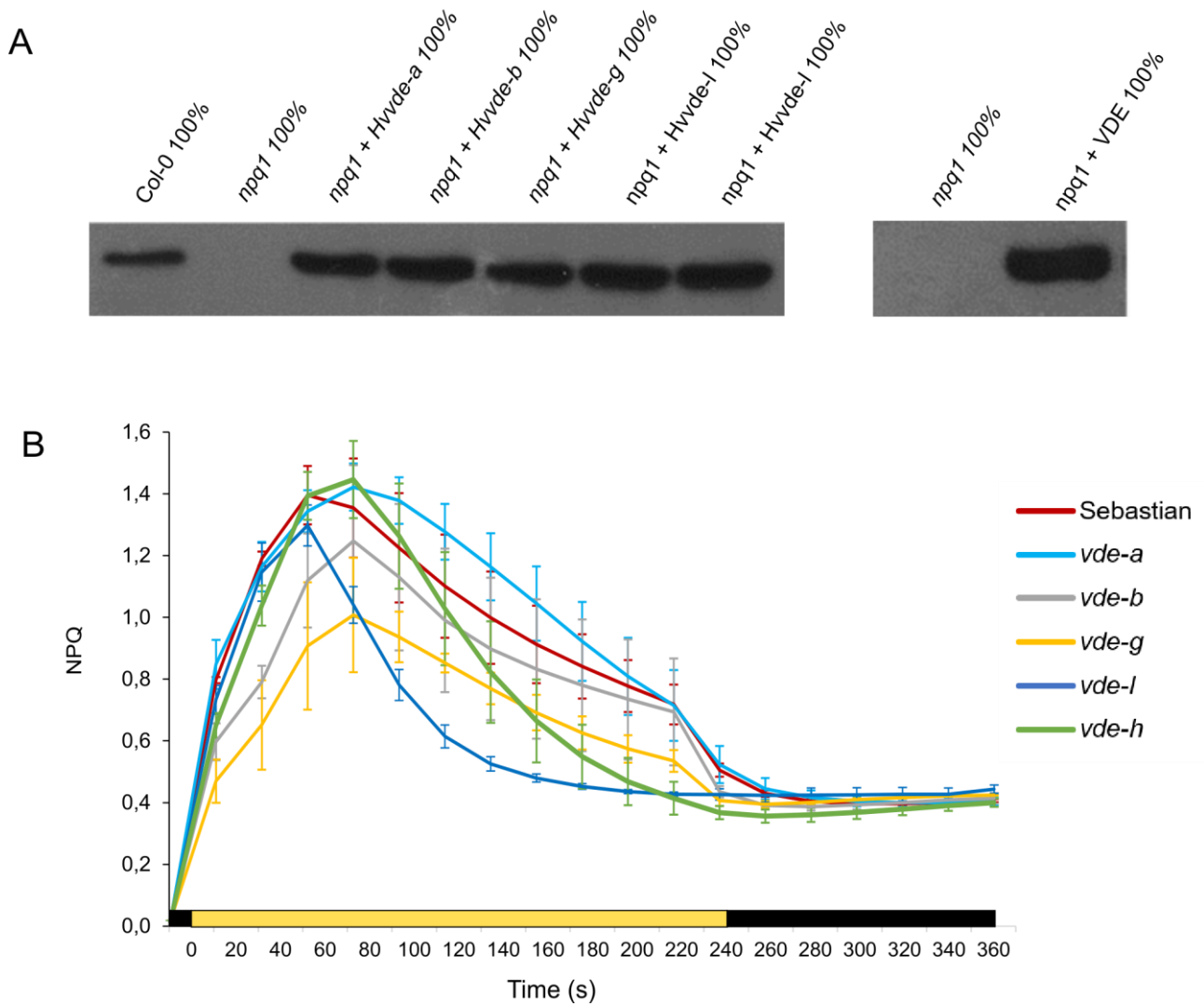


Figure 18 – Complementation assay of barley *VDE* allelic variants in *Arabidopsis npq1-2* mutant. (A) Immuno-blot assay of VDE protein in Col-0, *npq1-2*, *npq1-2 + Hvvd-e-a*, *npq1-2 + Hvvd-e-b*, *npq1-2 + Hvvd-e-g*, *npq1-2 + Hvvd-e-l*, *npq1-2 + Hvvd-e-h* and *npq1-2 + HvVDE* in T₁ generation. (B) Induction-relaxation curves of *VDE* allelic variants in *Arabidopsis npq1-2* mutant. NPQ measurements were performed using the Dual-PAM fluorometer. After 30 minutes of dark adaptation the plants were subjected to light ($36 \mu\text{mol}\cdot\text{photons m}^{-2}\cdot\text{s}^{-1}$) for 4 minutes and then incubated for 2 minutes into the dark. Curves represent the average of three technical replicates and error bars indicate standard deviation. Three independent biological replicates were analysed and a representative experiment is shown.

4.10 - Preliminary characterization of barley *ZEP* allelic variant

From the HorTILLUS population one allelic variant of *ZEP* (Zeaxanthin EPoxidase) gene was isolated as well (*HORVU.MOREX.r2.2HG0142080*). This line carries a SNP in position 3633 from the first ATG START codon (C->T), causing an amino acid change from a Proline-to-Leucine in position 407 (**Figure 19A**). Furthermore, very preliminary analysis shows that *zep-1* has an increased NPQ compared the control Sebastian (**Figure 19B**) as previously observed in the corresponding *Arabidopsis thaliana* mutant [103], making this allelic variant another promising candidate to modify the NPQ induction-relaxation kinetics in barley.

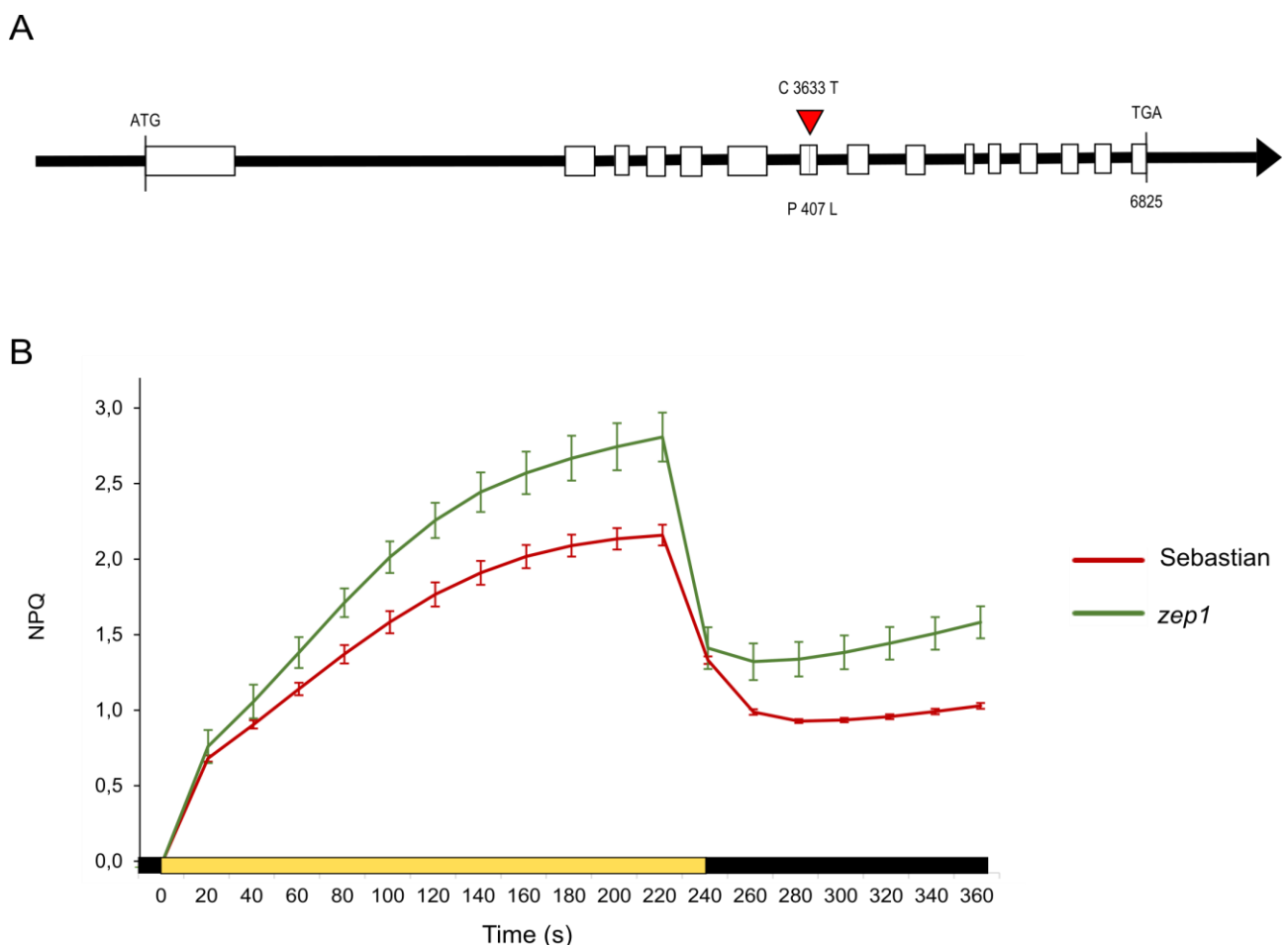


Figure 19 – Preliminary characterization of *zep1* allele. (A) Schematic representation of *HORVU.MOREX.r2.2HG0142080* gene. The white rectangles indicate the exons while the black lines the introns. The red triangle indicates the SNP mutation present in *zep1* allele. (B) Induction-

relaxation curves of Sebastian control and *zep1* mutant. NPQ measurements were performed using the Dual-PAM fluorometer. After 30 minutes of dark adaptation the plants were subjected to light ($166 \mu\text{mol}\cdot\text{photons m}^{-2}\cdot\text{s}^{-1}$) for 4 minutes and then incubated for 2 minutes into the dark. Curves represent the average of three technical replicates and error bars indicate standard deviation. Two independent biological replicates were analysed and a representative experiment is shown.

5 - Conclusions and future perspective

In this work we identified novel genes and alleles involved in antenna size determination and modulation of NPQ in barley. Using a forward genetic approach, the *hus1* mutant, isolated from the chemically mutagenized population HorTILLUS [39], showed a marked reduction of the antenna size and the increased photosynthetic performance upon low- and high-light illumination. *HUS1* turned out to be homologous to *cpSRP43*, encoding a chloroplast-located protein chaperone involved in LHCs insertion into the thylakoid membrane, characterized in several plant species [113][118][119][114]. Although in a natural environment, the natural selection has favoured the development of large antenna complexes able to capture large amount of light and compete with surrounding organisms, this trait might be disadvantageous in monoculture fields. In this context the competition among plants is counterproductive, while the large antenna size exposes the plant to the risks of over-absorption of solar irradiance at the top of the canopy, forcing the plant to waste energy in engaging photoprotection mechanisms, the leaves in the bottom part of the canopy are under shadow conditions and perform a low efficient photosynthesis [31].

According to previous studies and computational models, among the light-to-biomass optimization breeding strategies, the reduction of the light-harvesting antenna of the photosystems is an interesting trait to be explored for increasing crop productivity [18]. Chlorophyll-reduced crops are expected to distribute the light absorption more evenly in the canopy, due to the fact that the light can filter through the canopy and reach the bottom part [52][20], leading to overall higher photosynthetic performance [121]. This is corroborated by our studies on *hus1*, able to show an improved $Y_{(II)}$, the effective quantum yield of PSII, in low- and, especially, high-light conditions. Intriguingly, comparing field trials in Spain, north of Italy and Poland performed by partners of the BarPLUS project, *hus1* seems to be better performing in Spain, where the all over solar irradiance is higher during the summer. In fact, *hus1* produced 7.42 ± 0.30 t / ha of

grain and 1.380 g/m² of dry biomass, while Sebastian yielded 6.73 ± 0.53 t/ha of grain and 1.290 g/m² of biomass. In addition, *hus1* seems to better perform at high-density field cultivation, as observed in our very preliminary field measurements (data not shown), possibly due to the better light penetration through the dense canopy. Studies performed in tobacco have shown indeed that pale-green plants, grown at high density, produce more biomass [31]. Furthermore, the advantages listed are due not only to the plant density but also to the pale phenotype, as these crops would achieve canopy closure more quickly and thus (i) minimize losses of soil moisture, (ii) lower the amount of fertilizer needed, particularly nitrogen, which is largely used for chlorophyll and antenna protein synthesis. Also, smaller size higher density plots would minimize fertilizer runoff, and (iii) alleviate the need to use herbicides, as quick and unbroken canopy closure will create the shading needed to prevent, or minimize, the growth of weeds; (iv) lower the water requirement for growth since heat production from thermal dissipation of absorbed light (approx 96-99% in dark green plants) will be lower and less transpiration will be required furthermore regulation. Among the various bio-geo-engineering strategies, introducing the pale-green trait in crops also seems to be a very promising strategy for solar radiation management, potentially able to modify the local climate by mitigating the planet–surface temperature [70][67][122]. Indeed, the pale soybean mutant MinnGold can reflect a higher fraction of the solar radiation, compared to the green control, determining a temperature decrease at the level of the canopy [59]. For *hus1* mutant, further field analyses in different seasons and climate conditions are necessary to statistically validate the correlation between the improved *hus1* biomass production in hot and arid climates and high-density conditions.

Although the *hus1* phenotype is due to the silencing in an already known gene, *hus1* is the first mutant in *cpSRP43* locus identified in *Hordeum vulgare*. The exome capture sequencing led us to identify the *hus1* mutation in the *cpSRP43* gene, well characterised in *Arabidopsis thaliana* [113], in *Oryza sativa* ssp. *indica* [123], *Oryza sativa* ssp. *japonica* [124] and on maize [125]. The analysis of barley and *Arabidopsis hus1/chaos* mutants and the complementation of the *chaos* with the WT and mutated version of

barley *HUS1* led to conclude that *HUS1* is the functional orthologue of *AtcpSRP43* and the SNP identified in *HUS1* sequence is undoubtedly the cause of *hus1* phenotype. The yeast two hybrid assays displayed the physical interaction between cpSRP43/HUS1 and cpSRP54, as observed in Arabidopsis [120]. This heterodimerization is responsible for the translocation of antenna proteins in the thylakoid membrane, because the “transit complex” is a trimer composed of one cpSRP43 dimer and one cpSRP54 monomer [113][114][126][127]. Intriguingly, the heterodimer of cpSRP43 and cpSRP54 [120] is formed with *HUS1* WT sequence while it is abolished by *hus1* mutation. Although, the research for the *hus1*-like allele in the natural variability of the Whealbi and in the chemically mutagenized population of the TILLMore did not succeed, this led to the identification of new pale mutants suitable for further studies. The *TM-2490* line showed indeed a pale phenotype, reduced total chlorophyll and higher photosynthetic yield in low- and high-light. Moreover, the three slightly pale allelic variants WB-146, WB-401 and WB-418 could reflect environmental adaptations to climates where solar radiation is high (Ethiopia for WB-401 and Iraq for WB-418) and have been selected by local farmers for their increased productivity under field conditions, confirming that under specific environmental conditions the pale-green trait represents a major advantage for agriculture practices. A detail investigation of these accessions will allow to gain important information to be used in future breeding programs. A possible fast alternative to obtain the second allele of *HUS1* gene could be obtained through specific silencing of this gene via Virus-Induced Gene Silencing (VIGS) [128]. The transient silencing of the gene of interest was achieved exploiting the natural molecular mechanism of RNA interference.

Nevertheless, the reduction in the antenna size leads to a decrease in NPQ, as observed in *hus1*, possibly explaining the decrease in yield observed when *hus1* was cultivated in Italy and Poland (data obtained by partners of BarPLUS project). This reduction in yield has been also observed in the pale-green soybean mutant MiniGold [59], indicating that under fluctuating environmental conditions the activity of NPQ mechanism is a major determinant of plant yield. To address this issue, we used a

reverse genetics approach, to identify allelic series of VDE and ZEP enzymes involved in the xanthophyll cycle. The heterogeneity of the kinetics of the NPQ (Non-Photochemical Quenching) of the 5 allelic variants of the *VDE* (Violaxanthin De-Epoxidase) represents the ideal genetic material to compensate for the decrease in NPQ observed in *hus1* mutant. Further analysis in fluctuating light conditions are needed to select the best allelic variants to be combined by crossing with the *hus1* mutant. This strategy might lead to a new barley pale-green variety with an improved kinetic of NPQ induction-relaxation, possibly more productive under high density cultivation and being able to mitigate the global rise in temperature due to the increased albedo.

Overall, this Ph.D. thesis has provided preliminary evidence that support the potential of the pale-green phenotype and of the fine tuning of NPQ in agriculture. This knowledge, gained in barley, could be transferred to several other crops given the high degree of conservation of the photosynthetic process in higher plants and being at the basis of a second green revolution, with at the centre the improvement of the photosynthetic process.

6 - Bibliography

1. Foley, J.A.; DeFries, R.; Asner, G.P.; Barford, C.; Bonan, G.; Carpenter, S.R.; Chapin, F.S.; Coe, M.T.; Daily, G.C.; Gibbs, H.K.; et al. Global consequences of land use. *Science*. **2005**, *309*, 570–574, doi:10.1126/science.1111772.
2. Hosonuma, N.; Herold, M.; De Sy, V.; De Fries, R.S.; Brockhaus, M.; Verchot, L.; Angelsen, A.; Romijn, E. An assessment of deforestation and forest degradation drivers in developing countries. *Environ. Res. Lett.* **2012**, *7*, doi:10.1088/1748-9326/7/4/044009.
3. Campbell, B.M.; Beare, D.J.; Bennett, E.M.; Hall-Spencer, J.M.; Ingram, J.S.I.; Jaramillo, F.; Ortiz, R.; Ramankutty, N.; Sayer, J.A.; Shindell, D. Agriculture production as a major driver of the earth system exceeding planetary boundaries. *Ecol. Soc.* **2017**, *22*, doi:10.5751/ES-09595-220408.
4. Fischer, G.; Hizsnyik, E.; Prieler, S.; Velthuisen, H.V.; Wiberg, D. Scarcity and Abundance of Land Resources : competing uses and the shrinking land resource base Main Messages and Policy Conclusions. *IASA Food Water Res. Increasing* **2005**.
5. Mabee, W.E.; Gregg, D.J.; Saddler, J.N. Assessing the emerging biorefinery sector in Canada. *Appl. Biochem. Biotechnol. - Part A Enzym. Eng. Biotechnol.* **2005**, *123*, 765–778, doi:10.1007/978-1-59259-991-2_64.
6. Naik, S.N.; Goud, V. V.; Rout, P.K.; Dalai, A.K. Production of first and second generation biofuels: A comprehensive review. *Renew. Sustain. Energy Rev.* **2010**, *14*, 578–597, doi:10.1016/j.rser.2009.10.003.
7. De Fraiture, C.; Giordano, M.; Liao, Y. Biofuels and implications for agricultural water use: Blue impacts of green energy. *Water Policy* **2008**, *10*, 67–81, doi:10.2166/wp.2008.054.

8. Gressel, J. Transgenics are imperative for biofuel crops. *Plant Sci.* **2008**, *174*, 246–263, doi:10.1016/j.plantsci.2007.11.009.
9. Garrido, F.J.O.; Piston, F.; Gomez, L.D.; Mcqueen-Mason, S.J. Biomass recalcitrance in barley, wheat and triticale straw: Correlation of biomass quality with classic agronomical traits. *PLoS One* **2018**, *13*, 1–14, doi:10.1371/journal.pone.0205880.
10. Kang, Q.; Appels, L.; Tan, T.; Dewil, R. Bioethanol from lignocellulosic biomass: Current findings determine research priorities. *Sci. World J.* **2014**, *2014*, doi:10.1155/2014/298153.
11. Yue, D.; You, F.; Snyder, S.W. Biomass-to-bioenergy and biofuel supply chain optimization: Overview, key issues and challenges. *Comput. Chem. Eng.* **2014**, *66*, 36–56, doi:10.1016/j.compchemeng.2013.11.016.
12. Chandra, R.; Takeuchi, H.; Hasegawa, T. Methane production from lignocellulosic agricultural crop wastes: A review in context to second generation of biofuel production. *Renew. Sustain. Energy Rev.* **2012**, *16*, 1462–1476, doi:10.1016/j.rser.2011.11.035.
13. Cassman, K.G.; Dobermann, A.; Walters, D.T.; Yang, H. Meeting cereal demand while protecting natural resources and improving environmental quality. *Annu. Rev. Environ. Resour.* **2003**, *28*, 315–358, doi:10.1146/annurev.energy.28.040202.122858.
14. Price, D.L.; Casler, M.D. Predictive relationships between plant morphological traits and biomass yield in switchgrass. *Crop Sci.* **2014**, *54*, 637–645, doi:10.2135/cropsci2013.04.0272.
15. Lauria M.; Molinari F.; Motto M. Genetic Strategies to Enhance Plant Biomass Yield and Quality-Related Traits for Bio-Renewable Fuel and Chemical Productions. *Intechopen Sci.* **2015**, doi:http://dx.doi.org/10.5772/61005.
16. Jeon, J.S.; Jung, K.H.; Kim, H.B.; Suh, J.P.; Khush, G.S. Genetic and

- Molecular Insights into the Enhancement of Rice Yield Potential. *J. Plant Biol.* **2011**, *54*, 1–9, doi:10.1007/s12374-011-9144-0.
17. Hirel, B.; Le Gouis, J.; Ney, B.; Gallais, A. The challenge of improving nitrogen use efficiency in crop plants: Towards a more central role for genetic variability and quantitative genetics within integrated approaches. *J. Exp. Bot.* **2007**, *58*, 2369–2387, doi:10.1093/jxb/erm097.
 18. Ort, D.R.; Zhu, X.; Melis, A. Optimizing antenna size to maximize photosynthetic efficiency. *Plant Physiol.* **2011**, *155*, 79–85, doi:10.1104/pp.110.165886.
 19. Ort, D.R.; Merchant, S.S.; Alric, J.; Barkan, A.; Blankenship, R.E.; Bock, R.; Croce, R.; Hanson, M.R.; Hibberd, J.M.; Long, S.P.; et al. Redesigning photosynthesis to sustainably meet global food and bioenergy demand. *Proc. Natl. Acad. Sci. U. S. A.* **2015**, *112*, 8529–8536, doi:10.1073/pnas.1424031112.
 20. Long, S.P.; Marshall-Colon, A.; Zhu, X.G. Meeting the global food demand of the future by engineering crop photosynthesis and yield potential. *Cell* **2015**, *161*, 56–66, doi:10.1016/j.cell.2015.03.019.
 21. Kim, S.; Dale, B.E. Global potential bioethanol production from wasted crops and crop residues. *Biomass and Bioenergy* **2004**, *26*, 361–375, doi:10.1016/j.biombioe.2003.08.002.
 22. Haas, M.; Schreiber, M.; Mascher, M. Domestication and crop evolution of wheat and barley: Genes, genomics, and future directions. *J. Integr. Plant Biol.* **2019**, *61*, 204–225, doi:10.1111/jipb.12737.
 23. Zohary, D.; Hopf, M.; Weiss, E. Domestication of Plants in the Old World: The origin and spread of domesticated plants in Southwest Asia, Europe, and the Mediterranean Basin. In; Oxford Univ Press: Oxford, UK, **2013** ISBN 9780191810046.
 24. Badr, A.; Müller, K.; Schäfer-Pregl, R.; El Rabey, H.; Effgen, S.; Ibrahim,

- H.H.; Pozzi, C.; Rohde, W.; Salamini, F. On the origin and domestication history of barley (*Hordeum vulgare*). *Mol. Biol. Evol.* **2000**, *17*, 499–510, doi:10.1093/oxfordjournals.molbev.a026330.
25. Fuller D. & Allaby R. Dispersal and Crop Domestication: Shattering, Germination and Seasonality in Evolution Under Cultivation. In *Annual Plant Reviews book series*; **2018**; pp. 238–295.
 26. Doebley J. F., Brandon S.Gaut, B.D.S. The molecular genetics of crop domestication. *Cell* **2006**, *127*, 1309–1321, doi:https://doi.org/10.1016/j.cell.2006.12.006.
 27. Zohary, D. The progenitors of wheat and barley in relation to domestication and agricultural dispersal in the Old World. In *The Domestication and Exploitation of Plants and Animals*; Ucko, P.; Dibbleby, G., Ed.; Gerald Duckworth & Co., London, **1969**; pp. 47–66 ISBN 19701602487.
 28. Dawson, I.K.; Russell, J.; Powell, W.; Steffenson, B.; Thomas, W.T.B.; Waugh, R. Barley: A translational model for adaptation to climate change. *New Phytol.* **2015**, *206*, 913–931, doi:10.1111/nph.13266.
 29. Rotasperti, L.; Sansoni, F.; Mizzotti, C.; Tadini, L.; Pesaresi, P. Barley's second spring as a model organism for chloroplast research. *Plants* **2020**, *9*, 1–25, doi:10.3390/plants9070803.
 30. Song, Q.; Wang, Y.; Qu, M.; Ort, D.R.; Zhu, X.G. The impact of modifying photosystem antenna size on canopy photosynthetic efficiency—Development of a new canopy photosynthesis model scaling from metabolism to canopy level processes. *Plant Cell Environ.* **2017**, *40*, 2946–2957, doi:10.1111/pce.13041.
 31. Kirst, H.; Gabilly, S.T.; Niyogi, K.K.; Lemaux, P.G.; Melis, A. Photosynthetic antenna engineering to improve crop yields. *Planta* **2017**, *245*, 1009–1020, doi:10.1007/s00425-017-2659-y.
 32. Pogson, B.J.; Ganguly, D.; Albrecht-Borth, V. Insights into chloroplast

- biogenesis and development. *Biochim. Biophys. Acta - Bioenerg.* **2015**, 1847, 1017–1024, doi:10.1016/j.bbabi.2015.02.003.
33. Robertson, D.; Laetsch, W.M. Structure and Function of Developing Barley Plastids. *Plant Physiol.* **1974**, 54, 148–159, doi:10.1104/pp.54.2.148.
 34. Boffey, S.A.; Selldén, G.; Leech, R.M. Influence of Cell Age on Chlorophyll Formation in Light-grown and Etiolated Wheat Seedlings. *Plant Physiol.* **1980**, 65, 680–684, doi:10.1104/pp.65.4.680.
 35. Mullet, J.E. Chloroplast Development and Gene Expression. *Annu. Rev. Plant Physiol. Plant Mol. Biol.* **1988**, 39, 475–502, doi:10.1146/annurev.pp.39.060188.002355.
 36. Dubreuil, C.; Jin, X.; Barajas-López, J. de D.; Hewitt, T.C.; Tanz, S.K.; Dobrenel, T.; Schröder, W.P.; Hanson, J.; Pesquet, E.; Grönlund, A.; et al. Establishment of photosynthesis through chloroplast development is controlled by two distinct regulatory phases. *Plant Physiol.* **2018**, 176, 1199–1214, doi:10.1104/pp.17.00435.
 37. Hasan M., Hasibuzzaman A.S.M., Abdullah H.M., K.M.M.H. Genetic and Genomic Resources and Their Exploitation for Unlocking Genetic Potential from the Wild Relatives. In *Rediscovery of Genetic and Genomic Resources for Future Food Security*; Salgotra R.; Zargar S., Ed.; Springer, Singapore, **2020**.
 38. Bustos-Korts, D.; Dawson, I.K.; Russell, J.; Tondelli, A.; Guerra, D.; Ferrandi, C.; Strozzi, F.; Nicolazzi, E.L.; Molnar-Lang, M.; Ozkan, H.; et al. Exome sequences and multi-environment field trials elucidate the genetic basis of adaptation in barley. *Plant J.* **2019**, 99, 1172–1191, doi:10.1111/tpj.14414.
 39. Szurman-Zubrzycka, M.E.; Zbieszczak, J.; Marzec, M.; Jelonek, J.; Chmielewska, B.; Kurowska, M.M.; Krok, M.; Daszkowska-Golec, A.; Guzy-Wrobelska, J.; Gruszka, D.; et al. HorTILLUS—a rich and renewable source of induced mutations for forward/reverse genetics and pre-breeding programs in

barley (*Hordeum vulgare* L.). *Front. Plant Sci.* **2018**, *9*, 1–16, doi:10.3389/fpls.2018.00216.

40. Talamè, V.; Bovina, R.; Sanguineti, M.C.; Tuberosa, R.; Lundqvist, U.; Salvi, S. TILLMore, a resource for the discovery of chemically induced mutants in barley. *Plant Biotechnol. J.* **2008**, *6*, 477–485, doi:10.1111/j.1467-7652.2008.00341.x.
41. Schreiber, M.; Barakate, A.; Uzrek, N.; Macaulay, M.; Sourdille, A.; Morris, J.; Hedley, P.E.; Ramsay, L.; Waugh, R. A highly mutagenised barley (cv. Golden Promise) TILLING population coupled with strategies for screening-by-sequencing. *Plant Methods* **2019**, *15*, 99, doi:10.1186/s13007-019-0486-9.
42. Druka, A.; Franckowiak, J.; Lundqvist, U.; Bonar, N.; Alexander, J.; Houston, K.; Radovic, S.; Shahinnia, F.; Vendramin, V.; Morgante, M.; et al. Genetic dissection of barley morphology and development. *Plant Physiol.* **2011**, *155*, 617–627, doi:10.1104/pp.110.166249.
43. Dockter, C.; Gruszka, D.; Braumann, I.; Druka, A.; Druka, I.; Franckowiak, J.; Gough, S.P.; Janeczko, A.; Kurowska, M.; Lundqvist, J.; et al. Induced variations in brassinosteroid genes define barley height and sturdiness, and expand the green revolution genetic toolkit. *Plant Physiol.* **2014**, *166*, 1912–1927, doi:10.1104/pp.114.250738.
44. Jost, M.; Taketa, S.; Mascher, M.; Himmelbach, A.; Yuo, T.; Shahinnia, F.; Rutten, T.; Druka, A.; Schmutzer, T.; Steuernagel, B.; et al. A homolog of blade-on-petiole 1 and 2 (BOP1/2) controls internode length and homeotic changes of the barley inflorescence. *Plant Physiol.* **2016**, *171*, 1113–1127, doi:10.1104/pp.16.00124.
45. Komatsuda, T.; Pourkheirandish, M.; He, C.; Azhaguvel, P.; Kanamori, K.; Perovic, D.; Stein, N.; Graner, A.; Wicker, T.; Tagiri, A.; et al. Six-rowed barley originated from a mutation in a homeodomain-leucine zipper I-class

- homeobox gene. *Proc. Natl. Acad. Sci. U. S. A.* **2007**, *104*, 1424–1429, doi:10.1073/pnas.0608580104.
46. Ramsay, L.; Comadran, J.; Druka, A.; Marshall, D.F.; Thomas, W.T.B.; MacAulay, M.; MacKenzie, K.; Simpson, C.; Fuller, J.; Bonar, N.; et al. INTERMEDIUM-C, a modifier of lateral spikelet fertility in barley, is an ortholog of the maize domestication gene TEOSINTE BRANCHED 1. *Nat. Genet.* **2011**, *43*, 169–172, doi:10.1038/ng.745.
47. Henikoff, S.; Till, B.J.; Comai, L.; Division, B.S.; Hutchinson, F.; Washington, S.H. Perspectives on Translational Biology TILLING . Traditional Mutagenesis Meets Functional Genomics. *Cancer Res.* **2004**, *135*, 630–636, doi:10.1104/pp.104.041061.630.
48. Till, B.; Colbert, R.; Tompa, R.; Ennes, L.; Codomo, C.; Johnson J.; Reynolds, S.; Henikoff, S. High-Throughput TILLING for Functional Genomics. In *Plant Functional Genomics*; Humana Press Totowa, New Jersey, **2003**; pp. 205–220.
49. Henry, I.M.; Nagalakshmi, U.; Lieberman, M.C.; Ngo, K.J.; Krasileva, K. V.; Vasquez-Gross, H.; Akhunova, A.; Akhunov, E.; Dubcovsky, J.; Tai, T.H.; et al. Efficient genome-wide detection and cataloging of EMS-induced mutations using Exome capture and next-generation sequencing. *Plant Cell* **2014**, *26*, 1382–1397, doi:10.1105/tpc.113.121590.
50. Blankenship, R.E.; Chen, M. Spectral expansion and antenna reduction can enhance photosynthesis for energy production. *Curr. Opin. Chem. Biol.* **2013**, *17*, 457–461, doi:10.1016/j.cbpa.2013.03.031.
51. Evans, J.R. Improving photosynthesis. *Plant Physiol.* **2013**, *162*, 1780–1793, doi:10.1104/pp.113.219006.
52. Gu, J.; Zhou, Z.; Li, Z.; Chen, Y.; Wang, Z.; Zhang, H.; Yang, J. Photosynthetic properties and potentials for improvement of photosynthesis in pale green leaf rice under high light conditions. *Front. Plant Sci.* **2017**, *8*, 1082,

doi:10.3389/fpls.2017.01082.

53. Kromdijk, J.; Glowacka, K.; Leonelli, L.; Gabilly, S.; Iwai, M.; Niyogi, K.; Long, S. Improving photosynthesis and crop productivity by accelerating recovery from photoprotection. *Science (80-.)*. **2016**, *354*, 857–861.
54. Jansson, C.; Wullschleger, S.D.; Kalluri, U.C.; Tuskan, G.A. Phytosequestration: Carbon Biosequestration by Plants and the Prospects of Genetic Engineering. *Bioscience* **2010**, *60*, 685–696, doi:10.1525/bio.2010.60.9.6.
55. Jansson, S. A guide to the Lhc genes and their relatives in Arabidopsis. *Trends Plant Sci.* **1999**, *4*, 236–240, doi:10.1016/S1360-1385(99)01419-3.
56. Mazor, Y.; Borovikova, A.; Nelson, N. The structure of plant photosystem I super-complex at 2.8 Å resolution. *Elife* **2015**, *4*, 1–18, doi:10.7554/eLife.07433.
57. Zhu, X.-G.; Long, S.P.; Ort, D.R. Improving Photosynthetic Efficiency for Greater Yield. *Annu. Rev. Plant Biol.* **2010**, *61*, 235–261, doi:10.1146/annurev-arplant-042809-112206.
58. Beckmann, J.; Lehr, F.; Finazzi, G.; Hankamer, B.; Posten, C.; Wobbe, L.; Kruse, O. Improvement of light to biomass conversion by de-regulation of light-harvesting protein translation in *Chlamydomonas reinhardtii*. *J. Biotechnol.* **2009**, *142*, 70–77, doi:10.1016/j.jbiotec.2009.02.015.
59. Sakowska, K.; Alberti, G.; Genesio, L.; Peressotti, A.; Delle Vedove, G.; Gianelle, D.; Colombo, R.; Rodeghiero, M.; Panigada, C.; Juszczak, R.; et al. Leaf and canopy photosynthesis of a chlorophyll deficient soybean mutant. *Plant Cell Environ.* **2018**, *41*, 1427–1437, doi:10.1111/pce.13180.
60. Gu, J.; Zhou, Z.; Li, Z.; Chen, Y.; Wang, Z.; Zhang, H. Rice (*Oryza sativa* L.) with reduced chlorophyll content exhibit higher photosynthetic rate and efficiency, improved canopy light distribution, and greater yields than normally

- pigmented plants. *F. Crop. Res.* **2017**, *200*, 58–70, doi:10.1016/j.fcr.2016.10.008.
61. Slattery, R.A.; Vanlooche, A.; Bernacchi, C.J.; Zhu, X.G.; Ort, D.R. Photosynthesis, light use efficiency, and yield of reduced-chlorophyll soybean mutants in field conditions. *Front. Plant Sci.* **2017**, *8*, 1–19, doi:10.3389/fpls.2017.00549.
62. Li, Y.; Ren, B.; Gao, L.; Ding, L.; Jiang, D.; Xu, X.; Shen, Q.; Guo, S. Less Chlorophyll Does not Necessarily Restrain Light Capture Ability and Photosynthesis in a Chlorophyll-Deficient Rice Mutant. *J. Agron. Crop Sci.* **2013**, *199*, 49–56, doi:10.1111/j.1439-037X.2012.00519.x.
63. Pettigrew, W.; Hesketh, J.; Peters, D.; Woolley, J. Characterization of Canopy Photosynthesis of Chlorophyll-Deficient Soybean Isolines. *Crop Physiol. Metab.* **1989**, *29*, 1025–1029, doi:https://doi.org/10.2135/cropsci1989.0011183X002900040040x.
64. Tardy, F.; Créach, A.; Havaux, M. Photosynthetic pigment concentration, organization and interconversions in a pale green Syrian landrace of barley (*Hordeum vulgare* L., Tadmor) adapted to harsh climatic conditions. *Plant, Cell Environ.* **1998**, *21*, 479–489, doi:10.1046/j.1365-3040.1998.00293.x.
65. Royo, C.; Nazco, R.; Villegas, D. The climate of the zone of origin of Mediterranean durum wheat (*Triticum durum* Desf.) landraces affects their agronomic performance. *Genet. Resour. Crop Evol.* **2014**, *61*, 1345–1358, doi:10.1007/s10722-014-0116-3.
66. Zaharieva, M.; Gaulin, E.; Havaux, M.; Acevedo, E.; Monneveux, P. Drought and heat responses in the wild wheat relative *Aegilops geniculata* roth: Potential interest for wheat improvement. *Crop Sci.* **2001**, *41*, 1321–1329, doi:10.2135/cropsci2001.4141321x.
67. Bright, R.M.; Bogren, W.; Bernier, P.; Astrup, R. Carbon-equivalent metrics for

- albedo changes in land management contexts: Relevance of the time dimension. *Ecol. Appl.* **2016**, *26*, 1868–1880, doi:10.1890/15-1597.1.
68. Twomey, S. Pollution and the planetary albedo. *Atmos. Environ.* **1974**, *8*, 1251–1256, doi:https://doi.org/10.1016/0004-6981(74)90004-3.
69. Bett, A.; Ball, J. Albedo over the boreal forest. *J. Geophys. Res. Atmos.* **1997**, *102*, 901–909, doi:https://doi.org/10.1029/96JD03876.
70. Hirsch, A.L.; Wilhelm, M.; Davin, E.L.; Thiery, W.; Seneviratne, S.I. Can climate-effective land management reduce regional warming? *J. Geophys. Res.* **2017**, *122*, 2269–2288, doi:10.1002/2016JD026125.
71. Davin, E.L.; Seneviratne, S.I.; Ciais, P.; Olliso, A.; Wang, T. Preferential cooling of hot extremes from cropland albedo management. *Proc. Natl. Acad. Sci. U. S. A.* **2014**, *111*, 9757–9761, doi:10.1073/pnas.1317323111.
72. Colombo, M.; Suorsa, M.; Rossi, F.; Ferrari, R.; Tadini, L.; Barbato, R.; Pesaresi, P. Photosynthesis control: An underrated short-term regulatory mechanism essential for plant viability. *Plant Signal. Behav.* **2016**, *11*, 1–6, doi:10.1080/15592324.2016.1165382.
73. Rochaix, J.D. Regulation and dynamics of the light-harvesting system. *Annu. Rev. Plant Biol.* **2014**, *65*, 287–309, doi:10.1146/annurev-arplant-050213-040226.
74. Pesaresi, P.; Pribil, M.; Wunder, T.; Leister, D. Dynamics of reversible protein phosphorylation in thylakoids of flowering plants: The roles of STN7, STN8 and TAP38. *Biochim. Biophys. Acta - Bioenerg.* **2011**, *1807*, 887–896, doi:10.1016/j.bbabi.2010.08.002.
75. Allen, J.F. Protein phosphorylation in regulation of photosynthesis. *Biochim. Biophys. Acta - Bioenerg.* **1992**, *1098*, 275–335, doi:doi.org/10.1016/S0005-2728(09)91014-3.

76. Wollman, F.A. State transitions reveal the dynamics and flexibility of the photosynthetic apparatus. *EMBO J.* **2001**, *20*, 3623–3630, doi:10.1093/emboj/20.14.3623.
77. Bellaflore, S.; Barneche, F.; Peltler, G.; Rochaix, J.D. State transitions and light adaptation require chloroplast thylakoid protein kinase STN7. *Nature* **2005**, *433*, 892–895, doi:10.1038/nature03286.
78. Bonardi, V.; Pesaresi, P.; Becker, T.; Schleiff, E.; Wagner, R.; Pfannschmidt, T.; Jahns, P.; Leister, D. Photosystem II core phosphorylation and photosynthetic acclimation require two different protein kinases. *Nature* **2005**, *437*, 1179–1182, doi:10.1038/nature04016.
79. Pribil, M.; Pesaresi, P.; Hertle, A.; Barbato, R.; Leister, D. Role of plastid protein phosphatase TAP38 in LHCII dephosphorylation and thylakoid electron flow. *PLoS Biol.* **2010**, *8*, doi:10.1371/journal.pbio.1000288.
80. Shikanai, T. Central role of cyclic electron transport around photosystem I in the regulation of photosynthesis. *Curr. Opin. Biotechnol.* **2014**, *26*, 25–30, doi:10.1016/j.copbio.2013.08.012.
81. Shikanai, T. Chloroplast NDH: A different enzyme with a structure similar to that of respiratory NADH dehydrogenase. *Biochim. Biophys. Acta - Bioenerg.* **2016**, *1857*, 1015–1022, doi:10.1016/j.bbabi.2015.10.013.
82. Peltier, G.; Aro, E.M.; Shikanai, T. NDH-1 and NDH-2 Plastoquinone Reductases in Oxygenic Photosynthesis. *Annu. Rev. Plant Biol.* **2016**, *67*, 55–80, doi:10.1146/annurev-arplant-043014-114752.
83. Tikhonov, A.N. The cytochrome b6f complex at the crossroad of photosynthetic electron transport pathways. *Plant Physiol. Biochem.* **2014**, *81*, 163–183, doi:10.1016/j.plaphy.2013.12.011.
84. Tikhonov, A.N. Induction events and short-term regulation of electron transport in chloroplasts: An overview. *Photosynth. Res.* **2015**, *125*, 65–94,

doi:10.1007/s11120-015-0094-0.

85. Kramer, D.M.; Cruz, J.A.; Kanazawa, A. Balancing the central roles of the thylakoid proton gradient. *Trends Plant Sci.* **2003**, *8*, 27–32, doi:10.1016/S1360-1385(02)00010-9.
86. Rumberg, B., Siggel, U. pH changes in the inner phase of the thylakoids during photosynthesis. *Naturwissenschaften* **1969**, *56*, 130–132, doi:https://doi.org/10.1007/BF00601025.
87. Kohzuma, K.; Cruz, J.A.; Akashi, K.; Hoshiyasu, S.; Munekage, Y.N.; Yokota, A.; Kramer, D.M. The long-term responses of the photosynthetic proton circuit to drought. *Plant, Cell Environ.* **2009**, *32*, 209–219, doi:10.1111/j.1365-3040.2008.01912.x.
88. Kramer, D.M.; Evans, J.R. The importance of energy balance in improving photosynthetic productivity. *Plant Physiol.* **2011**, *155*, 70–78, doi:10.1104/pp.110.166652.
89. Niyogi, K.K.; Truong, T.B. Evolution of flexible non-photochemical quenching mechanisms that regulate light harvesting in oxygenic photosynthesis. *Curr. Opin. Plant Biol.* **2013**, *16*, 307–314, doi:10.1016/j.pbi.2013.03.011.
90. Ruban, A. V.; Johnson, M.P.; Duffy, C.D.P. The photoprotective molecular switch in the photosystem II antenna. *Biochim. Biophys. Acta - Bioenerg.* **2012**, *1817*, 167–181, doi:10.1016/j.bbabi.2011.04.007.
91. Demmig-Adams, B.; Cohu, C.M.; Muller, O.; Adams, W.W. Modulation of photosynthetic energy conversion efficiency in nature: From seconds to seasons. *Photosynth. Res.* **2012**, *113*, 75–88, doi:10.1007/s11120-012-9761-6.
92. Müller, P.; Li, X.P.; Niyogi, K.K. Update on Photosynthesis Non-Photochemical Quenching . A Response to Excess Light Energy 1. *Plant Physiol.* **2001**, *125*, 1558–1566.

93. Nilkens, M.; Kress, E.; Lambrev, P.; Miloslavina, Y.; Müller, M.; Holzwarth, A.R.; Jahns, P. Identification of a slowly inducible zeaxanthin-dependent component of non-photochemical quenching of chlorophyll fluorescence generated under steady-state conditions in *Arabidopsis*. *Biochim. Biophys. Acta - Bioenerg.* **2010**, *1797*, 466–475, doi:10.1016/j.bbabi.2010.01.001.
94. Takahashi, S.; Badger, M.R. Photoprotection in plants: A new light on photosystem II damage. *Trends Plant Sci.* **2011**, *16*, 53–60, doi:10.1016/j.tplants.2010.10.001.
95. Pérez-Bueno, M.L.; Johnson, M.P.; Zia, A.; Ruban, A. V.; Horton, P. The Lhcb protein and xanthophyll composition of the light harvesting antenna controls the Δ pH-dependency of non-photochemical quenching in *Arabidopsis thaliana*. *FEBS Lett.* **2008**, *582*, 1477–1482, doi:10.1016/j.febslet.2008.03.040.
96. Hubbart, S.; Smillie, I.R.A.; Heatley, M.; Swarup, R.; Foo, C.C.; Zhao, L.; Murchie, E.H. Enhanced thylakoid photoprotection can increase yield and canopy radiation use efficiency in rice. *Commun. Biol.* **2018**, *1*, 1–12, doi:10.1038/s42003-018-0026-6.
97. Simkin, A.J.; López-Calcagno, P.E.; Raines, C.A. Feeding the world: Improving photosynthetic efficiency for sustainable crop production. *J. Exp. Bot.* **2019**, *70*, 1119–1140, doi:10.1093/jxb/ery445.
98. Głowacka, K.; Kromdijk, J.; Kucera, K.; Xie, J.; Cavanagh, A.P.; Leonelli, L.; Leakey, A.D.B.; Ort, D.R.; Niyogi, K.K.; Long, S.P. Photosystem II Subunit S overexpression increases the efficiency of water use in a field-grown crop. *Nat. Commun.* **2018**, *9*, 868, doi:10.1038/s41467-018-03231-x.
99. Jahns, P.; Latowski, D.; Strzalka, K. Mechanism and regulation of the violaxanthin cycle: The role of antenna proteins and membrane lipids. *Biochim. Biophys. Acta - Bioenerg.* **2009**, *1787*, 3–14, doi:10.1016/j.bbabi.2008.09.013.
100. Magdaong, N.C.M.; Blankenship, R.E. Photoprotective, excited-state

- quenching mechanisms in diverse photosynthetic organisms. *J. Biol. Chem.* **2018**, *293*, 5018–5025, doi:10.1074/jbc.TM117.000233.
101. Arnoux, P.; Morosinotto, T.; Saga, G.; Bassi, R.; Pignol, D. A structural basis for the ph-dependent xanthophyll cycle in *Arabidopsis thaliana*. *Plant Cell* **2009**, *21*, 2036–2044, doi:10.1105/tpc.109.068007.
102. Havaux, M.; Bonfils, J.P.; Lutz, C.; Niyogi, K.K. Photodamage of the photosynthetic apparatus and its dependence on the leaf developmental stage in the npq1 *Arabidopsis* mutant deficient in the xanthophyll cycle enzyme violaxanthin de-epoxidase. *Plant Physiol.* **2000**, *124*, 273–284, doi:10.1104/pp.124.1.273.
103. Niyogi, K.K.; Grossman, A.R.; Björkman, O. *Arabidopsis* mutants define a central role for the xanthophyll cycle in the regulation of photosynthetic energy conversion. *Plant Cell* **1998**, *10*, 1121–1134, doi:10.1105/tpc.10.7.1121.
104. Niyogi, K.K.; Li, X.P.; Rosenberg, V.; Jung, H.S. Is PsbS the site of non-photochemical quenching in photosynthesis? *J. Exp. Bot.* **2005**, *56*, 375–382, doi:10.1093/jxb/eri056.
105. Werner, C.; Ryel, R.J.; Correia, O.; Beyschlag, W. Effects of photoinhibition on whole-plant carbon gain assessed with a photosynthesis model. *Plant, Cell Environ.* **2001**, *24*, 27–40, doi:10.1046/j.1365-3040.2001.00651.x.
106. Mascher, M.; Jost, M.; Kuon, J.E.; Himmelbach, A.; Abfal, A.; Beier, S.; Scholz, U.; Graner, A.; Stein, N. Mapping-by-sequencing accelerates forward genetics in barley. *Genome Biol.* **2014**, *15*, 1–15, doi:10.1186/gb-2014-15-6-r78.
107. Tadini, L.; Romani, I.; Pribil, M.; Jahns, P.; Leister, D.; Pesaresi, P. Thylakoid redox signals are integrated into organellar-gene-expression-dependent retrograde signaling in the prors1-1 mutant. *Front. Plant Sci.* **2012**, *3*, 1–13, doi:10.3389/fpls.2012.00282.

108. Mascher, M.; Richmond, T.A.; Gerhardt, D.J.; Himmelbach, A.; Clissold, L.; Sampath, D.; Ayling, S.; Steuernagel, B.; Pfeifer, M.; D'Ascenzo, M.; et al. Barley whole exome capture: A tool for genomic research in the genus *Hordeum* and beyond. *Plant J.* **2013**, *76*, 494–505, doi:10.1111/tpj.12294.
109. Clough, S.J.; Bent, A.F. Floral dip: A simplified method for *Agrobacterium*-mediated transformation of *Arabidopsis thaliana*. *Plant J.* **1998**, *16*, 735–743, doi:10.1046/j.1365-313X.1998.00343.x.
110. Schägger, H.; von Jagow, G. Tricine-sodium dodecyl sulfate-polyacrylamide gel electrophoresis for the separation of proteins in the range from 1 to 100 kDa. *Anal. Biochem.* **1987**, *166*, 368–379, doi:doi.org/10.1016/0003-2697(87)90587-2.
111. Monat, C.; Padmarasu, S.; Lux, T.; Wicker, T.; Gundlach, H.; Himmelbach, A.; Ens, J.; Li, C.; Muehlbauer, G.J.; Schulman, A.H.; et al. TRITEX: Chromosome-scale sequence assembly of Triticeae genomes with open-source tools. *Genome Biol.* **2019**, *20*, 284, doi:10.1186/s13059-019-1899-5.
112. Wang, W.; Czaplinski, K.; Rao, Y.; Peltz, S.W. The role of Upf proteins in modulating the translation read-through of nonsense-containing transcripts. *EMBO J.* **2001**, *20*, 880–890, doi:10.1093/emboj/20.4.880.
113. Klimyuk, V.I.; Persello-Cartieaux, F.; Havaux, M.; Contard-David, P.; Schuenemann, D.; Meierhoff, K.; Gouet, P.; Jones, J.D.G.; Hoffman, N.E.; Nussaume, L. A chromodomain protein encoded by the *Arabidopsis* CAO gene is a plant-specific component of the chloroplast signal recognition particle pathway that is involved in LHCP targeting. *Plant Cell* **1999**, *11*, 87–99, doi:10.1105/tpc.11.1.87.
114. Schuenemann, D.; Gupta, S.; Persello-Cartieaux, F.; Klimyuk, V.I.; Jones, J.D.G.; Nussaume, L.; Hoffman, N.E. A novel signal recognition particle targets light-harvesting proteins to the thylakoid membranes. *Proc. Natl. Acad.*

- Sci. U. S. A.* **1998**, *95*, 10312–10316, doi:10.1073/pnas.95.17.10312.
115. Jones, T.J.; Taylor, W.; Thornton, J. The rapid generation of mutation data matrices from protein sequences. *Bioinformatics* **1992**, *8*, 275–282, doi:https://doi.org/10.1093/bioinformatics/8.3.275.
116. Kumar, S.; Stecher, G.; Li, M.; Knyaz, C.; Tamura, K. MEGA X: Molecular evolutionary genetics analysis across computing platforms. *Mol. Biol. Evol.* **2018**, *35*, 1547–1549, doi:10.1093/molbev/msy096.
117. Ziehe, D.; Dünschede, B.; Schünemann, D. Molecular mechanism of SRP-dependent light-harvesting protein transport to the thylakoid membrane in plants. *Photosynth. Res.* **2018**, *138*, 303–313, doi:10.1007/s11120-018-0544-6.
118. Franklin, A.E.; Hoffman, N.E. Characterization of a chloroplast homologue of the 54-kDa subunit of the signal recognition particle. *J. Biol. Chem.* **1993**, *268*, 22175–22180, doi:10.1016/s0021-9258(20)80664-4.
119. Li, X.; Henry, R.; Yuan, J.; Cline, K.; Hoffman, N.E. A chloroplast homologue of the signal recognition particle subunit SRP54 is involved in the posttranslational integration of a protein into thylakoid membranes. *Proc. Natl. Acad. Sci. U. S. A.* **1995**, *92*, 3789–3793, doi:10.1073/pnas.92.9.3789.
120. Jonas-Straube, E.; Hutin, C.; Hoffman, N.E.; Schünemann, D. Functional Analysis of the Protein-interacting Domains of Chloroplast SRP43. *J. Biol. Chem.* **2001**, *276*, 24654–24660, doi:10.1074/jbc.M100153200.
121. Drewery, M.L.; Sawyer, J.E.; Pinchak, W.E.; Wickersham, T.A. Effect of increasing amounts of postextraction algal residue on straw utilization in steers. *J. Anim. Sci.* **2014**, *92*, 4642–4649, doi:10.2527/jas.2014-7795.
122. Ridgwell, A.; Singarayer, J.S.; Hetherington, A.M.; Valdes, P.J. Tackling Regional Climate Change By Leaf Albedo Bio-geoengineering. *Curr. Biol.* **2009**, *19*, 146–150, doi:10.1016/j.cub.2008.12.025.

123. Lv, X.G.; Shi, Y.F.; Xu, X.; Wei, Y.L.; Wang, H.M.; Zhang, X.B.; Wu, J.L. *Oryza sativa* chloroplast signal recognition particle 43 (OscpSRP43) is required for chloroplast development and photosynthesis. *PLoS One* **2015**, *10*, 1–17, doi:10.1371/journal.pone.0143249.
124. Ye, J.; Yang, Y.L.; Wei, X.H.; Niu, X.J.; Wang, S.; Xu, Q.; Yuan, X.P.; Yu, H.Y.; Wang, Y.P.; Feng, Y.; et al. PGL3 is required for chlorophyll synthesis and impacts leaf senescence in rice. *J. Zhejiang Univ. Sci. B* **2018**, *19*, 263–273, doi:10.1631/jzus.B1700337.
125. Guan, H.; Xu, X.; He, C.; Liu, C.; Liu, Q.; Dong, R.; Liu, T.; Wang, L. Fine mapping and candidate gene analysis of the leaf-color gene *ygl-1* in maize. *PLoS One* **2016**, *11*, 1–19, doi:10.1371/journal.pone.0153962.
126. Schuenemann, D.; Amin, P.; Hoffman, N.E. Functional divergence of the plastid and cytosolic forms of the 54-kDa subunit of signal recognition particle. *Biochem. Biophys. Res. Commun.* **1999**, *254*, 253–258, doi:10.1006/bbrc.1998.9923.
127. Tu, C.J.; Peterson, E.C.; Henry, R.; Hoffman, N.E. The L18 domain of light-harvesting chlorophyll proteins binds to chloroplast signal recognition particle 43. *J. Biol. Chem.* **2000**, *275*, 13187–13190, doi:10.1074/jbc.C000108200.
128. Holzberg, S.; Brosio, P.; Gross, C.; Pogue, G.P. Barley stripe mosaic virus-induced gene silencing in a monocot plant. *Plant J.* **2002**, *30*, 315–327, doi:10.1046/j.1365-313X.2002.01291.x.

7 – Acknowledgments

First of all, my thanks go to prof. Paolo Pesaresi for his guide in these three and a half years of Ph.D. and to give me the opportunity to be fascinated by barley and the mysteries of photosynthesis. The second thanks go to my laboratory “mamacita” Dr. Luca Tadini who endured me with immense patience listening to me from morning to evening. Thanks for your countless skills and practical problems solving skills: you have been the best laboratory tutor I could have. Thank you for translating my peculiar language into understandable English. I thank all the people in the lab who in some way have supported and helped me over the years: Nicolaj for his computer aids and use of any electronic device; all the master's students who have helped me with the experiments in these years, Francesca, Maria, Simona and Giorgia; the people from 3A, 5A, 5B especially Simona, Sara, Chiara, Stefano and all the other people of the Bioscience department that help me in any kind of stuff.

I also want to dedicate this Ph.D. thesis to my family: Davide, Mum and Dad, Ale and Vale, Dino and Anna and all my best friends Angi, Lucy, Illy and Ale.

8 – Appendices (Manuscripts)

Manuscript I

Paolo D., **Rotasperti L.**, Schnittger A., Masiero S., Colombo L., Mizzotti C. (2021) The Arabidopsis MADS-Domain Transcription Factor SEEDSTICK Controls Seed Size via Direct Activation of E2Fa. *Plants*. 10(2):192. doi: 10.3390/plants10020192.

This article shows the role of STK, a MADS-domain transcription factor, in modulating the seed size in *Arabidopsis thaliana*. In this work, I measured the size of seeds and performed the gene expression analyses by real-time PCR.

Manuscript II

Rotasperti L., Sansoni F., Mizzotti C., Tadini L., Pesaresi P. (2020) Barley's Second Spring as A Model Organism for Chloroplast Research. *Plants*. 9(7):803. doi: 10.3390/plants9070803.


This review article highlights the importance of barley as a model organism for studying of photosynthesis regulation and chloroplast development. Into details, I was involved in the conceptualization, the gathering of information and the writing of the manuscript.

Manuscript III

Mizzotti C., **Rotasperti L.**, Moretto M., Tadini L., Resentini F., Galliani B.M., Galbiati M., Engelen K., Pesaresi P., Masiero S. (2018) Time-Course Transcriptome Analysis of Arabidopsis Siliques Discloses Genes Essential for Fruit Development and Maturation. *Plant Physiol*. 178(3):1249-1268. doi: 10.1104/pp.18.00727.

In this manuscript the RNA-seq of *Arabidopsis thaliana* developing fruits (silique valves) is analysed and differentially expressed genes are described. For this work, I dealt with RNA extractions and RNA-seq validation through the analysis of 10 genes and their corresponding mutants. I performed the expression analysis of these differentially expressed genes via RT-qPCR, silique size measurement, GUS assay and trypan blue staining. I also performed the physiological analysis of the siliques using the Dual-PAM which measures chlorophyll fluorescence of PSII and the content of chlorophylls in these lines.

The *Arabidopsis* MADS-Domain Transcription Factor SEEDSTICK Controls Seed Size via Direct Activation of *E2Fa*

Dario Paolo ^{1,†}, Lisa Rotasperti ¹, Arp Schnittger ², Simona Masiero ¹, Lucia Colombo ¹ and Chiara Mizzotti ^{1,*} 

¹ Dipartimento di BioScienze, Università degli Studi di Milano, 20133 Milano, Italy; dario.paolo@ibba.cnr.it (D.P.); lisa.rotasperti@unimi.it (L.R.); simona.masiero@unimi.it (S.M.); lucia.colombo@unimi.it (L.C.)

² Abteilung für Entwicklungsbiologie, Institut für Pflanzenforschung und Mikrobiologie, Universität Hamburg, 22609 Hamburg, Germany; arp.schnittger@uni-hamburg.de

* Correspondence: chiara.mizzotti@unimi.it; Tel.: +39-02-503-14838

† Present address: Institute of Agricultural Biology and Biotechnology, CNR, 20133 Milan, Italy.

Abstract: Seed size is the result of complex molecular networks controlling the development of the seed coat (of maternal origin) and the two fertilization products, the embryo and the endosperm. In this study we characterized the role of *Arabidopsis thaliana* MADS-domain transcription factor SEEDSTICK (STK) in seed size control. STK is known to regulate the differentiation of the seed coat as well as the structural and mechanical properties of cell walls in developing seeds. In particular, we further characterized *stk* mutant seeds. Genetic evidence (reciprocal crosses) of the inheritance of the small-seed phenotype, together with the provided analysis of cell division activity (flow cytometry), demonstrate that STK acts in the earlier phases of seed development as a maternal activator of growth. Moreover, we describe a molecular mechanism underlying this activity by reporting how STK positively regulates cell cycle progression via directly activating the expression of *E2Fa*, a key regulator of the cell cycle. Altogether, our results unveil a new genetic network active in the maternal control of seed size in *Arabidopsis*.

Keywords: *Arabidopsis thaliana*; cell cycle; seed development; transcription factor



Citation: Paolo, D.; Rotasperti, L.; Schnittger, A.; Masiero, S.; Colombo, L.; Mizzotti, C. The *Arabidopsis* MADS-Domain Transcription Factor SEEDSTICK Controls Seed Size via Direct Activation of *E2Fa*. *Plants* **2021**, *10*, 192. <https://doi.org/10.3390/plants10020192>

Received: 23 December 2020

Accepted: 16 January 2021

Published: 20 January 2021

Publisher's Note: MDPI stays neutral with regard to jurisdictional claims in published maps and institutional affiliations.



Copyright: © 2021 by the authors. Licensee MDPI, Basel, Switzerland. This article is an open access article distributed under the terms and conditions of the Creative Commons Attribution (CC BY) license (<https://creativecommons.org/licenses/by/4.0/>).

1. Introduction

In spermatophyte plants, reproductive success depends on the ability to produce healthy seeds. Indeed, seed size represents one of the major traits that influence the fitness of the next plant generation. Despite their importance, molecular regulators of seed size have only begun to be identified in the last few years, mainly through studies on *Arabidopsis* [1–4]. Critical factors governing seed size include the parent-of-origin effect in fertilization tissues, overall plant fertility (balance between seed size/number), cell cycle/cell expansion regulation and hormonal signaling [5–8].

The final size of *Arabidopsis* seeds is achieved through coordinated growth of the three parts that compose the seeds: the seed coat, the endosperm and the embryo [9]. All three parts are characterized by a different genotype: the seed coat, deriving from the ovule integuments, is entirely of maternal origin, whereas both embryo and endosperm are the result of double fertilization. In *Arabidopsis*, seed size is established around four days after fertilization (DAF), when the dimension of the seed cavity has reached its maximum expansion as a result of seed coat growth and endosperm proliferation [10,11].

Many factors influencing ovule and seed development have been identified [1,12]. In particular, MADS-domain transcription factors have been found to be key determinants of female reproductive development [13]. Among them, the *Arabidopsis* transcription factor SEEDSTICK (STK) has been largely studied in relation to its function in ovule identity determination [14,15], transmitting tract development [16,17] seed abscission [15,18], seed coat development [19] and flavonoid biosynthesis [20]. We have also previously shown

how STK regulates size and differentiation of fruits by providing a link between signaling hormones (cytokinins) and other molecular developmental networks [21]. Loss-of-function *stk* mutants produce smaller seeds than wild-type, albeit with no obvious reduction in overall fertility [15]. However, the underlying molecular mechanisms of how STK promotes seed growth are not very well understood. We therefore conducted additional studies on the genetics of the small-seed phenotype of the *stk* mutant and we analyzed differences in mitotic activities emerging from the comparison with wild-type seeds. Moreover, we investigated possible downstream targets of STK involved in cell cycle progression. In this frame, we focused on E2Fa, a crucial transcription factor that regulates the mitotic activity of cells that is also co-expressed with STK in the seed coat of developing seeds [22–24]. The single *e2fa* mutant does not have a seed-related phenotype, while the double mutant *e2fa/b* has enlarged seeds, an indirect effect probably due to reduced fertility of the mutant which therefore diverts more allocated resources to the surviving seeds [24]. Here, we provide evidence of the involvement of STK in cell cycle control via the positive regulation of the expression of *E2Fa* in developing seeds.

2. Results and Discussion

2.1. STK Maternally Controls Seed Size and Controls Cell Cycle Progression in Seeds

To further characterize the reduction in seed size of *stk* seeds, we performed reciprocal crosses with wild-type plants. Our data confirmed that the smaller size and the rounder shape of *stk* seeds (Figure 1b,d,e) in comparison to wild-type (Figure 1a,c,e) only depend on the maternal origin of the seed coat, as suggested previously [15,25]. The maternally inherited small-seed phenotype of *stk* is also reflected in the reduction of average seed mass (Figure 1f).

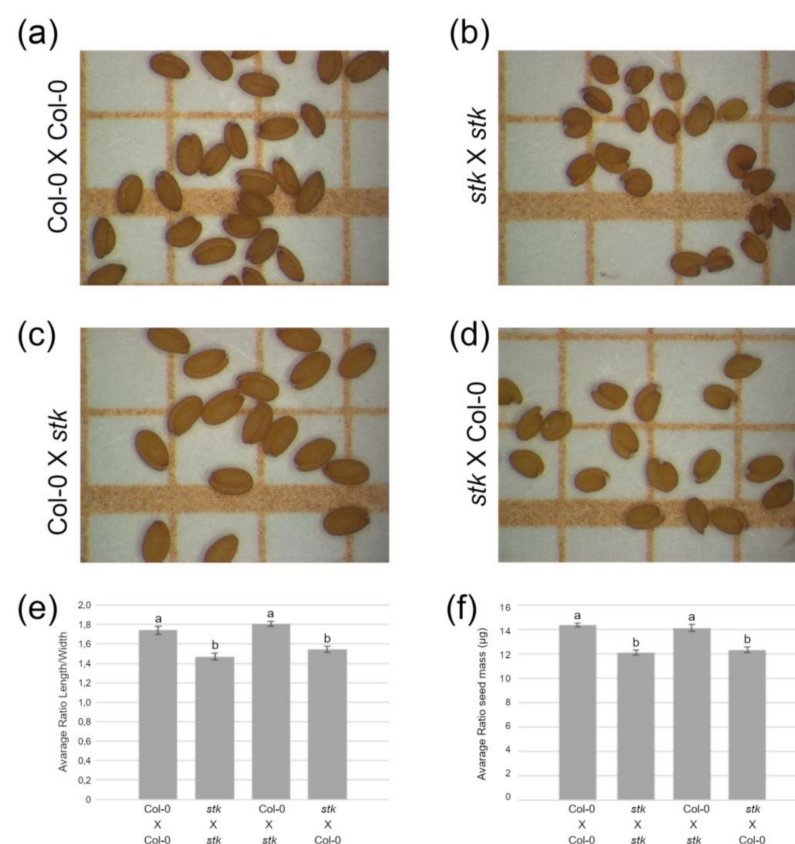


Figure 1. The phenotype of *stk* mutant seeds has a maternal sporophytic origin. (a–d) Seeds of reciprocal crosses between *stk* and wild-type Columbia (Col-0) plants on 1 mm squared graph paper. (e) Ratio between seed length and width. (f) Seed mass. Bars indicate means plus standard error; different letters above bars indicate statistically significant differences ($p < 0.01$).

A key parameter of organ growth is cell number, which is determined by cell division activity. Determining the ratio between 4C and 2C cells, i.e., before and after mitosis, can give a first estimate of cell cycle activity. In young seeds (0–6 DAF), the 4C/2C ratio is mainly influenced by seed coat cells, which are the predominant fraction of cells at this time point [26].

Previous flow cytometry analyses revealed that wild-type and *stk* seeds differ in terms of 4C and 2C peaks [25]. In *stk* seeds, nearly 50% of the cells reside in the gap before mitosis, whereas this is only the case for 35% of the cells in wild-type seeds (Supplementary Figure S1). This suggests that *stk* mutants either progress faster through the S-phase or are slowed down in their progression through mitosis.

Next, we investigated how *STK* could control cell proliferation by q-PCR (Figure 2), monitoring the expression levels of known cell cycle regulators, including transcription factors, cyclins (CYC) and cyclin-dependent kinases (CDK).

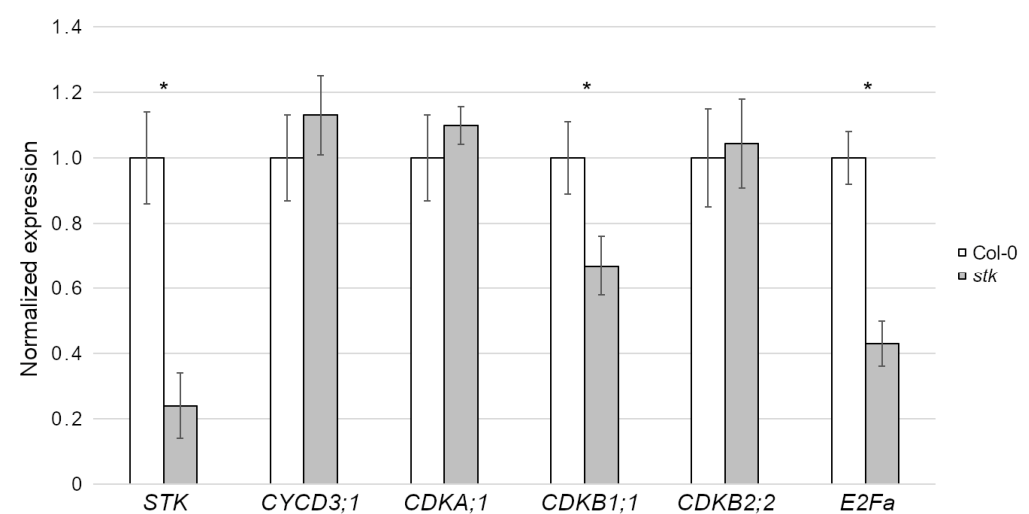


Figure 2. Expression level of cell cycle regulators in Col-0 and *stk* mutants. The q-PCR was conducted in triplicates using *ACTIN* (*ACT*) and *UBIQUITIN* (*UBQ*) as internal reference genes (Supplementary Table S1). Error bars represent the propagated standard deviation error value using three replicates; asterisks represent statistically significant differences ($p < 0.01$).

In *Arabidopsis*, the combined kinase activities of *CYCD3;1* and *CDKA;1* constitute a major positive force of cell cycle progression [27–29]. Despite evidence of an altered cell cycle progression in the seed coat of *stk* seeds, as shown by the flow cytometry analysis, we did not report significant downregulation of *CYCD3;1* nor *CDKA;1* (Figure 2). The checkpoint between the G2 and M phases is also controlled by CDKs of Type B. In particular, B1-type CDKs are characterized by maximum kinase activity during the transition from G2 to M phase, while B2-type CDKs reach their maximum activity during mitosis [30]. However, *CDKB1;1* is only slightly downregulated in *stk* and *CDKB2;2* expression is not affected in the mutant (Figure 2).

In proliferating cells, the transcription factor *E2Fa* acts in complex with RBR1 (RETINOBLASTOMA-RELATED PROTEIN 1) to maintain proliferation competence by inhibiting genes that control the switch from mitosis to the endocycle [31]. Moreover, similar to the *STK* protein, *E2Fa* accumulates in the nucleus of the outer integument cells [24]. For this reason, we tested the expression of *E2Fa* and interestingly, our analysis demonstrated that developing *stk* mutant seeds showed a partially reduced *E2Fa* expression in comparison to wild-type ones (Figure 2).

Since *E2Fa*-induced genes also encode proteins involved in cell wall biosynthesis, providing a possible link to *STK* function [19,32,33], we further investigated a possible regulation of *E2Fa* via *STK*.

2.2. STK Directly Regulates *E2Fa*

To understand the nature of *E2Fa* regulation via STK, we screened the *E2Fa* gene sequence and found two putative CaRG boxes, the CC[A/T]₆GG consensus sequences known to be recognized by the MADS-domain protein [34,35] (Supplementary Figure S2). To test if *E2Fa* could be a direct target of STK, we performed a chromatin immunoprecipitation (ChIP) assay using an anti-STK antibody (Figure 3). As a positive control, we tested *VERDANDI* (*VDD*), a known direct target of STK [35]. Immunoprecipitated chromatin obtained from 0–4 DAF fruits was tested via q-PCR analysis, which showed that the putative binding site “b” of STK on *E2Fa* was significantly enriched over the negative control (Figure 3). This data indicates that *E2Fa* expression is directly regulated by STK in developing seeds by the binding to regulative region “b”.

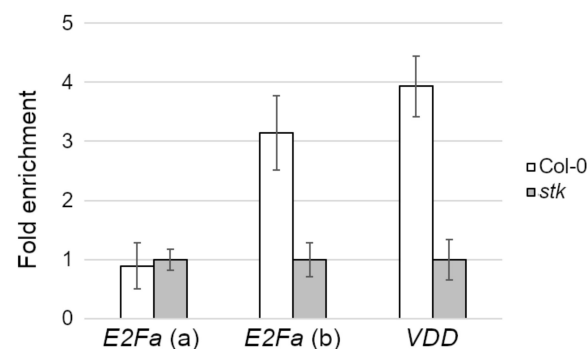


Figure 3. Chromatin immunoprecipitation (ChIP) enrichment by q-PCR of the STK binding site on *E2Fa*. Region “b” of *E2Fa* (see Supplementary Figure S2) is directly bound by STK during seed development, while region “a” is not. *VERDANDI* (*VDD*) was used as positive control. The q-PCR was conducted in duplicates. Fold enrichment was calculated over the negative controls. Error bars represent the propagated error value using three replicates.

Previous studies indicate that protein complexes involved in chromatin remodeling can be recruited on target genes by transcription factors of different families, including MADS [36]. For this reason, we investigated the chromatin landscape at the confirmed STK binding site on *E2Fa*, as we had previously done for *BANYULS* (*BAN*), another direct target of STK during the development of the seed coat [20]. This was done by means of a ChIP experiment on both wild-type and *stk* 0–4 DAF fruits, using a specific antibody to detect the level of H3-lysine9 acetylation (H3K9ac), an epigenetic mark usually associated with the activation of expression, choosing *INDOLE ACETIC ACID-INDUCED PROTEIN 8* (*IAA8*) as a positive control [37]. Indeed, we revealed a lower level of H3K9ac in the *stk* mutant background versus the wild-type (Figure 4), in accordance with our hypothesis of a direct positive regulation of *E2Fa* expression levels by STK.

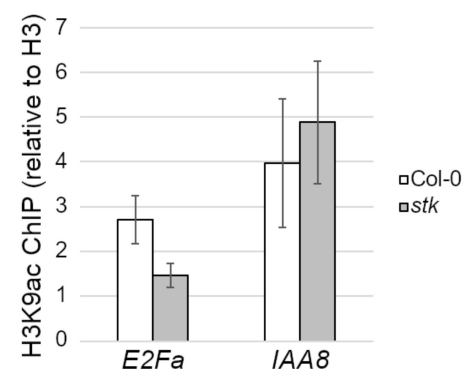


Figure 4. ChIP enrichment tests by q-PCR of H3-lysine9 acetylation (H3K9ac) level in *E2Fa* region “b” of wild-type and *stk* samples expressed as % input, normalized on total H3 level with error bars representing the propagated error value using three replicates. *IAA8* was used as positive control.

3. Conclusions

Based on our previous analyses [20,25] and the data presented here, we propose that STK controls cell cycle progression in the developing seed coat.

This mechanism involves the positive regulation of *E2Fa*. We also found that *CDKB1;1* expression is reduced and interestingly, the promoter of *CDKB1;1* is bound and regulated by *E2Fa* [38]. The activation of *E2Fa* likely involves local epigenetic remodeling of chromatin, as seen by the reduction in open and active chromatin at the STK-bound *E2Fa* locus in *stk* mutants. Thus, the regulation of ovule and seed development by STK expands to cell proliferation control, opening a new facet of MADS-domain transcription factors' action during reproduction.

4. Materials and Methods

4.1. Plant Material and Growth Condition

Arabidopsis thaliana wild-type (ecotype Columbia, Col-0) and *stk* mutant lines were grown on soil at 22 °C (3–6 plants per pot), initially in growth chambers under short-day conditions (8 h light/16 h dark) for two weeks and then moved to an experimental greenhouse under long-day conditions (16 h light/8 h dark). *stk* mutant lines are homozygous for the *stk-2* allele, which contains a 74 nucleotide insertion near the splice site of the 3rd intron; *stk* seeds were obtained by M. Yanosky's lab [15].

4.2. Genotyping

PCR-based genotyping for mutant alleles was performed with the primers listed in Supplementary Table S1 with the following conditions: 95 °C 3', 35 cycles of 95 °C 30'' + 61 °C 30'' + 72 °C 30'', 72 °C 5' and PCR products were checked on ethidium bromide-stained 1% agarose gel in 1 × TAE (Tris base, acetic acid and EDTA buffer).

4.3. Seed Analysis

Seeds were photographed using a Leica MZ6 stereomicroscope, and seed images ($n = 25$) were measured using ImageJ software. Average seed mass was determined by weighing mature dry seeds in batches of 500 and the weights of at least three replicates were measured for each seed lot. Measurements were statistically analyzed by one-way ANOVA with post-hoc Tukey honestly significant difference (HSD) comparison test and statistical differences marked as different letters reflect $p < 0.01$.

4.4. Ploidy Analysis

For flow cytometry analysis, flowers were emasculated 24 h before manual pollination with pollen of the same genotype. Seeds were collected from the siliques at 6 DAF and prepared for analysis using the CyStain[®] UV Precise kit (Partec, Cat. 05-5002). The staining with DAPI (4',6-diamidino-2-phenylindole) was performed as previously described [39]. The ploidy level was calibrated against the 2C nuclear DNA content peak derived from a preparation of young rosette leaves [25].

4.5. Expression Analyses

Total RNA was extracted in triplicate from flowers and siliques until 4 DAF using the LiCl method [40]. Total RNA was treated using Ambion TURBO DNA-free[™] DNase (Ambion, Cat. AM1907) and then reverse transcribed using the Bio-Rad iScript[™] kit (Bio-Rad, Cat. 170-8891). q-PCR was performed on three biological samples and on technical triplicates using the iQ5 real-time PCR detection system (Bio-Rad) in 20 µL reactions with 250 nM of each primer and the SYBR Green PCR Master Mix (Bio-Rad). The 3-step amplification protocol used was 95 °C 3' followed 40 cycles of 95 °C 10'' + 60 °C 30'', with melt curves calculated over the 60–95 °C interval with +0.5 °C increments. cDNA was standardized relative to *UBIQUITIN* (*UBQ*) and *ACTIN* (*ACT*) transcript levels and gene expression analysis was performed with the $2^{-\Delta\Delta Ct}$ method using Bio-Rad CFX Maestro software v.4.0 (Bio-Rad). Baseline and threshold levels were set according to the

manufacturer's instructions. Student's *t*-tests were run for each experiment and asterisks indicate significant differences ($p < 0.01$). The primers used in these experiments are listed in Supplementary Table S1.

4.6. Chromatin Immunoprecipitation Assay

ChIP experiments to evaluate the enrichment of *E2Fa* were performed with an antibody specific for the STK protein on fertilized flowers and siliques until 4 DAF. Plant material was collected from wild-type (Col-0) and *stk* plants. The q-PCR assay was conducted on biological duplicates, with three technical replicates for each sample. The q-PCR protocols used were the same as those listed in Section 4.5 of this manuscript. Data were obtained using the iQ5 real-time PCR detection system (Bio-Rad) with the SYBR Green PCR Master Mix (Bio-Rad) and, for the region of interest, fold enrichment over negative control (*ACT*) was evaluated with a method previously reported using *VDD* as a positive control [35].

Similarly, relative differences in acetylation levels between the wild-type (Col-0) and the *stk* mutant were tested by ChIP using the same developmental stages mentioned above. We used an antibody against an unmodified isoform of H3 ("total H3", Upstate, Cat. 06-753) and one specific for H3K9ac (Upstate, Cat. 07-532). For each sample, the percentage of enrichment in the acetylation versus input was calculated as previously shown [41], normalizing for total H3. *IAA8* was used as a positive control [20]. The primers used in these experiments are listed in Supplementary Table S1.

Supplementary Materials: The following are available online at <https://www.mdpi.com/2223-7747/10/2/192/s1>, Figure S1: DNA-content profile obtained from flow cytometry analysis of seeds; Figure S2: Schematic representation of the *E2Fa* gene; Table S1: List of primers.

Author Contributions: Conceptualization: D.P., L.C. and C.M.; formal analysis: D.P., L.R. and C.M.; supervision and funding acquisition: A.S., S.M. and L.C.; writing—original draft preparation: D.P. and C.M.; writing—review and editing: D.P. and C.M. All authors have read and agreed to the published version of the manuscript.

Funding: This work was supported by a fellowship from the Università degli Studi di Milano (D.P.) and by European Cooperation in Science and Technology (COST) Action FA0903 (D.P. and L.C.).

Data Availability Statement: The data presented in this study are available on request from the corresponding author.

Acknowledgments: The authors would like to thank L. Dreni, F. Galbiati and I. Ezquer for their preliminary assistance in conceptualization and data analysis and A. Cavalleri for critical reading of the manuscript, as well as V. Parravicini and M. Beretta for their technical assistance.

Conflicts of Interest: The authors declare no conflict of interest.

References

- Orozco-Arroyo, G.; Paolo, D.; Ezquer, I.; Colombo, L. Networks controlling seed size in Arabidopsis. *Plant Reprod.* **2015**, *28*, 17–32. [CrossRef]
- Li, N.; Li, Y. Signaling pathways of seed size control in plants. *Curr. Opin. Plant Biol.* **2016**, *33*, 23–32. [CrossRef]
- Li, N.; Li, Y. Maternal control of seed size in plants. *J. Exp. Bot.* **2015**, *66*, 1087–1097. [CrossRef]
- Li, N.; Xu, R.; Li, Y. Molecular Networks of Seed Size Control in Plants. *Annu. Rev. Plant Biol.* **2019**, *70*, 435–463. [CrossRef]
- Haig, D. Kin conflict in seed development: An interdependent but fractious collective. *Annu. Rev. Cell Dev. Biol.* **2013**, *29*, 189–211. [CrossRef]
- Hughes, R.; Spielman, M.; Schruff, M.C.; Larson, T.R.; Graham, I.A.; Scott, R.J. Yield assessment of integument-led seed growth following targeted repair of auxin response factor 2. *Plant Biotechnol. J.* **2008**, *6*, 758–769. [CrossRef]
- Jiang, W.-B.; Lin, W.-H. Brassinosteroid functions in Arabidopsis seed development. *Plant Signal. Behav.* **2013**, *8*, e25928. [CrossRef]
- Zhang, B.; Li, C.; Li, Y.; Yu, H. Mobile TERMINAL FLOWER1 determines seed size in Arabidopsis. *Nat. Plants* **2020**, *6*, 1146–1157. [CrossRef]
- Nowack, M.K.; Ungru, A.; Bjerkan, K.N.; Grini, P.E.; Schnittger, A. Reproductive cross-talk: Seed development in flowering plants. *Biochem. Soc. Trans.* **2010**, *38*, 604–612. [CrossRef]

10. Sun, X.; Shantharaj, D.; Kang, X.; Ni, M. Transcriptional and hormonal signaling control of Arabidopsis seed development. *Curr. Opin. Plant Biol.* **2010**, *13*, 611–620. [[CrossRef](#)]
11. Sundaresan, V. Control of seed size in plants. *Proc. Natl. Acad. Sci. USA* **2005**, *102*, 17887–17888. [[CrossRef](#)]
12. Cucinotta, M.; Colombo, L.; Roig-Villanova, I. Ovule development, a new model for lateral organ formation. *Front. Plant Sci.* **2014**, *5*, 117. [[CrossRef](#)]
13. Masiero, S.; Colombo, L.; Grini, P.E.; Schnittger, A.; Kater, M.M. The emerging importance of type I MADS box transcription factors for plant reproduction. *Plant Cell* **2011**, *23*, 865–872. [[CrossRef](#)]
14. Favaro, R.; Pinyopich, A.; Battaglia, R.; Kooiker, M.; Borghi, L.; Ditta, G.; Yanofsky, M.F.; Kater, M.M.; Colombo, L. MADS-box protein complexes control carpel and ovule development in Arabidopsis. *Plant Cell* **2003**, *15*, 2603–2611. [[CrossRef](#)]
15. Pinyopich, A.; Ditta, G.S.; Savidge, B.; Liljegren, S.J.; Baumann, E.; Wisman, E.; Yanofsky, M.F. Assessing the redundancy of MADS-box genes during carpel and ovule development. *Nature* **2003**, *424*, 85–88. [[CrossRef](#)]
16. Di Marzo, M.; Roig-Villanova, I.; Zanchetti, E.; Caselli, F.; Gregis, V.; Bardetti, P.; Chiara, M.; Guazzotti, A.; Caporali, E.; Mendes, M.A.; et al. MADS-Box and bHLH Transcription Factors Coordinate Transmitting Tract Development in Arabidopsis thaliana. *Front. Plant Sci.* **2020**, *11*, 526. [[CrossRef](#)]
17. Herrera-Ubaldo, H.; Lozano-Sotomayor, P.; Ezquer, I.; Di Marzo, M.; Chávez Montes, R.A.; Gómez-Felipe, A.; Pablo-Villa, J.; Diaz-Ramirez, D.; Ballester, P.; Ferrándiz, C.; et al. New roles of NO TRANSMITTING TRACT and SEEDSTICK during medial domain development in Arabidopsis fruits. *Development* **2019**, *146*. [[CrossRef](#)]
18. Balanzà, V.; Roig-Villanova, I.; Di Marzo, M.; Masiero, S.; Colombo, L. Seed abscission and fruit dehiscence required for seed dispersal rely on similar genetic networks. *Development* **2016**, *143*, 3372–3381. [[CrossRef](#)]
19. Ezquer, I.; Mizzotti, C.; Nguema-Ona, E.; Gotté, M.; Beauzamy, L.; Viana, V.E.; Dubrulle, N.; De Oliveira, A.C.; Caporali, E.; Koroney, A.-S.; et al. The developmental regulator SEEDSTICK controls structural and mechanical properties of the arabidopsis seed coat. *Plant Cell* **2016**, *28*, 2478–2492. [[CrossRef](#)]
20. Mizzotti, C.; Ezquer, I.; Paolo, D.; Rueda-Romero, P.; Guerra, R.F.; Battaglia, R.; Rogachev, I.; Aharoni, A.; Kater, M.M.; Caporali, E.; et al. SEEDSTICK is a Master Regulator of Development and Metabolism in the Arabidopsis Seed Coat. *PLoS Genet.* **2014**, *10*, 1–15. [[CrossRef](#)]
21. Di Marzo, M.; Herrera-Ubaldo, H.; Caporali, E.; Novák, O.; Strnad, M.; Balanzà, V.; Ezquer, I.; Mendes, M.A.; De Folter, S.; Colombo, L. SEEDSTICK Controls Arabidopsis Fruit Size by Regulating Cytokinin Levels and FRUITFULL. *Cell Rep.* **2020**, *30*, 2846–2857.e3. [[CrossRef](#)]
22. Vlieghe, K.; Boudolf, V.; Beemster, G.T.S.; Maes, S.; Magyar, Z.; Atanassova, A.; de Almeida Engler, J.; De Groodt, R.; Inzé, D.; De Veylder, L. The DP-E2F-like gene DEL1 controls the endocycle in Arabidopsis thaliana. *Curr. Biol.* **2005**, *15*, 59–63. [[CrossRef](#)]
23. Sozzani, R.; Maggio, C.; Varotto, S.; Canova, S.; Bergounioux, C.; Albani, D.; Cella, R. Interplay between Arabidopsis activating factors E2Fb and E2Fa in cell cycle progression and development. *Plant Physiol.* **2006**, *140*, 1355–1366. [[CrossRef](#)]
24. Leviczky, T.; Molnár, E.; Papdi, C.; Ószi, E.; Horváth, G.V.; Vizler, C.; Nagy, V.; Pauk, J.; Bögre, L.; Magyar, Z. E2FA and E2FB transcription factors coordinate cell proliferation with seed maturation. *Development* **2019**, *146*, dev179333. [[CrossRef](#)]
25. Mizzotti, C.; Mendes, M.A.; Caporali, E.; Schnittger, A.; Kater, M.M.; Battaglia, R.; Colombo, L. The MADS box genes SEEDSTICK and ARABIDOPSIS Bsisiter play a maternal role in fertilization and seed development. *Plant J.* **2012**, *70*, 409–420. [[CrossRef](#)]
26. Boudolf, V.; Vlieghe, K.; Beemster, G.T.S.; Magyar, Z.; Torres Acosta, J.A.; Maes, S.; Van Der Schueren, E.; Inze, D.; De Veylder, L. The plant-specific cyclin-dependent kinase CDKB1;1 and transcription factor E2Fa-DPa control the balance of mitotically dividing and endoreduplicating cells in Arabidopsis. *Plant Cell* **2004**, *16*, 2683–2692. [[CrossRef](#)]
27. Harashima, H.; Schnittger, A. Robust reconstitution of active cell-cycle control complexes from co-expressed proteins in bacteria. *Plant Methods* **2012**, *8*, 1–9. [[CrossRef](#)]
28. Schnittger, A.; Schöbinger, U.; Bouyer, D.; Weinl, C.; Stierhof, Y.-D.; Hülskamp, M. Ectopic D-type cyclin expression induces not only DNA replication but also cell division in Arabidopsis trichomes. *Proc. Natl. Acad. Sci. USA* **2002**, *99*, 6410–6415. [[CrossRef](#)]
29. Dewitte, W.; Riou-Khamlichi, C.; Scofield, S.; Healy, J.M.S.; Jacquard, A.; Kilby, N.J.; Murray, J.A.H. Altered cell cycle distribution, hyperplasia, and inhibited differentiation in Arabidopsis caused by the D-type cyclin CYCD3. *Plant Cell* **2003**, *15*, 79–92. [[CrossRef](#)]
30. Inze, D.; De Veylder, L. Cell cycle regulation in plant development. *Annu. Rev. Genet.* **2006**, *40*, 77–105. [[CrossRef](#)]
31. Magyar, Z.; Horváth, B.; Khan, S.; Mohammed, B.; Henriques, R.; De Veylder, L.; Bakó, L.; Scheres, B.; Bögre, L. Arabidopsis E2FA stimulates proliferation and endocycle separately through RBR-bound and RBR-free complexes. *EMBO J.* **2012**, *31*, 1480–1493. [[CrossRef](#)]
32. Vlieghe, K.; Vuylsteke, M.; Florquin, K.; Rombauts, S.; Maes, S.; Ormenese, S.; Van Hummelen, P.; Van de Peer, Y.; Inze, D.; De Veylder, L. Microarray analysis of E2Fa-DPa-overexpressing plants uncovers a cross-talking genetic network between DNA replication and nitrogen assimilation. *J. Cell Sci.* **2003**, *116*, 4249–4259. [[CrossRef](#)]
33. De Jager, S.M.; Scofield, S.; Huntley, R.P.; Robinson, A.S.; den Boer, B.G.W.; Murray, J.A.H. Dissecting regulatory pathways of G1/S control in Arabidopsis: Common and distinct targets of CYCD3;1, E2Fa and E2Fc. *Plant Mol. Biol.* **2009**, *71*, 345–365. [[CrossRef](#)]
34. Nurrish, S.; Treisman, R. DNA binding specificity determinants in MADS-box transcription factors. *Mol. Cell. Biol.* **1995**, *15*, 4076–4085. [[CrossRef](#)]

35. Matias-Hernandez, L.; Battaglia, R.; Galbiati, F.; Rubes, M.; Eichenberger, C.; Grossniklaus, U.; Kater, M.M.; Colombo, L. VERDANDI is a direct target of the MADS domain ovule identity complex and affects embryo sac differentiation in Arabidopsis. *Plant Cell* **2010**, *22*, 1702–1715. [[CrossRef](#)]
36. Hill, K.; Wang, H.; Perry, S.E. A transcriptional repression motif in the MADS factor AGL15 is involved in recruitment of histone deacetylase complex components. *Plant J.* **2008**, *53*, 172–185. [[CrossRef](#)]
37. Lauria, M.; Rossi, V. Epigenetic control of gene regulation in plants. *Biochim. Biophys. Acta* **2011**, *1809*, 369–378. [[CrossRef](#)]
38. Nowack, M.K.; Harashima, H.; Dissmeyer, N.; Zhao, X.; Bouyer, D.; Weimer, A.K.; De Winter, F.; Yang, F.; Schnittger, A. Genetic framework of cyclin-dependent kinase function in Arabidopsis. *Dev. Cell* **2012**, *22*, 1030–1040. [[CrossRef](#)]
39. Nowack, M.K.; Shirzadi, R.; Dissmeyer, N.; Dolf, A.; Endl, E.; Grini, P.E.; Schnittger, A. Bypassing genomic imprinting allows seed development. *Nature* **2007**, *447*, 312–315. [[CrossRef](#)]
40. Verwoerd, T.C.; Dekker, B.M.; Hoekema, A. A small-scale procedure for the rapid isolation of plant RNAs. *Nucleic Acids Res.* **1989**, *17*, 2362. [[CrossRef](#)]
41. Lin, X.; Tirichine, L.; Bowler, C. Protocol: Chromatin immunoprecipitation (ChIP) methodology to investigate histone modifications in two model diatom species. *Plant Methods* **2012**, *8*, 1–9. [[CrossRef](#)]

Review

Barley's Second Spring as a Model Organism for Chloroplast Research

Lisa Rotasperti , Francesca Sansoni , Chiara Mizzotti , Luca Tadini and Paolo Pesaresi * 

Dipartimento di Bioscienze, Università Degli Studi di Milano, 20133 Milano, Italy; lisa.rotasperti@unimi.it (L.R.); francesca.sansoni1@studenti.unimi.it (F.S.); chiara.mizzotti@unimi.it (C.M.); luca.tadini@unimi.it (L.T.)

* Correspondence: paolo.pesaresi@unimi.it

Received: 10 June 2020; Accepted: 24 June 2020; Published: 27 June 2020



Abstract: Barley (*Hordeum vulgare*) has been widely used as a model crop for studying molecular and physiological processes such as chloroplast development and photosynthesis. During the second half of the 20th century, mutants such as *albostrians* led to the discovery of the nuclear-encoded, plastid-localized RNA polymerase and the retrograde (chloroplast-to-nucleus) signalling communication pathway, while *chlorina-f2* and *xantha* mutants helped to shed light on the chlorophyll biosynthetic pathway, on the light-harvesting proteins and on the organization of the photosynthetic apparatus. However, during the last 30 years, a large fraction of chloroplast research has switched to the more “user-friendly” model species *Arabidopsis thaliana*, the first plant species whose genome was sequenced and published at the end of 2000. Despite its many advantages, *Arabidopsis* has some important limitations compared to barley, including the lack of a real canopy and the absence of the proplastid-to-chloroplast developmental gradient across the leaf blade. These features, together with the availability of large collections of natural genetic diversity and mutant populations for barley, a complete genome assembly and protocols for genetic transformation and gene editing, have relaunched barley as an ideal model species for chloroplast research. In this review, we provide an update on the genomics tools now available for barley, and review the biotechnological strategies reported to increase photosynthesis efficiency in model species, which deserve to be validated in barley.

Keywords: Barley; genome; functional genomics; chloroplast biogenesis; photosynthesis improvement

1. barley, the Crop and the Model Species

Barley (*Hordeum vulgare*) is a self-pollinating monocotyledonous plant species that belongs to the *Poaceae*, a grass family that includes several major crops exploited in modern agriculture. Its domestication dates back to 10,000 BC, took place in the Fertile Crescent and began with the wild species *Hordeum vulgare* ssp. *spontaneum* [1]. Barley ranks fourth in terms of annual grain tonnage after maize, wheat and rice, with a worldwide production level (2018/2019) of 141 million tons. The primary role of cultivated barley (*Hordeum vulgare* ssp. *vulgare*) is as a source of animal feed (about 75% of the global production), with subsidiary uses in alcoholic and non-alcoholic beverages (20%), and in human nutrition (5%)—partly due to its high content of beta-glucan, a beneficial fibre that can reduce levels of cholesterol in the blood. During the 20th century, barley was widely exploited as a model species for crop studies. As a self-pollinating species with a diploid (2n) genome and a haploid complement of only seven chromosomes, barley proved to be an excellent model organism for both basic and applied research. Furthermore, due to the fact that wild barley (*Hordeum vulgare* ssp. *spontaneum*) can grow in a wide range of environments and climates, from the Arctic Circle to the equatorial highlands, barley is cultivated more widely than any other major crop. This resilience relies on a wealth of natural genetic

diversity which enables the plant to adapt effectively to various environmental challenges such as cold temperatures, drought, alkalinity and salinity, and makes it a perfect model species for investigating crop adaptation to abiotic stresses [2].

1.1. A Brief History of Genome Manipulation in Barley

Hordeum vulgare was one of the very first crops used in cereal improvement programs based on different induced mutation strategies. In 1930, Stadler studied the mutagenic effects of different types of radiation on maize and barley, describing chlorophyll-deficient and virescent phenotypes in seedlings [3]. In 1938, Nilsson-Ehle and Gustafsson tested X-rays and UV light on the barley cultivar (cv.) ‘Gull’ and isolated several mutants, which were named *albina*, *xantha*, *alboviridis*, *viridis*, *tigrina*, *striata* and *maculata*, categorizing them by their carotenoid and chlorophyll contents and distribution within the leaf blade [4]. The characteristics of several mutated lines were recognized as being very valuable for potential use in agriculture, since they exhibited alterations in grain yield, straw stiffness, straw length and tillering capacity, as well as changes in spike firmness, kernel maturation and pigmentation [5]. Later on, two varieties of barley ‘Trebí’ and ‘Moister’ were exposed to the radiation generated by the first aerial atomic explosion at Bikini atoll in 1946 [6]. Meanwhile, Gustafsson and Mackey applied mustard gas to barley to observe the effect of chemical mutagenesis [7], whereas Ehrenberg and collaborators tested various mutagenic compounds on barley and evaluated their impact on chlorophyll accumulation [8]. After these pioneering experiments, a broad range of chemical and physical mutagens were tested systematically. During this phase, alkylating agents able to generate G/C to A/T transitions in DNA, such as EMS (Ethyl Methane Sulfonate), ENU (N-nitroso-N-ethylurea), MNU (N-nitroso-N-methylurea), DES (diEthyl Sulfate) and sodium azide (NaN_3), were widely used for the mutagenesis of barley. The first chemically induced barley variety, ‘Luther’, was released in the US in 1966. ‘Luther’ was obtained by exposing the variety ‘Alpine’ to DES. In 1965, in Czechoslovakia, the variety ‘Diamant’ was obtained after gamma-ray irradiation. This new variety was ~ 15 cm shorter than the parental ‘Valticky’ and displayed an increase in grain yield amounting to about 12% [9]. At around the same time, in the UK, ‘Golden Promise’ was registered. This semi-dwarf cultivar originated from exposure of the salt-sensitive variety ‘Maythorpe’ to gamma rays [10]. The generation of ‘Golden Promise’ represented an important step towards the development of tissue culture and barley transformation techniques (see below).

1.2. Early Studies and Milestones in Understanding of Chloroplast Biogenesis and Physiology in Barley

Genetic studies of barley have not been restricted to breeding programs. The plant has also been used as a model species to dissect the molecular mechanisms that underlie plant development and physiology and, for a large part of the 20th century, it served as a major experimental system for the investigation of chloroplast biogenesis and photosynthesis. In particular, several studies during the 1970s characterized different aspects of plastid structure and development, such as plastid growth, replication and differentiation. Dark-grown barley seedlings were used to determine the protochlorophyll content and structure of the etioplasts. Exposure to different light conditions allowed chloroplast development to be characterised from both structural and biochemical points of view [11–14].

The organization of chloroplast membranes was analysed in chloroplast preparations solubilised with digitonin and fractionated by electrophoresis, proving the existence of distinct sets of membranes [15]. The functionality and structural organization of thylakoids were also studied in barley mutants altered in chlorophyll biosynthesis [16] and revealed the impact of such changes on thylakoid membrane organization. For instance, the *chlorina-f2* mutant, which is impaired in chlorophyll b accumulation, led to the discovery of light-harvesting chlorophyll-binding proteins [17–20]. *Chlorina-f2* was also used to assess the impact of protein-chlorophyll complexes on the ultrastructure of thylakoid membranes, shedding light on the organisation of the photosynthetic apparatus [17,21]. In addition, the *tigrina-d* mutant [22], originally suggested to be involved in the early steps of tetrapyrrole

biosynthesis prior to ALA formation, was recently identified as the barley orthologue [23] of the *FLU* gene of *Arabidopsis thaliana*, a nuclear-encoded, plastid-localized protein that plays a key role in the negative-feedback control of chlorophyll biosynthesis, with an essential role during the dark-to-light switch [24]. Moreover, the barley *xantha* mutants helped to elucidate key steps in chlorophyll biosynthesis [25]: *xantha-l* was shown to code for a mutated form of Mg-protoporphyrin IX monomethyl ester cyclase, while *xantha-f*, *-g*, and *-h* carry genetic lesions at three distinct loci encoding the three Mg-chelatase subunits [26,27].

From a physiological point of view, Smith et al. [28] documented changes in chloroplast activity during de-etiolation of barley seedlings by measuring the Hill reaction in relation to chlorophyll accumulation. The correlation between plastid ultrastructure, chlorophyll synthesis and development of photosynthetic activity was also evaluated by measuring O₂ evolution [29].

Besides the characterization of the photosynthetic apparatus, barley played an important part in the dissection of the chloroplast's gene expression machinery. Indeed, evidence for a fully nuclear-encoded transcriptional activity in plastids, later named the Nuclear-Encoded RNA Polymerase (NEP; [30]), was first reported in barley, based on analysis of the *albostrians* mutant. In particular, the synthesis of RNA was reported in the white sectors of *albostrians* leaves, which harbor plastids that are devoid of ribosomes. These data provided initial evidence for the existence of a nuclear-encoded and plastid-localized RNA polymerase [31]. In addition, ribosome-free plastids of *albostrians* were helpful in distinguishing between the set of plastid genes preferentially transcribed by NEP, such as *rRNA*, *rpo* and *rps15*, and the set transcribed by the Plastid-Encoded RNA polymerase (PEP), which is enriched in photosynthesis-related genes such as *psbA*, *rbcL*, *atpI-H* [31,32]. Furthermore, the barley *albostrians* mutant was essential to the initial detection of communication between organellar and nuclear genomes. By analyzing *albostrians*, which is characterized by reduced amounts and/or activities of nucleus-encoded chloroplast proteins including the small subunit of ribulose-1,5-bisphosphate carboxylase/oxygenase (Rubisco), ferredoxin NADP⁺ reductase, and enzymes of the Calvin cycle, Börner provided the first evidence for plastid signals that control nuclear gene expression, leading to the discovery of chloroplast-to-nucleus retrograde communication [33–35].

2. *Arabidopsis thaliana* as the Model Plant of Modern Times

In the 1990s, crop models lost their dominant position in basic research on plants to *Arabidopsis thaliana*, which has now reigned supreme for three decades. Its small size, short life cycle, ability to produce thousands of seeds from a single plant and simple growth requirements were perfectly compatible with lab facilities and research workflows. Moreover, its small diploid nuclear genome (~135 Mb on 5 chromosomes) and the *Agrobacterium tumefaciens*-based transformation protocol made *Arabidopsis* ideal for use in basic research [36]. The *Arabidopsis* Genome Project was initiated in 1990, and led to the publication of the first sequenced plant genome in 2000 [37]. This, together with large collections of insertional mutants (SIGnAL, <http://signal.salk.edu/cgi-bin/tdnaexpress>), permitted the functional characterization of large numbers of genes and biological processes, thus laying the foundations for the modern age of plant biology.

Although *Arabidopsis* has been considered the “golden” model species in plant science, it does have some limitations in terms of the extent to which lessons on development and physiology learnt from this model species can be extrapolated to monocots, including barley. This is particularly true for processes such as chloroplast biogenesis and photosynthesis. For instance, *Arabidopsis* does not produce an overhead canopy, and therefore cannot be employed in studies of plant architecture and optimization of photosynthesis under field conditions [38,39]. Moreover, the biogenesis of the multisubunit photosynthetic complexes, and indeed the chloroplast more generally, appear to differ significantly between monocotyledonous and dicotyledonous plants [40]. In monocots, the process of chloroplast development from the proplastid to functional chloroplasts can be observed as a gradient along the leaf blade, since leaves have a basal meristem and, as a consequence, the youngest cells carrying proplastids are found at the leaf base, while the leaf tip consists of the oldest cells with

mature chloroplasts [29,41,42]. In contrast, in dicots like *Arabidopsis thaliana* chloroplast development varies between plant organs—i.e., between cotyledons and leaves—and with respect to the leaves, most of the events take place inside the shoot apex, which constitutes a major limitation for functional studies [43,44]. In light of these limitations, the widely accepted knowledge transfer route from *Arabidopsis* to crops is not always the most convenient and effective strategy, especially in the era of next-generation sequencing technologies and gene-editing approaches that make functional genomics studies feasible in species with complex genomes.

3. The Genomes of Barley

3.1. The Nuclear Genome

For a long time, the absence of a reference genome has been the major obstacle to the exploitation of barley genomic resources in both research and breeding programs. The relatively large size of the barley genome (5.3 Gb), together with its high proportion of repetitive DNA (more than 80%), has severely compromised the assembly of the whole-genome shotgun sequence and the generation of a reference genome (Figure 1). However, in 2012 the International Barley Sequencing Consortium circumvented these problems by integrating several different strategies. This involved coupling a detailed physical map of the barley cv. 'Morex' (a US spring six-row malting barley) with high-density genetic maps, superimposing deep short-read whole-genome shotgun assemblies, and annotating the resulting linear genomic sequence with dense-coverage RNA-derived, i.e., full-length cDNA and RNA-seq, data. This strategy allowed approximately 4 Gb (80%) of the genome to be delineated, including more than 90% of the expressed genes, together with their physical distribution and patterns of expression [45]. This partially ordered sequence assembly has since been substantially improved by Mascher and collaborators [46] through the release of a map-based reference sequence of the barley cv. 'Morex' genome that included the first comprehensively ordered assembly of the pericentromeric regions. The final genome sequence covered 4.79 Gb (approximately 95% of the total genome size), of which 4.54 Gb were assigned to precise chromosomal locations. Mapping of transcriptome data and reference protein sequences from other plant species to the assembly identified 39,734 high- and 41,949 low-confidence genes, representing 98% of the Morex gene complement. Furthermore, homology-guided repeat annotation identified 3.7 Gb (80.8%) of the assembled sequence as derived from transposable elements, most of which were present as truncated and degenerated copies, with only 10% of mobile elements being intact and potentially active. A second improved version of the barley cv. 'Morex' reference genome has recently been released [47]. This is based on the use of TRITEX, an open-source computational workflow, whose output is available on the IPK Barley BLAST server (https://webblast.ipk-gatersleben.de/barley_ibsc/, see Table 1). The need for an improved assembly arose from large sequence gaps and local mis-assemblies present in the first reference sequence. A total of 32,787 high- and 30,871 low-confidence gene models were annotated in the second version of the barley genome. The smaller number of high-confidence gene models described in the second version of the genome (32,787 vs 39,734) is certainly due to the more precise annotation process, making the TRITEX-based assembly a greatly improved version of the reference genome. More recently, a reference genome assembly for the barley cv. Golden Promise has been reported [48]. The assembled genome of seven chromosomes comprising 4.13 Gb contains 95.2% of complete and single-copy genes and will prove particularly useful for functional genomics studies, given that Golden Promise is the most readily transformable barley genotype.

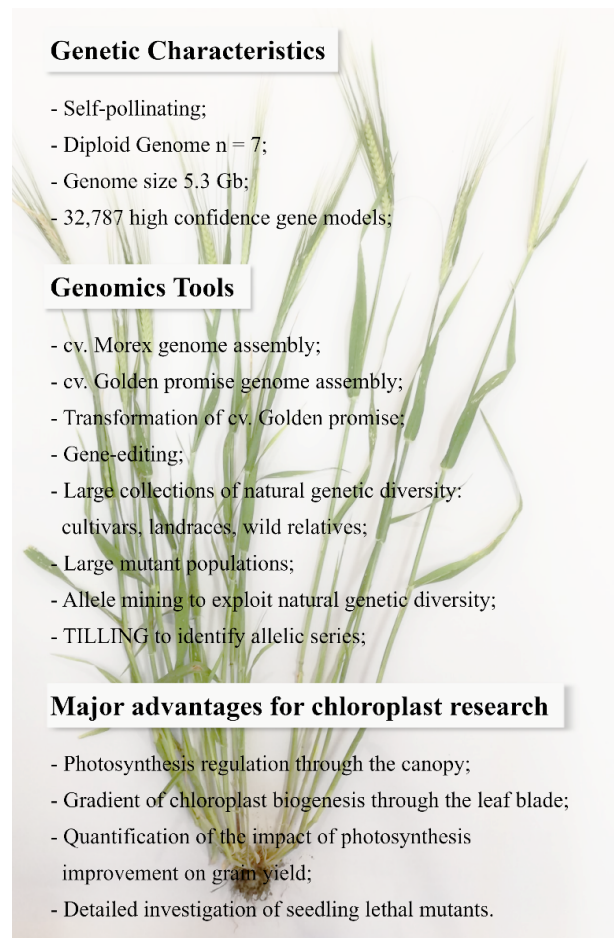


Figure 1. Overview of the genetic characteristics and genomics tools available for barley. These features, together with its canopy architecture and developmental properties, make barley an optimal model for chloroplast research.

Table 1. List of databases, genome browsers and bioinformatics tools available for barley genome analyses.

Tool	Description/Application	URL	Reference
BARLEX	The Barley Genome Explorer permits visual inspection of BAC overlaps, and comparisons of BACs and provides useful information on genes and markers	http://barlex.barleysequence.org	[49]
EnsemblPlants	A genome browser that incorporates genomic data from diverse organisms, including numerous plant species. It enables users to compare genome-scale datasets with the aid of a single collection of interfaces	http://plants.ensembl.org	[50]
IPK Barley BLAST Server	Barley BLAST server for genome-scale homology-based searches	http://webblast.ipk-gatersleben.de/barley	[51]

Table 1. Cont.

Tool	Description/Application	URL	Reference
Golden Promise Genome	GMAP and BLAST server for barley (cv. Golden Promise) genome comparisons, including mapping of transcripts	https://ics.hutton.ac.uk/gmapper/	[48]
Gramene	Integrated data resource for comparative functional genomics in crops and model plant species	http://www.gramene.org	[52]
PlantsDB	Provides data and information resources for individual plant species and a platform for integrative and comparative plant genome research.	http://pgsb.helmholtz-muenchen.de/plant/	[53]
BaRTv1.0	Barley Reference Transcript Dataset provides access to 177,240 barley-expressed transcripts covering 60,444 genes	https://ics.hutton.ac.uk/barleyrtd/	[54]

3.2. The Exomes

A broader knowledge of the genetic diversity of barley is an essential prerequisite for the development of new varieties with increased yields and greater environmental robustness. A comprehensive genotyping of germplasm based on exome sequencing currently offers the best route to this goal. Sequencing of the coding DNA alone dramatically decreases the complexity of the task, and reduces the computational effort and associated costs compared with whole-genome approaches. This makes it highly suitable for crops like barley, which contain very high proportions of transposon DNA [46]. The application of the exome approach to barley was initially reported in Mascher et al. [55], and was first applied to examine the crop's adaptive responses in an analysis of 267 geo-referenced landraces and wild accessions [56]. This analysis combined exome capture and sequencing with field trials, bioclimatic data and various statistical approaches to investigate the genomic signatures that underlie barley's adaptive responses to various environmental stresses. A total of 1,688,807 SNPs and 143,872 short InDels were identified in 59.5 Mb of genomic sequence. The study yielded a large pool of genetic variation to be exploited in future breeding programs, as many of the SNPs identified were rare, showing an overall allele frequency below 5% and being more highly represented in wild accessions. A similar strategy based on exome capture sequencing [57] explored the genetics of barley adaptation to multiple contrasting environments in 371 domesticated lines, comprising cultivars and landraces of both two- and six-rowed types. The identification of 435,431 SNPs uncovered significant genetic diversity—including a well-defined subset of spring-growth-habit barleys, made up of 111 cultivars and 63 landraces—as well as revealing strong differentiation at specific chromosome positions between two- and six-row barley lines, and high adaptation and heritability of phenotypes such as days to heading, plant height, 1000-grain weight and awn length.

4. Barley Genetic Resources: Natural and Induced Genetic Diversity

4.1. Natural Genetic Diversity

Crop improvement through crossing of high-performance cultivars has resulted in the loss of genetic diversity across cultivated genomes, a phenomenon known as the “domestication bottleneck” [58]. Therefore, landraces and wild accessions of barley are a precious pristine source of natural allelic variability that can be exploited in barley breeding programs, as has now been verified by exome sequencing assays (see above). Over the years, several research institutes around the world have collected barley accessions with the aim of preserving this genetic variability and making it accessible to breeders through the adoption of advanced methods that are better able to discover, dissect and deploy useful variations [46,59]. The major collections are maintained in institutions around the

world, and the most representative are listed in Table 2. Among them, the ICARDA Collection hosts 222,704 barley accessions. Most of these are advanced materials, such as released cultivars and research lines, while 22% are geo-referenced wild barley relatives and landraces. The International Barley Core Collection (BCC) is a research collection that aims to represent the fullest possible range of the extant diversity of wild and cultivated barley. About 1300 accessions are currently available. Of these, some 300 varieties and landraces are held in the IPK Gatersleben Genebank. Of special relevance is the WHEALBI collection (<http://www.whealbi.eu/>), which comprises 511 accessions. This source of material represents a worldwide selection of barley's genetic diversity, including landraces, cultivars and progenitors. In particular, the WHEALBI panel includes accessions originating from a wide range of locations covering key crop production regions in Europe, Africa, the Middle East and Asia. A subset of 371 domesticated lines chosen from the entire WHEALBI germplasm has been subjected to exome sequencing in order to correlate genomic and phenotypic data [57]. Various online platforms have been developed to facilitate searches of germplasm collections and provide detailed information on their origins and characteristics. Some of these are listed in Table 2.

Table 2. List of representative collections of natural variants of barley available at different institutions worldwide, together with online platforms that provide information about barley genetic resources.

Collections of natural genetic diversity		
Gene Bank	Country	URL
PGRC Plant Gene Resources of Canada, Saskatoon Research Centre, Agriculture and Agri-Food Canada)	Canada	https://pgrc.agr.gc.ca/index_e.html
NSGC The National Small Grains Collection is part of the National Plant Germplasm System (NPGS) of the United States Department of Agriculture - Agricultural Research Service (USDA-ARS)	USA	https://www.ars.usda.gov/pacific-west-area/aberdeen-id/small-grains-and-potato-germplasm-research/docs/barley-wheat-genetic-stocks-collections-1/
ICARDA International Centre for Agricultural Research in the Dry Areas	Global	https://grs.icarda.org/
IPK Leibniz Institute of Plant Genetics and Crop Plant Research	Germany	http://gbis.ipk-gatersleben.de
WHEALBI WHEAt and barley Legacy for Breeding Improvement	France	http://wheat-urgi.versailles.inra.fr/Projects/Achieved-projects/Whealbi
NORDGEN Nordic Genetic Resources Centre	Sweden	https://www.nordgen.org/bgs/
GRU Germplasm Resource Unit, John Innes Centre	UK	https://www.seedstor.ac.uk/
NARO NIAS, National Institute of Agrobiological Sciences	Japan	https://www.gene.affrc.go.jp/databases_en.php
Online platforms for barley germplasm searches		
Name	Description	URL
GENESIS	An online platform containing information about plant genetic resources for food and agriculture, conserved in gene banks worldwide	https://www.genesys-pgr.org/
SINGER (The system-wide Information Network for Genetic Resources)	An online catalogue of crop collections together with their locations	https://www.gbif.org/dataset/85818aea-f762-11e1-a439-00145eb45e9a
EURISCO (The European Search Catalogue for Plant Genetic Resources)	Information on more than 2 million crop plant accessions and their wild relatives, preserved ex situ by almost 400 institutes in Europe and beyond	https://www.ecpgr.cgiar.org/resources/germplasm-databases/eurisco-catalogue/

4.2. Induced Genetic Diversity: Random Chemical and Physical Mutagenesis

Besides natural genetic diversity, the availability of barley mutants is very important for understanding gene functions and their links with phenotypical traits (Figure 1). As described above (see Section 1.1), chemical and physical agents have been used to generate random mutagenized barley populations by several research groups. A few of these populations, derived from diverse genetic backgrounds, are listed in Table 3. Two large-scale EMS mutant populations from the cv. Optic, for instance, have been developed [60] and comprise approximately 20,000 M₂ plants. TILLMore, a sodium azide-mutagenized population of cv. Morex, has also been created [61] and consists of 4906 M₃ families. More recently, the *HorTILLUS* (*Hordeum*—TILLING—University of Silesia) population, derived from the spring barley cultivar Sebastian following treatment of seeds with two chemical mutagens (NaN₃ and MNU) and consisting of more than 9600 M₂ plants, was reported [62]. However, one limitation of the available resources is that the parental cultivars used for mutant population development are all recalcitrant to genetic transformation. Consequently, gene-specific complementation assays, which are essential for phenotype-to-genotype association, are generally not possible. To mitigate this drawback, a heavily mutagenized EMS population of cv. Golden Promise (the reference variety used across the barley research community for genetic transformation and functional genomics) has been developed [63]. This population permits direct complementation of candidate mutations, opening up new possibilities for efficient functional genomics studies.

Table 3. List of representative barley mutant populations obtained by either chemical or physical mutagenesis in different genetic backgrounds, i.e., cultivars.

Induced Mutant Populations		
Cultivar	Mutagen	Reference
Optic	EMS	[60]
Barke	EMS	[64]
Morex	NaN ₃	[61]
Lux	NaN ₃	[65]
DH-930-36	MNU	[66]
DH-930-36	Gamma rays	[66]
Sebastian	NaN ₃ +MNU	[62]
Golden Promise	EMS	[63]

During the last 15 years, mutagenized populations have emerged as a key resource for gene discovery [67]. Using forward genetics approaches, many genes, especially those that confer morphological or developmental phenotypes, have now been isolated [68–71]. In addition, Targeting Induced Local Lesions in Genomes (TILLING; [72]) has become particularly powerful for gene validation studies, and for exploring the roles of genes for which no obvious visual phenotype can be predicted, i.e., the reverse genetics approach [73]. Moreover, the TILLING approach produces allelic series, which are important for genes whose knock-out would be lethal, but also in cases where proteins/enzymes with novel properties are needed. Identification of the DNA sequence changes responsible for mutant phenotypes has been performed, so far, through heteroduplex analysis [74]. This involves amplification of the gene of interest from a DNA pool, enzymatic cleavage of heteroduplexes formed by allelic mismatches, and detection of the cleaved strands in polyacrylamide gels, followed by sequencing for confirmation of the variation. However, with the advent of Next Generation Sequencing (NGS) technologies and the availability of reference genomes, the use of exome capture sequencing and/or pooled amplicon sequencing of multiple target genes appears to be more effective in the case of barley [63,75]. Moreover, it is worth mentioning that these mutagenized barley plants are not

considered as Genetically Modified (GM), and can be used in field trials to evaluate their performance, even in countries in which the cultivation of GM organisms is forbidden.

4.3. Induced Genetic Diversity: Genome Transformation and Insertional Mutagenesis

The need for complete sequencing of the barley genome, the range of genetic diversity and the numerous mutant populations all underline the importance of developing an efficient and versatile transformation protocol for functional genomics studies. In barley, many types of explant tissues have been used for tissue culture and plant regeneration, and immature embryos have proven to be the most suitable for barley transformation. Immature embryos were first used as explants for barley transformation in 1986 [76], and gradually became the most popular system. However, plant regeneration from immature embryo-derived callus is influenced by genotype, with the highest rates of success having been obtained in the cv. Golden Promise [77]. Up to now, a variety of DNA delivery methods, which involve biological, chemical, mechanical and/or physical treatment, have proven effective in barley. However, *Agrobacterium*-mediated transformation seems to be the best strategy, since it is characterised by low cost, high efficiency, simple integration, stable inheritance and expression of the transgene over generations. Indeed, the current transformation protocol integrates *Agrobacterium* and immature embryos, yielding an average transformation efficiency of 25% [78]. This protocol is widely used for overexpression, RNAi (RNA interference) applications and, more recently, CRISPR/Cas 9-mediated gene editing, as discussed below. Transgenic approaches have been employed to control pathogens such as Barley Yellow Dwarf Virus (BYDV; [79]), *Fusarium graminearum* [80], leaf stripe disease (*Pyrenophora graminea*; [81]), powdery mildew (*Blumeria graminis* f. sp. *Hordei*; [82]) and stem rust (*Puccinia graminis* f. sp. *Tritici*; [83]). Moreover, the transgenic technology has also been used to increase tolerance to environmental stresses, such as drought [84,85] and frost [86–88], and to modify enzymes, such as α -amylase, β -amylase, β -glucanase and (1,3;1,4)- β -D-glucan endohydrolase [89–93], which have an influence on the brewing process. The transgenic technology is also essential for mutagenesis. In barley, insertional mutagenesis has been used to produce loss-of-function mutations based on transposable elements such as the Ac/Ds-based tagging system [94–96], and gain-of-function mutations using the activation tagging strategy that promotes or enhances, through random genomic insertion, the expression of neighbouring regions [95]. However, unlike the case in *Arabidopsis*, no large-scale T-DNA insertional populations are currently available for barley.

4.4. Induced Genetic Diversity: Gene Editing

The availability of the whole genome sequence, together with the recently developed gene-editing strategies, makes targeted mutagenesis possible in barley [97]. Among the various customized endonucleases used in plant research, the type II Clustered Regularly Interspaced Short Palindromic repeat (CRISPR)/CRISPR-associated protein 9 (Cas9) system has proven to be the best tool for gene editing [98]. The CRISPR/Cas9 gene-editing technology is easy to design and very precise. It requires the synthesis of oligonucleotides which, once transcribed into RNA, guide the Cas9 enzyme to the desired target. Being based on RNA–DNA interaction, the method is quite specific. The CRISPR/Cas9 technology can be used to create null alleles (i.e., gene knock-outs), and by adding a designed DNA template to the CRISPR/Cas9 system, it is possible to replace the target sequence via the error-free homology-directed repair pathway [99]. Furthermore, the system can be used to modulate gene expression [100]. In the past few years, the CRISPR/Cas9 technique has been increasingly applied to barley. In particular, a simple and efficient CRISPR/Cas9 platform for the induction of single and multiple, heritable mutations has been introduced [101]. The CRISPR/Cas9 technique has also been utilised to study genes involved in responses to pathogens, such as *HvMORC1*, whose protein product is one of the seven MORC members encoded by the barley genome [102]. Knock-out alleles of *HvCKX1* or *HvCKX3*, which are involved in the regulation of cytokinin metabolism and root morphology [103], as well as mutants in the *D-hordein* gene, which participates in the control of grain size and grain composition in barley [104], were also generated with the aid of CRISPR/Cas9.

5. Barley is Ready for a New Age of Functional Genomics Studies and Genetic Improvements

With the aid of the recently acquired collection of functional genomics tools, in a large part described above, the unique potential of barley as an ideal system for functional genomics studies can now be fully exploited. These new methods can elucidate, for instance, the molecular mechanisms behind chloroplast-to-nucleus communication, which is essential for chloroplast biogenesis and leaf emergence, leaf senescence and adaptation to environmental stresses. They can also be used to test—in an established crop plant—strategies intended to increase photosynthesis efficiency and biomass production, which have been shown to work in model species (Figure 2).

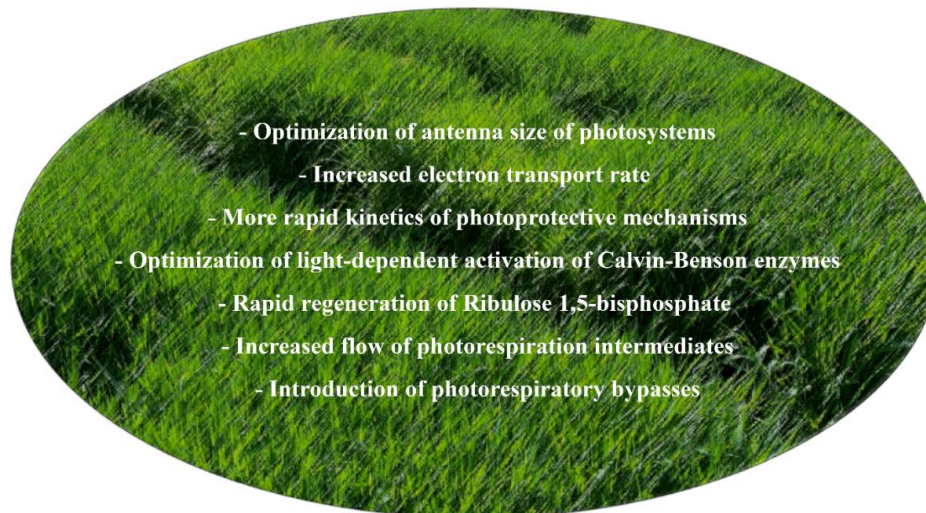


Figure 2. Biotechnological strategies that have been shown to enhance photosynthetic efficiency in model species. All of them can be applied to barley using the available genetic tools, and can potentially be improved by exploiting the genetic diversity of barley.

5.1. Plastid-to-Nucleus Retrograde Signalling

The chloroplast genome in barley encodes only 78 of the 3000 proteins that compose the plastid proteome [105,106]. The rest now reside in the nuclear DNA. Hence, signalling pathways that allow plastid and nuclear genomes to communicate with each other are essential for proper chloroplast development and functionality. The plastid-to-nucleus component of this circuit is often referred as “retrograde signalling” and it was first discovered in the barley mutant *albostrians* (see Section 1.2), which lacks plastid ribosomes and, concomitantly, shows reduced amounts and/or activities of nuclear-encoded plastidic proteins [33–35]. This channel is used to keep the nucleus informed of the developmental state of plastids (known as biogenic control), but it also signals changes in the functional status of fully developed chloroplasts in response to environmental factors, a process termed operational control [107]. Thus, chloroplast-to-nucleus communication is vital for chloroplast biogenesis and leaf emergence, as well as for the transition from chloroplast to gerontoplast during leaf senescence. Since the modulation of early leaf emergence and leaf senescence extends the proportion of the photosynthetically active radiation (PAR) that is intercepted by the crop over the growing season (the interception efficiency), both aspects of this communication are likely to be important determinants of crop yield. In addition, leaf senescence is a central process in maximising the efficiency of nutrient use, i.e., the ability of the plant to mobilise and translocate nutrients from leaves to grains. This is particularly true for small-grained cereals like barley, where up to 90% of the nitrogen is mobilised to the grains, mainly from the photosynthetic apparatus present in the leaves, and including Rubisco.

During the last 15 years, studies performed mainly in *Arabidopsis thaliana* have revealed a complex network of signals that allows chloroplasts to communicate their functional status to the nucleus. Singlet oxygen [108], H₂O₂ [109], the redox state of the photosynthetic electron transport

chain [110], 3'-phosphoadenosine 5'-phosphate [111], the isoprenoid precursor methylerythritol cyclodiphosphate [112], β -cyclocitral [113,114] and other potential candidates [115–119] have been added to the list of operational control signals [107]. Understanding the degree to which these pathways are operative in monocot species like barley, together with a deeper knowledge of the regulatory, biochemical and redox networks that control the stability, functionality and disassembly of the photosynthetic apparatus under stress conditions and during induced senescence is pivotal for the identification of novel genes and favourable allelic variants for use in breeding programs.

Chloroplast biogenesis during leaf emergence is initiated upon light perception and is also dependent on plastid retrograde signals. Over the past two decades, many publications have explored the role of plastid gene expression and tetrapyrrole biosynthesis as sources of biogenic signals. This system is disrupted in 'genomes uncoupled' mutants (*gun*; [120]). Five of the six GUN proteins (GUN2-6) are enzymes of the tetrapyrrole biosynthesis pathway and control the branched pathways downstream of Protoporphyrin IX (for a review see [121]). GUN1, however, does not take part in tetrapyrrole biosynthesis, but is required for the generation of retrograde signals triggered by the accumulation of tetrapyrrole precursors and inhibition of plastid gene expression (PGE) [122]. More recently, GUN1 has been reported to play a prominent role in the maintenance of chloroplast protein homeostasis by modulating plastid protein synthesis through its interaction with the plastid ribosomal protein S1 [123], and to control the activity of the plastid protein import machinery [124,125], suggesting that unimported preproteins in the cytosol could act as messenger molecules. Although most of the information on biogenic retrograde signalling has been obtained in *Arabidopsis*, the barley mutant *albostrians* has proved to be a valuable system for studying the regulation of tetrapyrrole biosynthesis and the involvement of these compounds in communication between plastids and the nucleus. Due to the lack of plastid-encoded proteins in this mutant, low levels of tRNA^{Glu}, which serves as a substrate activator in tetrapyrrole biosynthesis, are observed in bleached *albostrians* leaves, and this might be one reason for the much lower chlorophyll content in *albostrians* plastids [126–128]. In the mutant, the common precursors of all tetrapyrroles are channelled in the direction of heme synthesis, while the formation of chlorophylls is repressed [127]. This, in turn, suggests that excess heme might leave the chloroplast and act as a signalling molecule, as has been observed in *Arabidopsis* [129]. Recently, the mutation responsible for the *albostrians* phenotype has been identified. It lies in the barley gene *HvCMF7*, which codes for a putative plastid protein that belongs to the CCT motif family (CMF), which includes CONSTANS, CO-like and TOC1 [130]. This gene is likely to play a crucial role in plastid ribosome formation during early embryo development and hence for chloroplast development. The identification of the gene defect that causes the *albostrians* phenotype represents a major step forward in the understanding of the molecular mechanisms that mediate chloroplast biogenesis in barley. In this context, it would be interesting to determine whether a GUN1-like protein exists in barley. Furthermore, the gradient in chloroplast biogenesis observed in the barley leaf blade provides access to leaf sectors that contain cells of the same developmental stage, which facilitates the use of RNA-seq and proteomics approaches to investigate the molecular network at the basis of proplastid-to-chloroplast differentiation.

5.2. Photosynthesis and Yield

Doubling agricultural production by 2050 is essential if the demands of a constantly growing population for food and biomass are to be satisfied. Among cereals, barley straw is characterised by the highest content of carbohydrates [131]. Barley is therefore an ideal feedstock for the bio-based economy, since it can be used for the production of food/feed/spirits from grains, and renewable resources, including biofuel, from straw. It is worth mentioning here that none of the huge improvements in agricultural production made during the 'Green Revolution' were directly related to manipulations of photosynthesis. Hence, the process remains an unexplored target with a high potential for crop improvement. Indeed, the theoretical maximum efficiency of the conversion of solar energy into biomass in a C3 crop like barley is around 4.6% and this value decreases to 2.4% under field conditions

across the entire growing season. Therefore, the conversion efficiency of visible solar energy is considerably below its theoretical maximum, and several promising targets for its improvement have been identified in model species, some of which are described below (Figure 2 and Table 4).

5.3. Optimization of Antenna Size in Crop Canopies

One of the main reasons for the lower conversion efficiency of solar radiation is the saturation of the photosynthetic machinery with light. Indeed, it has been demonstrated that the photosynthetic apparatus operates with near maximum efficiency when light levels are low. For instance, the photosynthetic process in a C3 plant is already saturated at approximately 25% of maximum sunlight [153]. As light absorption increases, photosynthetic efficiency declines. In fact, the antennal apparatus of photosystems is larger than optimal, since under competitive natural conditions, shading of neighbouring plants confers an important selective advantage on the upper storey [154]. However, this behaviour is clearly disadvantageous for cultivated crops. Reducing the size of the antenna systems in the leaves of the upper canopy can offer important advantages, saving the metabolic resources required for the production of the antenna complex and the activity of photoprotective mechanisms, while increasing the amount and quality of light able to reach the lower leaves [155]. Several studies have provided evidence that the reduction of antenna size can improve photosynthetic efficiency. For instance, cell suspensions of *Synechocystis* PCC6714 and *Chlorella pyrenoidosa* with reduced contents of light-harvesting pigments showed a photosynthetic activity 20–30% higher than the wild type [156]. An engineered *Chlamydomonas reinhardtii* strain with a small PSII antenna size exhibited about a 50% increase in photosynthetic efficiency under saturating levels of light [157]. In the same alga, a partial reduction in chlorophyll b levels resulted in a two-fold increase in photosynthetic rate at high light intensities [158]. The hypothesis that a constitutively smaller antenna size should improve canopy photosynthetic efficiency by minimizing the over-absorption of the incident sunlight, and improving canopy light penetration, has also been tested in higher plants. A decrease in antenna size in tobacco, for instance, led to an increase of about 25% in plant–canopy biomass accumulation under high-density cultivation conditions [39]. Similarly, beneficial effects were observed in a rice genotype with pale green leaves cultivated under high light conditions [132].

5.4. Increased Photosynthetic Electron Transport

The modification of the thylakoid electron transport chain has also been reported to contribute to the improvement of photosynthetic performance and biomass accumulation. For instance, Chida et al. [133] showed that the expression of the algal *Porphyra yezoensis* cytochrome c_6 in the chloroplasts of *Arabidopsis* led to an increase of CO₂ assimilation, and biomass production [133]. The overexpression of cytochrome c_6 from *Ulva fasciata* in tobacco gave similar results [134]. Moreover, overexpression of plastocyanin in *Arabidopsis* resulted in 1.6-fold increase in leaf area [135]. A large increase in biomass and seed yield was also obtained in *Arabidopsis* upon overexpression of its endogenous Rieske FeS protein, a subunit of the cytochrome b_6/f [136].

Table 4. Brief summary of biotechnological strategies that are being employed for photosynthesis improvement in barley.

Target	Efficiency Gain	Strategy	Outcome	References
Retrograde signalling				
1. Investigating the existence of a GUN1-dependent retrograde signalling pathway in barley	Not expected	Knock-out of the HORVU.MOREX.r2.5HG0366860.1 gene through gene editing	Molecular details of the retrograde signalling pathway involved in chloroplast biogenesis with possible repercussions for the control of leaf life-cycle	[122]
Light phase of photosynthesis				
1. Optimisation of the antenna size	20–50%	Reduction of photosystem antenna size obtained by either reducing chlorophyll production or decreasing levels of the photosystem antenna proteins by gene editing or introgression of induced mutations. Identification of allelic variants by allele mining and TILLING.	More uniform photosynthetic performance throughout the crop canopy and prevention of photo-oxidative damage in the upper layers of the canopy. Increases in land–surface reflectivity to offset greenhouse gas warming.	[39,132]
2. Increased photosynthetic electron transport	30–70%	Increased accumulation of electron carriers, such as cytochrome <i>c</i> ₆ , plastocyanin and Rieske proteins, by transgenic approaches. Identification of allelic variants by allele mining and TILLING.	Increased electron transport rate through the thylakoid membranes	[133–136]
3. Fine-Tuning of NPQ	30%	Increased accumulation of VDE, ZEP and PsbS by transgenic approaches. Identification of allelic variants by allele mining and TILLING.	More rapid induction and relaxation of heat dissipation at PSII.	[137]
Dark phase of photosynthesis				
1. Increasing the abundance of different enzymes of the Calvin–Benson cycle	>30%	Increased accumulation of SBPase and FBPA enzymes by transgenic approaches. Identification of allelic variants by allele mining and TILLING.	Optimization of ribulose 1,5-bisphosphate (RuBP) regeneration.	[138–142]
2. Increasing the efficiency of light activation of Calvin–Benson enzymes	>20%	Increased accumulation of Rubisco activase, TRX <i>f</i> and NTRC by transgenic approaches. Identification of allelic variants by allele mining and TILLING.	More efficient light-dependent activation of Calvin–Benson enzyme optimises CO ₂ fixation.	[143–147]
Photorespiration				
1. Increasing the photorespiration flow of intermediates	>15%	Increased accumulation of H- and L-proteins by transgenic approaches.	Reduced accumulation of photorespiration intermediates and increased CO ₂ assimilation rate	[148–150]
2. Synthetic bypasses to photorespiration	>20%	Introduction of natural and synthetic glycolate catabolic pathways in the chloroplast	Increased CO ₂ assimilation rates	[151,152]

5.5. Improving the Adaptation to Fluctuating Light: Dissipation of Excess Energy through Non-Photochemical Quenching

Non-Photochemical Quenching (NPQ) serves as photoprotective mechanism in leaves, and is responsible for the dissipation of excess absorbed light energy as heat, thus preventing oxidative damage. Dissipation takes place in photosystem II (PSII) and involves the enzymes violaxanthin de-epoxidase (VDE) and zeaxanthin epoxidase (ZEP) [159], together with PsbS, a PSII protein subunit [160]. Activation and relaxation of NPQ take place over timescales of seconds to minutes, which are rather slow with respect to the instantaneous changes in light intensities observable within plant canopies in field settings. This leads to loss of photosynthetic efficiency, as heat dissipation continues even when light does not exceed the photosynthetic capacity [161]. Recently, the overexpression of *PsbS*, *ZEP* and *VDE* genes was reported in tobacco plants. These plants displayed an improved kinetics of NPQ, resulting in about 20% increase in biomass accumulation under both greenhouse and field conditions [137].

5.6. Transgenic Manipulation of the Calvin–Benson Cycle

Attempts to improve photosynthetic efficiency through transgenic manipulations have also focused on the overexpression of single enzymes of the Calvin–Benson cycle (Table 4). For example, overexpression of sedoheptulose-1,7-bisphosphatase (SBPase) in *Arabidopsis* [139], tobacco [138,140] and tomato [141] has shown that an increased SBPase activity results in a 30–40% increase in biomass yield, depending on the species. More recently it was shown that significant increases in photosynthetic rates, biomass and grain yield can be achieved by augmenting SBPase activity in wheat [162]. In 2012, the overexpression of the fructose 1,6-bisphosphate aldolase (FBPA) enzyme in tobacco also resulted in an increase in biomass production of 10–30% [142]. Overall, these findings demonstrated that SBPase and FBPA are enzymes that can exert control over the flow of carbon in the Calvin–Benson cycle in a number of different species, and proved that their manipulation also benefits grain yield. Efforts to increase the light activation rate of the Calvin–Benson cycle have also yielded very promising results. For instance, the overexpression of maize Rubisco activase in rice increased the rate of Rubisco activation by light and at high temperature (40 °C; [143]). Increased levels of thioredoxin *f* (TRX *f*), which is known to reductively activate enzymes of the Calvin–Benson cycle, have also increased leaf weight and sugar content under both ambient and increased CO₂ conditions [144,145]. Overexpression of the chloroplast NADPH-dependent thioredoxin reductase (NTRC), also reported to interact with several Calvin–Benson enzymes, has also been shown to be beneficial for productivity in *Arabidopsis*. Indeed, the biomass increases in the NTRC-overexpressing *Arabidopsis* plants were between 2- and 2.5-fold in plants grown under long- and short-day conditions, respectively, at fluence levels of 600 μmol m⁻² s⁻¹ light [146,147]. Additionally, overexpression of NTRC has been reported to enhance tolerance to oxidative and drought stresses. These are traits of great significance for improvement of crop productivity under field conditions [163].

5.7. Photorespiration and Photorespiratory Bypasses

Photorespiration is also an important target to improve photosynthesis. For instance, the reversible conversion of glycine into serine that takes place in mitochondria is crucial for plants [164–169]. These reactions involve the pyridoxal phosphate-dependent enzyme glycine decarboxylase (P-protein), the THF-dependent enzyme aminomethyltransferase (T-protein), the NAD⁺-dependent enzyme dihydrolipoyl dehydrogenase (L-protein) and the lipoic acid-containing H-protein. In *Arabidopsis*, overexpression of the H- or L-protein resulted in an improvement in photosynthetic efficiency and larger biomass accumulation [148,149]. Similar results were also obtained with the mesophyll-specific overexpression of the H-protein in tobacco [150]. Besides increasing photorespiration flow and reducing accumulation of photorespiratory intermediates, the most promising strategies for enhancing productivity are based on photorespiratory bypasses, i.e., the introduction of alternative pathways to metabolize 2PG, thus liberating CO₂ in the chloroplast stroma for Rubisco fixation [151,152].

In particular, Kebeish et al. introduced the *Escherichia coli* glycolate catabolic pathway into *Arabidopsis*. In these transgenic plants, the glycolate derived from the dephosphorylation of 2-phosphoglycolate was converted into glycerate in the chloroplast without the release of ammonia, which can make nitrogen use more efficient. Moreover, CO₂ release was shifted from mitochondria to chloroplasts, based on the idea that CO₂ should have a better chance to be re-fixed by Rubisco if it is released in the chloroplast rather than in the mitochondria. As a result of the increased concentration of CO₂ in the chloroplasts and the reduced energy demand for photorespiration, transgenic plants grew faster and produced more biomass, indicating that the bypass effectively reduced photorespiration and enhanced photosynthesis. Inspired by this work, another group [152] introduced synthetic glycolate metabolic pathways that are more efficient than the endogenous pathway into tobacco chloroplasts. Flux through the synthetic pathways was maximized by inhibiting glycolate export from the chloroplast. These synthetic pathways were able to improve photosynthetic quantum yield by 20% and biomass productivity by >40% in replicated field trials.

It is reasonable to expect that the various transgenic approaches described above will result in increased photosynthetic quantum yield, biomass and, eventually, grain yield also in barley, although species-dependent effects were observed in the multigene manipulation of the Calvin–Benson cycle [138,139]. In addition to that, the large genetic diversity readily available in barley also allows the exploitation of natural and/or induced allelic variants of enzymes involved in defining the antenna size of photosystems, in thylakoid electron transport, NPQ, the Calvin–Benson cycle, and photorespiration, which could ameliorate barley yield (Table 4). These allelic variants can be identified either by allele mining of exome sequences of barley cultivars, landraces and wild varieties (see Table 2), or through TILLING of mutant populations (Table 3). As mentioned above, the latter approaches enable one to obtain new barley varieties by using the classical breeding approach based on crosses. Thus, the performance of the new varieties can be verified under field conditions and they could be grown even in countries that have banned the cultivation of genetically modified plants.

6. Conclusions

Its genetic diversity and the availability of a large collection of molecular tools make barley an ideal model crop for functional genomics studies related to chloroplast biogenesis and retrograde communication. Such studies will reveal to what extent retrograde signalling mechanisms are conserved between *Arabidopsis* and barley, and permit us to learn more about aspects of chloroplast biogenesis that are specific to monocots. The recent identification of the genetic factor responsible for the *albostrians* phenotype demonstrates that this type of analysis can now be effectively conducted in barley. The fact that the gene concerned, *HvCMF7*, encodes a protein that is apparently located exclusively in plastids highlights the need for systematic investigation of barley mutants with defects in chloroplast biogenesis. Furthermore, novel approaches to the screening of barley mutant populations are required to elucidate the molecular details of the chloroplast-to-nucleus communication. The genes and allelic variants identified in future studies could have an important impact in breeding programs, since retrograde communication controls the leaf life cycle.

Barley can also make a significant contribution to the testing of novel biotechnological strategies for improving photosynthesis, and the validation of their effects on biomass accumulation and grain yield. In recent decades, our knowledge of the photosynthetic process has increased substantially, and improvements in its efficiency have been demonstrated in different model species. The high level of conservation of the photosynthetic process strongly argues that similar enhancements can be achieved in barley. Thanks to the high content of sugars in the straw, barley could be transformed into a dual-purpose crop suitable for the production of biofuel from the straw, and food, feed and spirits from the grain. Furthermore, the use of barley varieties characterised by high photosynthetic efficiency and reduced antenna size of photosystems is a promising strategy for boosting productivity and water use efficiency, while increasing land–surface reflectivity to offset greenhouse gas warming. In light of the foreseeable rise in the demand for food by the middle of this century, and the fact that

the development and commercialization of a new plant variety with improved quality takes 10 to 15 years, concerted efforts to increase agricultural yields through manipulation of photosynthesis must be initiated immediately. The “redesign” of photosynthesis must represent one of the main pillars of the next “Green Revolution”.

Author Contributions: Conceptualization, P.P., L.R., F.S., and L.T.; methodology, P.P., L.R., F.S., and L.T.; validation, P.P., L.R., and F.S.; resources, P.P.; data curation, P.P., L.R., and F.S.; writing—original draft preparation, P.P., L.R., F.S., and L.T.; writing—review and editing, P.P. and L.R.; visualization, C.M.; supervision, P.P.; project administration, P.P.; funding acquisition, P.P. All authors have read and agreed to the published version of the manuscript.

Funding: This research received funding from ERA-NET Cofund FACCE SURPLUS (BarPLUS grant id. 93).

Acknowledgments: We apologize to the authors who did not get their work discussed in this review due to space limitation. The authors thank Paul Hardy for critical reading of the manuscript.

Conflicts of Interest: The authors declare no conflict of interest.

References

- Zohary, D.; Hopf, M.; Weiss, E. Domestication of Plants in the Old World: The origin and spread of domesticated plants in Southwest Asia, Europe, and the Mediterranean Basin. In *Domestication of Plants in the Old World: The Origin and Spread of Domesticated Plants in Southwest Asia, Europe, and the Mediterranean Basin*; Oxford University Press: Oxford, UK, 2013; ISBN 9780191810046.
- Dawson, I.K.; Russell, J.; Powell, W.; Steffenson, B.; Thomas, W.T.B.; Waugh, R. Barley: A translational model for adaptation to climate change. *New Phytol.* **2015**, *206*, 913–931. [[CrossRef](#)] [[PubMed](#)]
- Stadler, L.J. Some genetic effect of X-rays in plants. *J. Hered.* **1930**, *21*, 3–20. [[CrossRef](#)]
- Afsson, Å.K.E.G. Studies on the genetic basis of chlorophyll formation and the mechanism of induced mutating. *Hereditas* **1938**, *24*, 33–93. [[CrossRef](#)]
- Afsson, A.K.E.G. Mutation experiments in barley. *Hereditas* **1941**, *27*, 225–242. [[CrossRef](#)]
- Smith, L. Effects of atomic bomb radiations and x-rays on seeds of cereals: A comparison of the effects of ionizing radiations from the “ test able” atomic bomb and from x-rays on seeds of barley, wheat and oats. *J. Hered.* **1950**, *41*, 125–130. [[CrossRef](#)] [[PubMed](#)]
- Gustafsson, Å.; Key, J.M. The genetical effects of musterd gas substances and neutrons. *Hereditas* **1948**, *34*, 371–386. [[CrossRef](#)]
- Ehrenberg, L.; Gustafsson, Å.; Lundqvist, U.; Stenhagen, E.; Thorell, B. Chemically induced mutation and sterility in Barley. *Acta Chem. Scand.* **1956**, *10*, 492–494. [[CrossRef](#)]
- Bouma, J.; Ohnoutka, Z. Importance and application of the mutant “Diamant” in spring barley breeding. *Plant Mutat. Breed. Crop Improv.* **1991**, *1*, 127–134.
- Forster, B.P. Mutation genetics of salt tolerance in barley: An assessment of Golden Promise and other semi-dwarf mutants. *Euphytica* **2001**, *120*, 317–328. [[CrossRef](#)]
- Henningsen, K.W.; Boynton, J.E. Macromolecular physiology of plastids. VII. The effect of a brief illumination on plastids of dark-grown barley leaves. *J. Cell Sci.* **1969**, *5*, 757–793.
- Kannanga, G.; Gamini, C. The formation of Ribulose Diphosphate Carboxylase Protein during chloroplast development in Barley. *Plant Physiol.* **1969**, *44*, 1533–1537. [[CrossRef](#)] [[PubMed](#)]
- Wellburn, A.R.; Robinson, D.C.; Wellburn, F.A.M. Chloroplast development in low light-grown barley seedlings. *Planta* **1982**, *154*, 259–265. [[CrossRef](#)] [[PubMed](#)]
- Apel, K.; Gollmer, I.; Batschauer, A. The light-dependent control of chloroplast development in barley (*Hordeum vulgare* L.). *J. Cell. Biochem.* **1983**, *23*, 181–189. [[CrossRef](#)] [[PubMed](#)]
- Fradkin, L.I.; Kolyago, V.M.; Nisenbaum, G.D.; Domanskaya, I.N. Disintegration and fractionation of Barley chloroplast membranes at different concentrations of digitonin and chloroplasts. *Biokhimiya* **1978**, *43*, 723–733.
- Nielsen, N.C.; Smillie, R.M.; Henningsen, K.W.; Von Wettstein, D.; French, C.S. Composition and function of thylakoid membranes from grana-rich and grana-deficient chloroplast mutants of barley. *Plant Physiol.* **1979**, *63*, 174–182. [[CrossRef](#)]
- Thornber, J.P.; Highkin, H.R. Composition of the photosynthetic apparatus of normal barley leaves and a mutant lacking chlorophyll b. *Eur. J. Biochem.* **1974**, *41*, 109–116. [[CrossRef](#)]

18. Król, M.; Spangfort, M.D.; Huner, N.P.; Oquist, G.; Gustafsson, P.; Jansson, S. Chlorophyll a/b-binding proteins, pigment conversions, and early light-induced proteins in a chlorophyll b-less barley mutant. *Plant Physiol.* **1995**, *107*, 873–883. [[CrossRef](#)]
19. Król, M.; Ivanov, A.G.; Jansson, S.; Kloppstech, K.; Huner, N.P.A. Greening under high light or cold temperature affects the level of xanthophyll-cycle pigments, early light-inducible proteins, and light-harvesting polypeptides in wild-type barley and the chlorina f2 mutant. *Plant Physiol.* **1999**, *120*, 193–203. [[CrossRef](#)]
20. Bossmann, B.; Knoetzel, J.; Jansson, S. Screening of chlorina mutants of barley (*Hordeum vulgare* L.) with antibodies against light-harvesting proteins of PS I and PS II: Absence of specific antenna proteins. *Photosynth. Res.* **1997**, *52*, 127–136. [[CrossRef](#)]
21. Goodchild, D.J.; Highkin, H.R.; Boardman, N.K. The fine structure of chloroplasts in a barley mutant lacking chlorophyll B. *Exp. Cell Res.* **1966**, *43*, 684–688. [[CrossRef](#)]
22. Von Wettstein, D.; Kahn, A.; Nielsen, O.F.; Gough, S. Genetic Regulation of Chlorophyll Synthesis Analyzed with Mutants in Barley. *Science* **1974**, *184*, 800–802. [[CrossRef](#)] [[PubMed](#)]
23. Lee, K.P.; Kim, C.; Lee, D.W.; Apel, K. TIGRINA d, required for regulating the biosynthesis of tetrapyrroles in barley, is an ortholog of the FLU gene of Arabidopsis thaliana. *FEBS Lett.* **2003**, *553*, 119–124. [[CrossRef](#)]
24. Meskauskiene, R.; Nater, M.; Goslings, D.; Kessler, F.; Op den Camp, R.; Apel, K. FLU: A negative regulator of chlorophyll biosynthesis in Arabidopsis thaliana. *Proc. Natl. Acad. Sci. USA* **2001**, *98*, 12826–12831. [[CrossRef](#)]
25. Gustafsson, Å. Drastic morphological mutation in Barley. *Hereditas* **1946**, *32*, 120–122. [[CrossRef](#)]
26. Rzeznicka, K.; Walker, C.J.; Westergren, T.; Kannangara, C.G.; Von Wettstein, D.; Merchant, S.; Gough, S.P.; Hansson, M. Xantha-I encodes a membrane subunit of the aerobic Mg-protoporphyrin IX monomethyl ester cyclase involved in chlorophyll biosynthesis. *Proc. Natl. Acad. Sci. USA* **2005**, *102*, 5886–5891. [[CrossRef](#)] [[PubMed](#)]
27. Jensen, P.E.; Willows, R.D.; Petersen, B.L.; Vothknecht, U.C.; Stummann, B.M.; Kannangara, C.G.; Von Wettstein, D.; Henningsen, K.W. Structural genes for Mg-chelatase subunits in barley: Xantha-f, -g and -h. *Mol. Gen. Genet.* **1996**, *250*, 383–394. [[CrossRef](#)] [[PubMed](#)]
28. Smith, J.H.C.; French, C.S.; Koski, V.M. The Hill Reaction: Development of Chloroplast Activity During Greening of Etiolated Barley Leaves. *Plant Physiol.* **1952**, *27*, 212–213. [[CrossRef](#)] [[PubMed](#)]
29. Robertson, D.; Laetsch, W.M. Structure and Function of Developing Barley Plastids. *Plant Physiol.* **1974**, *54*, 148–159. [[CrossRef](#)]
30. Hajdukiewicz, P.T.J.; Allison, L.A.; Maliga, P. The two RNA polymerases encoded by the nuclear and the plastid compartments transcribe distinct groups of genes in tobacco plastids. *EMBO J.* **1997**, *16*, 4041–4048. [[CrossRef](#)]
31. Siemenroth, A.; Wollgiehn, R.; Neumann, D.; Börner, T. Synthesis of ribosomal RNA in ribosome-deficient plastids of the mutant “albostrians” of *Hordeum vulgare* L. *Planta* **1981**, *153*, 547–555. [[CrossRef](#)]
32. Hess, W.R.; Prombona, A.; Fieder, B.; Subramanian, A.R.; Börner, T. Chloroplast rps15 and the rpoB/C1/C2 gene cluster are strongly transcribed in ribosome-deficient plastids: Evidence for a functioning non-chloroplast-encoded RNA polymerase. *EMBO J.* **1993**, *12*, 563–571. [[CrossRef](#)] [[PubMed](#)]
33. Hagemann, R.; Börner, T.; Knoth, R. Plastid ribosome deficiency in plastid mutants of Pelargonium and Hordeum. *Genetics* **1973**, *74*, 103–104.
34. Börner, T.; Schumann, B.; Hagemann, R. Biochemical studies on a plastid ribosome-deficient mutant of *Hordeum vulgare*. In *Genetics Biogenesis of Chloroplasts Mitochondria*; Bücher, T., Neupert, W., Sebald, W., Werner, S., Eds.; Elsevier/North-Hill Medical Press: Amsterdam, The Netherlands, 1976; pp. 41–48.
35. Börner, T. The discovery of plastid-to-nucleus retrograde signaling—a personal perspective. *Protoplasma* **2017**, *254*, 1845–1855. [[CrossRef](#)] [[PubMed](#)]
36. Chilton, M.D.; Drummond, M.H.; Merlo, D.J.; Sciaky, D.; Montoya, A.L.; Gordon, M.P.; Nester, E.W. Stable incorporation of plasmid DNA into higher plant cells: The molecular basis of crown gall tumorigenesis. *Cell* **1977**, *11*, 263–271. [[CrossRef](#)]
37. Kaul, S.; Koo, H.L.; Jenkins, J.; Rizzo, M.; Rooney, T.; Tallon, L.J.; Feldblyum, T.; Nierman, W.; Benito, M.I.; Lin, X.; et al. Analysis of the genome sequence of the flowering plant Arabidopsis thaliana. *Nature* **2000**, *408*, 796–815. [[CrossRef](#)]

38. Song, W.; Li, C.; Sun, X.; Wang, P.; Zhao, S. Effects of ridge direction on growth and yield of tomato in solar greenhouse with diffuse film. *Nongye Gongcheng Xuebao/Trans. Chinese Soc. Agric. Eng.* **2017**, *33*, 242–248. [[CrossRef](#)]
39. Kirst, H.; Gabilly, S.T.; Niyogi, K.K.; Lemaux, P.G.; Melis, A. Photosynthetic antenna engineering to improve crop yields. *Planta* **2017**, *245*, 1009–1020. [[CrossRef](#)]
40. Pogson, B.J.; Ganguly, D.; Albrecht-Borth, V. Insights into chloroplast biogenesis and development. *Biochim. Biophys. Acta Bioenerg.* **2015**, *1847*, 1017–1024. [[CrossRef](#)]
41. Boffey, S.A.; Selldén, G.; Leech, R.M. Influence of Cell Age on Chlorophyll Formation in Light-grown and Etiolated Wheat Seedlings. *Plant Physiol.* **1980**, *65*, 680–684. [[CrossRef](#)]
42. Mullet, J.E. Chloroplast Development and Gene Expression. *Annu. Rev. Plant Physiol. Plant Mol. Biol.* **1988**, *39*, 475–502. [[CrossRef](#)]
43. Pogson, B.J.; Albrecht, V. Genetic dissection of chloroplast biogenesis and development: An overview. *Plant Physiol.* **2011**, *155*, 1545–1551. [[CrossRef](#)] [[PubMed](#)]
44. Jarvis, P.; López-Juez, E. Biogenesis and homeostasis of chloroplasts and other plastids. *Nat. Rev. Mol. Cell Biol.* **2013**, *14*, 787–802. [[CrossRef](#)] [[PubMed](#)]
45. Mayer, K.F.X.; Waugh, R.; Langridge, P.; Close, T.J.; Wise, R.P.; Graner, A.; Matsumoto, T.; Sato, K.; Schulman, A.; Ariyadasa, R.; et al. A physical, genetic and functional sequence assembly of the barley genome. *Nature* **2012**, *491*, 711–771. [[CrossRef](#)] [[PubMed](#)]
46. Mascher, M.; Gundlach, H.; Himmelbach, A.; Beier, S.; Twardziok, S.O.; Wicker, T.; Radchuk, V.; Dockter, C.; Hedley, P.E.; Russell, J.; et al. A chromosome conformation capture ordered sequence of the barley genome. *Nature* **2017**, *544*, 427–433. [[CrossRef](#)] [[PubMed](#)]
47. Monat, C.; Padmarasu, S.; Lux, T.; Wicker, T.; Gundlach, H.; Himmelbach, A.; Ens, J.; Li, C.; Muehlbauer, G.J.; Schulman, A.H.; et al. TRITEX: Chromosome-scale sequence assembly of Triticeae genomes with open-source tools. *Genome Biol.* **2019**, *20*, 284. [[CrossRef](#)] [[PubMed](#)]
48. Schreiber, M.; Mascher, M.; Wright, J.; Padmarasu, S.; Himmelbach, A.; Heavens, D.; Milne, L.; Clavijo, B.; Stein, N.; Waugh, R. A Genome Assembly of the Barley “Transformation Reference” Cultivar Golden Promise. *G3 Genes Genomes Genet.* **2020**, *10*, 1823–1827. [[CrossRef](#)]
49. Colmsee, C.; Beier, S.; Himmelbach, A.; Schmutzer, T.; Stein, N.; Scholz, U.; Mascher, M. BARLEX—The barley draft genome explorer. *Mol. Plant* **2015**, *8*, 964–966. [[CrossRef](#)]
50. Bolser, D.; Staines, D.M.; Pritchard, E.; Kersey, P. Ensembl plants: Integrating tools for visualizing, mining, and analyzing plant genomics data. *Methods Mol. Biol.* **2016**, *1533*, 1–31. [[CrossRef](#)]
51. Deng, W.; Nickle, D.C.; Learn, G.H.; Maust, B.; Mullins, J.I. ViroBLAST: A stand-alone BLAST web server for flexible queries of multiple databases and user’s datasets. *Bioinformatics* **2007**, *23*, 2334–2336. [[CrossRef](#)]
52. Tello-Ruiz, M.K.; Naithani, S.; Stein, J.C.; Gupta, P.; Campbell, M.; Olson, A.; Wei, S.; Preece, J.; Geniza, M.J.; Jiao, Y.; et al. Gramene 2018: Unifying comparative genomics and pathway resources for plant research. *Nucleic Acids Res.* **2018**, *46*, D1181–D1189. [[CrossRef](#)]
53. Spannagl, M.; Nussbaumer, T.; Bader, K.C.; Martis, M.M.; Seidel, M.; Kugler, K.G.; Gundlach, H.; Mayer, K.F.X. PGSB plantsDB: Updates to the database framework for comparative plant genome research. *Nucleic Acids Res.* **2016**, *44*, D1141–D1147. [[CrossRef](#)] [[PubMed](#)]
54. Rapazote-Flores, P.; Bayer, M.; Milne, L.; Mayer, C.D.; Fuller, J.; Guo, W.; Hedley, P.E.; Morris, J.; Halpin, C.; Kam, J.; et al. BaRTv1.0: An improved barley reference transcript dataset to determine accurate changes in the barley transcriptome using RNA-seq. *BMC Genom.* **2019**, *20*, 968. [[CrossRef](#)] [[PubMed](#)]
55. Mascher, M.; Richmond, T.A.; Gerhardt, D.J.; Himmelbach, A.; Clissold, L.; Sampath, D.; Ayling, S.; Steuernagel, B.; Pfeifer, M.; D’Ascenzo, M.; et al. Barley whole exome capture: A tool for genomic research in the genus *Hordeum* and beyond. *Plant J.* **2013**, *76*, 494–505. [[CrossRef](#)] [[PubMed](#)]
56. Russell, J.; Mascher, M.; Dawson, I.K.; Kyriakidis, S.; Calixto, C.; Freund, F.; Bayer, M.; Milne, I.; Marshall-Griffiths, T.; Heinen, S.; et al. Exome sequencing of geographically diverse barley landraces and wild relatives gives insights into environmental adaptation. *Nat. Genet.* **2016**, *48*, 1024–1030. [[CrossRef](#)]
57. Bustos-Korts, D.; Dawson, I.K.; Russell, J.; Tondelli, A.; Guerra, D.; Ferrandi, C.; Strozzi, F.; Nicolazzi, E.L.; Molnar-Lang, M.; Ozkan, H.; et al. Exome sequences and multi-environment field trials elucidate the genetic basis of adaptation in barley. *Plant J.* **2019**, *99*, 1172–1191. [[CrossRef](#)]

58. Hasan, M.; Hasibuzzaman, A.S.M.; Abdullah, H.M.; Kallol, M.M.H. Rediscovery of Genetic and Genomic Resources for Future Food Security. In *Genetic and Genomic Resources and their Exploitation for Unlocking Genetic Potential from the Wild Relatives*; Springer: Singapore, 2020; pp. 193–210.
59. Dempewolf, H.; Baute, G.; Anderson, J.; Kilian, B.; Smith, C.; Guarino, L. Past and future use of wild relatives in crop breeding. *Crop Sci.* **2017**, *57*, 1070–1082. [[CrossRef](#)]
60. Caldwell, D.G.; McCallum, N.; Shaw, P.; Muehlbauer, G.J.; Marshall, D.F.; Waugh, R. A structured mutant population for forward and reverse genetics in Barley (*Hordeum vulgare* L.). *Plant J.* **2004**, *40*, 143–150. [[CrossRef](#)]
61. Talamè, V.; Bovina, R.; Sanguineti, M.C.; Tuberosa, R.; Lundqvist, U.; Salvi, S. TILLMore, a resource for the discovery of chemically induced mutants in barley. *Plant Biotechnol. J.* **2008**, *6*, 477–485. [[CrossRef](#)]
62. Szurman-Zubrzycka, M.E.; Zbieszczczyk, J.; Marzec, M.; Jelonek, J.; Chmielewska, B.; Kurowska, M.M.; Krok, M.; Daszkowska-Golec, A.; Guzy-Wrobelska, J.; Gruszka, D.; et al. HorTILLUS—a rich and renewable source of induced mutations for forward/reverse genetics and pre-breeding programs in barley (*Hordeum vulgare* L.). *Front. Plant Sci.* **2018**, *9*, 216. [[CrossRef](#)]
63. Schreiber, M.; Barakate, A.; Uzrek, N.; Macaulay, M.; Sourdille, A.; Morris, J.; Hedley, P.E.; Ramsay, L.; Waugh, R. A highly mutagenised barley (cv. Golden Promise) TILLING population coupled with strategies for screening-by-sequencing. *Plant Methods* **2019**, *15*, 99. [[CrossRef](#)]
64. Gottwald, S.; Bauer, P.; Komatsuda, T.; Lundqvist, U.; Stein, N. TILLING in the two-rowed barley cultivar “Barke” reveals preferred sites of functional diversity in the gene HvHox1. *BMC Res. Notes* **2009**, *2*, 258. [[CrossRef](#)] [[PubMed](#)]
65. Lababidi, S.; Mejlhede, N.; Rasmussen, S.K.; Backes, G.; Al-Said, W.; Baum, M.; Jahoor, A. Identification of barley mutants in the cultivar “lux” at the dhn loci through tilling. *Plant Breed.* **2009**, *128*, 332–336. [[CrossRef](#)]
66. Kurowska, M.; Labocha-Pawłowska, A.; Gnizda, D.; Maluszynski, M.; Szarejko, I. Molecular analysis of point mutations in a barley genome exposed to MNU and Gamma rays. *Mutat. Res. Fundam. Mol. Mech. Mutagen.* **2012**, *738–739*, 52–70. [[CrossRef](#)] [[PubMed](#)]
67. Druka, A.; Franckowiak, J.; Lundqvist, U.; Bonar, N.; Alexander, J.; Houston, K.; Radovic, S.; Shahinnia, F.; Vendramin, V.; Morgante, M.; et al. Genetic dissection of barley morphology and development. *Plant Physiol.* **2011**, *155*, 617–627. [[CrossRef](#)] [[PubMed](#)]
68. Dockter, C.; Gruszka, D.; Braumann, I.; Druka, A.; Druka, I.; Franckowiak, J.; Gough, S.P.; Janeczko, A.; Kurowska, M.; Lundqvist, J.; et al. Induced variations in brassinosteroid genes define barley height and sturdiness, and expand the green revolution genetic toolkit. *Plant Physiol.* **2014**, *166*, 1912–1927. [[CrossRef](#)]
69. Jost, M.; Taketa, S.; Mascher, M.; Himmelbach, A.; Yuo, T.; Shahinnia, F.; Rutten, T.; Druka, A.; Schmutzer, T.; Steuernagel, B.; et al. A homolog of blade-on-petiole 1 and 2 (BOP1/2) controls internode length and homeotic changes of the barley inflorescence. *Plant Physiol.* **2016**, *171*, 1113–1127. [[CrossRef](#)]
70. Komatsuda, T.; Pourkheirandish, M.; He, C.; Azhaguvel, P.; Kanamori, K.; Perovic, D.; Stein, N.; Graner, A.; Wicker, T.; Tagiri, A.; et al. Six-rowed barley originated from a mutation in a homeodomain-leucine zipper I-class homeobox gene. *Proc. Natl. Acad. Sci. USA* **2007**, *104*, 1424–1429. [[CrossRef](#)]
71. Ramsay, L.; Comadran, J.; Druka, A.; Marshall, D.F.; Thomas, W.T.B.; MacAulay, M.; MacKenzie, K.; Simpson, C.; Fuller, J.; Bonar, N.; et al. INTERMEDIUM-C, a modifier of lateral spikelet fertility in barley, is an ortholog of the maize domestication gene TEOSINTE BRANCHED 1. *Nat. Genet.* **2011**, *43*, 169–172. [[CrossRef](#)]
72. Henikoff, S.; Till, B.J.; Comai, L. TILLING. Traditional mutagenesis meets functional genomics. *Plant Physiol.* **2004**, *135*, 630–636. [[CrossRef](#)]
73. Waugh, R.; Leader, D.J.; McCallum, N.; Caldwell, D. Harvesting the potential of induced biological diversity. *Trends Plant Sci.* **2006**, *11*, 71–79. [[CrossRef](#)]
74. Till, B.J.; Reynolds, S.H.; Greene, E.A.; Codomo, C.A.; Enns, L.C.; Johnson, J.E.; Burtler, C.; Odden, A.R.; Young, K.; Taylor, N.E.; et al. Large-scale discovery of induced point mutations with high-throughput TILLING. *Genome Res.* **2003**, *13*, 524–530. [[CrossRef](#)] [[PubMed](#)]
75. Henry, I.M.; Nagalakshmi, U.; Lieberman, M.C.; Ngo, K.J.; Krasileva, K.V.; Vasquez-Gross, H.; Akhunova, A.; Akhunov, E.; Dubcovsky, J.; Tai, T.H.; et al. Efficient genome-wide detection and cataloging of EMS-induced mutations using Exome capture and next-generation sequencing. *Plant Cell* **2014**, *26*, 1382–1397. [[CrossRef](#)] [[PubMed](#)]

76. Goldstein, C.S.; Kronstad, W.E. Tissue culture and plant regeneration from immature embryo explants of Barley, *Hordeum vulgare*. *Theor. Appl. Genet.* **1986**, *71*, 631–636. [[CrossRef](#)] [[PubMed](#)]
77. Dahleen, L.S.; Bregitzer, P. An improved media system for high regeneration rates from barley immature embryo-derived callus cultures of commercial cultivars. *Crop Sci.* **2002**, *42*, 934–938. [[CrossRef](#)]
78. Harwood, W.A. A protocol for high-throughput agrobacterium-mediated barley transformation. *Methods Mol. Biol.* **2014**, *1099*, 251–260. [[CrossRef](#)] [[PubMed](#)]
79. McGrath, P.F.; Vincent, J.R.; Lei, C.H.; Pawlowski, W.P.; Torbert, K.A.; Gu, W.; Kaeppler, H.F.; Wan, Y.; Lemaux, P.G.; Rines, H.R.; et al. Coat protein-mediated resistance to isolates of barley yellow dwarf in oats and barley. *Eur. J. Plant Pathol.* **1997**, *103*, 695–710. [[CrossRef](#)]
80. Hüchelhoven, R. BAX Inhibitor-1, an ancient cell death suppressor in animals and plants with prokaryotic relatives. *Apoptosis* **2004**, *9*, 299–307. [[CrossRef](#)]
81. Bulgarelli, D.; Biselli, C.; Collins, N.C.; Consonni, G.; Stanca, A.M.; Schulze-Lefert, P.; Valè, G. The CC-NB-LRR-Type RDG2a resistance gene confers immunity to the seed-borne barley leaf stripe pathogen in the absence of hypersensitive cell death. *PLoS ONE* **2010**, *5*, e12599. [[CrossRef](#)]
82. Eichmann, R.; Bischof, M.; Weis, C.; Shaw, J.; Lacomme, C.; Schweizer, P.; Duchkov, D.; Hensel, G.; Kumlehn, J.; Hüchelhoven, R. Bax inhibitor-1 is required for full susceptibility of barley to powdery mildew. *Mol. Plant-Microbe Interact.* **2010**, *23*, 1217–1227. [[CrossRef](#)]
83. Horvath, H.; Rostoks, N.; Brueggeman, R.; Steffenson, B.; Von Wettstein, D.; Kleinhofs, A. Genetically engineered stem rust resistance in barley using the Rpg1 gene. *Proc. Natl. Acad. Sci. USA* **2003**, *100*, 364–369. [[CrossRef](#)]
84. Morran, S.; Eini, O.; Pyvovarenko, T.; Parent, B.; Singh, R.; Ismagul, A.; Eliby, S.; Shirley, N.; Langridge, P.; Lopato, S. Improvement of stress tolerance of wheat and barley by modulation of expression of DREB/CBF factors. *Plant Biotechnol. J.* **2011**, *9*, 230–249. [[CrossRef](#)]
85. Seiler, C.; Harshavardhan, V.T.; Reddy, P.S.; Hensel, G.; Kumlehn, J.; Eschen-Lippold, L.; Rajesh, K.; Korzun, V.; Wobus, U.; Lee, J.; et al. Abscisic acid flux alterations result in differential abscisic acid signaling responses and impact assimilation efficiency in barley under terminal drought stress. *Plant Physiol.* **2014**, *164*, 1677–1696. [[CrossRef](#)] [[PubMed](#)]
86. Soltész, A.; Vágújfalvi, A.; Rizza, F.; Kerepesi, I.; Galiba, G.; Cattivelli, L.; Coraggio, I.; Crosatti, C. The rice Osmyb4 gene enhances tolerance to frost and improves germination under unfavourable conditions in transgenic barley plants. *J. Appl. Genet.* **2012**, *53*, 133–143. [[CrossRef](#)]
87. Soltész, A.; Smedley, M.; Vashegyi, I.; Galiba, G.; Harwood, W.; Vágújfalvi, A. Transgenic barley lines prove the involvement of TaCBF14 and TaCBF15 in the cold acclimation process and in frost tolerance. *J. Exp. Bot.* **2013**, *64*, 1849–1862. [[CrossRef](#)] [[PubMed](#)]
88. Kovalchuk, N.; Jia, W.; Eini, O.; Morran, S.; Pyvovarenko, T.; Fletcher, S.; Bazanova, N.; Harris, J.; Beck-Oldach, K.; Shavrukov, Y.; et al. Optimization of TaDREB3 gene expression in transgenic barley using cold-inducible promoters. *Plant Biotechnol. J.* **2013**, *11*, 659–670. [[CrossRef](#)] [[PubMed](#)]
89. Murray, F.; Matthews, P.; Jacobsen, J.; Gubler, F. Increased expression of HvGAMYB in transgenic barley increases hydrolytic enzyme production by aleurone cells in response to gibberellin. *J. Cereal Sci.* **2006**, *44*, 317–322. [[CrossRef](#)]
90. Kihara, M.; Okada, Y.; Kuroda, H.; Saeki, K.; Yoshigi, N.; Ito, K. Improvement of β -amylase thermostability in transgenic barley seeds and transgene stability in progeny. *Mol. Breed.* **2000**, *6*, 511–517. [[CrossRef](#)]
91. Tull, D.; Phillipson, B.A.; Kramhøft, B.; Knudsen, S.; Olsen, O.; Svensson, B. Enhanced amyolytic activity in germinating barley through synthesis of a bacterial Alpha-amylase. *J. Cereal Sci.* **2003**, *37*, 71–80. [[CrossRef](#)]
92. Jensen, L.G.; Olsen, O.; Kops, O.; Wolf, N.; Thomsen, K.K.; Von Wettstein, D. Transgenic barley expressing a protein-engineered, thermostable (1,3-1,4)- β -glucanase during germination. *Proc. Natl. Acad. Sci. USA* **1996**, *93*, 3487–3491. [[CrossRef](#)]
93. Nuutila, A.M.; Ritala, A.; Skadsen, R.W.; Mannonen, L.; Kauppinen, V. Expression of fungal thermotolerant endo-1,4- β -glucanase in transgenic barley seeds during germination. *Plant Mol. Biol.* **1999**, *41*, 777–783. [[CrossRef](#)]
94. Koprek, T.; McElroy, D.; Louwerse, J.; Williams-Carrier, R.; Lemaux, P.G. An efficient method for dispersing Ds elements in the barley genome as a tool for determining gene function. *Plant J.* **2000**, *24*, 253–263. [[CrossRef](#)] [[PubMed](#)]

95. Ayliffe, M.A.; Pallotta, M.; Langridge, P.; Pryor, A.J. A barley activation tagging system. *Plant Mol. Biol.* **2007**, *64*, 329–347. [[CrossRef](#)] [[PubMed](#)]
96. Lazarow, K.; Lütticke, S. An Ac/Ds-mediated gene trap system for functional genomics in barley. *BMC Genom.* **2009**, *10*, 55. [[CrossRef](#)] [[PubMed](#)]
97. Ryder, P.; McHale, M.; Fort, A.; Spillane, C. Generation of stable nulliplex autopolyploid lines of *Arabidopsis thaliana* using CRISPR/Cas9 genome editing. *Plant Cell Rep.* **2017**, *36*, 1005–1008. [[CrossRef](#)] [[PubMed](#)]
98. Jinek, M.; Chylinski, K.; Fonfara, I.; Hauer, M.; Doudna, J.A.; Charpentier, E. A Programmable Dual-RNA – Guided DNA Endonuclease S figs. *Science* **2012**, *337*, 816–821. [[CrossRef](#)]
99. Lawrenson, T.; Shorinola, O.; Stacey, N.; Li, C.; Østergaard, L.; Patron, N.; Uauy, C.; Harwood, W. Induction of targeted, heritable mutations in barley and *Brassica oleracea* using RNA-guided Cas9 nuclease. *Genome Biol.* **2015**, *16*, 258. [[CrossRef](#)]
100. Holme, I.B.; Wendt, T.; Gil-Humanes, J.; Deleuran, L.C.; Starker, C.G.; Voytas, D.F.; Brinch-Pedersen, H. Evaluation of the mature grain phytase candidate HvPAPhy_a gene in barley (*Hordeum vulgare* L.) using CRISPR/Cas9 and TALENs. *Plant Mol. Biol.* **2017**, *95*, 111–121. [[CrossRef](#)]
101. Gasparis, S.; Kała, M.; Przyborowski, M.; Łyżnik, L.A.; Orczyk, W.; Nadolska-Orczyk, A. A simple and efficient CRISPR/Cas9 platform for induction of single and multiple, heritable mutations in barley (*Hordeum vulgare* L.). *Plant Methods* **2018**, *14*, 111. [[CrossRef](#)]
102. Kumar, N.; Galli, M.; Ordon, J.; Stuttmann, J.; Kogel, K.H.; Imani, J. Further analysis of barley MORC1 using a highly efficient RNA-guided Cas9 gene-editing system. *Plant Biotechnol. J.* **2018**, *16*, 1892–1903. [[CrossRef](#)]
103. Gasparis, S.; Przyborowski, M.; Kała, M.; Nadolska-Orczyk, A. Knockout of the HvCKX1 or HvCKX3 Gene in Barley (*Hordeum vulgare* L.) by RNA-Guided Cas9 Nuclease Affects the Regulation of Cytokinin Metabolism and Root Morphology. *Cells* **2019**, *8*, 782. [[CrossRef](#)]
104. Yang, Q.; Zhong, X.; Li, Q.; Lan, J.; Tang, H.; Qi, P.; Ma, J.; Wang, J.; Chen, G.; Pu, Z.; et al. Mutation of the D-hordein gene by RNA-guided Cas9 targeted editing reducing the grain size and changing grain compositions in barley. *Food Chem.* **2020**, *311*, 125892. [[CrossRef](#)] [[PubMed](#)]
105. Saski, C.; Tomkins, J.; Lee, S.-B.; Daniell, H.; Fjellheim, S.; Rognli, O.A.; Guda, C.; Jansen, R.K.; Luo, H.; Clarke, J.L. Complete chloroplast genome sequences of *Hordeum vulgare*, *Sorghum bicolor* and *Agrostis stolonifera*, and comparative analyses with other grass genomes. *Theor. Appl. Genet.* **2007**, *115*, 571–590. [[CrossRef](#)] [[PubMed](#)]
106. Petersen, J.; Rogowska-Wrzesinska, A.; Jensen, O.N. Functional proteomics of barley and barley chloroplasts-strategies, methods and perspectives. *Front. Plant Sci.* **2013**, *4*, 52. [[CrossRef](#)] [[PubMed](#)]
107. Pogson, B.J.; Woo, N.S.; Förster, B.; Small, I.D. Plastid signalling to the nucleus and beyond. *Trends Plant Sci.* **2008**, *3*, 602–609. [[CrossRef](#)]
108. Wagner, D.; Przybyla, D.; Op Den Camp, R.; Kim, C.; Landgraf, F.; Keun, P.L.; Würsch, M.; Laloi, C.; Nater, M.; Hideg, E.; et al. The genetic basis of singlet oxygen-induced stress response of *Arabidopsis thaliana*. *Science* **2004**, *306*, 1183–1185. [[CrossRef](#)]
109. Maruta, T.; Noshi, M.; Tanouchi, A.; Tamoi, M.; Yabuta, Y.; Yoshimura, K.; Ishikawa, T.; Shigeoka, S. H₂O₂-triggered retrograde signaling from chloroplasts to nucleus plays specific role in response to stress. *J. Biol. Chem.* **2012**, *287*, 11717–11729. [[CrossRef](#)]
110. Pfalz, J.; Liebers, M.; Hirth, M.; Grübler, B.; Holtzegel, U.; Schröter, Y.; Dietzel, L.; Pfannschmidt, T. Environmental control of plant nuclear gene expression by chloroplast redox signals. *Front. Plant Sci.* **2012**, *3*, 257. [[CrossRef](#)]
111. Estavillo, G.M.; Crisp, P.A.; Pornsiriwong, W.; Wirtz, M.; Collinge, D.; Carrie, C.; Giraud, E.; Whelan, J.; David, P.; Javot, H.; et al. Evidence for a SAL1-PAP chloroplast retrograde pathway that functions in drought and high light signaling in *Arabidopsis*. *Plant Cell* **2011**, *23*, 3992–4012. [[CrossRef](#)]
112. Xiao, Y.; Savchenko, T.; Baidoo, E.E.K.; Chehab, W.E.; Hayden, D.M.; Tolstikov, V.; Corwin, J.A.; Kliebenstein, D.J.; Keasling, J.D.; Dehesh, K. Retrograde signaling by the plastidial metabolite MEcPP regulates expression of nuclear stress-response genes. *Cell* **2012**, *149*, 1525–1535. [[CrossRef](#)]
113. Ramel, F.; Birtic, S.; Ginies, C.; Soubigou-Taconnat, L.; Triantaphylidès, C.; Havaux, M. Carotenoid oxidation products are stress signals that mediate gene responses to singlet oxygen in plants. *Proc. Natl. Acad. Sci. USA* **2012**, *109*, 5535–5540. [[CrossRef](#)]
114. D’Alessandro, S.; Havaux, M. Sensing β -carotene oxidation in photosystem II to master plant stress tolerance. *New Phytol.* **2019**, *223*, 1776–1783. [[CrossRef](#)] [[PubMed](#)]

115. Chi, W.; Feng, P.; Ma, J.; Zhang, L. Metabolites and chloroplast retrograde signaling. *Curr. Opin. Plant Biol.* **2015**, *25*, 32–38. [[CrossRef](#)] [[PubMed](#)]
116. Tian, L. Recent advances in understanding carotenoid-derived signaling molecules in regulating plant growth and development. *Front. Plant Sci.* **2015**, *6*, 790. [[CrossRef](#)] [[PubMed](#)]
117. Chan, K.X.; Phua, S.Y.; Crisp, P.; McQuinn, R.; Pogson, B.J. Learning the Languages of the Chloroplast: Retrograde Signaling and Beyond. *Annu. Rev. Plant Biol.* **2016**, *67*, 25–53. [[CrossRef](#)] [[PubMed](#)]
118. Kleine, T.; Leister, D. Retrograde signaling: Organelles go networking. *Biochim. Biophys. Acta Bioenerg.* **2016**, *1857*, 1313–1325. [[CrossRef](#)] [[PubMed](#)]
119. de Souza, A.; Wang, J.-Z.; Dehesh, K. Retrograde Signals: Integrators of Interorganellar Communication and Orchestrators of Plant Development. *Annu. Rev. Plant Biol.* **2017**, *68*, 85–108. [[CrossRef](#)]
120. Susek, R.E.; Ausubel, F.M.; Chory, J. Signal transduction mutants of arabidopsis uncouple nuclear CAB and RBCS gene expression from chloroplast development. *Cell* **1993**, *74*, 787–799. [[CrossRef](#)]
121. Larkin, R.M.; Stefano, G.; Ruckler, M.E.; Stavoe, A.K.; Sinkler, C.A.; Brandizzi, F.; Malmstrom, C.M.; Osteryoung, K.W.; Chory, J. REDUCED CHLOROPLAST COVERAGE genes from Arabidopsis thaliana help to establish the size of the chloroplast compartment. *Proc. Natl. Acad. Sci. USA* **2016**, *113*, E1116–E1125. [[CrossRef](#)]
122. Koussevitzky, S.; Nott, A.; Mockler, T.C.; Hong, F.; Sachetto-Martins, G.; Surpin, M.; Lim, J.; Mittler, R.; Chory, J. Signals from Chloroplasts Converge to Regulate Nuclear Gene Expression. *Science* **2007**, *316*, 715–719. [[CrossRef](#)]
123. Tadini, L.; Pesaresi, P.; Kleine, T.; Rossi, F.; Guljamow, A.; Sommer, F.; Mühlhaus, T.; Schroda, M.; Masiero, S.; Pribil, M.; et al. Gun1 controls accumulation of the plastid ribosomal protein S1 at the protein level and interacts with proteins involved in plastid protein homeostasis. *Plant Physiol.* **2016**, *170*, 1817–1830. [[CrossRef](#)]
124. Tadini, L.; Peracchio, C.; Trotta, A.; Colombo, M.; Mancini, I.; Jeran, N.; Costa, A.; Faoro, F.; Marsoni, M.; Vannini, C.; et al. GUN1 influences the accumulation of NEP-dependent transcripts and chloroplast protein import in Arabidopsis cotyledons upon perturbation of chloroplast protein homeostasis. *Plant J.* **2020**, *101*, 1198–1220. [[CrossRef](#)]
125. Wu, G.Z.; Meyer, E.H.; Richter, A.S.; Schuster, M.; Ling, Q.; Schöttler, M.A.; Walther, D.; Zoschke, R.; Grimm, B.; Jarvis, R.P.; et al. Control of retrograde signalling by protein import and cytosolic folding stress. *Nat. Plants* **2019**, *5*, 525–538. [[CrossRef](#)] [[PubMed](#)]
126. Börner, T.; Meister, A. Chlorophyll and carotenoid content of ribosome-deficient plastids. *Photosynthetica* **1980**, *14*, 589–593.
127. Yaronskaya, E.; Ziemann, V.; Walter, G.; Averina, N.; Börner, T.; Grimm, B. Metabolic control of the tetrapyrrole biosynthetic pathway for porphyrin distribution in the barley mutant albostrians. *Plant J.* **2003**, *35*, 512–522. [[CrossRef](#)] [[PubMed](#)]
128. Feierabend, J.; Mikus, M. Occurrence of a High Temperature Sensitivity of Chloroplast Ribosome Formation in Several Higher Plants. *Plant Physiol.* **1977**, *59*, 863–867. [[CrossRef](#)]
129. Woodson, J.D.; Perez-Ruiz, J.M.; Chory, J. Heme synthesis by plastid ferrochelatase i regulates nuclear gene expression in plants. *Curr. Biol.* **2011**, *21*, 897–903. [[CrossRef](#)]
130. Li, M.; Hensel, G.; Mascher, M.; Melzer, M.; Budhagatapalli, N.; Rutten, T.; Himmelbach, A.; Beier, S.; Korzun, V.; Kumlehn, J.; et al. Leaf variegation and impaired chloroplast development caused by a truncated CCT domain gene in albostrians barley. *Plant Cell* **2019**, *31*, 1430–1445. [[CrossRef](#)]
131. Kim, S.; Dale, B.E. Global potential bioethanol production from wasted crops and crop residues. *Biomass Bioenergy* **2004**, *26*, 361–375. [[CrossRef](#)]
132. Gu, J.; Zhou, Z.; Li, Z.; Chen, Y.; Wang, Z.; Zhang, H.; Yang, J. Photosynthetic properties and potentials for improvement of photosynthesis in pale green leaf rice under high light conditions. *Front. Plant Sci.* **2017**, *8*, 1082. [[CrossRef](#)]
133. Chida, H.; Nakazawa, A.; Akazaki, H.; Hirano, T.; Suruga, K.; Ogawa, M.; Satoh, T.; Kadokura, K.; Yamada, S.; Hakamata, W.; et al. Expression of the algal cytochrome c6 gene in Arabidopsis enhances photosynthesis and growth. *Plant Cell Physiol.* **2007**, *48*, 948–957. [[CrossRef](#)]
134. Yadav, S.K.; Khatri, K.; Rathore, M.S.; Jha, B. Introgression of UfCyt c 6, a thylakoid lumen protein from a green seaweed *Ulva fasciata* Delile enhanced photosynthesis and growth in tobacco. *Mol. Biol. Rep.* **2018**, *45*, 1745–1758. [[CrossRef](#)] [[PubMed](#)]

135. Pesaresi, P.; Hertle, A.; Pribil, M.; Kleine, T.; Wagner, R.; Strissel, H.; Lhnatowicz, A.; Bonardi, V.; Scharfenberg, M.; Schneider, A.; et al. Arabidopsis STN7 kinase provides a link between short- and long-term photosynthetic acclimation. *Plant Cell* **2009**, *21*, 2402–2423. [[CrossRef](#)]
136. Simkin, A.J.; McAusland, L.; Lawson, T.; Raines, C.A. Overexpression of the rieskeFeS protein increases electron transport rates and biomass yield. *Plant Physiol.* **2017**, *175*, 134–145. [[CrossRef](#)]
137. Kromdijk, J.; Glowacka, K.; Leonelli, L.; Gabilly, S.T.; Iwai, M.; Niyogi, K.K.; Long, S.P. Improving photosynthesis and crop productivity by accelerating recovery from photoprotection. *Science* **2016**, *354*, 857–861. [[CrossRef](#)] [[PubMed](#)]
138. Simkin, A.J.; McAusland, L.; Headland, L.R.; Lawson, T.; Raines, C.A. Multigene manipulation of photosynthetic carbon assimilation increases CO₂ fixation and biomass yield in tobacco. *J. Exp. Bot.* **2015**, *66*, 4075–4090. [[CrossRef](#)] [[PubMed](#)]
139. Simkin, A.J.; Lopez-Calcagno, P.E.; Davey, P.A.; Headland, L.R.; Lawson, T.; Timm, S.; Bauwe, H.; Raines, C.A. Simultaneous stimulation of sedoheptulose 1,7-bisphosphatase, fructose 1,6-bisphosphate aldolase and the photorespiratory glycine decarboxylase-H protein increases CO₂ assimilation, vegetative biomass and seed yield in Arabidopsis. *Plant Biotechnol. J.* **2017**, *15*, 805–816. [[CrossRef](#)]
140. Lefebvre, S.; Lawson, T.; Zakhleniuk, O.V.; Lloyd, J.C.; Raines, C.A. Increased sedoheptulose-1,7-bisphosphatase activity in transgenic tobacco plants stimulates photosynthesis and growth from an early stage in development. *Plant Physiol.* **2005**, *138*, 451–460. [[CrossRef](#)]
141. Ding, F.; Wang, M.; Zhang, S.; Ai, X. Changes in SBPase activity influence photosynthetic capacity, growth, and tolerance to chilling stress in transgenic tomato plants. *Sci. Rep.* **2016**, *6*, 32741. [[CrossRef](#)] [[PubMed](#)]
142. Uematsu, K.; Suzuki, N.; Iwamae, T.; Inui, M.; Yukawa, H. Increased fructose 1,6-bisphosphate aldolase in plastids enhances growth and photosynthesis of tobacco plants. *J. Exp. Bot.* **2012**, *63*, 3001–3009. [[CrossRef](#)]
143. Yamori, W.; Masumoto, C.; Fukayama, H.; Makino, A. Rubisco activase is a key regulator of non-steady-state photosynthesis at any leaf temperature and, to a lesser extent, of steady-state photosynthesis at high temperature. *Plant J.* **2012**, *71*, 871–880. [[CrossRef](#)]
144. Sanz-Barrio, R.; Corral-Martinez, P.; Ancin, M.; Segui-Simarro, J.M.; Farran, I. Overexpression of plastidial thioredoxin f leads to enhanced starch accumulation in tobacco leaves. *Plant Biotechnol. J.* **2013**, *11*, 618–627. [[CrossRef](#)]
145. Farran, I.; Fernandez-San Millan, A.; Ancin, M.; Larraya, L.; Veramendi, J. Increased bioethanol production from commercial tobacco cultivars overexpressing thioredoxin f grown under field conditions. *Mol. Breed.* **2014**, *34*, 457–469. [[CrossRef](#)]
146. Toivola, J.; Nikkanen, L.; Dahlström, K.M.; Salminen, T.A.; Lepistö, A.; Vignols, F.; Rintamäki, E. Overexpression of chloroplast NADPH-dependent thioredoxin reductase in Arabidopsis enhances leaf growth and elucidates in vivo function of reductase and thioredoxin domains. *Front. Plant Sci.* **2013**, *4*, 389. [[CrossRef](#)] [[PubMed](#)]
147. Nikkanen, L.; Toivola, J.; Rintamäki, E. Crosstalk between chloroplast thioredoxin systems in regulation of photosynthesis. *Plant Cell Environ.* **2016**, *39*, 1691–1705. [[CrossRef](#)] [[PubMed](#)]
148. Timm, S.; Florian, A.; Arrivault, S.; Stitt, M.; Fernie, A.R.; Bauwe, H. Glycine decarboxylase controls photosynthesis and plant growth. *FEBS Lett.* **2012**, *586*, 3692–3697. [[CrossRef](#)] [[PubMed](#)]
149. Timm, S.; Wittmiß, M.; Gamlien, S.; Ewald, R.; Florian, A.; Frank, M.; Wirtz, M.; Hell, R.; Fernie, A.R.; Bauwe, H. Mitochondrial dihydrolipoyl dehydrogenase activity shapes photosynthesis and photorespiration of Arabidopsis Thaliana. *Plant Cell* **2015**, *27*, 1968–1984. [[CrossRef](#)] [[PubMed](#)]
150. López-Calcagno, P.E.; Fisk, S.; Brown, K.L.; Bull, S.E.; South, P.F.; Raines, C.A. Overexpressing the H-protein of the glycine cleavage system increases biomass yield in glasshouse and field-grown transgenic tobacco plants. *Plant Biotechnol. J.* **2019**, *7*, 141–151. [[CrossRef](#)]
151. Kebeish, R.; Niessen, M.; Thiruveedhi, K.; Bari, R.; Hirsch, H.J.; Rosenkranz, R.; Stäbler, N.; Schönfeld, B.; Kreuzaler, F.; Peterhänsel, C. Chloroplastic photorespiratory bypass increases photosynthesis and biomass production in Arabidopsis thaliana. *Nat. Biotechnol.* **2007**, *25*, 593–599. [[CrossRef](#)]
152. South, P.F.; Cavanagh, A.P.; Liu, H.W.; Ort, D.R. Synthetic glycolate metabolism pathways stimulate crop growth and productivity in the field. *Science* **2019**, *367*, 45. [[CrossRef](#)]
153. Jansson, C.; Wullschleger, S.D.; Kalluri, U.C.; Tuskan, G.A. Phytosequestration: Carbon Biosequestration by Plants and the Prospects of Genetic Engineering. *Bioscience* **2010**, *60*, 685–696. [[CrossRef](#)]

154. Zhu, X.-G.; Long, S.P.; Ort, D.R. Improving Photosynthetic Efficiency for Greater Yield. *Annu. Rev. Plant Biol.* **2010**, *61*, 235–261. [[CrossRef](#)] [[PubMed](#)]
155. Blankenship, R.E.; Chen, M. Spectral expansion and antenna reduction can enhance photosynthesis for energy production. *Curr. Opin. Chem. Biol.* **2013**, *17*, 457–461. [[CrossRef](#)]
156. Nakajima, Y.; Ueda, R. Improvement of photosynthesis in dense microalgal suspension by reduction of light harvesting pigments. *J. Appl. Phycol.* **1997**, *9*, 503–510. [[CrossRef](#)]
157. Beckmann, J.; Lehr, F.; Finazzi, G.; Hankamer, B.; Posten, C.; Wobbe, L.; Kruse, O. Improvement of light to biomass conversion by de-regulation of light-harvesting protein translation in *Chlamydomonas reinhardtii*. *J. Biotechnol.* **2009**, *142*, 70–77. [[CrossRef](#)] [[PubMed](#)]
158. Perrine, Z.; Negi, S.; Sayre, R.T. Optimization of photosynthetic light energy utilization by microalgae. *Algal Res.* **2012**, *1*, 134–142. [[CrossRef](#)]
159. Demmig-Adams, B.; Adams, W.W. Chlorophyll and carotenoid composition in leaves of *Euonymus kiautschovicus* acclimated to different degrees of light stress in the field. *Aust. J. Plant Physiol.* **1996**, *23*, 649–659. [[CrossRef](#)]
160. Li, X.P.; Müller-Moulé, P.; Gilmore, A.M.; Niyogi, K.K. PsbS-dependent enhancement of feedback de-excitation protects photosystem II from photoinhibition. *Proc. Natl. Acad. Sci. USA* **2002**, *99*, 15222–15227. [[CrossRef](#)]
161. Pérez-Bueno, M.L.; Johnson, M.P.; Zia, A.; Ruban, A.V.; Horton, P. The Lhcb protein and xanthophyll composition of the light harvesting antenna controls the Δ pH-dependency of non-photochemical quenching in *Arabidopsis thaliana*. *FEBS Lett.* **2008**, *582*, 1477–1482. [[CrossRef](#)]
162. Driever, S.M.; Simkin, A.J.; Alotaibi, S.; Fisk, S.J.; Madgwick, P.J.; Sparks, C.A.; Jones, H.D.; Lawson, T.; Parry, M.A.J.; Raines, C.A. Increased sbpase activity improves photosynthesis and grain yield in wheat grown in greenhouse conditions. *Philos. Trans. R. Soc. B Biol. Sci.* **2017**, *372*, 20160384. [[CrossRef](#)]
163. Kim, M.R.; Khaleda, L.; Jung, I.J.; Kim, J.Y.; Lee, S.Y.; Cha, J.Y.; Kim, W.Y. Overexpression of chloroplast-localized NADPH-dependent thioredoxin reductase C (NTRC) enhances tolerance to photo-oxidative and drought stresses in *Arabidopsis thaliana*. *J. Plant Biol.* **2017**, *60*, 175–180. [[CrossRef](#)]
164. Kisaki, T.; Tolbert, N.E. Glycine as a substrate for photorespiration. *Plant Cell Physiol.* **1970**, *11*, 247–258. [[CrossRef](#)]
165. Kisaki, T.; Imai, A.; Tolbert, N.E. Intracellular localization of enzymes related to photorespiration in green leaves. *Plant Cell Physiol.* **1971**, *12*, 267–273. [[CrossRef](#)]
166. Eisenhut, M.; Ruth, W.; Haimovich, M.; Bauwe, H.; Kaplan, A.; Hagemann, M. The photorespiratory glycolate metabolism is essential for cyanobacteria and might have been conveyed endosymbiotically to plants. *Proc. Natl. Acad. Sci. USA* **2008**, *105*, 17199–17204. [[CrossRef](#)] [[PubMed](#)]
167. Kikuchi, G.; Motokawa, Y.; Yoshida, T.; Hiraga, K. Glycine cleavage system: Reaction mechanism, physiological significance, and hyperglycinemia. *Proc. Japan Acad. Ser. B Phys. Biol. Sci.* **2008**, *84*, 246–263. [[CrossRef](#)] [[PubMed](#)]
168. Zelitch, I.; Schultes, N.P.; Peterson, R.B.; Brown, P.; Brutnell, T.P. High glycolate oxidase activity is required for survival of maize in normal air. *Plant Physiol.* **2009**, *149*, 195–204. [[CrossRef](#)]
169. Hackenberg, C.; Kern, R.; Hüge, J.; Stal, L.J.; Tsuji, Y.; Kopka, J.; Shiraiwa, Y.; Bauwe, H.; Hagemann, M. Cyanobacterial lactate oxidases serve as essential partners in N₂ fixation and evolved into photorespiratory glycolate oxidases in plants. *Plant Cell* **2011**, *23*, 2978–2990. [[CrossRef](#)]



Time-Course Transcriptome Analysis of Arabidopsis Siliques Discloses Genes Essential for Fruit Development and Maturation¹

Chiara Mizzotti,^a Lisa Rotasperti,^a Marco Moretto,^b Luca Tadini,^a Francesca Resentini,^{a,2} Bianca M. Galliani,^a Massimo Galbiati,^a Kristof Engelen,^b Paolo Pesaresi,^c and Simona Masiero^{a,3,4}

^aDepartment of Biosciences, Università degli Studi di Milano, 20133 Milan, Italy

^bComputational Biology Unit, Fondazione E. Mach, 38010 S. Michele all'Adige, Trentino, Italy

^cDepartment of Agricultural and Environmental Sciences-Production, Landscape, Agroenergy, Università degli Studi di Milano, 20133 Milan, Italy

ORCID IDs: 0000-0003-3644-2890 (C.M.); 0000-0001-9595-9828 (L.R.); 0000-0003-4555-7243 (M.M.); 0000-0003-0033-6930 (F.R.); 0000-0002-9827-4506 (M.G.); 0000-0002-3236-7005 (P.P.); 0000-0002-7563-7634 (S.M.)

Fruits protect the developing seeds of angiosperms and actively contribute to seed dispersion. Furthermore, fruit and seed development are highly synchronized and require exchange of information between the mother plant and the developing generations. To explore the mechanisms controlling fruit formation and maturation, we performed a transcriptomic analysis on the valve tissue of the Arabidopsis (*Arabidopsis thaliana*) silique using RNA sequencing. In doing so, we have generated a data set of differentially regulated genes that will help to elucidate the molecular mechanisms that underpin the initial phase of fruit growth and, subsequently, trigger fruit maturation. The robustness of our data set has been tested by functional genomic studies. Using a reverse genetics approach, we selected 10 differentially expressed genes and explored the consequences of their disruption for both silique growth and senescence. We found that genes contained in our data set play essential roles in different stages of silique development and maturation, indicating that our transcriptome-based gene list is a powerful tool for the elucidation of the molecular mechanisms controlling fruit formation in Arabidopsis.

In angiosperms fruit formation is triggered by fertilization, which occurs in the ovule. As a consequence of fertilization, the ovule develops into a seed while the ovary differentiates into a fruit (Coombe, 1975). Fruits evolved to protect and provide nutrients for the embryos, which grow and differentiate within the seeds (Müntz et al., 1978). Once embryos have completed their development, fruits contribute to their dispersal. To perform these functions, fruits and seeds must

communicate throughout their development. Coordination between the mother plant and the developing generation is a highly complex process that relies on a variety of chemical mediators, such as hormones, proteins, peptides, mRNAs, small RNAs, and noncoding RNAs (Lindsey, 2001; Jones-Rhoades et al., 2006; Corbesier et al., 2007; Tamaki et al., 2007; Kalantidis et al., 2008; McAtee et al., 2013). Moreover, signals derived from pollen (O'Neill, 1997; O'Neill and Nadeau, 2010), ovules (Gillaspy et al., 1993), or other vegetative tissues (Nitsch, 1952) can stimulate fruit development. Indeed, the occurrence of seedless fruits, whether parthenocarpic (in which case they develop in the absence of fertilization) or stenospermocarpic (in which case fertilization occurs but seeds abort precociously), indicates that fruit and seed communication can be outflanked (Mazzucato et al., 1998; Varoquaux et al., 2000; Pandolfini, 2009; Rojas-Gracia et al., 2017).

The fruit of the model plant species Arabidopsis (*Arabidopsis thaliana*), known as the silique, is a dry dehiscent fruit that mechanically opens at maturity, releasing the seeds. Siliques develop from a gynoecium composed of two fused carpels linked by a central tissue named the septum (Rollins, 1993). Fertilization induces a rapid transformation of the gynoecium, leading to the development of the silique; this process can be divided into two distinct phases, encompassing growth and maturation. The first phase begins immediately after fertilization and determines the final size of the silique, which is reached at 6 to 7 DPA (Vivian-Smith

¹The work has been supported by Cariplo Foundation [grant number 2011-2257 to C.M. and S.M.], by MIUR PRIN [grant number 2015BPM9H3_005 to S.M.] and by post doc and PhD fellowships from the Università degli Studi di Milano [to C.M., L.T., and B.G.].

²Current address: Instituto de Biología Molecular y Celular de Plantas, Consejo Superior de Investigaciones Científicas (CSIC)-Universidad Politécnica de Valencia, 46022 Valencia, Spain.

³ Author for contact: simona.masiero@unimi.it.

⁴Senior author.

The author responsible for distribution of materials integral to the findings presented in this article in accordance with the policy described in the Instructions for Authors (www.plantphysiol.org) is: Simona Masiero (simona.masiero@unimi.it).

C.M. and S.M. planned and designed the research; C.M., L.R., B.G., and F.R. extracted the RNA; M.M. and K.E. carried out the bioinformatics analysis; C.M. and L.R. performed all the experiments; P.P. and L.T. were involved in the measurement of the quantum efficiency of the PSII electron transport chain and immunoblot analysis; M.G. constructed the transgenic lines; C.M., P.P., and S.M. wrote the article.

www.plantphysiol.org/cgi/doi/10.1104/pp.18.00727

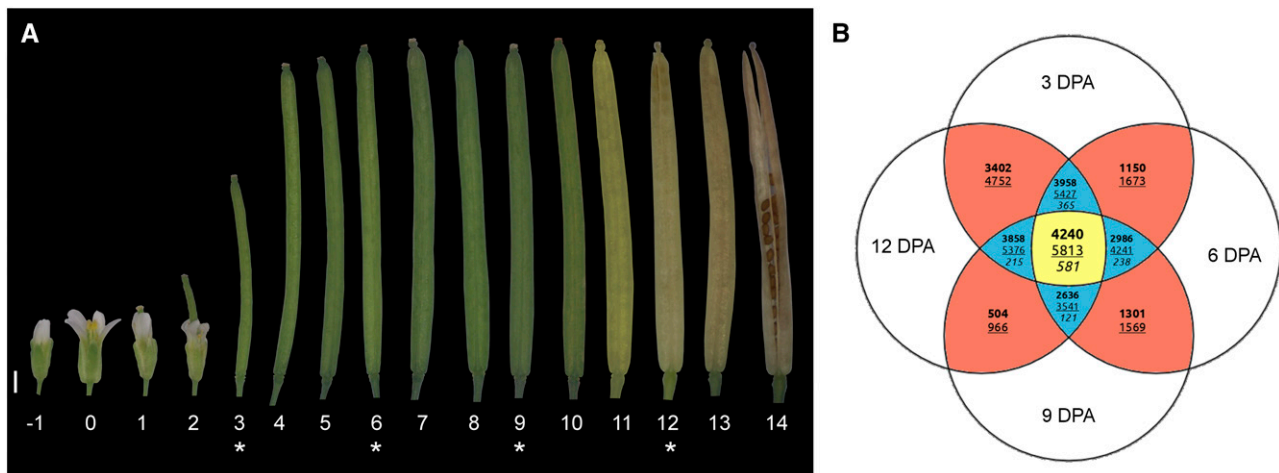


Figure 1. RNA sequencing (RNAseq) strategy used to explore the mechanisms controlling fruit formation and maturation. A, Developmental series of Arabidopsis siliques from the flower bud (–1 DPA) to the mature fruit (14 DPA). Numbers below the siliques indicate the DPA. The siliques at 3, 6, 9, and 12 DPA, marked with asterisks, were opened and the seeds were removed prior to use for RNAseq analysis. The image shown is a composite image. Bar = 1 mm. B, Venn diagram shows the number of up-regulated (boldface), down-regulated (underlined), and alternative behavior (italics) genes across all comparisons performed using the selected cutoff (fold change of 2.5 and $P = 0.001$; see “Materials and Methods”). The four pairwise comparisons (6 versus 3 DPA, 9 versus 6 DPA, 12 versus 9 DPA, and 12 versus 3 DPA) show only two values, since, by definition, genes can only be either up-regulated or down-regulated. The center of the Venn diagram (i.e. the yellow portion) shows the number of differentially expressed genes considered in this work: 4,240 up-regulated genes (Supplemental Table S1), 5,813 down-regulated genes (Supplemental Table S2), and 581 genes that showed an alternative behavior (Supplemental Table S3–S6).

and Koltunow, 1999). Growth of the silique in length and width involves cell division and cell expansion (Vivian-Smith and Koltunow, 1999). Once the silique has reached its final size, it quickly enters the maturation phase, which leads to the ripening and the subsequent senescence of the fruit. The effect of maturation is clearly visible by around 12 DPA, when the green color of the silique begins to turn yellowish. However, this visible phenotype is anticipated by several molecular events, such as the decline in chlorophyll content that begins before the yellowing becomes apparent.

The transcriptomic data on Arabidopsis fruit development currently available derive from a few surveys based on microarray analysis (Wagstaff et al., 2009; Carbonell-Bejerano et al., 2010; Jaradat et al., 2014). Furthermore, these studies analyzed mutant lines (*eceriferum*) or explored relatively late developmental stages (10 and 20 DPA) or siliques including the seeds, making it almost impossible to distinguish between fruit and seed development at the molecular level.

In our investigation, we have used next-generation sequencing to extend our knowledge of the molecular mechanisms that control the early stages of silique formation and the sequence of maturation events. We provide a comprehensive transcriptomic analysis of Arabidopsis fruits, devoid of seeds, at 3, 6, 9, and 12 DPA, which allows us to identify genes with potential roles in silique formation and maturation. Through a reverse genetics approach, we demonstrate that transcription factors, cytoskeletal proteins, and enzymes

that modulate hormone homeostasis are intimately involved in these processes.

RESULTS

Expression Analysis Identifies Three Classes of Differentially Expressed Genes

In order to determine which genes are involved in Arabidopsis silique development, siliques at 3, 6, 9, and 12 DPA from Columbia-0 (Col-0) plants (Fig. 1A) were collected. The first two time points (3 and 6 DPA) are representative of the growth stage of the siliques, while the other two (9 and 12 DPA) correspond to the silique’s maturation phase. Seeds were removed manually, such that the poly(A) RNA extracted and subjected to Illumina sequencing was derived solely from maternal fruit tissues. The number of reads for each replicate is reported in Supplemental Figure S1A.

Principal component analysis of the sequences sampled at the four time points shows that they are well separated along the first component, which explains 56% of the variability (Supplemental Fig. S1B). Biological replicates were grouped together, with the second and third time points (6 and 9 DPA, respectively) showing higher variability than the first and last time points (3 and 12 DPA).

Two computational packages were used to identify differentially expressed genes, edgeR and Limma, which

have been shown previously to have a Spearman correlation coefficient of 0.9 through the analysis of mouse data sets (Seyednasrollah et al., 2015). In our case, the two packages also gave very similar results, although Limma was more stringent (Supplemental Fig. S2). Therefore, we decided to consider the Limma outputs for further analyses, even though all the genes analyzed by reverse genetics in this study were differentially expressed according to both computational tools.

Based on the adopted cutoff (fold change of 2.5 and $P = 0.001$; see “Materials and Methods”), genes were grouped into three classes (Fig. 1B). Up-regulated genes consistently and significantly increased their transcription rate between the two end points in the time series; conversely, the expression of down-regulated genes diminished steadily from the first time point to the last. All genes displaying both up- and down-regulated profiles, depending on the time points considered, were defined as exhibiting alternative behavior (Fig. 1B). Among the alternative behavior genes, we performed a visual inspection of the hierarchical clustering results to identify meaningful subgroups; thus, four different clusters were defined (Supplemental Fig. S3; see “Materials and Methods”). With this approach, we defined 4,240 up-regulated genes (Supplemental Table S1), 5,813 down-regulated genes (Supplemental Table S2), and 581 genes with alternative behaviors (Supplemental Table S3–S6). In all, 11,274 genes showed no significant change in their expression level over the four stages analyzed.

Gene Ontology Analysis Reveals the Functions of the Differentially Expressed Genes

Changes in gene expression underlie differences in biological functions; using the agriGO software (Du et al., 2010), we explored the gene ontologies (GO) that were enriched among the previously defined groups (up- and down-regulated genes and genes showing alternative behaviors; see Supplemental Figs. S4, S5, and S6, respectively). Within the group of up-regulated genes, we identified GO categories for biological processes (GO:0050789/GO:0065007), cell communication (GO:0007154), regulation of cellular processes (GO:0050794), response to stimuli (GO:0050896), together with some of their child terms, and participation in secondary metabolism (GO:0019748). Functions in secondary metabolism (GO:0019748) also were associated with genes assigned to the alternative behavior sets. This reflects the fact that siliques are sink organs (Robinson and Hill, 1999), in which secondary metabolites, like trehalose and ascorbic acid, are produced soon after fertilization, whereas others, such as maltose, sorbitol, and galactinol, accumulate during silique maturation (Watanabe et al., 2013).

Among the down-regulated genes, GO terms related to cellular component organization (GO:0016043), cell cycle (GO:0007049), photosynthesis (GO:0015979), and carbohydrate metabolic processes (GO:0005975) were enriched. The down-regulation of these gene sets reflects

alterations in cell division and cell expansion rates, which are high during the early phases of fruit growth and diminish in later stages of fruit development and maturation (Vivian-Smith and Koltunow, 1999). Furthermore, chlorophylls are degraded, without being replaced, during silique maturation (Wagstaff et al., 2009; Jaradat et al., 2014); consequently, photosynthesis-related genes are found consistently in this group.

Expression Analysis of Genes with Known Functions Proves the Robustness of the Transcriptome Data Set

The expression profiles of genes already known to be involved in silique formation and maturation were used to verify the quality of our data set (Table 1). For instance, the MADS box gene *AGAMOUS* (*AG*), which encodes a transcription factor that is responsible for determining the fate of the fourth whorl of the flower and later orchestrates silique shattering (Ferrándiz, 2002; Dinneny et al., 2005), is highly expressed at all of the four time points analyzed. Furthermore, among genes known to promote cell expansion, *LONGIFOLIA1* (*LNG1*), *LNG2*, *ROTUNDIFOLIA3* (*ROT3*), *ANGUSTIFOLIA* (*AN*), and *ATHB13* (*Homeobox-Leu zipper protein ATHB-13*; Tsuge et al., 1996; Kim et al., 1998, 1999, 2002, 2005; Hanson et al., 2001; Lee et al., 2006; Prasad et al., 2010) are present in our data set. More specifically, *ROT3* expression increases between 3 and 6 DPA and then decreases until 12 DPA; therefore, *ROT3* is found among the alternative behavior genes. In contrast, *LNG1*, *LNG2*, *AN*, and *ATHB13* are among the down-regulated group, since they are strongly expressed at 3 DPA and their expression decreases with the onset of maturation, in agreement with their role in promoting cell expansion, which is concluded at 6 DPA.

Fruit development and maturation are strictly regulated by hormones (Kumar et al., 2014). In Supplemental Table S7, a list of genes involved in hormone metabolism, and differentially expressed in our samples, is provided. Among the five classical hormones, ethylene is known to play a key role in silique maturation (Kou et al., 2012). Ethylene is synthesized from Met, which is converted into *S*-adenosylmethionine by ACS (1-aminocyclopropane-1-carboxylate synthase) enzymes. Of the nine Arabidopsis ACS genes, only a few were found to be up-regulated in our data sets (Supplemental Table S7), such as ACS2 (Kou et al., 2012) and ACS7 (Tsuchisaka et al., 2009). ACS6 is found in the down-regulated gene set, although it is robustly transcribed during all the stages of fruit development taken into consideration. The ACC oxidase (ACO) enzymes, which are involved in the final step of the ethylene biosynthetic pathway, convert 1-aminocyclopropane-1-carboxylic acid (ACC) into ethylene. Among the five Arabidopsis ACO enzymes, ACO2 and ACO4 are assigned to the group of up-regulated genes, whereas ACO3 transcription increases quickly and reaches its maximum at 9 DAP before decreasing slightly by 12 DAP. Interestingly, *AtNAP* (*NAC-LIKE*,

Table 1. Expression of genes known from the literature to be involved in fruit formation or maturation

ATG Code	Name	Acronym	3 DAP	6 DAP	9 DAP	12 DAP	Group
AT5G15580	<i>LONGIFOLIA1</i>	<i>LNG1</i>	6.385	3.924	1.427	-0.115	Down
AT3G02170	<i>LONGIFOLIA2</i>	<i>LNG2</i>	6.329	3.373	2.947	3.794	Down
AT4G36380	<i>ROTUNDIFOLIA3</i>	<i>ROT3</i>	4.098	5.461	4.864	3.525	Alternative
AT1G01510	<i>ANGUSTIFOLIA</i>	<i>AN</i>	5.622	5.192	4.414	4.099	Down
AT1G69780	<i>ATHB13</i>	<i>ATHB13</i>	5.629	4.127	3.247	1.261	Down
AT4G18960	<i>AGAMOUS</i>	<i>AG</i>	5.511	5.126	5.213	5.274	
AT5G67110	<i>ALCATRAZ</i>	<i>ALC</i>	6.802	6.989	7.099	5.845	
AT5G60910	<i>FRUITFULL</i>	<i>FUL</i>	7.216	6.413	7.079	7.079	
AT4G00120	<i>INDEHISCENT</i>	<i>IND</i>	3.698	3.950	4.413	3.982	
AT2G45190	<i>FILAMENTOUS FLOWER</i>	<i>FIL</i>	3.439	3.864	3.822	2.664	
AT1G68480	<i>JAGGED</i>	<i>JAG</i>	-1.461	-0.659	-4.440	-4.592	Down
AT5G02030	<i>REPLUMLESS</i>	<i>RPL</i>	5.176	5.458	5.825	6.368	
AT4G09960	<i>SEEDSTICK</i>	<i>STK</i>	6.365	5.582	6.691	6.001	
AT2G42830	<i>SHATTERPROOF2</i>	<i>SHP2</i>	4.358	5.042	4.400	3.565	
AT3G58780	<i>SHATTERPROOF1</i>	<i>SHP1</i>	6.315	5.088	5.933	7.010	Up
AT4G00180	<i>YABBY3</i>	<i>YAB3</i>	1.451	2.668	2.796	1.663	
AT1G69490	<i>NAC-LIKE, ACTIVATED BY AP3/PI</i>	<i>AtNAP</i>	-0.021	2.244	3.231	4.413	Up
AT1G04580	<i>ALDEHYDE OXIDASES4</i>	<i>AAO4</i>	3.422	8.012	9.495	9.552	Up

ACTIVATED BY AP3/PI, NAC029), a NAC transcription factor whose expression increases over the course of silique development and whose product orchestrates ethylene biosynthesis (Kou et al., 2012), also is represented in the list of up-regulated genes. Besides *AtNAP*, 41 more NAC-encoding genes are assigned to the up-regulated group, 4 NAC genes are listed as alternative behavior, and 15 are part of the down-regulated gene set (Supplemental Table S8). NAC DNA-binding proteins are plant-specific transcription factors; in Arabidopsis, the NAC family so far includes 138 genes whose products play pivotal roles in plant development, hormone signal transduction, and stress responses (Shao et al., 2015). In agreement with the up-regulation of *AtNAP*, the transcription factor *EIN3* (*ETHYLENE INSENSITIVE3*), a positive regulator of ethylene signal (Kou et al., 2012), also is found among the up-regulated genes. *AtNAP* expression is triggered by *EIN3* (Kim et al., 2014), which modulates the expression of several ethylene-responsive factors that act in response to ethylene, abscisic acid, and jasmonic acid as well as to biotic and abiotic stresses. Indeed, several ethylene-responsive factor genes are differentially expressed in our data sets (Supplemental Table S8), including *ABI4* (*ABSCISIC ACID INSENSITIVE4*; Dong et al., 2016) among the up-regulated genes and *CYTOKININ RESPONSE FACTOR2* (*CRF2*) and *CRF4* among the down-regulated genes. *ABI4* is an intriguing transcription factor, since it antagonizes ethylene production (Dong et al., 2016) and is involved in plastid-to-nucleus and mitochondrion-to-nucleus retrograde signaling (Giraud et al., 2009; León et al., 2013).

The latter phase of silique development also is characterized by events relating to dehiscence, which together result in seed release upon pod shattering. Silique shattering includes the gradual breakdown of silique tissues, and this process is tightly regulated (for review, see Matilla, 2007). However, since the last time point considered here is 12 DPA, before any

signs of shattering become manifest, we do not expect the genes involved in this process to be differentially expressed yet. Indeed, all the genes known to be involved in pod shattering are present in our data set, but only *SHATTERPROOF1* (*SHP1*) shows a statistically significant increase in its expression during silique development (Liljegren et al., 2000). *SHP1* is a MIKC MADS box transcription factor (Masiero et al., 2011), and nine other MIKC MADS box genes are included in the list of up-regulated genes; among them are *AGAMOUS-LIKE15* (*AGL15*), *AGL18*, and *SHORT VEGETATIVE PHASE*, which might cooperate to slow down fruit maturation (Fernandez et al., 2014).

To further assess the reliability of the RNAseq data set, the expression profiles of 202 nuclear genes known to be involved in chloroplast-related functions, such as photosynthesis (42 genes), tetrapyrrole biosynthesis (26 genes), plastid protein translation (31 genes), RNA metabolism (13 genes), chlorophyll degradation (nine genes), plastid protein chaperone and degradation (35 genes), plastid protein import (20 genes), plastid membrane metabolism (five genes), nucleus-to-plastid anterograde signaling (seven genes), and plastid-to-nucleus retrograde signaling (14 genes), were investigated (Fig. 2A; Supplemental Fig. S7; Supplemental Table S8). As expected, the expression profiles of genes coding for components of the photosynthetic machinery, including PSI and PSII, the light-harvesting complexes a (Lhca) and b (Lhcb), cytochrome *b_f*, the small subunit of Rubisco (RbcS), and subunits of ATP synthase, showed no significant change between 3 and 6 DPA before exhibiting a marked decrease at 9 and 12 DPA. The tetrapyrrole biosynthesis pathway, including its chlorophyll and heme branches, followed a similar general trend, with a slight decrease between 3 and 6 DPA and a marked reduction at 9 and 12 DPA. A similar expression pattern also was exhibited by genes encoding proteins involved in plastid gene expression, such as plastid ribosomes and plastid factors with a

role in RNA metabolism. In particular, the expression of nuclear genes coding for plastid ribosomal proteins, for plastid RNA helicases of the DEAD/DEAH box family, and for plastid pentatricopeptide repeat proteins displayed a general decrease over the sampling time frame from 3 to 12 DPA. Conversely, the expression profiles of genes involved in chlorophyll degradation were characterized by a continuous increase from 3 to 12 DPA, in accordance with the marked structural alterations that chloroplasts undergo in the course of their metamorphosis into gerontoplasts during fruit maturation. Chloroplasts as well as the other plastid types, such as gerontoplasts and chromoplasts, need to communicate with the nucleus to modulate and harmonize the expression of the nuclear and plastid genomes. Our data show that the expression of nuclear genes involved in nucleus-to-chloroplast communication (i.e. anterograde signaling), including the nucleus-encoded RNA polymerase and the RNA polymerase Sigma factors (*SigA–SigF*), was down-regulated once chloroplasts were committed to turn into gerontoplasts, the only exception being *SigE*, whose expression doubled from 3 to 12 DPA (Supplemental Fig. S7; Supplemental Table S8). In contrast, the expression of genes involved in chloroplast-to-nucleus communication (i.e. retrograde signaling pathway) remained rather stable during fruit aging, and only small differences in the expression of *STN7* (up-regulated by 33% from 3 to 12 DPA) and *PRIN2* (down-regulated by 31% from 3 to 12 DPA) could be detected. The transition from chloroplast to gerontoplast also is accomplished through modifications of plastid membranes and the plastid proteome. As expected, nuclear genes encoding the CURT proteins, involved in the maintenance of thylakoid membrane ultrastructure, were down-regulated, whereas the expression of the *VIPP1* gene, encoding VESICLE-INDUCING PROTEIN IN PLASTIDS1, remained constant. In general, genes for the plastid import apparatus (i.e. TIC and TOC proteins) were slightly down-regulated from 3 to 12 DPA. Only in a few cases were larger changes in gene expression observed, such as for *TIC20-IV* (up-regulated by about 4-fold from 3 to 12 DPA) and *TIC62* (down-regulated by 4-fold). In contrast, no major changes in expression were observed among genes encoding plastid chaperones or proteases, indicating that the plastid proteome also is controlled at the posttranscriptional level.

To verify the collinearity between transcript levels and photosynthesis-related protein accumulation, as shown previously for the Calvin cycle and amino acid biosynthesis pathways in the chloroplast (Piechulla et al., 1985; Kleffmann et al., 2004), immunoblot analyses were performed (Fig. 2B). Using Lhca2- and Lhcb3-specific antibodies, we measured the accumulation of the proteins that harvest the light energy and transfer it to the photosystems. In agreement with the transcriptomic data, Lhc accumulation decreased in old siliques at 9 and 12 DPA. The same behavior was observed for PsbO, a subunit of the oxygen-evolving complex and part of the PSII (Suorsa et al., 2016), and for the plastid

ribosomal proteins of both the small (30S) and large (50S) subunits (PRPS1 [PLASTID RIBOSOMAL PROTEIN SMALL1] and PRPL4 [PLASTID RIBOSOMAL PROTEIN LARGE4]; Romani et al., 2012). Furthermore, Coomassie Brilliant Blue staining of total protein extracts demonstrated that, at 12 DPA, both the large and small subunits of Rubisco accumulate poorly (Fig. 2B), in agreement with a previous observation in leaves, where the degradation of Rubisco was proposed at the basis of senescence (Breeze et al., 2011). In contrast, proteins with a key role in senescence-associated changes accumulate in large amounts in fruits at 12 DPA, such as the enzyme PHEOPHORBIDE A OXYGENASE (PAO), which catalyzes the key reaction of chlorophyll catabolism (Ghandchi et al., 2016). A small amount of PAO mRNA is present at 3 DPA but a lot is accumulated at 12 DPA, showing a perfect collinearity with the enzyme amount. Filters also were immunodecorated with an anti-H3 antibody, as a control for loading (Chen et al., 2016).

RNAseq Data Validation through Promoter Expression Analysis

To further validate the RNAseq data, the silique transcriptome data sets were analyzed using promoter-driven GUS assays. In particular, we analyzed the promoter activity of the *FLOWERING LOCUS T* (pFT), *LIPOXYGENASE3* (pLOX3), and *LOX4* (pLOX4) genes from the up-regulated group, *ABA INSENSITIVE5* (pABI5) from the alternative behavior group, and *RESPONSE REGULATOR15* (pARR15) and *LOX2* (pLOX2) genes as representative of the down-regulated gene set (Fig. 3; Supplemental Table S9). The putative promoter regions of these genes were cloned upstream of the *GUS* reporter gene, and the siliques of the corresponding transgenic lines were analyzed at 3, 6, 9, and 12 DPA, the same time points used for the RNAseq analysis (Fig. 3). These genes were selected because they display high levels of expression or pronounced variations among at least three of the four different time points, facilitating the observation and quantification of the differences.

In fruits at 3 and 6 DPA, the enzymatic activity of the GUS protein expressed under the control of pFT is detected in the replum, in the septum, and in the pedicel, while at 9 and 12 DPA, the blue staining also is visible in the valves, thus confirming the transcriptome data, which show a consistent increase of FT transcripts during the development of the silique.

For pLOX3 and pLOX4, the signal at 3, 6, and 9 DPA is restricted to the basal part of the siliques, in the pedicel for pLOX4 and in the abscission zone for pLOX3. At 12 DPA, pLOX3 also drives GUS activity in the valves, in the replum, in the septum, and in the pedicel, while the signal of pLOX4 is visible only in some areas of the valves. The expression of pLOX3 and pLOX4 in the two early stages and at 12 DPA confirm the transcriptome data. Nevertheless, we could not detect any GUS activity at 9 DPA, although the transcriptome data set indicates that both genes are expressed strongly at this

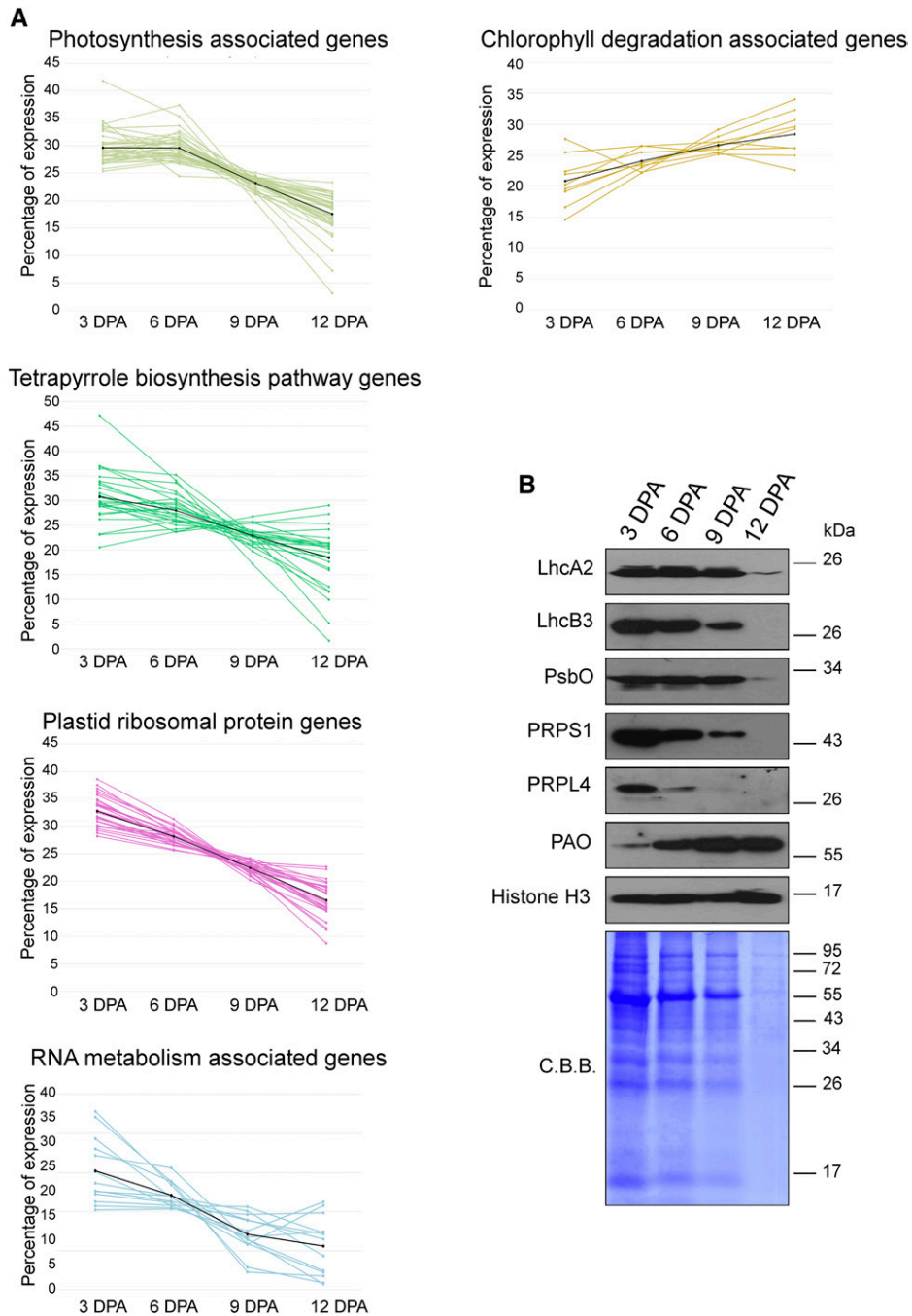


Figure 2. Expression patterns of genes involved in chloroplast-related functions. A, Expression of genes involved in photosynthesis (i.e. encoding subunits of the thylakoid electron transport chain, tetrapyrrole biosynthesis, plastid ribosomal protein, RNA metabolism, and chlorophyll degradation). Each line describes the expression pattern of a single gene; the core values for each cluster are plotted in black. The percentage of expression was defined as the ratio between expression values at every single time point and the sum of the values of all the time points, given as 100%. The expression values of all the genes are reported in Supplemental Table S9. B, Immunoblot analyses of total protein extracts from 3-, 6-, 9-, and 12-DPA developing Col-0 siliques, whose seeds have been removed manually. Total protein extracts obtained from identical silique fresh weight were fractionated by SDS-PAGE (12% polyacrylamide) and transferred on polyvinylidene difluoride filters. Filters were then immunodecorated using antibodies specific for LhcA2, LhcB3, PsbO, PRPS1, PRPL4, PAO, and Histone H3 proteins. A replicate SDS-PAGE gel stained with Coomassie Brilliant Blue (C.B.B.) is shown as a loading control. One out of three immunoblots for each antibody is shown.

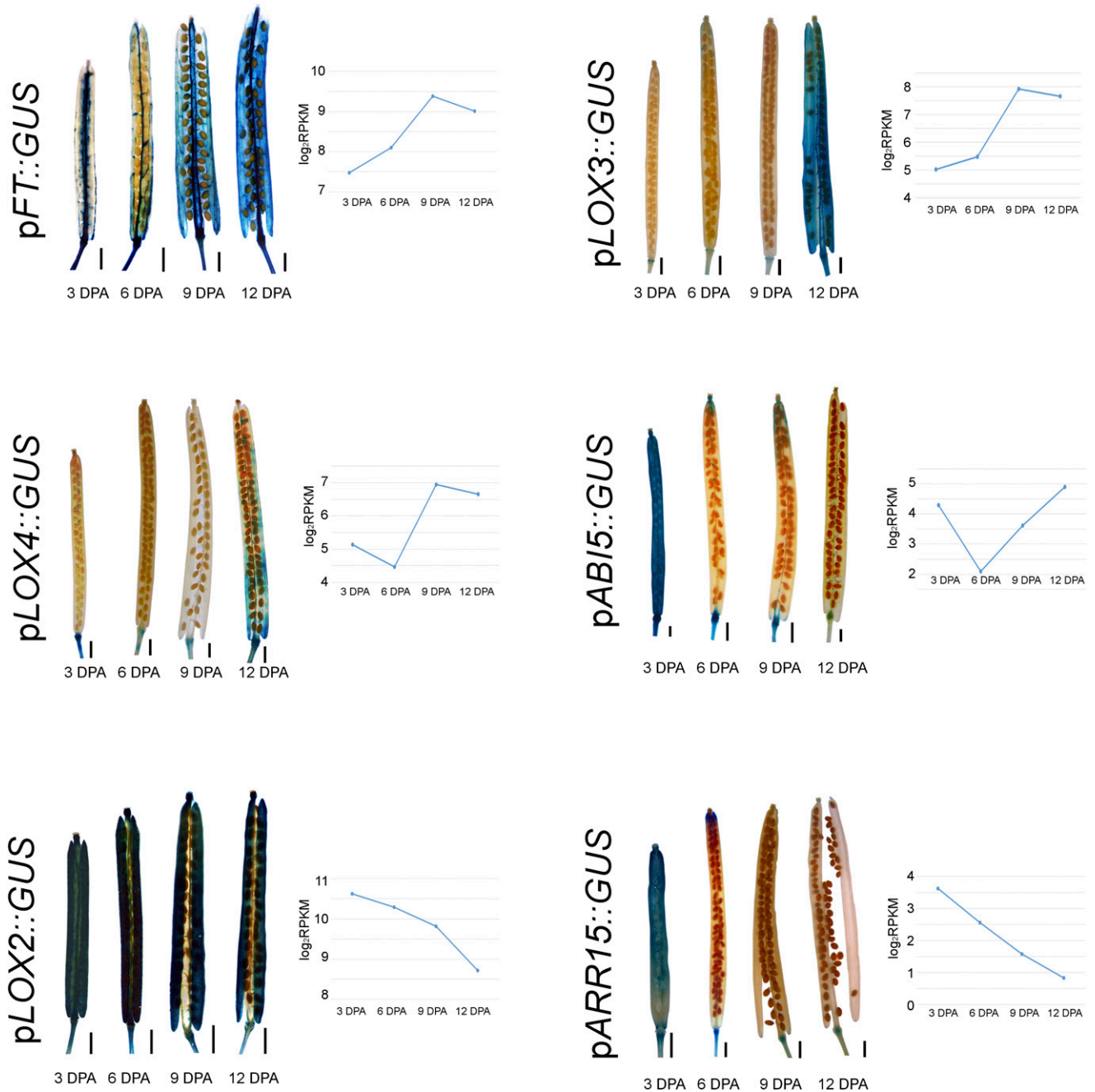


Figure 3. Promoter-driven *GUS* expression analysis to validate RNAseq data. The expression of the promoters of *FT*, *LOX3*, *LOX4*, *ABI5*, *LOX2*, and *ARR15* fused to the *GUS* reporter gene was evaluated on the basis of *Uida* enzymatic activity. Silique images are representative of analyses performed on 10 siliques for each stage and transgenic line. At right, the level of expression of each gene (according to the RNAseq data reported in Supplemental Table S10) is shown. The images shown are composite images. Bars = 1 mm.

stage, suggesting the lack of important regulatory elements in the cloned DNA fragments.

By contrast, in *pABI5::GUS* fruits at 3 DPA, the enzymatic activity of the *GUS* protein is detected in the valves, in the style, and in the pedicel. After this stage, the signal dropped off drastically, remaining only in the pedicel, in the apical part of the valve tissue, in

the style, and in some funiculi. These data confirm the trend of transcriptome levels detected by RNAseq between 3 and 6 DPA, while at 9 and 12 DPA, the *GUS* assay failed to reveal the *ABI5* transcript increase.

In the case of *pLOX2*, *GUS* activity is detected in the whole silique and in the pedicel from 3 to 12 DPA, in agreement with the high level of transcript

Table 2. Expression of selected genes analyzed in this study

ATG Code	Name	Acronym	3 DAP	6 DAP	9 DAP	12 DAP	References
Cluster: up-regulated							
<i>AT5G13790</i>	<i>AGAMOUS-LIKE15</i>	<i>AGL15</i>	1,607	3,617	4,514	3,233	Fang and Fernandez (2002)
<i>AT2G36750</i>	<i>UDP-GLUCOSYL TRANSFERASE73C1</i>	<i>UGT73C1</i>	1,752	1,005	2,022	3,629	Hou et al. (2004)
<i>AT3G60670</i>	PLATZ transcription factor family gene		-3,388	1,290	2,847	4,129	
<i>AT5G10625</i>	Unknown function		-2,349	-1,859	2,712	7,879	
Cluster: down-regulated							
<i>AT3G44750</i>	<i>HISTONE DEACETYLASE2A/HISTONE DEACETYLASE3</i>	<i>HDA2A/HDA3</i>	4,790	4,728	2,935	3,370	Wu et al. (2000)
<i>AT5G12250</i>	<i>BETA-6 TUBULIN</i>	<i>TUB6</i>	8,886	8,821	6,727	4,167	Czechowski et al. (2005); Gutierrez et al. (2008)
<i>AT3G57920</i>	<i>SQUAMOSA PROMOTER BINDING PROTEIN-LIKE15</i>	<i>SPL15</i>	2,635	0,085	-0,857	-1,661	Schwarz et al. (2008)
<i>AT2G30810</i>	GA-regulated family gene		7,416	2,513	-2,858	-3,818	
<i>AT3G01323</i>	Unknown function		4,008	-0,564	-1,851	-4,592	
Cluster: alternative behavior							
<i>AT3G18400</i>	<i>NAC DOMAIN CONTAINING PROTEIN58</i>	<i>NAC058</i>	-4,691	-3,143	4,759	1,802	Coego et al. (2014)

accumulation observed by RNAseq, although the enzyme assay failed to reveal the decrease in *LOX2* transcript observed in the transcriptome data set, possibly due to the lower sensitivity of the GUS staining.

On the other hand, *ARR15* promoter activity is observed in the entire silique and in the pedicel at 3 DPA, but its expression is restricted to the apical part of the silique and the pedicel at 6 DPA and persists only in the pedicel at 9 and 12 DPA, which is consonant with the transcriptome data.

Novel Genes Involved in Fruit Development and Maturation

Our data set indicates that more than 10,000 genes are differentially expressed among the four time points we chose, and the extent of the differences confirms the notion that our samples represent four different developmental stages. Furthermore, the robustness of our RNAseq-based silique transcriptome could be confirmed by several independent approaches, as detailed above, prompting us to query the data set for novel genes with key roles in fruit formation. To this end, we selected a few genes whose expression levels change substantially among the selected time points. These genes (Table 2) were chosen from all three classes of differentially expressed genes and are associated with different GO classes, including transcription factors (*AGL15*, *SPL15*, *NAC058*, and *AT3G60670*), hormone signaling (*AT2G30810*), metabolic processes (*UGT73C1*), histone modification (*HDA3*), housekeeping roles (*TUB6*), and genes of unknown function (*AT5G10625* and *AT3G01323*).

The expression profile of each of the selected genes was first validated by reverse transcription

quantitative PCR (RT-qPCR) analysis (Fig. 4). However, the most common reference genes used for normalization in Arabidopsis, such as *ACTIN2/ACT2*, *ACT7*, *ACT8*, *ELONGATION FACTOR 1 α /EF1 α* , *EUKARYOTIC TRANSLATION INITIATION FACTOR4A-1/eIF4A*, *TUBULIN2/TUB2*, *TUB6*, *TUB9*, *UBIQUITIN4/UBQ4*, *UBQ5*, *UBQ10*, *UBQ11*, and *GLYCERALDEHYDE-3-PHOSPHATE DEHYDROGENASE/GAPDH* (Czechowski et al., 2005; Gutierrez et al., 2008), showed quite variable and stage-dependent expression in our data set (Supplemental Table S11). For instance, *ACT2*, *TUB2*, and *TUB6* were in the group of down-regulated genes. Therefore, stably expressed genes that could be used as internal reference genes first had to be identified. In particular, we selected *UBC9* and *PP2A* as internal reference genes (already suggested by Czechowski et al. [2005] as two of the best housekeeping genes for developmental series), which are highly and stably expressed at all four time points considered in our transcriptome analysis (Supplemental Table S10). The RT-qPCR results (Fig. 4) support our transcriptome data, with the sole exception of *UGT73C1* at the 12-DPA stage. This gene belongs to a multigene family encoding UDP-glycosyltransferases, whose members share a high degree of similarity (Li et al., 2001), which complicates the expression analyses. Insertion mutant lines for the selected genes also were isolated, and the transcript levels in mutant and Col-0 siliques were compared by RT-qPCR. The sampling time points for RT-qPCR analysis were chosen based on the gene expression patterns (Fig. 4) in order to detect the gene expression peak; thus, the down-regulated genes were analyzed at 3 DPA while all the up-regulated genes and *NAC058* were examined at 9 DPA. As shown in Figure 5A, nine T-DNA insertion lines exhibited

marked reductions in transcript abundance relative to Col-0, while the T-DNA insertion into the *AT2G30810* gene caused an overaccumulation of the corresponding transcripts.

The length and width of Col-0 and mutant siliques were then measured to deduce possible roles for the corresponding gene products in fruit growth (Fig. 5, B and C). Forty siliques for each genotype were measured in two different biological replicates, and interestingly, the siliques of *agl15*, *hda3*, *tub6*, *spl15*, *at5g10625*, and *at3g01323* were reduced significantly in length with respect to Col-0, whereas reductions in silique width were observed in *hda3* and *at5g10625* mutant lines. Thus, *HDA3* and *AT5G10625* appear to be involved in the silique growth program in terms of both length and width, while *AGL15*, *TUB6*, *SPL15*, and *AT3G01323* seem to be involved in functions that affect only one of these dimensions.

We also considered silique maturation, and this trait was evaluated by three different approaches that are used routinely to detect leaf senescence: (1) Trypan Blue assay (van Wees, 2008); (2) measurements of the quantum efficiency of PSII electron transport (Wingler et al., 2004); and (3) visual assessment of yellowing, combined with chlorophyll *a* and *b* measurements, during silique senescence (Ougham et al., 2008).

The viability of the silique cells was explored using the Trypan Blue dye-exclusion method (Fig. 6A; Supplemental Figs. S8 and S9), which allows one to visualize dead and dying cells (van Wees, 2008). In Col-0 siliques, we detected cell death in the stigma and in the gynophore, starting from 3 DPA and continuing to 12 DPA (Fig. 6A). Moreover, at later stages (9 and 12 DPA), portions of the funiculi and septum were found to be positive for Trypan Blue staining. A similar staining pattern was observed in eight of the 10 mutants analyzed, the exceptions being *hda3* and *at2g30810*. More specifically, in *hda3* fruits at 12 DPA, most of the funiculi and the septum displayed a markedly intense coloration, indicating widespread cell death in these regions. In contrast, in *at2g30810*, portions of the valves were already blue at 6 DPA, suggesting premature senescence of the silique; moreover, the blue cells are grouped in spots with a typical pattern (Fig. 6A; Supplemental Fig. S8). The precise quantification of the blue area (Supplemental Fig. S9) revealed that *hda3* differs from Col-0 siliques only at 12 DPA, while *at2g30810* siliques already show differences at 3 DPA and in all the other considered time points.

In order to monitor fruit senescence, we also measured the photosynthetic performance of PSII in the siliques with a Dual-PAM chlorophyll fluorometer (Wingler et al., 2004; Brooks and Niyogi, 2011; Scarpeci et al., 2017). Before analyzing the selected mutants with respect to the quantum efficiency of PSII, we conducted a preliminary experiment to exclude any contribution to PSII photosynthetic performance from embryo chloroplasts, as proplastids differentiate into photosynthetically active chloroplasts during embryo development in *Arabidopsis* (Mansfield and Briarty, 1991). To this

end, we chose *arf8-4* plants, which can develop parthenocarpic fruits if the anthers are removed manually (Vivian-Smith et al., 2001; Goetz et al., 2006). Measurements of the quantum efficiency of PSII at 3 and 6 DPA were performed on the Landsberg *erecta* (*Ler*) ecotype and compared with the data for self-pollinated and emasculated *arf8-4* flowers, respectively. Moreover, to exclude the possibility that the removal of all of the floral organs surrounding the carpel in the emasculated *arf8-4* siliques might affect the photosynthetic efficiency of the mutant, we also removed all the floral organs prior to manual pollination of *Ler* and *arf8-4* pistils (we called these samples *Ler* naked and *arf8-4* naked). Interestingly, measurements of the quantum efficiency of PSII did not reveal any differences among the mutants and the control, supporting the notion that the measured PSII efficiency refers to silique chloroplasts and does not include any contribution from the chlorophyll in embryos (Supplemental Fig. S10A). To further validate this observation, we used *PRPL28/prpl28* heterozygotes (Romani et al., 2012), in which one-fourth of the embryos that develop inside the siliques are albinos. Once again, we failed to detect any differences in photosynthetic efficiency between the mutant and Col-0 siliques (Supplemental Fig. S10B). The analysis of the photosynthetic ability of the mutant siliques revealed several degrees of phenotype (Fig. 7): in *agl15*, *ugt73c1*, *tub6*, and *spl15*, photosynthetic efficiency was identical to that in the Col-0 siliques, while *hda3*, *at5g10625*, *at2g30810*, and *at3g01323* displayed a slight reduction in photosynthetic ability with respect to Col-0. *at3g60670* and *nac058* mutants instead presented a marked reduction in photosynthetic efficiency at 12 DPA, which also was observed at 9 DPA in the case of *nac058* (Fig. 7) and in agreement with the precocious senescence phenotype shown in Figure 6B, while visual assessment of yellowing during silique senescence failed to uncover any differences between Col-0 and *at3g60670*. To further validate the precocious yellowing observed in *nac058*, we extracted and quantified the total chlorophyll content in the valves of Col-0 and *nac058* (Fig. 6C). This analysis confirmed that *nac058* contains half of the chlorophyll present in Col-0 valves at 12 DPA, suggesting the premature breakdown of chloroplasts in this mutant.

DISCUSSION

Time-Course Transcriptome Profiling of Developing Seedless Fruits

Fruits are essential for humans, as an integrative part of our diet, and they also are an essential element in the plant life cycle, serving first to protect seeds and then facilitating their dispersal (Van der Pijl, 1982; Seymour et al., 2013). Beyond their role in the protection of the offspring, fruits also contain active chloroplasts that contribute to plant fitness (Blanke and Lenz, 1989; Raghavan, 2003; Gnan et al., 2017).

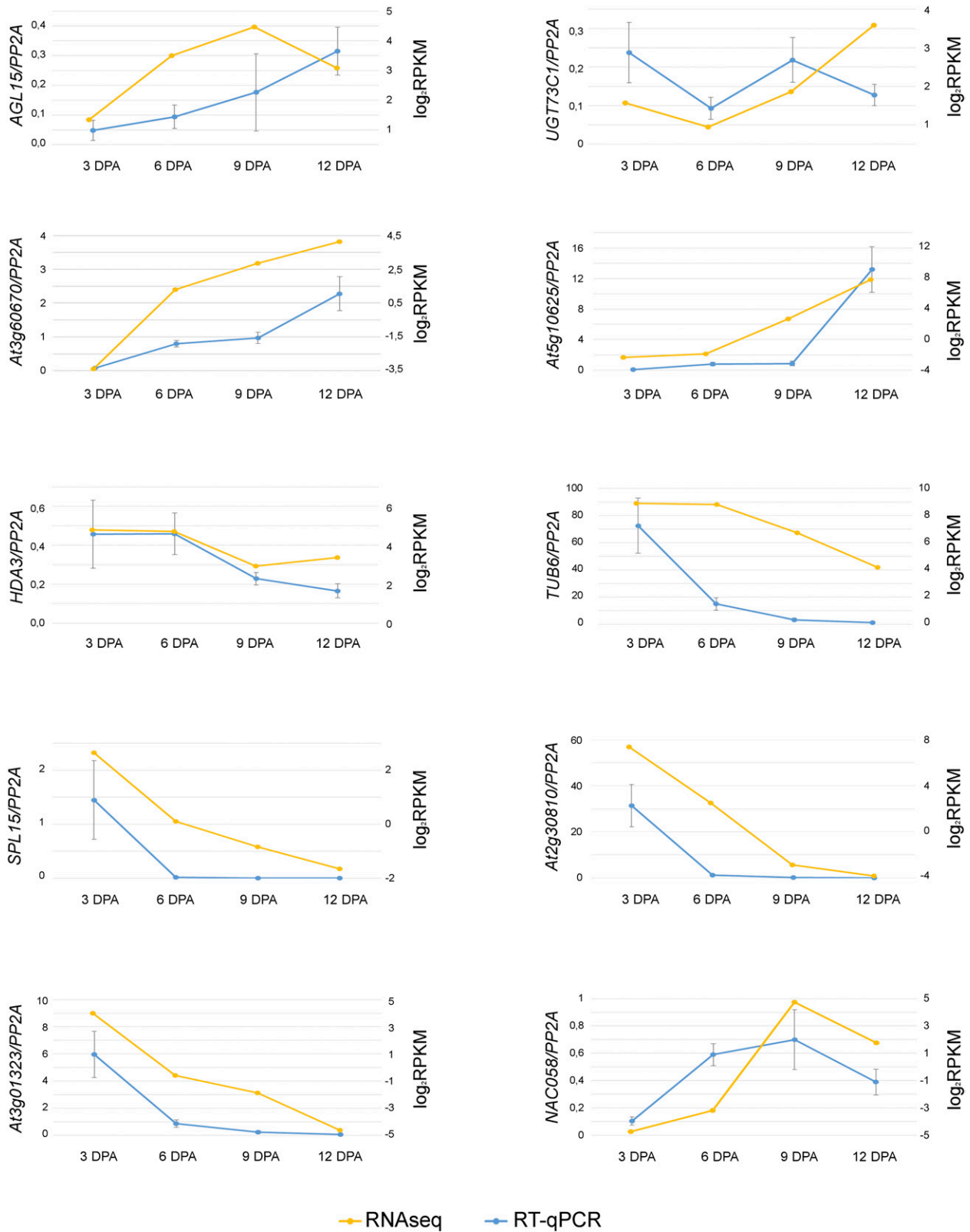


Figure 4. Expression patterns of selected genes by RT-qPCR analysis and RNAseq. The x axis indicates the four selected time points, while the y axis shows the mRNA levels: the scale at left indicates gene expression level based on RT-qPCR, and the scale at right is based on RNAseq. The blue lines correspond to RT-qPCR and the orange ones to RNAseq. RT-qPCR was performed on cDNA extracted from Col-0 siliques devoid of seeds and collected at the same time points chosen for RNAseq.

To analyze the molecular networks responsible for mediating and coordinating fruit growth and maturation in *Arabidopsis*, we have carried out a transcriptomic analysis of Col-0 valve tissues. We decided to manually remove the seeds to exclude any embryo/seed contribution to our data set, in order to increase the probability of pinpointing genes involved specifically in fruit development and maturation. Fruit growth is controlled by signals, most probably produced by the female gametophyte, aimed to communicate that fertilization has occurred successfully and to promote ovule conversion into seeds and pistils into fruits (Dorcey et al., 2009). As a matter of fact, in the absence of fertilization, pistils undergo senescence after a few days (Carbonell-Bejerano et al., 2010). Furthermore, fruit growth relies on seed development, and some evidence pinpoints that hormones are at the basis of seed-fruit communication. Because of that, the siliques used for our analyses were the result of natural, and not of manual, fertilization, to avoid flower organ removal and, as a consequence, hormone homeostasis perturbation.

We have identified thousands of genes differentially expressed among the four chosen time points. Based on previously published microarray data (de Folter et al., 2004; Wagstaff et al., 2009; Carbonell-Bejerano et al., 2010; Jaradat et al., 2014), RNAseq appears to be a more powerful strategy, since almost 7,000 genes annotated in the TAIR10 genome are not represented on the Affymetrix ATH1 microarray platform (Giorgi et al., 2013). Thus, RNAseq can probe portions of transcripts never analyzed before. For instance, *AT3G01323*, *AT3G60670*, and *AT5G10625* are not present in the ATH1 platform, while our analyses pinpoint that they are differentially expressed and that their disruption affects fruit photosynthetic efficiency.

In our experimental design, we set the zero time point to coincide with flower anthesis, and we collected the material at 3, 6, 9, and 12 DPA in order to cover both the growing and the maturation phases. These time points also allow us to explore events that occur in the phase immediately following fertilization, which is characterized by rapid changes in the silique structure, since fruit size increases 5-fold within a few days (Fig. 1A; Kleindt et al., 2010). Indeed, at least three out of the four selected time points are included in the classical stage 17 of silique formation (Ferrándiz et al., 1999). However, our four data sets are clearly different from each other, suggesting that fruits normally annotated as stage 17 are undergoing highly dynamic development or that development is quite asynchronous. Our results support the idea that stage 17 should be disassembled into several different classes, in agreement with the data reported in some previous publications

(Kleindt et al., 2010; He et al., 2018). In total, we have been able to detect 21,908 protein-coding genes, while 25,706 differentially expressed genes were reported by Klepikova et al. (2016), where RNAseq data of 79 *Arabidopsis* samples, including organs at different developmental stages, were analyzed, thus supporting the robustness of our approach. According to our analyses, 4,240 genes are consistently up-regulated and 5,813 genes are consistently down-regulated in *Arabidopsis* siliques from the first time point to the last, while 581 exhibit alternative behaviors (i.e. transient changes in expression within the period examined; Supplemental Tables S1–S6). Interestingly, 11,274 genes do not change their expression significantly, although we cannot exclude the possibility that some of these genes code for regulators of fruit development and maturation, since posttranscriptional regulation also plays an important role in generating rapid responses to environmental and intracellular signals.

New Genes Involved in Silique Growth and Maturation

Given the large numbers of genes differentially expressed in developing siliques, the main question is whether one can readily uncover information about new regulatory networks and genes involved in silique formation and maturation. Therefore, we selected 10 genes based on the following criteria: (1) their expression changes substantially among the selected time points; (2) they cover each of the three classes of differentially expressed genes; and (3) they are associated with different GO terms. The selected genes encode transcription factors (*AGL15*, *SPL15*, *NAC058*, and *AT3G60670*), proteins with a role in hormone signaling (*AT2G30810*), in metabolic processes (*UGT73C1*), in histone modification (*HDA3*), and in housekeeping functions (*TUB6*), and proteins of unknown function (*AT5G10625* and *AT3G01323*). The corresponding T-DNA insertional mutants were isolated, and their involvement in determining fruit size and maturation was investigated. In particular, the disruption of two of the four genes encoding transcription factors affected fruit size or maturation, indicating that our transcriptome data sets allow the identification of master regulators of important developmental cascades. For instance, the *agl15* knockout mutant develops shorter siliques but fruit maturation seems unaffected. Previous studies indicate that *AGL15* overexpression (Fernandez et al., 2000; Fang and Fernandez, 2002) delays sepal and petal falls and that *AGL15* is responsible, together with *AGL18*, for organ senescence (Adamczyk et al., 2007). Indeed, *AGL18* also is included in the up-regulated gene data set and probably compensates for the absence of *AGL15*, thus explaining why *agl15*

Figure 4. (Continued.)

RT-qPCR was conducted in triplicate using *PP2A* and *UBC9* as internal reference genes (Supplemental Table S11). The graphs depict the results obtained using *PP2A* as the internal reference gene; identical results were obtained using *UBC9* as the internal reference gene. Error bars represent the propagated SD value using three biological replicates.

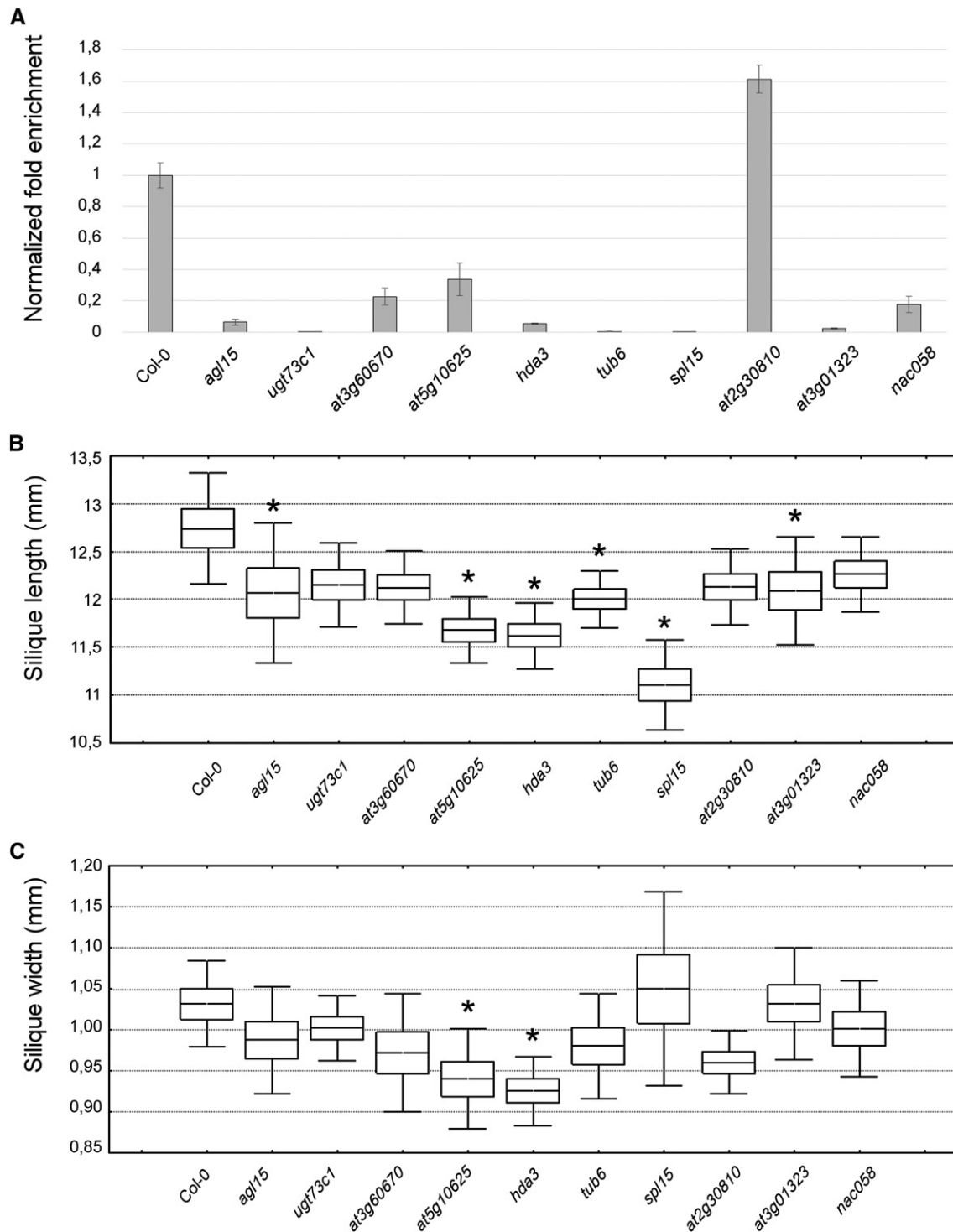


Figure 5. Molecular and morphological characterization of the phenotypic effects of the selected mutations on silique formation. A, RT-qPCR analysis to verify transcript accumulation in the mutant lines examined (Supplemental Table S12). RT-qPCR was conducted in triplicate using *PP2A* and *UBC9* as internal reference genes (Supplemental Table S11). The graphs depict the results obtained using *PP2A* as the internal reference gene; identical results were obtained using *UBC9* as the internal reference gene. Error bars represent the propagated SD value using three replicates. B and C, Measurements of the length (B) and width (C) of the siliques produced by the selected lines. The length and width of the mature siliques were evaluated by measuring 40 siliques for each genotype in two different biological replicates. Boxes indicate means plus SE , while error bars indicate SD . One-way ANOVA combined with Dunnett's comparison test indicated that the mutants marked with asterisks were significantly different from the Col-0 control ($P < 0.05$; $n = 40$).

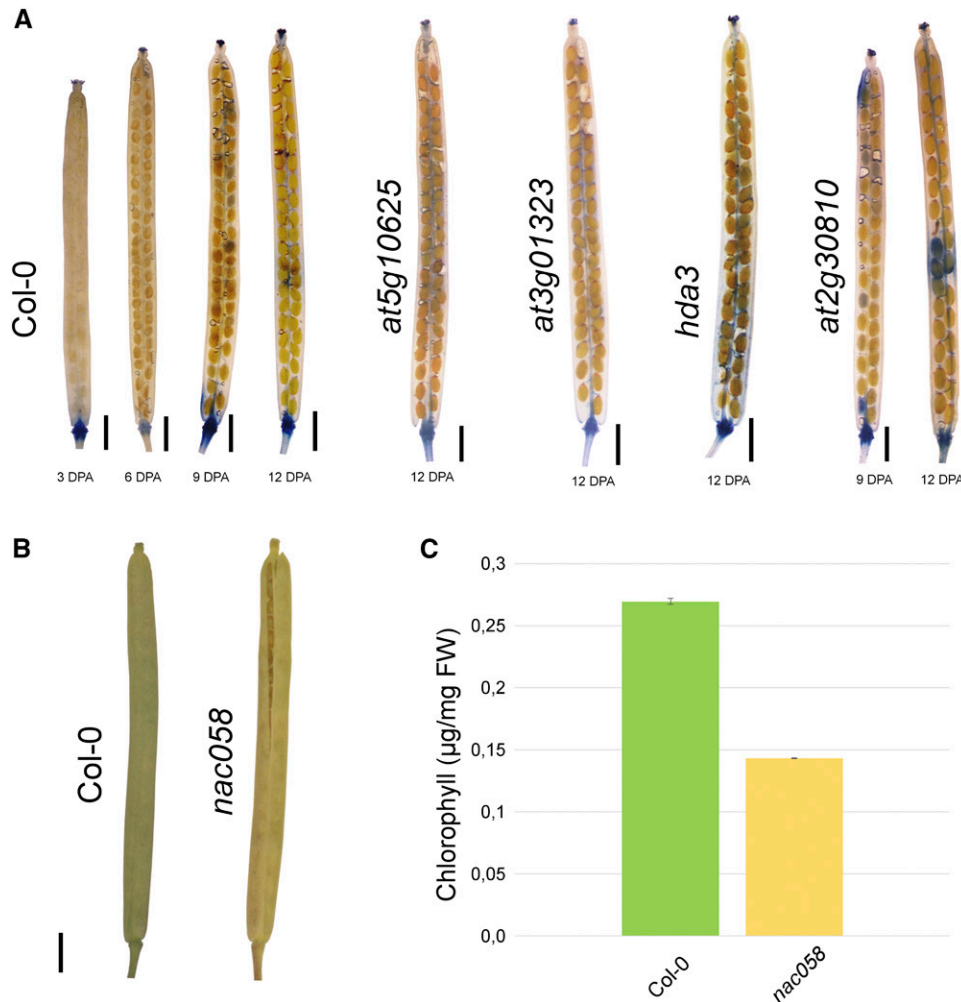


Figure 6. Phenotypic effects of the selected mutations on silique maturation. A, The Trypan Blue dye-exclusion method allows the detection of cell death. A complete analysis is reported in Supplemental Figure S8. Trypan Blue also was quantified, and the quantification is reported in Supplemental Figure S9. The image shown is a composite image. B, Visual evaluation of the yellowing of Col-0 and *nac058* siliques at 12 DPA. C, Measurements of chlorophyll content in Col-0 and *nac058*. Error bars represent SD of three independent measurements. FW, Fresh weight. Bars in A and B = 1 mm.

siliques are not positive to the Trypan Blue staining and show wild-type-like photosynthetic performance (Fig. 7; Supplemental Figs. S8 and S9). Also in the case of the *spl15* mutant, siliques were shorter, implying that silique length is a rather complex trait controlled by multiple regulatory pathways. SPL15 is a transcription factor that belongs to the SQUAMOSA Promoter Binding Protein (SBP) family. Four more SBP genes are found to be down-regulated in our data sets, while only two genes are included in the group of up-regulated genes, and no SBP gene is listed in the alternative behavior group. SBP genes are involved in organ formation (Wang et al., 2008; Usami et al., 2009), nutritional changes (Jung et al., 2011), copper metabolism (Yamasaki et al., 2009), and GA response (Zhang et al., 2007). On the other hand, the *nac58* mutant displayed a reduced photosynthetic performance in fruits at 9 DPA, but no alteration in silique growth was observed.

Many more NAC genes, 60 out of the 138, are differentially expressed in our data sets. Previous works (Breeze et al., 2011; Kim et al., 2014, 2016) pinpointed a pivotal role for the NAC genes in leaf aging, and several NAC-encoding genes have been found to be differentially expressed in aging leaves at different time points (Balazadeh et al., 2008; Breeze et al., 2011; Christiansen and Gregersen, 2014).

Overall, seven out of the 10 selected mutants showed either altered morphology in silique length and silique width or precocious senescence of mature siliques. These findings, together with the fact that several other transcription factors, such as the Auxin-Responsive Factor and the Ethylene-Responsive Factor families (Supplemental Table S8), and many genes already known to have a role in silique growth, like CKX5 (cytokinin oxidase/dehydrogenase), are present in our list of differentially regulated genes (Bartrina et al.,

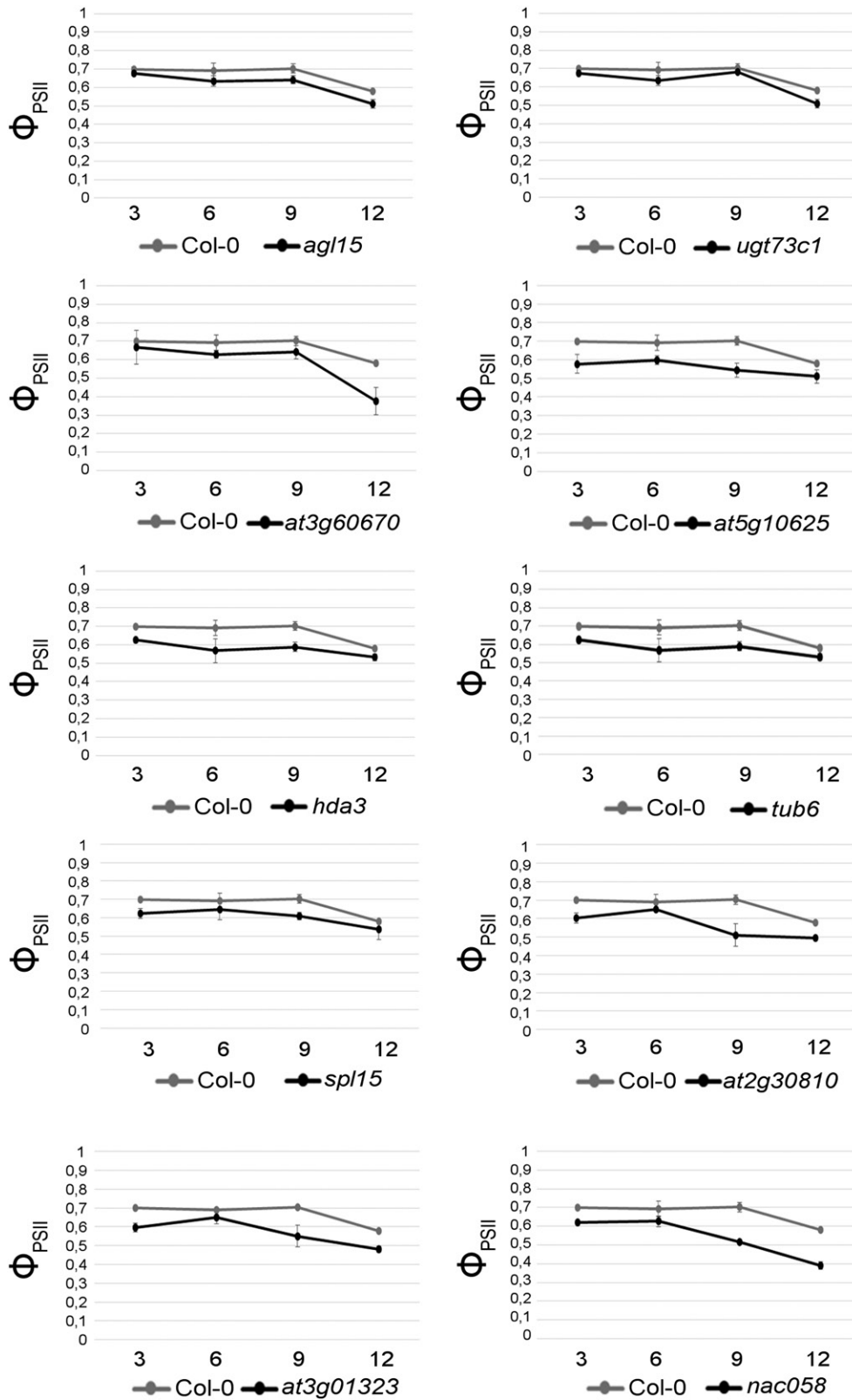


Figure 7. Photosynthetic efficiency (Φ_{PSII}) of wild-type and mutant siliques. Three measurements for each stage were performed (using five siliques for each developmental stage for a single measurement), and three biological replicates were used. Mean values \pm SD are reported.

2011) or are among the genes expressed at high levels in all the analyzed stages, such as *FATA2* (Wang et al., 2013), strongly indicate that our data set can be considered a reservoir from which genes with a role in fruit formation can be drawn.

Coordination of Chloroplast and Nuclear Gene Expression Is Fundamental during Fruit Development and Maturation

The unifying theory, based on the observation of a Jurassic plant with free central placentation, suggests that carpels are composed of an ovule-bearing shoot (the placenta) and its enclosing foliar structure (Wang, 2010). Cytological and molecular observations also confirm the ontogenic relationship between leaves and fruits (Gillaspy et al., 1993). However, unlike leaves, silique maturation is strictly regulated by seed formation and strictly controlled by the progression of embryogenesis.

Chlorophyll breakdown is the clearest marker of both leaf senescence and fruit ripening, but the pathways that control these processes differ between the two organs. For instance, the disruption of *PHEOPHYTYNASE* causes a stay-green phenotype in leaves, although greening of seeds and fruits is not affected (Guyer et al., 2014; Zhang et al., 2014; Chen et al., 2017). By contrast, *AtNAP* plays a pivotal role during leaf natural and dark-induced senescence, since it modulates the transcription of several genes, including *PAO* (Yang et al., 2014), whose accumulation at later stages of silique development and maturation was confirmed by our RNAseq data sets and by immunoblot analysis. Indeed, the *AtNAP* transcription factor couples plastid physiological status to hormone metabolism, since it modulates ethylene metabolism in both senescing leaves and maturing siliques (Kou et al., 2012) and abscisic acid in senescing leaves (Yang et al., 2014). In particular, ethylene promotes or inhibits growth and senescence processes depending on its concentration and the timing of its production or application. Therefore, leaf senescence and silique senescence might vary in relation to the growth conditions. For instance, differences might be expected between plants grown in greenhouses as opposed to growth chambers. Under the latter conditions, the small volumes of the growth chambers might facilitate ethylene accumulation, which, in turn, might accelerate senescence mechanisms. Therefore, chlorophyll accumulation in *Arabidopsis* might reach its peak on different DPAs, depending on the precise growth conditions. In different studies, chlorophyll accumulation in the siliques has been reported to reach its maximum level between 6 and 8 DPA (Wagstaff et al., 2009; Kou et al., 2012). In this respect, our data set is extremely useful, since it contains specific genes, such as *NAC058* and *AT2G30810*, that can be used as reliable molecular markers for the accurate staging of fruit maturation in place of chlorophyll amount. For instance, the tomato (*Solanum lycopersicum*) mutants *lutescent1* and *lutescent2*

display a precocious loss of chlorophyll in leaves and fruits (Barry et al., 2012), but the onset of fruit ripening is delayed by approximately 1 week, indicating a major role for the chloroplast in mediating the onset of fruit ripening.

Furthermore, it was demonstrated recently that the chloroplast transcriptome, but not the mitochondrial transcriptome, undergoes major changes during leaf aging, which are accompanied by a largely unchanged expression pattern of nuclear genes coding for plastid-targeted proteins (Woo et al., 2016). Thus, unlike animal aging, leaf senescence proceeds with tight temporal and distinct interorganellar coordination of various transcriptomes, which presumably are critical for the highly regulated degeneration process and the recycling of nutrients, which contributes to plant fitness and productivity. This is in agreement with the observation that the cellular degeneration process during leaf aging begins with the decay of chloroplasts, while nuclei and mitochondria remain intact until the end of the leaf's lifespan (Lim et al., 2007). The expression pattern of nuclear genes encoding plastid proteins involved in photosynthesis, protein translation, tetrapyrrole biosynthesis, RNA metabolism, and chlorophyll degradation (Fig. 2) observed in our data set resembles the behavior of these genes during the leaf senescence process, indicating that fruit maturation and leaf senescence have several features in common and pointing to a major role of the chloroplast in both processes. Furthermore, the strong linear correlation between the physiological state of chloroplasts and plastid-associated nuclear gene expression implies, also in the case of fruits, the need for chloroplast-nucleus retrograde and anterograde signaling to coordinate the activities of the two genomes (Pesaresi et al., 2014). Nevertheless, the importance of photosynthesis in fruit metabolism is still under debate and deserves further investigation (Piechulla et al., 1987; Wanner and Gruissem, 1991; Schaffer and Petreikov, 1997; Carrari et al., 2006; Steinhauser et al., 2010). For instance, several studies used tomato cultivars carrying the *uniform ripening (u)* light green fruit phenotype (Powell et al., 2012). The *U* gene encodes a transcription factor named *GOLDEN2-LIKE*, which belongs to the AP2 family. The *u* mutants produce fewer chloroplasts, which are abnormal and whose thylakoid grana are reduced. Furthermore, *u* fruits are paler than normal and they have less sugars and lycopene, but they have normal size and ripen normally, suggesting that photosynthesis is not essential for fruit formation. On the other hand, experiments on *Brassica napus* plants shaded or defoliated soon after fertilization suggest a close relationship among leaf area, pod number, and seed per pod number (Pechan and Morgan, 1985). ¹⁴C-labeling experiments indicated that the fruit photosynthates are transported to the developing seeds; thus, the photosynthetic ability of the siliques strongly contributes to *B. napus* seed oil content (Hua et al., 2012).

Overall, the analysis of our RNAseq data clearly justifies our decision to monitor transcript accumulation in siliques devoid of seeds at four different

developmental stages. This is shown by the fact that several genes known to have a role in fruit development and maturation are represented in our data set. Moreover, by exploring the consequences of the disruption of a few of the genes contained in our data set, we have detected significant alterations in fruit development and maturation, proving that our transcriptomic data sets are highly enriched in genes with specific roles in fruit formation and, therefore, should be very useful in the elucidation of the molecular mechanisms controlling fruit growth and maturation in *Arabidopsis*.

MATERIALS AND METHODS

Plant Growth

Arabidopsis (*Arabidopsis thaliana*) wild-type (Col-0 and *Ler*) and mutant plants were grown under controlled growth chamber conditions at 22°C with 16 h of light and 8 h of darkness, as described previously (Mizzotti et al., 2012). For RNAseq, RT-qPCR, and all the characterization analyses, plants were inspected daily, and flowers at anthesis (time zero) were marked. Fruits were then collected 4 h after the lights were turned on at 3, 6, 9, and 12 DPA. For RNAseq and RT-qPCR, seeds were removed manually: siliques were opened along the dehiscence zone using a needle attached to a syringe that also was used to remove the seeds.

All mutants described in this article are in the Col-0 ecotype, except for *arf8-4* (Goetz et al., 2006), which is in the *Ler* background. Mutant alleles were identified by searching the T-DNA Express database (<http://signal.salk.edu/cgi-bin/tdnaexpress>), and mutant lines were obtained from the SALK (Alonso et al., 2003) and GABI-KAT collections (Rosso et al., 2003; Supplemental Table S12). T-DNA insertions were confirmed by sequencing PCR products obtained using gene- and T-DNA-specific primers (Supplemental Table S13).

Nucleic Acid Isolation, cDNA Library Preparation, RNAseq, and RT-qPCR Analysis

For RNAseq analysis, total RNA was extracted from Col-0 siliques at 3, 6, 9, and 12 DPA from three biological replicates using the NucleoSpin RNA kit (Macherey Nagel), according to the supplier's instructions. RNA concentrations and integrity were determined using the 2100 Bioanalyzer (Agilent Technologies). For each biological replicate, we grew together five different Col-0 plants, and we collected the material from at least 10 siliques deprived of seeds.

Sequencing libraries were prepared using the TruSeq RNA Sample Prep kit (Illumina), according to the manufacturer's instructions, and sequenced on an Illumina HiSeq2000 (50-bp single read). The processing of fluorescent images into sequences, base calling, and quality value calculations were performed using the Illumina data-processing pipeline (version 1.8).

For RT-qPCR analyses, 0.5- μ g samples of total RNA were used for first-strand cDNA synthesis with the ImProm-II Reverse Transcription System, as already described by Mizzotti et al. (2017). RT-qPCR profiling was carried out using the iQ SYBR Green Supermix (Bio-Rad) and the Bio-Rad iCycler iQ Optical System (software version 3.0a), with the primers listed in Supplemental Table S13. *UBC9* and *PP2A* transcripts were used as internal standards (Czechowski et al., 2005). Data from two biological and three technical replicates were analyzed as reported previously by Mizzotti et al. (2014). For each biological replicate, we grew at the same time five different plants (Col-0 or mutant), and we collected the material from at least 10 siliques deprived of seeds. Briefly, the normalized expression of a gene corresponds to $2^{-\Delta\Delta C_T}$, which is calculated as the difference between the cycle threshold of the gene and the cycle threshold of the internal standard.

RNAseq Analysis and Identification of Differentially Expressed Genes

Raw reads were preprocessed for quality using FastQC (Andrews, 2010) version 0.11.5, cleaned, and trimmed with Trimmomatic version 0.36 (Bolger

et al., 2014). The resulting reads were aligned to the *Arabidopsis* genome (TAIR10) using STAR version 2.5.1bb software (Dobin et al., 2013). Raw read counts were calculated using the featureCounts (<http://bioinf.wehi.edu.au/featureCounts/>) software (Liao et al., 2014). Read count data were used to identify differentially expressed genes by comparisons among different time points using both edgeR (Robinson et al., 2010) and the Limma empirical Bayes analysis pipeline (Smyth, 2005) and voom (Law et al., 2014), which estimates the mean variance trend of the log counts to predict the variance and to generate a precision weight to be incorporated in the linear model. To show that consistency holds for our data set, we performed differentially expressed gene analysis with edgeR using the same thresholds used for Limma/voom to rank genes (see below) and plotted the results using Venn diagrams. As expected, the results between the two tools were consistent, as most genes detected by Limma/voom also were detected by edgeR. edgeR usually reports more differentially expressed genes with respect to Limma/voom (~1,000 in every contrast). A double cutoff on both *P* value and fold change was used to select differentially expressed genes; a maximum *P* value of 0.001 and a fold change of 2.5 were set. Contrasts were defined by considering all six possible combinations of the four time points, and genes were grouped based on their expression profiles as up-regulated (i.e. genes that were found to be significantly up-regulated between any two consecutive time points), down-regulated (i.e. genes that were significantly down-regulated between any two consecutive time points), and alternative behavior (i.e. all the other genes that exhibited various other expression profiles and that were clustered to further assess the different behaviors). Gene clustering was performed employing the hierarchical clustering method using the Pearson correlation coefficient as the distance metric to calculate pairwise distances and the unweighted pair group method with arithmetic mean to calculate the distances between the clusters thus formed. After visual inspection of the dendrogram, a cutoff of 0.6 was selected and four clusters were defined. All RNAseq files are available from the European Nucleotide Archive database (accession no. PRJEB25745).

GO Enrichment Analysis

All six groups (up-regulated genes, down-regulated genes, and the four clusters generated from the genes marked as alternative behavior) were used to perform a GO enrichment analysis with agriGO (Du et al., 2010), using a hypergeometric statistical test, with the Benjamini-Hochberg (false discovery rate) correction for multiple tests, a significance level of 0.01, and the plant GOSlim as parameters.

Immunoblot Analyses

For immunoblot analyses, developing siliques were collected at 3, 6, 9, and 12 DAP and total protein extracts were prepared as described by Martínez-García et al. (1999). Protein extracts, corresponding to 2 mg of silique fresh weight, were fractionated by SDS-PAGE (12% [w/v] polyacrylamide; Schägger and von Jagow, 1987) and transferred to polyvinylidene difluoride membranes (Ihnatowicz et al., 2004). Replicate filters were immunodecorated using antibodies specific for LhcA2, LhcB3, PsbO, PRPS1, PRPL4, PAO, and Histone H3 proteins. LhcA2, LhcB3, PsbO, and PAO antibodies were obtained from Agrisera. PRPS1 and PRPL4 were obtained from UniPlastomic. Histone H3 antibody was purchased from Sigma-Aldrich.

Silique Measurements

The length and width of the mature siliques were evaluated by measuring 40 siliques for each genotype in two different biological replicates. For each biological replicate, we grew at the same time 10 different plants (Col-0 or mutant), and we collected the material from 40 siliques for each genotype. Samples were first photographed using a Leica MZ6 stereomicroscope, and silique images were measured using ImageJ software (Schneider et al., 2012). Measurements were statistically analyzed by one-way ANOVA combined with Dunnett's comparison test using StatSoft software.

GUS Assays and Trypan Blue Staining

The GUS assay was carried out as reported by Resentini et al. (2017). Marker lines were kindly provided by Takashi Araki (*pFT*; Takada and Goto, 2003), Jan U. Lohmann (*pARR15*; Zhao et al., 2010), and Ian Graham (*pAB5::GUS*;

Penfield et al., 2006). *pLOX2::GUS*, *pLOX3::GUS*, and *pLOX4::GUS* were generated by Massimo Galbiati. Primers are listed in Supplemental Table S13, and fragments were cloned by Gateway cloning into pBGWFS7.

For Trypan Blue staining, the Cold Spring Harbor protocol was adopted (van Wees, 2008). For the measurement of the stained area, we used a modified version of the Phenotype Quant plugin for ImageJ (Abd-El-Haliem, 2012), while for the total area of the silique, we developed an ImageJ plugin that calculates the area of the silique through threshold levels. Measurements were analyzed statistically by two-way ANOVA combined with Dunnett's and Duncan's comparison test using StatSoft software.

Chlorophyll Fluorescence of Col-0 and Mutant Siliques

In vivo chlorophyll *a* fluorescence of Arabidopsis siliques was measured at 3, 6, 9, and 12 DPA using the pulse-modulated fluorometer Dual-PAM 100 (Walz; Tadini et al., 2012). Five siliques for each developmental stage were placed on a 24 × 24-mm coverslip and used for a single measurement. Three measurements for each stage (i.e. 15 siliques in total) were performed, and three biological replicates were used. Siliques were first dark adapted for 30 min, and minimal fluorescence (F_0) was measured. Then, pulses (0.8 s) of saturating light ($5,000 \mu\text{mol photons m}^{-2} \text{s}^{-1}$) were employed to determine the maximum fluorescence (F_m), and the ratio $(F_m - F_0)/F_m = F_v/F_m$ (maximum quantum yield of PSII) was calculated. A 2-min exposure to actinic red light ($37 \mu\text{mol photons m}^{-2} \text{s}^{-1}$) served to drive electron transport between PSII and PSI. Then, the steady-state fluorescence (F_s) and the maximum fluorescence after light adaptation (F_m') were determined. Finally, the ratio $(F_m' - F_0)/F_m'$, representing the effective quantum yield of PSII, was calculated.

Chlorophyll Contents of Col-0 and *nac058* Siliques

Pigments were extracted using 90% (v/v) acetone from valves at 12 DPA, after manual seed removal. The chlorophyll (*a* and *b*) content was measured, at 663- and 645-nm wavelength, using a spectrophotometer. Chlorophyll (*a* + *b*) values were determined as described previously by Arnon (1949) and normalized relative to tissue fresh weight.

Accession Numbers

Sequence data from this article can be found in the European Nucleotide Archive database under accession number PRJEB25745.

Supplemental Data

The following supplemental materials are available.

Supplemental Figure S1. Number of reads obtained from each replicate by Illumina sequencing and principal component analysis.

Supplemental Figure S2. Comparison of the outputs obtained by analyzing the RNAseq datasets with the Limma and edgeR packages.

Supplemental Figure S3. Heat map of differentially expressed genes that belong to the alternative behavior group.

Supplemental Figure S4. Singular enrichment analysis of GO annotation terms overrepresented in the list of the up-regulated genes.

Supplemental Figure S5. Singular enrichment analysis of GO annotation terms overrepresented in the list of the down-regulated genes.

Supplemental Figure S6. Singular enrichment analysis of GO annotation terms overrepresented in the list of the genes showing alternative behaviors.

Supplemental Figure S7. Expression pattern of genes involved in chloroplast-nucleus communication.

Supplemental Figure S8. Detection of cell death using the Trypan Blue dye-exclusion method.

Supplemental Figure S9. Quantification of the Trypan Blue dye-exclusion method.

Supplemental Figure S10. The photosynthetic performance of the siliques is not influenced by green embryos.

Supplemental Table S1. Average expression levels, log fold change, and *P* values across all comparisons of the up-regulated genes, according to the criteria described in the text.

Supplemental Table S2. Average expression levels, log fold change, and *P* values across all comparisons of the down-regulated genes, according to the criteria described in the text.

Supplemental Table S3. Average expression levels, log fold change, and *P* values across all comparisons of the genes in the first cluster of the alternative behavior group, according to the criteria described in the text.

Supplemental Table S4. Average expression levels, log fold change, and *P* values across all comparisons of the genes in the second cluster of the alternative behavior group, according to the criteria described in the text.

Supplemental Table S5. Average expression levels, log fold change, and *P* values across all comparisons of the genes in the third cluster of the alternative behavior group, according to the criteria described in the text.

Supplemental Table S6. Average expression levels, log fold change and *P* values across all comparisons of the genes in the fourth cluster of the alternative behavior group, according to the criteria described in the text.

Supplemental Table S7. Expression levels, at the indicated time points, of genes involved in hormonal pathways.

Supplemental Table S8. List of transcription factors present in our differentially expressed gene list.

Supplemental Table S9. Expression levels, at the indicated time points, of genes involved in chloroplast-related functions.

Supplemental Table S10. Expression levels of genes analyzed by GUS assay.

Supplemental Table S11. Expression levels of commonly used housekeeping genes.

Supplemental Table S12. List of Arabidopsis T-DNA insertional mutants used in this study.

Supplemental Table S13. Primer sequences used in this work.

ACKNOWLEDGMENTS

We thank Takashi Araki, Jan U. Lohmann, and Ian Graham for providing seeds of *pFT::GUS*, *pARR15::GUS*, and *pAB15::GUS*. We thank Luca Mizzi and Giorgio Binelli for help with the Trypan Blue area measurement and the statistical analysis, respectively. We also thank Carolina Cozzi for help with chlorophyll content assays, Valerio Parravicini for excellent technical assistance, and Paul Hardy for critical reading of the article.

Received September 4, 2018; accepted September 16, 2018; published October 1, 2018.

LITERATURE CITED

- Abd-El-Haliem A** (2012) An unbiased method for the quantitation of disease phenotypes using a custom-built macro plugin for the program ImageJ. *Methods Mol Biol* **835**: 635–644
- Adamczyk BJ, Lehti-Shiu MD, Fernandez DE** (2007) The MADS domain factors AGL15 and AGL18 act redundantly as repressors of the floral transition in Arabidopsis. *Plant J* **50**: 1007–1019
- Alonso JM, Stepanova AN, Leisse TJ, Kim CJ, Chen H, Shinn P, Stevenson DK, Zimmerman J, Barajas P, Cheuk R** (2003) Genome-wide insertional mutagenesis of Arabidopsis thaliana. *Science* **301**: 653–657
- Andrews S** (2010) FastQC: a quality control tool for high throughput sequence data. <http://www.bioinformatics.babraham.ac.uk/projects/fastqc>
- Arnon DI** (1949) Copper enzymes in isolated chloroplasts: polyphenoloxidase in *Beta vulgaris*. *Plant Physiol* **24**: 1–15

- Balazadeh S, Riaño-Pachón DM, Mueller-Roeber B (2008) Transcription factors regulating leaf senescence in *Arabidopsis thaliana*. *Plant Biol (Stuttg) (Suppl 1)* 10: 63–75
- Barry CS, Aldridge GM, Herzog G, Ma Q, McQuinn RP, Hirschberg J, Giovannoni JJ (2012) Altered chloroplast development and delayed fruit ripening caused by mutations in a zinc metalloprotease at the *lutulent2* locus of tomato. *Plant Physiol* 159: 1086–1098
- Bartrina I, Otto E, Strnad M, Werner T, Schmülling T (2011) Cytokinin regulates the activity of reproductive meristems, flower organ size, ovule formation, and thus seed yield in *Arabidopsis thaliana*. *Plant Cell* 23: 69–80
- Blanke MM, Lenz F (1989) Fruit photosynthesis. *Plant Cell Environ* 12: 31–46
- Bolger AM, Lohse M, Usadel B (2014) Trimmomatic: a flexible trimmer for Illumina sequence data. *Bioinformatics* 30: 2114–2120
- Breeze E, Harrison E, McHattie S, Hughes L, Hickman R, Hill C, Kiddle S, Kim YS, Penfold CA, Jenkins D, (2011) High-resolution temporal profiling of transcripts during *Arabidopsis* leaf senescence reveals a distinct chronology of processes and regulation. *Plant Cell* 23: 873–894
- Brooks MD, Niyogi KK (2011) Use of a pulse-amplitude modulated chlorophyll fluorometer to study the efficiency of photosynthesis in *Arabidopsis* plants. *Methods Mol Biol* 775: 299–310
- Carbonell-Bejerano P, Urbez C, Carbonell J, Granell A, Perez-Amador MA (2010) A fertilization-independent developmental program triggers partial fruit development and senescence processes in pistils of *Arabidopsis*. *Plant Physiol* 154: 163–172
- Carrari F, Baxter C, Usadel B, Urbanczyk-Wochniak E, Zanon MI, Nunes-Nesi A, Nikiforova V, Centero D, Ratzka A, Pauly M, (2006) Integrated analysis of metabolite and transcript levels reveals the metabolic shifts that underlie tomato fruit development and highlight regulatory aspects of metabolic network behavior. *Plant Physiol* 142: 1380–1396
- Chen J, Zhu X, Ren J, Qiu K, Li Z, Xie Z, Gao J, Zhou X, Kuai B (2017) Suppressor of Overexpression of CO 1 negatively regulates dark-induced leaf degreening and senescence by directly repressing pheophytinase and other senescence-associated genes in *Arabidopsis*. *Plant Physiol* 173: 1881–1891
- Chen X, Lu L, Mayer KS, Scalf M, Qian S, Lomax A, Smith LM, Zhong X (2016) POWERDRESS interacts with HISTONE DEACETYLASE 9 to promote aging in *Arabidopsis*. *eLife* 5: e17214
- Christiansen MW, Gregersen PL (2014) Members of the barley NAC transcription factor gene family show differential co-regulation with senescence-associated genes during senescence of flag leaves. *J Exp Bot* 65: 4009–4022
- Coego A, Brizuela E, Castillejo P, Ruíz S, Koncz C, del Pozo JC, Piñeiro M, Jarillo JA, Paz-Ares J, León J; TRANSPLANTA Consortium (2014) The TRANSPLANTA collection of *Arabidopsis* lines: a resource for functional analysis of transcription factors based on their conditional overexpression. *Plant J* 77: 944–953 24456507
- Coombe BG (1975) The development of fleshy fruits. *Annu Rev Plant Physiol* 27: 507–528
- Corbesier L, Vincent C, Jang S, Fornara F, Fan Q, Searle I, Giakountis A, Farrona S, Gissot L, Turnbull C, (2007) FT protein movement contributes to long-distance signaling in floral induction of *Arabidopsis*. *Science* 316: 1030–1033
- Czechowski T, Stitt M, Altmann T, Udvardi MK, Scheible WR (2005) Genome-wide identification and testing of superior reference genes for transcript normalization in *Arabidopsis*. *Plant Physiol* 139: 5–17
- de Folter S, Busscher J, Colombo L, Losa A, Angenent GC (2004) Transcript profiling of transcription factor genes during silique development in *Arabidopsis*. *Plant Mol Biol* 56: 351–366 15604749
- Dinneny JR, Weigel D, Yanofsky MF (2005) A genetic framework for fruit patterning in *Arabidopsis thaliana*. *Development* 132: 4687–4696
- Dobin A, Davis CA, Schlesinger F, Drenkow J, Zaleski C, Jha S, Batut P, Chaisson M, Gingeras TR (2013) STAR: ultrafast universal RNA-seq aligner. *Bioinformatics* 29: 15–21
- Dong Z, Yu Y, Li S, Wang J, Tang S, Huang R (2016) Abscisic acid antagonizes ethylene production through the ABI4-mediated transcriptional repression of ACS4 and ACS8 in *Arabidopsis*. *Mol Plant* 9: 126–135
- Dorcey E, Urbez C, Blázquez MA, Carbonell J, Perez-Amador MA (2009) Fertilization-dependent auxin response in ovules triggers fruit development through the modulation of gibberellin metabolism in *Arabidopsis*. *Plant J* 58: 318–332
- Du Z, Zhou X, Ling Y, Zhang Z, Su Z (2010) agriGO: a GO analysis toolkit for the agricultural community. *Nucleic Acids Res* 38: W64–W70
- Fang SC, Fernandez DE (2002) Effect of regulated overexpression of the MADS domain factor AGL15 on flower senescence and fruit maturation. *Plant Physiol* 130: 78–89
- Fernandez DE, Heck GR, Perry SE, Patterson SE, Bleecker AB, Fang SC (2000) The embryo MADS domain factor AGL15 acts postembryonically: inhibition of perianth senescence and abscission via constitutive expression. *Plant Cell* 12: 183–198
- Fernandez DE, Wang CT, Zheng Y, Adamczyk BJ, Singhal R, Hall PK, Perry SE (2014) The MADS-domain factors AGAMOUS-LIKE15 and AGAMOUS-LIKE18, along with SHORT VEGETATIVE PHASE and AGAMOUS-LIKE24, are necessary to block floral gene expression during the vegetative phase. *Plant Physiol* 165: 1591–1603
- Ferrándiz C (2002) Regulation of fruit dehiscence in *Arabidopsis*. *J Exp Bot* 53: 2031–2038
- Ferrándiz C, Pelaz S, Yanofsky MF (1999) Control of carpel and fruit development in *Arabidopsis*. *Annu Rev Biochem* 68: 321–354
- Ghandchi FP, Caetano-Anolles G, Clough SJ, Ort DR (2016) Investigating the control of chlorophyll degradation by genomic correlation mining. *PLoS ONE* 11: e0162327
- Gillaspy G, Ben-David H, Gouissem W (1993) Fruits: a developmental perspective. *Plant Cell* 5: 1439–1451
- Giorgi FM, Del Fabbro C, Licausi F (2013) Comparative study of RNA-seq and microarray-derived coexpression networks in *Arabidopsis thaliana*. *Bioinformatics* 29: 717–724
- Giraud E, Van Aken O, Ho LHM, Whelan J (2009) The transcription factor ABI4 is a regulator of mitochondrial retrograde expression of ALTERNATIVE OXIDASE1a. *Plant Physiol* 150: 1286–1296
- Gnan S, Marsh T, Kover PX (2017) Inflorescence photosynthetic contribution to fitness releases *Arabidopsis thaliana* plants from trade-off constraints on early flowering. *PLoS ONE* 12: e0185835
- Goetz M, Vivian-Smith A, Johnson SD, Koltunow AM (2006) AUXIN RESPONSE FACTOR8 is a negative regulator of fruit initiation in *Arabidopsis*. *Plant Cell* 18: 1873–1886
- Gutierrez L, Mauriat M, Guénin S, Pelloux J, Lefebvre JF, Louvet R, Rusterucci C, Moritz T, Guérineau F, Bellini C, (2008) The lack of a systematic validation of reference genes: a serious pitfall undervalued in reverse transcription-polymerase chain reaction (RT-PCR) analysis in plants. *Plant Biotechnol J* 6: 609–618
- Guyer L, Hofstetter SS, Christ B, Lira BS, Rossi M, Hörtensteiner S (2014) Different mechanisms are responsible for chlorophyll dephytylation during fruit ripening and leaf senescence in tomato. *Plant Physiol* 166: 44–56
- Hanson J, Johannesson H, Engström P (2001) Sugar-dependent alterations in cotyledon and leaf development in transgenic plants expressing the HDZ-dip gene ATHB13. *Plant Mol Biol* 45: 247–262
- He H, Bai M, Tong P, Hu Y, Yang M, Wu H (2018) CELLULASE6 and MANANASE7 affect cell differentiation and silique dehiscence. *Plant Physiol* 176: 2186–2201
- Hou B, Lim EK, Higgins GS, Bowles DJ (2004) N-glycosylation of cytokinins by glycosyltransferases of *Arabidopsis thaliana*. *J Biol Chem* 279: 47822–47832 15342621
- Hua W, Li RJ, Zhan GM, Liu J, Li J, Wang XF, Liu GH, Wang HZ (2012) Maternal control of seed oil content in *Brassica napus*: the role of silique wall photosynthesis. *Plant J* 69: 432–444
- Ihnatowicz A, Pesaresi P, Varotto C, Richly E, Schneider A, Jahns P, Salamini F, Leister D (2004) Mutants for photosystem I subunit D of *Arabidopsis thaliana*: effects on photosynthesis, photosystem I stability and expression of nuclear genes for chloroplast functions. *Plant J* 37: 839–852
- Jaradat MR, Ruegger M, Bowling A, Butler H, Cutler AJ (2014) A comprehensive transcriptome analysis of silique development and dehiscence in *Arabidopsis* and *Brassica* integrating genotypic, interspecies and developmental comparisons. *GM Crops Food* 5: 302–320
- Jones-Rhoades MW, Bartel DP, Bartel B (2006) MicroRNAs and their regulatory roles in plants. *Annu Rev Plant Biol* 57: 19–53
- Jung JH, Seo PJ, Kang SK, Park CM (2011) miR172 signals are incorporated into the miR156 signaling pathway at the SPL3/4/5 genes in *Arabidopsis* developmental transitions. *Plant Mol Biol* 76: 35–45
- Kalantidis K, Schumacher HT, Alexiadis T, Helm JM (2008) RNA silencing movement in plants. *Biol Cell* 100: 13–26
- Kim GT, Tsukaya H, Uchimiya H (1998) The ROTUNDIFOLIA3 gene of *Arabidopsis thaliana* encodes a new member of the cytochrome P-450 family that is required for the regulated polar elongation of leaf cells. *Genes Dev* 12: 2381–2391
- Kim GT, Tsukaya H, Saito Y, Uchimiya H (1999) Changes in the shapes of leaves and flowers upon overexpression of cytochrome P450 in *Arabidopsis*. *Proc Natl Acad Sci USA* 96: 9433–9437

- Kim GT, Shoda K, Tsuge T, Cho KH, Uchimiya H, Yokoyama R, Nishitani K, Tsukaya H (2002) The *ANGUSTIFOLIA* gene of *Arabidopsis*, a plant CtBP gene, regulates leaf-cell expansion, the arrangement of cortical microtubules in leaf cells and expression of a gene involved in cell-wall formation. *EMBO J* 21: 1267–1279
- Kim GT, Fujioka S, Kozuka T, Tax FE, Takatsuto S, Yoshida S, Tsukaya H (2005) CYP90C1 and CYP90D1 are involved in different steps in the brassinosteroid biosynthesis pathway in *Arabidopsis thaliana*. *Plant J* 41: 710–721
- Kim HJ, Hong SH, Kim YW, Lee IH, Jun JH, Phee BK, Rupak T, Jeong H, Lee Y, Hong BS, (2014) Gene regulatory cascade of senescence-associated NAC transcription factors activated by ETHYLENE-INSENSITIVE2-mediated leaf senescence signalling in *Arabidopsis*. *J Exp Bot* 65: 4023–4036
- Kim HJ, Nam HG, Lim PO (2016) Regulatory network of NAC transcription factors in leaf senescence. *Curr Opin Plant Biol* 33: 48–56
- Kleffmann T, Russenberger D, von Zychlinski A, Christopher W, Sjölander K, Gruissem W, Baginsky S (2004) The *Arabidopsis thaliana* chloroplast proteome reveals pathway abundance and novel protein functions. *Curr Biol* 14: 354–362
- Kleindt CK, Stracke R, Mehrrens F, Weisshaar B (2010) Expression analysis of flavonoid biosynthesis genes during *Arabidopsis thaliana* silique and seed development with a primary focus on the proanthocyanidin biosynthetic pathway. *BMC Res Notes* 3: 255
- Klepikova AV, Kasianov AS, Gerasimov ES, Logacheva MD, Penin AA (2016) A high resolution map of the *Arabidopsis thaliana* developmental transcriptome based on RNA-seq profiling. *Plant J* 88: 1058–1070
- Kou X, Watkins CB, Gan SS (2012) *Arabidopsis* AtNAP regulates fruit senescence. *J Exp Bot* 63: 6139–6147
- Kumar R, Khurana A, Sharma AK (2014) Role of plant hormones and their interplay in development and ripening of fleshy fruits. *J Exp Bot* 65: 4561–4575
- Law CW, Chen Y, Shi W, Smyth GK (2014) voom: precision weights unlock linear model analysis tools for RNA-seq read counts. *Genome Biol* 15: R29
- Lee YK, Kim GT, Kim JJ, Park J, Kwak SS, Choi G, Chung WI (2006) *LONGIFOLIA1* and *LONGIFOLIA2*, two homologous genes, regulate longitudinal cell elongation in *Arabidopsis*. *Development* 133: 4305–4314
- León P, Gregorio J, Cordoba E (2013) *ABI4* and its role in chloroplast retrograde communication. *Front Plant Sci* 3: 304
- Li Y, Baldauf S, Lim EK, Bowles DJ (2001) Phylogenetic analysis of the UDP-glycosyltransferase multigene family of *Arabidopsis thaliana*. *J Biol Chem* 276: 4338–4343
- Liao Y, Smyth GK, Shi W (2014) featureCounts: an efficient general purpose program for assigning sequence reads to genomic features. *Bioinformatics* 30: 923–930
- Liljehgren SJ, Ditta GS, Eshed Y, Savidge B, Bowman JL, Yanofsky MF (2000) SHATTERPROOF MADS-box genes control seed dispersal in *Arabidopsis*. *Nature* 404: 766–770
- Lim PO, Kim HJ, Nam HG (2007) Leaf senescence. *Annu Rev Plant Biol* 58: 115–136
- Lindsey K (2001) Plant peptide hormones: the long and the short of it. *Curr Biol* 11: R741–R743
- Mansfield SG, Briarty LG (1991) Early embryogenesis in *Arabidopsis thaliana*. II. The developing embryo. *Can J Bot* 69: 461–476
- Martínez-García JE, Monte E, Quail PH (1999) A simple, rapid and quantitative method for preparing *Arabidopsis* protein extracts for immunoblot analysis. *Plant J* 20: 251–257
- Masiero S, Colombo L, Grini PE, Schnittger A, Kater MM (2011) The emerging importance of type I MADS box transcription factors for plant reproduction. *Plant Cell* 23: 865–872
- Matilla AJ (2007) How is the silique fruit dismantled over its maturation? *Funct Plant Sci Biotechnol* 1: 85–93
- Mazzucato A, Taddei AR, Soressi GP (1998) The parthenocarpic fruit (pat) mutant of tomato (*Lycopersicon esculentum* Mill.) sets seedless fruits and has aberrant anther and ovule development. *Development* 125: 107–114
- McAtee P, Karim S, Schaffer R, David K (2013) A dynamic interplay between phytohormones is required for fruit development, maturation, and ripening. *Front Plant Sci* 4: 79
- Mizzotti C, Mendes MA, Caporali E, Schnittger A, Kater MM, Battaglia R, Colombo L (2012) The MADS box genes *SEEDSTICK* and *ARABIDOPSIS* Bsister play a maternal role in fertilization and seed development. *Plant J* 70: 409–420
- Mizzotti C, Ezquer I, Paolo D, Rueda-Romero P, Guerra RF, Battaglia R, Rogachev I, Aharoni A, Kater MM, Caporali E, (2014) *SEEDSTICK* is a master regulator of development and metabolism in the *Arabidopsis* seed coat. *PLoS Genet* 10: e1004856
- Mizzotti C, Galliani BM, Dreni L, Sommer H, Bombarely A, Masiero S (2017) *ERAMOSA* controls lateral branching in snapdragon. *Sci Rep* 7: 41319
- Müntz K, Rudolph A, Schlesier G, Silhengst P (1978) The function of the pericarp in fruits of crop legumes. *Die Kult* 26: 37–67
- Nitsch JP (1952) Plant hormones in the development of fruits. *Q Rev Biol* 27: 33–57
- O'Neill SD (1997) POLLINATION REGULATION OF FLOWER DEVELOPMENT. *Annu Rev Plant Physiol Plant Mol Biol* 48: 547–574
- O'Neill SD, Nadeau JA (2010) Postpollination flower development. *Hortic Rev* 19: 1–58
- Ougham H, Hörtensteiner S, Armstead I, Donnison I, King I, Thomas H, Mur L (2008) The control of chlorophyll catabolism and the status of yellowing as a biomarker of leaf senescence. *Plant Biol (Stuttg) (Suppl 1)* 10: 4–14
- Pandolfini T (2009) Seedless fruit production by hormonal regulation of fruit set. *Nutrients* 1: 168–177
- Pechan PA, Morgan DG (1985) Defoliation and its effects on pod and seed development in oil seed rape (*Brassica napus* L.). *J Exp Bot* 36: 458–468
- Penfield S, Li Y, Gilday AD, Graham S, Graham IA (2006) *Arabidopsis* *ABA INSENSITIVE4* regulates lipid mobilization in the embryo and reveals repression of seed germination by the endosperm. *Plant Cell* 18: 1887–1899
- Pesaresi P, Mizzotti C, Colombo M, Masiero S (2014) Genetic regulation and structural changes during tomato fruit development and ripening. *Front Plant Sci* 5: 124
- Piechulla B, Imlay KR, Gruissem W (1985) Plastid gene expression during fruit ripening in tomato. *Plant Mol Biol* 5: 373–384
- Piechulla B, Glick RE, Bahl H, Melis A, Gruissem W (1987) Changes in photosynthetic capacity and photosynthetic protein pattern during tomato fruit ripening. *Plant Physiol* 84: 911–917
- Powell ALT, Nguyen CV, Hill T, Cheng KL, Figueroa-Balderas R, Aktas H, Ashrafi H, Pons C, Fernández-Muñoz R, Vicente A, (2012) Uniform ripening encodes a Golden 2-like transcription factor regulating tomato fruit chloroplast development. *Science* 336: 1711–1715
- Prasad K, Zhang X, Tobón E, Ambrose BA (2010) The *Arabidopsis* B-sister MADS-box protein, *GORDITA*, represses fruit growth and contributes to integument development. *Plant J* 62: 203–214
- Raghavan V (2003) Some reflections on double fertilization, from its discovery to the present. *New Phytol* 159: 565–583
- Resentini E, Cyprys P, Steffen JG, Alter S, Morandini P, Mizzotti C, Lloyd A, Drews GN, Dresselhaus T, Colombo L, (2017) *SUPPRESSOR OF FRIGIDA* (*SUF4*) supports gamete fusion via regulating *Arabidopsis* *EC1* gene expression. *Plant Physiol* 173: 155–166
- Robinson CK, Hill SA (1999) Altered resource allocation during seed development in *Arabidopsis* caused by the *abi3* mutation. *Plant Cell Environ* 22: 117–123
- Robinson MD, McCarthy DJ, Smyth GK (2010) edgeR: a Bioconductor package for differential expression analysis of digital gene expression data. *Bioinformatics* 26: 139–140
- Rojas-Gracia P, Roque E, Medina M, Rochina M, Hamza R, Angarita-Díaz MP, Moreno V, Pérez-Martín F, Lozano R, Cañas L, (2017) The parthenocarpic hydra mutant reveals a new function for a *SPOCYTELESS*-like gene in the control of fruit set in tomato. *New Phytol* 214: 1198–1212
- Rollins RC (1993) The Cruciferae of Continental North America: Systematics of the Mustard Family from the Arctic to Panama. Stanford University Press, Stanford, CA
- Romani I, Tadini L, Rossi F, Masiero S, Pribil M, Jahns P, Kater M, Leister D, Pesaresi P (2012) Versatile roles of *Arabidopsis* plastid ribosomal proteins in plant growth and development. *Plant J* 72: 922–934
- Rosso MG, Li Y, Strizhov N, Reiss B, Dekker K, Weisshaar B (2003) An *Arabidopsis thaliana* T-DNA mutagenized population (*GABI-Kat*) for flanking sequence tag-based reverse genetics. *Plant Mol Biol* 53: 247–259
- Scarpeci TE, Frea VS, Zanon MI, Valle EM (2017) Overexpression of *AtERF019* delays plant growth and senescence, and improves drought tolerance in *Arabidopsis*. *J Exp Bot* 68: 673–685
- Schaffer AA, Petreikov M (1997) Sucrose-to-starch metabolism in tomato fruit undergoing transient starch accumulation. *Plant Physiol* 113: 739–746
- Schägger H, von Jagow G (1987) Tricine-sodium dodecyl sulfate-polyacrylamide gel electrophoresis for the separation of proteins in the range from 1 to 100 kDa. *Anal Biochem* 166: 368–379

- Schneider CA, Rasband WS, Eliceiri KW (2012) NIH Image to ImageJ: 25 years of image analysis. *Nat Methods* **9**: 671–675
- Schwarz S, Grande AV, Bujdosó N, Saedler H, Huijser P (2008) The microRNA regulated SBP-box genes SPL9 and SPL15 control shoot maturation in *Arabidopsis*. *Plant Mol Biol* **67**: 183–195 18278578
- Seyednasrollah F, Laiho A, Elo LL (2015) Comparison of software packages for detecting differential expression in RNA-seq studies. *Brief Bioinform* **16**: 59–70
- Seymour GB, Østergaard L, Chapman NH, Knapp S, Martin C (2013) Fruit development and ripening. *Annu Rev Plant Biol* **64**: 219–241
- Shao H, Wang H, Tang X (2015) NAC transcription factors in plant multiple abiotic stress responses: progress and prospects. *Front Plant Sci* **6**: 902
- Smyth G (2005) Limma: linear models for microarray data. In R Gentleman, V Carey, S Dudoit, R Irizarry, W Huber, eds, *Bioinformatics and Computational Biology Solutions Using R and Bioconductor*. Springer, New York, pp 397–420
- Steinhauser MC, Steinhauser D, Koehl K, Carrari F, Gibon Y, Fernie AR, Stitt M (2010) Enzyme activity profiles during fruit development in tomato cultivars and *Solanum pennellii*. *Plant Physiol* **153**: 80–98
- Suorsa M, Rossi F, Tadini L, Labs M, Colombo M, Jahns P, Kater MM, Leister D, Finazzi G, Aro EM, (2016) PGR5-PGRL1-dependent cyclic electron transport modulates linear electron transport rate in *Arabidopsis thaliana*. *Mol Plant* **9**: 271–288
- Tadini L, Romani I, Pribil M, Jahns P, Leister D, Pesaresi P (2012) Thylakoid redox signals are integrated into organellar-gene-expression-dependent retrograde signaling in the prors1-1 mutant. *Front Plant Sci* **3**: 282
- Takada S, Goto K (2003) Terminal flower2, an *Arabidopsis* homolog of heterochromatin protein1, counteracts the activation of flowering locus T by constans in the vascular tissues of leaves to regulate flowering time. *Plant Cell* **15**: 2856–2865
- Tamaki S, Matsuo S, Wong HL, Yokoi S, Shimamoto K (2007) Hd3a protein is a mobile flowering signal in rice. *Science* **316**: 1033–1036
- Tsuchisaka A, Yu G, Jin H, Alonso JM, Ecker JR, Zhang X, Gao S, Theologis A (2009) A combinatorial interplay among the 1-aminocyclopropane-1-carboxylate isoforms regulates ethylene biosynthesis in *Arabidopsis thaliana*. *Genetics* **183**: 979–1003
- Tsuge T, Tsukaya H, Uchimiya H (1996) Two independent and polarized processes of cell elongation regulate leaf blade expansion in *Arabidopsis thaliana* (L.) Heynh. *Development* **122**: 1589–1600
- Usami T, Horiguchi G, Yano S, Tsukaya H (2009) The more and smaller cells mutants of *Arabidopsis thaliana* identify novel roles for SQUAMOSA PROMOTER BINDING PROTEIN-LIKE genes in the control of heteroblasty. *Development* **136**: 955–964
- Van der Pijl L (1982) *Principles of Dispersal in Higher Plants*. Springer-Verlag, New York
- van Wees S (2008) Phenotypic analysis of *Arabidopsis* mutants: trypan blue stain for fungi, oomycetes, and dead plant cells. *CSH Protoc* **2008**: pdb.prot4982
- Varoquaux F, Blanvillain R, Delseny M, Gallois P (2000) Less is better: new approaches for seedless fruit production. *Trends Biotechnol* **18**: 233–242
- Vivian-Smith A, Koltunow AM (1999) Genetic analysis of growth-regulator-induced parthenocarpy in *Arabidopsis*. *Plant Physiol* **121**: 437–451
- Vivian-Smith A, Luo M, Chaudhury A, Koltunow A (2001) Fruit development is actively restricted in the absence of fertilization in *Arabidopsis*. *Development* **128**: 2321–2331
- Wagstaff C, Yang TJW, Stead AD, Buchanan-Wollaston V, Roberts JA (2009) A molecular and structural characterization of senescing *Arabidopsis* siliques and comparison of transcriptional profiles with senescing petals and leaves. *Plant J* **57**: 690–705
- Wang X (2010) *The Dawn Angiosperms: Uncovering the Origin of Flowering Plants*. Springer-Verlag, Berlin
- Wang JW, Schwab R, Czech B, Mica E, Weigel D (2008) Dual effects of miR156-targeted SPL genes and CYP78A5/KLUH on plastochron length and organ size in *Arabidopsis thaliana*. *Plant Cell* **20**: 1231–1243
- Wang Q, Huang W, Jiang Q, Lian J, Sun J, Xu H, Zhao H, Liu Z (2013) Lower levels of expression of FATA2 gene promote longer siliques with modified seed oil content in *Arabidopsis thaliana*. *Plant Mol Biol Rep* **31**: 1368–1375
- Wanner LA, Gruissem W (1991) Expression dynamics of the tomato rbcS gene family during development. *Plant Cell* **3**: 1289–1303
- Watanabe M, Balazadeh S, Tohge T, Erban A, Giavalisco P, Kopka J, Mueller-Roeber B, Fernie AR, Hoefgen R (2013) Comprehensive dissection of spatiotemporal metabolic shifts in primary, secondary, and lipid metabolism during developmental senescence in *Arabidopsis*. *Plant Physiol* **162**: 1290–1310
- Wingler A, Marès M, Pourtau N (2004) Spatial patterns and metabolic regulation of photosynthetic parameters during leaf senescence. *New Phytol* **161**: 781–789
- Woo HR, Koo HJ, Kim J, Jeong H, Yang JO, Lee IH, Jun JH, Choi SH, Park SJ, Kang B, (2016) Programming of plant leaf senescence with temporal and inter-organellar coordination of transcriptome in *Arabidopsis*. *Plant Physiol* **171**: 452–467
- Wu K, Tian L, Malik K, Brown D, Miki B (2000) Functional analysis of HD2 histone deacetylase homologues in *Arabidopsis thaliana*. *Plant J* **22**: 19–27 10792817
- Yamasaki H, Hayashi M, Fukazawa M, Kobayashi Y, Shikanai T (2009) SQUAMOSA Promoter Binding Protein-Like7 is a central regulator for copper homeostasis in *Arabidopsis*. *Plant Cell* **21**: 347–361
- Yang J, Worley E, Udvardi M (2014) A NAP-AAO3 regulatory module promotes chlorophyll degradation via ABA biosynthesis in *Arabidopsis* leaves. *Plant Cell* **26**: 4862–4874
- Zhang W, Liu T, Ren G, Hörtensteiner S, Zhou Y, Cahoon EB, Zhang C (2014) Chlorophyll degradation: the tocopherol biosynthesis-related phytyl hydrolase in *Arabidopsis* seeds is still missing. *Plant Physiol* **166**: 70–79
- Zhang Y, Schwarz S, Saedler H, Huijser P (2007) SPL8, a local regulator in a subset of gibberellin-mediated developmental processes in *Arabidopsis*. *Plant Mol Biol* **63**: 429–439
- Zhao Z, Andersen SU, Ljung K, Dolezal K, Miotk A, Schultheiss SJ, Lohmann JU (2010) Hormonal control of the shoot stem-cell niche. *Nature* **465**: 1089–1092